

DOCTORAL THESIS

**Tracing environmental variability in the
changing Arctic Ocean with optical
measurements of dissolved organic matter**

**Dissertation zur Erlangung des
Doktorgrades der Naturwissenschaften
- Dr. rer. nat. -**

vorgelegt von

RAFAEL GONÇALVES ARAUJO

am 28. 10. 2016

an der Universität Bremen
im Fachbereich Biologie/Chemie

THESIS' SUPERVISION

- Supervisor:** Prof. Dr. Astrid Bracher,
Universität Bremen
Alfred Wegener Institute Helmholtz Centre for Polar and
Marine Research
- Co-supervisor:** Associate Prof. Dr. Colin Andrew Stedmon
National Institute of Aquatic Resources, Technical
University of Denmark

THESIS' EVALUATION

- 1. Gutachter:** Prof. Dr. Astrid Bracher,
Universität Bremen
Alfred Wegener Institute Helmholtz Centre for Polar and
Marine Research
- 2. Gutachter:** Associate Prof. Dr. Colin Andrew Stedmon
National Institute of Aquatic Resources, Technical
University of Denmark
- 3. Gutachter:** Prof. Dr. Oliver Zielinski
Institute for Chemistry and Biology of the Marine
Environment, Carl von Ossietzky Universität Oldenburg
- 1. Prüfer:** Prof. Dr. Kai Bischof
Universität Bremen
- 2. Prüfer:** Prof. Dr. Tilmann Harder
Universität Bremen

Datum des Kolloquiums: 08. 12. 2016

Versicherung an Eides Statt

Ich, Rafael Gonçalves Araujo, Anschrift: Bürgermeister-Smidt-Straße 48 – 27568 – Bremerhaven, Matr.-Nr. 2951561, versichere an Eides Statt durch meine Unterschrift, dass ich die vorstehende Arbeit selbständig und ohne fremde Hilfe angefertigt und alle Stellen, die ich wörtlich dem Sinne nach aus Veröffentlichungen entnommen habe, als solche kenntlich gemacht habe, mich auch keiner anderen als der angegebenen Literatur oder sonstiger Hilfsmittel bedient habe.

Ich versichere an Eides Statt, dass ich die vorgenannten Angaben nach bestem Wissen und Gewissen gemacht habe und dass die Angaben der Wahrheit entsprechen und ich nichts verschwiegen habe.

Die Strafbarkeit einer falschen eidesstattlichen Versicherung ist mir bekannt, namentlich die Strafandrohung gemäß § 156 StGB bis zu drei Jahren Freiheitsstrafe oder Geldstrafe bei vorsätzlicher Begehung der Tat bzw. Gemäß § 161 Abs. 1 StGB bis zu einem Jahr Freiheitsstrafe oder Geldstrafe bei fahrlässiger Begehung.

Bremen, 28.10.2016

Rafael Gonçalves Araujo

Valeu a pena? Tudo vale a pena se a alma não é pequena.

Was it worth it? Everything is worthy if the soul is not small.

Fernando Pessoa, Portuguese Sea, 1934

Acknowledgements

There are many people that I would like to thank for helping and inspiring me, both personal and professionally, over the last several years.

First, I would like to thank my supervisors, Prof. Dr. Astrid Bracher and Assistant Prof. Dr. Colin A. Stedmon for accepting me in their groups and for supporting, guiding and inspiring me along those years with a lot of motivation and massive learning. I also would emphasize that I am very grateful in particular that both of you have trusted and encouraged me.

I thank my colleagues of the Phytooptics group (Mariana Soppa, Sonja Wiegmann, Aleksandra Wolanin, Tilman Dinter, Svetlana Loza, Bettina Taylor, Wee Cheah, Alexandra Cherkasheva, Julia Oelker, Yangyang Liu and Sebastian Hellmann), for their support, friendship and the great moments we have spent together.

I am tremendously thankful to Lumi Haraguchi not only for being my best friend, but also my critic scientific advisor since our bachelor studies in Brazil.

It is worth it to thank the many friends, who helped me to solve some problems during my PhD with programming, reading my manuscripts and/or providing many great discussions and insights. These friends are Amália Detoni, Marta Ramírez-Pérez, Ingrid Angel-Benavides, Abel Machado, Tatiane Combi, Márcio Silva de Souza, Amábile Ferreira, Catarina Cecílio and many others.

I am thankful to all the co-authors who helped me improve the manuscripts of this thesis with their constructive comments and discussions.

This thesis would not have been possible without the support and infrastructure provided by the Alfred Wegener Institute Helmholtz Centre for Polar and Marine Research through the Section for Physical Oceanography of Polar Seas.

I would like to express my appreciation to Prof. Dr. Oliver Zielinski who agreed to be a reviewer of this thesis. I am also grateful to other thesis defense committee members: Prof. Dr. Kai Bischof, Prof. Dr. Tilmann Harder, Rita Melo Franco Santos and Timothy Thomson.

I also acknowledge the members of my PhD Committee (Prof. Dr. Boris Koch, Prof. Dr. Oliver Zielinski and Dr. Benjamin Rabe), who used of their time to meet me twice a year, and give very constructive suggestions to my thesis. Those meetings were very important for delineating the outline of this thesis.

I am grateful to the POLMAR Graduate School, particularly to Claudia Hanfland and Claudia Sprengel, for their time, confidence, motivation, attention and continuous tracking of my progress. I am very thankful for the courses I have attended, which were always helpful and insightful, and for making the PhD Committee meetings mandatory. I also would like to express my thankfulness to POLMAR for providing funding for attending conferences and, in particular, for funding my first visit to the Technical University of Denmark (from August to October 2014), which was the best think I could have done in my PhD.

A special thanks to the Coordination for the Improvement of Higher Level Personnel (CAPES, Brazil) for funding my PhD studies in Germany through the research grant 12362/12-3. I also thank the University of Bremen for accepting me as a PhD student and also for funding my research stay at the Technical University of Denmark between January and February 2016.

I thank the German Academic Exchange Service (DAAD) for providing the very intensive German classes in Leipzig before starting my PhD. That course made my life in Germany much easier.

I acknowledge to all principal investigators and contributors for collecting, analyzing and sharing part of the data used in this thesis. I also thank to all the colleagues from the four expeditions I participated in during my PhD: the Lena group for all the patience and hard work, but especially for keeping up the good mood; the PEBCAO group and my beloved Mandy, Jonathan and Sinna, for preventing me to get crazy during the Polarstern expedition; and finally, to all the PHYTOSCOPE members for the extremely friendly, amazing and positive atmosphere during the campaigns, even when we were rescued by the coast guard. You guys rock!

I will be forever thankful to Prof. Dr. Carolous Vooren and Prof. Dr. Virginia Tavano from the Federal University of Rio Grande (Brazil) for transmitting their love for science through the brightness in their eyes during their classes. You made me feel in love with it as well.

I thank the AWI Volleyball team for the great time we spent together.

I am very thankful to all the good friends I have made in Germany, who put some light in the dark Bremerhaven: Giulia, Ivan, Diana, Ole, Ritinha, Cami, Lauris, Mariam, Ingrid, Miguel, Meri, Ale, Alemão, Alessandra, Camila, Tremembé, Dragos, Eric, Felix, Lera, Nok, and many others.

I thank to the lovely Niller, for being the best flat mate I could have had in Copenhagen.

It is impossible not to mention the long skype/beer meetings with my beloved Lumi, Naty, Pati, Fer, Amalia, Pi, Tatileine, Fernandinho and Juba. You guys made my days much happier for many times without even knowing it. However, I would like to highlight how important was to talk to Lumi, Naty and Pati, who always had wisdom words! Love you, Gatas!

I am very thankful to all the social media groups, which kept me close to my friends along all these years. And, mostly, those groups make me give some great laughs.

I thank to all my friends from the studies and hometown living in Europe for the awesome trips, moments and sleepovers we had. Those were definitely the moments to “recharge the batteries”. I could not forget to thank my beloved friends Susi and Colômbia for teaching me how to conjugate the verb “titanium”. I am also very thankful to the “Santa” for blessing our lives and guiding us to the success.

Many thanks to all the friends I have left in Brazil (especially my beloved girls from the “Sapa Bonde”, Mau and Denão) for always receiving me with love and many kisses and hugs, and, mostly, for proving that true friendships last forever. The love I have for you guys will never change!

I thank my fiancée’s family, or my second family, for being so welcoming, supportive and making me feel part of the family, especially Fatiminha, whom I love very much and took me like her own son.

My sincere gratitude to my family for supporting me and my career choices, since always. However, I would like to highlight my Grandparents and uncle Biba, who always trusted and supported me, no matter what. I love you!

I am thankful to my sister, for simply being the best sister in this world. Love you, Gordinha!

I would like to express my most sincere gratitude to two persons, for their unconditional love during all those years: my Mom and Bruno, my fiancée. Both of them encouraged me, cheered me up, were patient and, without your love, I would not have made it. I love you so much and seeing you proud of me makes me certain that it was worth it. Finally, to Bruno, I am fortunate to have you in my life. You make me the happiest man in the world.

Table of Contents

Abstract.....	1
Zusammenfassung.....	3
List of Abbreviations.....	6
List of Publications.....	10
List of Figures.....	11
List of Tables.....	17
1. Introduction.....	19
1.1. Motivation and objectives of the thesis.....	20
1.2. Thesis outline and author's contribution.....	25
2. Scientific Background.....	27
2.1. The Arctic Ocean.....	28
2.2. Tools for assessing content, speciation and origin of DOM in aquatic systems.....	34
Abstract.....	34
2.2.1. Objectives.....	35
2.2.2. Quantitative and qualitative methods for DOM assessment.....	35
2.2.2.1. Molecular analyses.....	35
2.2.2.2. Bulk analyses.....	37
2.2.3. DOM as an environmental tracer.....	41
2.2.4. Conclusions.....	42
2.2.4. Acknowledgements.....	42
3. From fresh to marine waters: Characterization and fate of dissolved organic matter in the Lena River Delta region, Siberia.....	43
Abstract.....	45
3.1. Introduction.....	45
3.2. Material and Methods.....	47
3.2.1. Sampling.....	47
3.2.2. Water column structure assessment.....	48
3.2.3. DOC and DOM sample processing and data analysis... ..	48
3.2.4. DOM modification indices, statistical analyses and graphical tools.....	50
3.3. Results.....	51
3.3.1. Hydrography and water column structure.....	51

3.3.2. CDOM and DOC spatial variability.....	52
3.3.3. FDOM components by PARAFAC.....	54
3.3.4. Optical indices of DOM modification.....	56
3.4. Discussion.....	57
3.4.1. Characterization and transformation of DOM.....	57
3.4.2. Dynamics and fate of DOM in the Lena Delta region....	59
3.5. Summary.....	62
3.6. Acknowledgements.....	63
4. Using fluorescent dissolved organic matter to trace and distinguish the origin of Arctic surface waters.....	65
Abstract.....	67
4.1. Introduction.....	67
4.2. Material and methods.....	70
4.2.1. Sampling strategy.....	70
4.2.2. Analyses of salinity, dissolved inorganic nutrients, dissolved oxygen and $\delta^{18}\text{O}$	71
4.2.3. DOM samples processing.....	71
4.2.4. Spectroscopic measurements and PARAFAC modeling...	72
4.2.5. Water masses fractionation.....	72
4.3. Results.....	73
4.3.1. Water mass distribution.....	73
4.3.2. Dissolved organic matter fluorescence characterization....	76
4.3.3. Distribution of water fractions.....	78
4.3.4. Linking visible organic matter fluorescence to water fractions.....	78
4.4. Discussion.....	79
4.5. Summary.....	84
4.6. Acknowledgements.....	85
4.7. Supplementary material.....	86
5. High colored dissolved organic matter (CDOM) absorption by waters of central-eastern Arctic Ocean: implications for biogeochemistry and ocean color algorithms.....	89
Abstract.....	91
5.1. Introduction.....	91
5.2. Methods.....	94
5.2.1. Sampling.....	94
5.2.2. Particulate absorption analysis.....	95

5.2.3. Dissolved organic matter absorption analysis.....	95
5.2.4. Chlorophyll- <i>a</i> analysis.....	96
5.2.5. Radiometric measurements.....	96
5.2.6. Ocean color algorithms.....	97
5.2.7. Statistical analyses.....	99
5.3. Results and discussion.....	100
5.3.1. Hydrography.....	100
5.3.2. Absorption coefficients of phytoplankton, NAP, and CDOM.....	101
5.3.3. Geographic clustering.....	105
5.3.4. Arctic bio-optical provinces.....	108
5.3.5. Evaluation of ocean color algorithms.....	109
5.4. Summary and scope.....	114
5.5. Acknowledgements.....	116
6. Synthesis and major outcomes.....	117
7. References.....	125
8. Addendum.....	151
Gonçalves-Araujo (2016), <i>Proceedings of YOUMARES 7</i>	152
Gonçalves-Araujo et al. (2015), <i>Frontiers in Marine Science</i>	163
Gonçalves-Araujo et al. (2016), <i>Scientific Reports</i>	176

Abstract

The Arctic Ocean plays an important role on the global hydrological and carbon cycles. It contributes 5–14% to the global balance of CO₂ sinks and sources. Carbon is also cycled in the Arctic Ocean through the primary producers, with high primary production observed in the marginal ice zones, ice-free zones and melt ponds, with increased biogenic carbon export to the deep layers. Although being the smallest ocean basin, the Arctic Ocean receives ~11% of the global riverine runoff. Along with the freshwater, high loads of organic carbon are introduced in the Arctic Ocean. Most of it is observed in the fraction of dissolved organic matter (DOM). With the ongoing global warming, glacier melt and permafrost thaw are observed and pointed as the main drivers for increasing the freshwater discharge into the Arctic basin. Along side, permafrost thaw coupled with increased coastal erosion lead to an increase in mobilization of carbon from permafrost, which could have critical implications for microbial processes, primary production, terrestrial carbon fluxes to the shelf seas and, thus, carbon cycling in the Arctic.

This thesis is focusing on tracing the mixing of DOM along the Siberian shelves and developing potential applications of DOM as an environmental tracer. Four main objectives have been pursued: (1) to quantify, characterize and assess the distribution and transformation of DOM across the river-shelf transition and provide insights into the fate of Arctic riverine DOM; (2) to assess the potential of DOM, especially its fluorescent fraction (FDOM), as a tracer of freshwater in the surface layers in the Arctic Ocean; (3) to characterize the non-water absorption in the surface central and eastern Arctic Ocean and further test whether bio-optical properties (such as absorption and reflectance) can reproduce hydrographical variability; (4) to evaluate the performance of ocean color algorithms frequently applied for studies in the Arctic Ocean using novel data from a central-eastern Arctic expedition.

In the first study the fluorescent components of DOM isolated with PARAFAC model were characterized along the river to sea transition in the Laptev Sea and Lena River delta region. Results showed a strong dominance of visible wavelength DOM fluorescence (VIS-FDOM), which is associated to terrestrial signal (or humic-like compounds). The results corroborate previous reports showing strong removal of DOM at low salinity. However, our results showed that the removal occurs preferentially for VIS-FDOM, whereas ultraviolet wavelength FDOM (UV-FDOM, associated to autochthonous marine production) differed in behavior, with an increase during estuarine mixing. DOM removal occurred primarily in the surface layer, under direct influence of the Lena River runoff (salinity <10), which indicates that it was mainly driven by photodegradation and flocculation.

The second study explored the potential of VIS-FDOM components isolated with PARAFAC analysis as an environmental tracer in the Fram and Davis Straits. VIS-FDOM was strongly correlated to the fractions of meteoric water (f_{mw}) in polar waters. Furthermore, a pattern allowed the distinction between the sources of polar waters exiting the Fram Strait as being from the Eurasian or Canadian basins. In the bottom waters of the Davis Strait, VIS-FDOM was correlated to apparent oxygen utilization (AOU), tracing deep-water turnover of DOM and production of VIS-FDOM fluorescence. The findings presented in this study show which wavelengths carry information on sources and mixing of DOM, which therefore can be applied to monitor freshwater and carbon export to the North Atlantic.

The third study shows that colored DOM (CDOM) dominates the non-water absorption in the surface waters of the central and eastern Arctic. Spatial variability observed in the non-water absorbers (phytoplankton, CDOM and non-algal particles–NAP) clustered the sampling sites in agreement with hydrographic variability. Such variability was also detected by the analysis of hyperspectral remote sensing reflectance (R_{rs}). The empirical and semi-analytical ocean color algorithms frequently applied in studies in the Arctic Ocean were applied to *in situ* measured R_{rs} to evaluate their performance. The retrievals (chlorophyll-a, and the absorption coefficients of CDOM and phytoplankton) were then validated to the correspondent *in situ* measurements. The results showed that empirical algorithms have poor performance, whereas the semi-analytical algorithms appeared to be robust for application in the Arctic Ocean; however still with considerable errors embedded to the retrievals.

The main findings of this thesis are that bio-optical measurements have strong potential to trace environmental variability in the Arctic Ocean, and those can therefore provide insights on the Arctic hydrological and biogeochemical cycles. These parameters can be monitored by bio-optical sensors (e.g., radiometers, transmissometers, fluorometers, etc.). Such sensors can be further coupled to autonomous platforms such as satellites, gliders, automated underwater vehicles (AUVs) and ice-tethered profilers (ITPs), and significantly increase the amount of biogeochemical data in the Arctic Ocean, filling the gap left by classical sampling methods (i.e., oceanographic expeditions) and ocean color remote sensing, restricted to spring and summer seasons.

Zusammenfassung

Der Arktische Ozean spielt eine wichtige Rolle für die globalen hydrologischen und Kohlenstoffkreisläufe. Er trägt mit 5–14% zur globalen Bilanz der CO₂-Quellen und Senken bei. Kohlenstoff wird auch im Arktischen Ozean durch die Primärerzeuger mit einer hohen Primärproduktion, die insbesondere in den Randeiszonen, den eisfreien Zonen und den Schmelztümpeln beobachtet wird, effizient in die tiefen Schichten des Ozeans transportiert. Obwohl es sich um das kleinste Ozeanbecken weltweit handelt, umfasst der Zufluss in den Arktischen Ozean ca. 11% des globalen Flusseintrags in die Meere. Zusammen mit dem Süßwasser werden im arktischen Ozean große Mengen an organischem Kohlenstoff eingetragen. Der größte Anteil gehört dabei zur Fraktion des gelösten organischen Kohlenstoffes (DOM). Die mit dem anhaltenden Klimawandel einhergehenden Prozesse, wie das Schmelzen der Gletscher oder Tauen des Permafrosts, gelten als wesentliche Faktoren für einen erhöhten Süßwassereintrag in das arktische Becken. Daneben führte das Tauen des Permafrosts in Verbindung mit einer erhöhten Küstenerosion zu einer Zunahme der Mobilisierung von im Permafrost gespeicherten Kohlenstoff, was wiederum kritische Auswirkungen auf mikrobielle Prozesse, Primärproduktion, terrestrische Kohlenstoffströme in die Schelfmeere und somit auf den Kohlenstoffkreislauf in der Arktis haben könnte.

Diese Arbeit konzentriert sich auf die Analyse (oder Untersuchung) der Vermischung von DOM entlang der sibirischen Schelfmeere und die Entwicklung potenzieller Anwendungen von DOM als Umwelt-Tracer. Vier Ziele wurden hierbei verfolgt: (1) die Quantifizierung, Charakterisierung und Beurteilung der Verteilung und Veränderung von DOM im Übergangsbereich von den Flüssen in die Schelfmeere und ein Einblick in die Bedeutung von fluvialen DOM in der Arktis; (2) die Bewertung des Potenzials von DOM insbesondere seiner fluoreszierenden Fraktion (FDOM) als Tracer von Süßwasser in den Oberflächenschichten des Arktischen Ozeans; (3) die Charakterisierung der Absorption von Wasserinhaltsstoffen in den oberflächennahen Schichten der zentralen und östlichen Arktis und darüber hinaus eine Analyse, ob die abgeleiteten biooptischen Eigenschaften wie Absorption und Streuung die hydrographische Variabilität reproduzieren können; (4) die Bewertung der Leistungsfähigkeit von Ocean-Colour-Algorithmen, die häufig für Studien im Arktischen Ozean verwendet werden, wobei hierzu Daten von einer Polarstern-Expedition in 2011 aus der zentralen sibirischen Arktis verwendet wurden.

In der ersten Studie wurden die fluoreszierenden Komponenten des DOM, die mit dem PARAFAC-Modell isoliert wurden, erstmals entlang des Flusses zum Meeresübergang in der Laptev-See und dem Lena-Delta-Gebiet charakterisiert. Die Ergebnisse zeigten eine starke Dominanz der DOM-

Fluoreszenz im Bereich des sichtbaren Lichts (VIS-FDOM), die mit dem terrestrischen Signal (oder Humin-Anteilen) assoziiert ist. Die Ergebnisse bestätigen frühere Untersuchungen, die eine starke Abnahme von DOM bei geringem Salzgehalt zeigen. Jedoch zeigten unsere Ergebnisse, dass die Abnahme bevorzugt für VIS-FDOM erfolgt, wohingegen die Fluoreszenz im Bereich ultravioletter Wellenlängen (UV-FDOM, assoziiert mit der autochthonen marinen Produktion) im Bereich der Flussmündungen eher zu nimmt. Die DOM-Abnahme erfolgte primär in der oberflächennahen Schicht unter direktem Einfluß des Lena-Abflusses (Salzgehalt <10), was darauf hinweist, dass diese Abnahme hauptsächlich durch fotochemischen Abbau und Ausfällung bedingt war.

Die zweite Studie untersuchte das Potenzial von VIS-FDOM-Komponenten, die mit der PARAFAC-Analyse als Umwelt-Tracer in den Fram- und Davis-Straßen isoliert wurden. VIS-FDOM korrelierte stark mit den Fraktionen von meteorischem Wasser (f_{mw}) in polaren Gewässern. Außerdem erlaubten die Messungen weiter den Ursprung der polaren Wassermassen, die die Framstraße verlassen, entweder aus dem eurasischen oder aus dem kanadischen Becken abzuleiten. In den Bodenwässern der Davis Straße wurde VIS-FDOM mit der offensichtlichen Sauerstoffnutzung (AOU) korreliert, was dem Umsatz von DOM im Tiefenwasser und der Produktion von VIS-FDOM-Fluoreszenz folgte. Die Ergebnisse dieser Studie zeigen, welche Wellenlängen Informationen über Quellen und die Vermischung von DOM haben, welche daher angewendet werden können, um Süßwasser- und Kohlenstoff-Export in dem Nordatlantik zu bestimmen.

Die dritte Studie zeigt, dass farbiges DOM (CDOM) die Absorption der Wasserinhaltsstoffe in den oberen Bereichen der Wassermassen der zentralen und östlichen Arktis dominiert. Die räumliche Variabilität, die in den Wasserinhaltsstoffen (Phytoplankton, CDOM und Nicht-Algen-Partikel–NAP) beobachtet wurde, ermöglichte eine Eingruppierung der Probenahmestellen in Übereinstimmung mit der hydrographischen Variabilität. Diese Variabilität wurde auch durch die Analyse der mit hyperspektralen Satelliten gemessenen Reflektanz (R_{rs}) nachgewiesen. Die empirischen und semianalytischen Ocean Color – Algorithmen, die häufig in Studien im Arktischen Ozean angewendet wurden, wurden auf in-situ gemessene Reflektanzen (R_{rs}) angewendet, und dabei ihre Leistungsfähigkeit bewertet. Die aus den Algorithmen bestimmten Daten (Chlorophyll-*a*, und die Absorptionskoeffizienten von CDOM und Phytoplankton) wurden dann mit den entsprechenden in-situ-Messungen validiert. Die Ergebnisse zeigen, dass empirische Algorithmen keine verlässliche Ergebnisse erzielen, wohin gegen die semianalytischen Algorithmen im Arktischen Ozean zuverlässig angewendet werden können, jedoch immer noch deutliche Abweichungen im Vergleich zu den in-situ-Daten aufweisen.

Die wichtigsten Ergebnisse dieser Arbeit zeigen, dass bio-optische Messungen ein starkes Potenzial haben, um die Umweltvariabilität im Arktischen Ozean zu verfolgen. Sie können daher Einblicke in die hydrologischen und biogeochemischen Kreisläufe der Arktis geben. Diese Parameter können durch bio-optische Sensoren (z. B. Radiometer, Transmissometer, Fluorometer usw.) langfristig gemessen werden. Solche Sensoren können darüber hinaus an autonomen Plattformen wie Satelliten, Segelflugzeuge, automatisierte Unterwasserfahrzeuge (AUVs) und am Eis befestigt profilierend (sog. Ice-tethered profilers, ITPs) implementiert werden. Dadurch können sie dazu beitragen, die Menge an biogeochemischen Daten im Arktischen Ozean erheblich zu steigern, um so die Lücke zu schließen, die durch die Methoden der klassischen Probenahme und Verwendung von Ocean-Colour-Fernerkundungsdaten und ihre technisch bedingte Limitierung auf das Sommerhalbjahr offen bleibt.

List of Abbreviations

a_{350}	Absorption coefficient of CDOM at 350 nm
a_{375}	Absorption coefficient of CDOM at 375 nm
a_{440}	Absorption coefficient of CDOM at 440 nm
AB	Amundsen Basin
a_{CDOM}	Absorption coefficient of CDOM
a_{dg}	Absorption coefficient of CDOM and NAP
a_{λ}	Absorbance at specific wavelength
a_{NAP}	Absorption coefficient of NAP
AOU	Apparent Oxygen Usage
a_{ph}	Absorption coefficient of phytoplankton
AQY	Apparent Fluorescence Quantum Yield
ASW	Arctic Surface Water
a_{tw}	Total non-water absorption coefficient
AUV	Automated Underwater Vehicle
AW	Atlantic Water
BBDW	Baffin Bay Deep Water
BG	Beaufort Gyre
BIC	Baffin Island Current
BIX	Biological/autochthonous index
BPLR	Boreal Polar Province
BSBW	Barents Sea Branch Water
c	Cophenetic correlation coefficient
C1	Fluorescent component 1
C2	Fluorescent component 2
C3	Fluorescent component 3
C4	Fluorescent component 4
C5	Fluorescent component 5
C6	Fluorescent component 6
CAA	Canadian Arctic Archipelago
CAPES	Coordination for the Improvement of Higher Level Personnel
CB	Canada Basin

CDOM	Colored dissolved organic matter
Chl- <i>a</i>	Chlorophyll- <i>a</i>
CPW	Canadian Polar Water
CTD	Conductivity-Temperature-Depth
cUHW	Canadian Upper Halocline Water
DAAD	German Academic Exchange Service
DFF	Danish Research Council for Independent Research
DFG	German Science Foundation
DOC	Dissolved Organic Carbon
DOM	Dissolved Organic Matter
DSR	Deep-sea reference
<i>E</i>	Stability parameter
EB	Eurasian Basin
EEM	Excitation-Emission-Matrix
EGC	East Greenland Current
EGS	East Greenland shelf
EPW	Eurasian Polar Water
eUHW	Eurasian Upper Halocline Water
f_{aw}	Fraction of Atlantic Water
FDOM	Fluorescent dissolved organic matter
FI	Fluorescence Index
F_{max}	Maximum fluorescence
f_{mw}	Fraction of meteoric water
f_{pw}	Fraction of Pacific Water
f_{sim}	Fraction of sea-ice melt
FT-ICR MS	Fourier transform ion cyclotron resonance mass spectrometry
FYI	First year ice
GIOP	Generalized Inherent Optical Property model
GSM	Garver-Siegel-Maritorena
HIX	Humification index
HPLC	High-performance liquid chromatography
IOP	Inherent Optical Property
ITP	Ice-tethered profiler

<i>L</i>	Cuvette path length
IAIW	Lower Arctic Intermediate Water
LHW	Lower Halocline Water
LS	Laptev Sea
LSS	Laptev Sea Shelf
LSSW	Laptev Sea Shelf Water
MB	Markarov Basin
MBR	Maximum band ratio
MODIS	Moderate Resolution Imaging Spectroradiometer
MW	Meteoric Water
NAP	Non-algal particles
NB	Nansen Basin
NMR	Nuclear magnetic resonance
NSDW	Norwegian Sea Deep Water
OD	Optical density
ODV	Ocean Data View
PARAFAC	Parallel Factor Analysis
PML	Polar Mixed Layer
POC	Particulate organic carbon
RMSE	Root mean square error
ROV	Remotely Operated Vehicle
R_{rs}	Remote sensing reflectance
RV	Research Vessel
<i>S</i>	Spectral slope of absorption spectra
SAA	Semi-analytical algorithm
S_{CDOM}	Spectral slope of CDOM absorption spectra
SeaWiFS	Sea-Viewing Wide Field-of-View Sensor
SIM	Sea-ice melt
SMOW	Standard mean ocean water
SPE	Solid phase extraction
S_R	Slope ratio
S_{ratio}	Slope ratio
SUVA	Specific UV absorbance

TPD	Transpolar Drift
TrW	Transitional Water
uAIW	Upper Arctic Intermediate Water
UHW	Upper Halocline Water
UMLD	Upper mixed layer depth
UV	Ultra-violet wavelength range
UV-FDOM	Ultra-violet wavelength DOM fluorescence
VIS	Visible wavelength range
VIS-FDOM	Visible wavelength DOM fluorescence
WGC	West Greenland Current
WGIW	West Greenland Irminger Water
WGSC	West Greenland Slope Current
WGSW	West Greenland Shelf Water
WOCE	World Ocean Circulation Experiment

List of Publications

Peer-reviewed manuscripts composing the thesis:

1. **Gonçalves-Araujo, R.** (2016). Tools for assessing content, speciation and origin of DOM in aquatic systems. *YOUMARES 7 Proceedings*, 32–42.
2. **Gonçalves-Araujo, R.**; Stedmon, C.A.; Heim, B.; Dubinenkov, I.; Kraberg, A.; Moiseev, D.; Bracher, A. (2015). From fresh to marine waters: characterization and fate of dissolved organic matter in the Lena River Delta region, Siberia. *Frontiers in Marine Science*, 2:108, 1–13, doi: 10.3389/fmars.2015.00108.
3. **Gonçalves-Araujo, R.**; Granskog, M.A.; Bracher, A.; Azetsu-Scott, K.; Dodd, P.A.; Stedmon, C.A. (2016). Using fluorescent dissolved organic matter to trace and distinguish the origin of Arctic surface waters. *Scientific Reports*, 6: 33978, doi: 10.1038/srep33978.
4. **Gonçalves-Araujo, R.**; Rabe, B.; Peeken, I.; Bracher, A. (*submitted*). High colored dissolved organic matter (CDOM) absorption by waters of central-eastern Arctic Ocean: implications for biogeochemistry and ocean color algorithms.

Peer-reviewed manuscripts not included in the thesis:

- a. **Gonçalves-Araujo, R.**; de Souza, M.S.; Tavano, V.M., Garcia, C.A.E. (2015). Influence of oceanographic features on spatial and interannual variability of phytoplankton in the Bransfield Strait, Antarctica. *Journal of Marine Systems*, 142, 1–15, doi: 10.1016/j.jmarsys.2014.09.007.
- b. **Gonçalves-Araujo, R.**; de Souza, M.S.; Mendes, C.R.B.; Tavano, V.M.; Garcia, C.A.E. (2016), Seasonal change of phytoplankton (spring vs. summer) in the southern Patagonian shelf. *Continental Shelf Research*, 124, 142–152, doi: 10.1016/j.csr.2016.03.023.
- c. Machado, A.A.S.; **Gonçalves-Araujo, R.**; Teixeira, P.F.; Tavano, V.M.; Bianchini, A. (2014), Effects of zinc on *in vivo* fluorescence, chlorophyll a and growth of the diatom *Conticribra weissflogii* (Thalassiosirales, Thalassiosiraceae). *Pan-American Journal of Aquatic Sciences*, 9(4), 278–287.
- d. Ramírez-Pérez, M.; **Gonçalves-Araujo, R.**; Wiegmann, S.; Torrecilla, E.; Bardají, R.; Röttgers, R.; Bracher, A.; Piera, J. (2017). Towards cost-effective operational monitoring systems for complex waters: analyzing small-scale coastal processes with optical transmissometry. *PLoS ONE*, 12(1): e0170706, doi: 10.1371/journal.pone.0170706.
- e. Heim, B.; Abramova, E.; Bracher, A.; Doerffer, R.; **Gonçalves-Araujo, R.**; Hellman, S.; Juhls, B.; Kraberg, A.; Martynov, F.; Overduin, P.; Wegner, C. Book chapter: Ocean Colour Remote Sensing in the Shallow Laptev Sea and Eastern Siberian Shelf Seas. (Eds.: Vittorio Barale and Martin Gade) (*Submitted to the EARSeL – European Association of Remote Sensing Laboratories*).
- f. **Gonçalves-Araujo, R.**; de Souza, M.S.; Mendes, C.R.B.; Souza, R.B.; Tavano, V.M.; Schultz, C.; Pollery, R.C. (*accepted*). Response of winter phytoplankton assemblages to hydrographic variability in the southern Brazilian shelf. *Journal of Marine Systems*.

List of Figures

Figure 1.1. The global carbon cycle. The diagram shows the storage and annual exchange of carbon between the atmosphere, hydrosphere and geosphere in gigatons of Carbon (GtC). Credit: NASA Earth Observatory....**20**

Figure 1.2. Schematic diagram of the total DOM-pool with respect to the chromophoric (CDOM) and fluorescent (FDOM) fractions. Examples of CDOM absorption spectra and excitation-emission matrices are shown over the CDOM and FDOM domains, respectively. Structure of tryptophan, a natural amino acid, and vanillin, a constituent of lignin, are shown as examples of fluorescent CDOM. The grey lines indicate the position of their respective fluorescence excitation-emission peaks. Taken from *Stedmon and Álvarez-Salgado [2011]*..... **23**

Figure 1.3. The brownish waters of the Lena River Plume. Surface waters in the southern Laptev Sea during the Lena Expedition (September 2013). The brownish color of the water denotes the strong influence of the Lena River waters, with high loads of terrestrial organic matter (*Photo: Rafael Gonçalves-Araujo*)..... **24**

Figure 2.1. The Arctic seas and surface circulation. Arrows represent the main surface circulation patterns in the Arctic Ocean [*Rudels, 2009*] colored as follows: major rivers (light green); riverine runoff (dark green) inflowing currents (red); out flowing currents (blue). Produced with Ocean Data View [*Schlitzer, 2015*]..... **29**

Figure 2.2. Hydrography of the Arctic Ocean. Schematic vertical distribution of the major water masses in the Arctic Ocean based on a hypothetical transect from 175°W to 5°E (black line in the map) [adapted from *Aagaard and Carmack, 1989*] (top). Typical vertical distribution of potential temperature (°C) and salinity for Nansen Basin (NB), Amundsen Basin (AB), Markarov Basin (MB) and Canada (CB). PML indicates Polar Mixed Layer [*Rudels, 2009*] (bottom)..... **30**

Figure 2.3. Strategies in the chemical analyses of DOM with respect to the pre-processing of samples [adapted from *Dubinenkov, 2015*]..... **36**

Figure 2.4. Strategies in the chemical analyses of DOM regarding the methods of analysis [adapted from *Dubinenkov, 2015*]..... **36**

Figure 3.1. A) View of the Northern Hemisphere with the coverage of the sampled area in the black box, which is zoomed in highlighting the Lena delta region and southern Laptev Sea, as well as oceanographic stations and transects occupied during the Lena Expedition 2013. B) Surface distribution of salinity (colorbar) and a_{350} (m^{-1} ; solid black lines). C) T-S- a_{350} diagram for all the stations, with the plume-influenced and marine-influenced stations displayed in blue and red, respectively. Marine-influenced stations (surface salinity >10) are displayed in red in (A) and in the transects. Produced with Ocean Data View [*Schlitzer, 2015*]..... **51**

Figure 3.2. A) DOC (μM) against salinity and depth for all the samples related to this study (m; colorbar). B) a_{350} (m^{-1}) against salinity and DOC for the entire dataset used in this study (μM ; colorbar), which was split into two subsets regard to the hydrographical conditions: the plume-influenced stations (C) and the marine-influenced stations (D) that are plotted against salinity and DOC (μM ; colorbar). In all the plots, samples above the pycnocline are displayed as circles, samples at the pycnocline as squares, and samples below the pycnocline are displayed as triangles. Gray dashed-lines indicate the hypothetical conservative mixing line between DOM (or DOC) and salinity. Inset graph in (A) shows the relationship between a_{350} (m^{-1}) and DOC (μM) and the dashed line shows the fit exhibited for the coastal Canadian Arctic [Walker et al., 2009]. Inset graph in (B) exhibits vertical distribution of salinity (red dots) and a_{350} (m^{-1} ; blue line) for one typical plume-influenced station..... **53**

Figure 3.3. a_{350} against salinity plot with for the Plume-influenced (A) and Marine-influenced (B) stations. Samples above the pycnocline are displayed in blue whereas the ones below it are presented in red. Samples located in the pycnocline are displayed in black. All the fits presented in this figure are significant ($p < 0.0001$). Gray dashed-lines indicate the hypothetical conservative mixing line between DOM and salinity for each of the plots..... **54**

Figure 3.4. Three-dimensional fluorescence landscapes (left), the excitation (solid line) and emission (dashed line) spectra (center) and F_{max} (nm^{-1}) against salinity and depth (m) (right) for each of the six fluorescent components identified by PARAFAC model for all the samples. Gray lines displayed in components spectra graphs (center) show the spectra for components previously found in the major Arctic Rivers [Walker et al., 2013]. Gray dashed-lines in F_{max} against salinity plots (right) indicate the hypothetical conservative mixing line between each of the components and salinity. Red diamonds in y-axis indicate averaged F_{max} values for similar components found in the Lena River during periods of peak discharge (for C1 and C2) and mid flow (for C5 and C6) [Walker et al., 2013]..... **55**

Figure 3.5. The relationship between the optical indices of DOM modification and salinity for all the samples: S_{CDOM} (μm^{-1}) (A); SUVA ($\text{m}^2 \text{g}^{-1}$) (B); HIX (C); BIX (D); S_{Ratio} (E). Colorbar indicates the relative contribution (%) of the humic-like signal (C1+C2+C4+C5) to the total FDOM (A-D) and depth (m; E). Black lines indicate the regression lines between each parameter and salinity..... **57**

Figure 3.6. Schematic diagram showing the complex interactions occurring in the Laptev Sea continental shelf, close to the Lena River delta region. The vertical distribution of the two water masses found within the region (Lena River plume and Laptev Sea Shelf waters) is presented. A strong gradient between the two water masses with limited exchanges between them is depicted. Salinity, DOM concentration and the humic-like contribution are shown in the colorbar. The main removal processes within the surface layer (photodegradation and flocculation) are demonstrated by the symbols presented in the inset legend. Inset graphs show the DOM (a_{350} ; m^{-1}) against salinity plots for the Lena plume (A) and Laptev Sea shelf Waters (B)..... **62**

Figure 4.1. Study area and water masses. (a) Map of the study area and sampling stations in 2012 and 2013. (b) T-S diagram for all the oceanographic stations (except Davis2013) considered for this study with the identified water masses [Swift and Aagaard, 1981; Pavlov et al., 2015] (Table S1): Atlantic Water, Polar Water, Arctic Surface Water (ASW), upper Arctic Intermediate Water (uAIW), lower Arctic Intermediate Water (lAIW) and Norwegian Sea Deep Water (NSDW). (c) T-S diagram showing the eastern Greenland cruises (gray) and Davis2013 (black) with the identified water masses for the latter region (adapted from Tang et al. [Tang et al., 2004], Azetsu-Scott et al. [Azetsu-Scott et al., 2012], Curry et al. [Curry et al., 2014]): West Greenland Shelf Water (WGSW), West Greenland Irminger Water (WGIW), Polar Water, Arctic Surface Water (ASW), Baffin Bay Deep Water (BBDW) and Transitional Water (TrW). Isopycnals [potential density (σ , kg m⁻³)] are indicated as gray lines in (b) and (c). Produced with Ocean Data View [Schlitzer, 2015]..... **70**

Figure 4.2. Vertical sections across the surface layer of Fram Strait in September 2012. (a) temperature (°C), (b) salinity, fractions of (c) meteoric water (f_{mw}), (d) sea-ice melt (f_{sim}), (e) Atlantic water (f_{aw}), and (f) Pacific water (f_{pw}), (g) C1 (R.U.) and (h) C2 (R.U.). In (b) black lines indicate the potential density (σ , kg m⁻³) and the abbreviations indicate the position of the water masses defined based on T-S diagrams (Figure 1). Produced with Ocean Data View [Schlitzer, 2015]..... **74**

Figure 4.3. Vertical sections across the surface layer of Fram Strait in September 2013. (a) temperature (°C), (b) salinity, fractions of (c) meteoric water (f_{mw}), (d) sea-ice melt (f_{sim}), (e) Atlantic water (f_{aw}) and (f) Pacific water (f_{pw}), (g) C1 (R.U.) and (h) C2 (R.U.). In (b) black lines indicate the potential density (σ , kg m⁻³) and the abbreviations indicate the position of the water masses defined based on T-S diagrams (Figure 1). Produced with Ocean Data View [Schlitzer, 2015]..... **75**

Figure 4.4. Vertical sections across Davis Strait in September 2013. (a) temperature (°C), (b) salinity, fractions of (c) meteoric water (f_{mw}), (d) sea-ice melt (f_{sim}), (e) Atlantic water (f_{aw}) and (f) Pacific water (f_{pw}), (g) C1 (R.U.), (h) C2 (R.U.) and (i) apparent oxygen utilization (AOU, $\mu\text{mol kg}^{-1}$). (j) AOU ($\mu\text{mol kg}^{-1}$) vs. C1 (R.U.) for samples under influence of TrW and BBDW (below 300 m). (k) C2 vs. C1 plots for all the samples collected in the Davis Strait 2013, with colorbar indicating depth (m). In (b) black lines indicate the potential density (σ , kg m⁻³) and the abbreviations indicate the position of the water masses defined based on T-S diagrams (Figure 1). Produced with Ocean Data View [Schlitzer, 2015]..... **76**

Figure 4.5. PARAFAC model and isolated components. (top) Three-dimensional fluorescence landscapes example of the measured, modeled and residual EEMs of the PARAFAC analysis. (bottom) The excitation (solid line) and emission (dashed line) spectra for the three fluorescent components identified by PARAFAC model for each of the cruises. Inset plots show the three-dimensional fluorescence landscapes for each of the final PARAFAC-derived component used in this work (with all cruises merged into one dataset)..... **77**

Figure 4.6. T-S diagram and correlations between salinity and C1 in the east of Greenland. (a) Temperature (°C) vs. salinity with colorbar indicating C1 (R.U.) for all the samples collected in the eastern Greenland cruises. (b-d) Salinity vs. C1 (R.U.) and f_{pw} as colorbar for polar waters and ASW for each of the eastern Greenland cruises. Black solid line (I) indicates the mixing curve for the polar waters (based on Fram 2012 and 2013 datasets). Gray dashed lines (II and III) indicate the two distinct mixing curves of polar waters over the Greenland shelf. The regressions were obtained by combining the three datasets. (I) $y = -0.02 * (\text{Sal}) + 0.723$, $r^2=0.90$, $p<0.0001$, $n=240$. (II) $y = 0.0042 * (\text{Sal}) - 0.0698$, $r^2=0.90$, $p<0.0001$, $n=126$. (III) $y = 0.0183 * (\text{Sal}) - 0.4816$, $r^2=0.98$, $p<0.0001$, $n=18$ **79**

Figure 4.7. VIS-FDOM as a water mass tracer in the Davis Strait. Plots for the Davis2013 cruise. (a) T-S diagram with longitude (°W) as colorbar.. (b) Salinity vs. C1 (R.U.), with colorbar indicating longitude (°W). (c) C1 (R.U.) vs. f_{pw} for the surface layer (<300 m) and f_{sim} as colorbar. (d) C2 (R.U.) vs. C1–C1* (R.U.) for the surface layer (<300 m), with longitude (°W) as colorbar. Triangles indicate the samples within the eastern part of Davis Strait, whereas circles refer to samples located in the western sector (separated by the 57.5 °W longitude). Black line in (c) indicates the best fit..... **80**

Figure 4.8. Schematic graphs for eastern Greenland. Schematic graphs showing the behavior during mixing of distinct waters defined in the text (Atlantic water, Eurasian and Canada basin polar waters, whose end members in this study are colored accordingly): for (a) C1 and salinity, (b) C1 and f_{mw} , (c) temperature and salinity, (d) f_{sim} and f_{mw} . All data used in this study is shown with gray dots. Lines indicate the mixing between different waters, whose end-members for this study are tabulated below. Arrows represent the approximate direction of the deviation expected by dilution with sea-ice melt and precipitation (including glacial melt). The table shows information (range and average) on some parameters for the end members of each water type identified in this study..... **84**

Figure S4.1. Water fractionation. (a) Phosphate (µM) vs. nitrate (µM) with the equations and source lines for the Atlantic and Pacific waters [Dodd et al., 2012]. (b) Salinity vs. $\delta^{18}\text{O}$ (‰) with the end members for Atlantic Water (AW), Meteoric Water (MW) and Sea-ice melt (SIM) and corresponding conservative mixing lines [Dodd et al., 2012]..... **86**

Figure S4.2. Vertical distribution of Chlorophyll-a and UV-FDOM for the EGC2012 cruise. Vertical distribution of (a) chlorophyll-a fluorescence (A.U.) and (b) C3 (R.U.) for the EGC2012 cruise, and (c) the correlation between chlorophyll-a fluorescence (A.U.) and C3 (R.U.)..... **87**

Figure S4.3. Scatter plots each of the cruises performed in the eastern Greenland, considering only PW and ASW (salinity<34.3). (top panel) C1 (R.U.) vs. $\delta^{18}\text{O}$ (‰) vs. f_{sim} . (middle panel) C1 (R.U.) vs. f_{mw} vs. f_{sim} . (bottom panel) C1 (R.U.) vs. f_{sim} vs. salinity..... **87**

Figure S4.4. Vertical distribution of UV-fluorescent C3 (R.U.) along the transects. (a) Fram2012, (b) Fram2013 and (c) Davis2013. Note the

differences in color bar ranges for the cruises. Produced with Ocean Data View [Schlitzer, 2015]..... 88

Figure 5.1. Study region and sea-ice conditions. AMRSR-2 sea-ice concentration (<http://meereisportal.de>) for August (a) and September (b) 2011. ODV maps [Schlitzer, 2015] showing the sampling stations occupied during the ARK-XXVI/3 (PS-78) cruise where CTD casts (c), water sampling and hyperspectral radiometric measurements (d) were performed. Arrows in (c) represent the main surface circulation patterns in the Arctic Ocean colored as follows: major rivers (green); inflowing currents (red); out flowing currents (blue) [Rudels, 2009]..... 94

Figure 5.2. Hydrography in the surface Central and Eastern Arctic Ocean. (a) T-S diagram with depth (m) as color bar. (b) Surface distribution of temperature (°C) and salinity (c) with the approximate occupation of the water masses with the PML within the study region. Produced with Ocean Data View [Schlitzer, 2015]..... 101

Figure 5.3. Absorption coefficients in the surface waters of Central and Eastern Arctic Ocean. (a) Surface distribution of $a_{\text{CDOM}}(443)$ (m^{-1}) and correlation between $a_{\text{CDOM}}(443)$ and $a_{\text{CDOM}}(350)$ (inset graph); produced with Ocean Data View [Schlitzer, 2015]. (b) Ternary plot denoting the contribution of the non-water absorbers (a_{CDOM} , a_{ph} , a_{NAP}) to total non-water absorption (a_{tw}) at surface; colorbar indicates salinity. (c) Station 207 (indicated by the arrow in a) as example of a_{CDOM} , a_{CDOM} , a_{ph} and a_{NAP} spectra (m^{-1}). Dashed line indicates the position of 443 nm. (d) Correlation between Chl-a (mg m^{-3}) and $a_{\text{ph}}(443)$ (m^{-1}); for the colors, please refer to Figure 5.4..... 103

Figure 5.4. Environmental clustering. (left) Dendrogram (cophenetic correlation coefficient: $c=0.91$) for sampling stations based on surface normalized values of an environmental matrix containing environmental and bio-optical parameters: temperature, salinity, $a_{\text{CDOM}}(443)$, $a_{\text{NAP}}(443)$ and $a_{\text{ph}}(443)$. (right) ODV map [Schlitzer, 2015] showing the position of each station according to the classification based on the hierarchical clustering. Inset graph shows the correlation between $a_{\text{CDOM}}(443)$ and salinity colored with respect to the clusters; black line indicates the best fit ($p<0.01$)..... 106

Figure 5.5. Hyperspectral clustering. (a) Dendrogram (cophenetic correlation coefficient: $c=0.87$) for sampling stations based on hierarchical cluster analysis applied to the 2nd derivative of $R_{\text{rs}}(\lambda)/R_{\text{rs}}(555)$ (following Torrecilla et al., 2011). (b) ODV map [Schlitzer, 2015] showing the position of each station according to the classification based on the hierarchical clustering. (c) 2nd derivative of normalized hyperspectral remote sensing reflectance, $R_{\text{rs}}(\lambda)/R_{\text{rs}}(555)$, with respect to the wavelength range of 435–510 nm (following Torrecilla et al., 2011). (d) Normalized hyperspectral remote sensing reflectance, $R_{\text{rs}}(\lambda)/R_{\text{rs}}(555)$ in the visible wavelength range. Colored circles in (a) refer to the environmental clusters presented in Figure 5.4. Colors in (c) and (d) are in accordance with the clusters presented in (a) and (b)..... 107

Figure 5.6. Evaluation of empirical ocean color algorithms frequently applied to the Arctic Ocean. (a) Chl-a estimated by empirical algorithms (mg m^{-3} ;

indicated by different colors) versus *in situ* Chl-*a* (mg m^{-3}). Stations belonging to the low a_{CDOM} cluster (Cluster 1) are presented as circles, whereas stars represent stations grouped in the high a_{CDOM} cluster (Cluster 2; Figure 5.5). (b) Chl-*a* estimated by empirical algorithms (mg m^{-3} ; indicated by different symbols) versus *in situ* Chl-*a* (mg m^{-3}), with $a_{\text{CDOM}}(443)$ (m^{-1}) as colorbar. (c) *In situ* Chl-*a* (mg m^{-3}) versus maximum band ratio [MBR; $R_{rs}(443>490>510/555)$]. (d) Chl-*a* estimated by empirical algorithms (mg m^{-3} ; indicated by different colors) versus $a_{\text{CDOM}}(443)$ (m^{-1}). Information on the fits displayed in (d) is given in Table 5.4..... **111**

Figure 5.7. Evaluation of the semi-analytical algorithms. Modeled geophysical parameters calculated used *in situ* R_{rs} versus *in situ* measured parameters: $a_{\text{ph}}(443)$ (a); Chl-*a* (b); $a_{\text{dg}}(443)$ (c) and $a_{\text{CDOM}}(443)$ (d). Red points refer to the GIOP [Werdell *et al.*, 2013a, 2013b] retrievals, whereas blue points to the retrievals from the GSM model adapted to the Arctic [Matsuoka *et al.*, 2013]..... **114**

List of Tables

- Table S4.1.** Water masses classification. Thermohaline ranges used to characterize the water masses in the Fram Strait and east Greenland [Swift and Aagaard, 1981; Pavlov et al., 2015]..... **86**
- Table 5.1.** Relative absorption of non-water absorbers. Averaged contribution of the absorption coefficients for each of the non-water absorbers to a_{tw} in this and other studies carried out in different regions..... **104**
- Table 5.2.** Environmental parameters for the geographic clusters based on the environmental matrix. Averaged values \pm standard deviation of environmental/bio-optical parameters and geographic region for each of the clusters presented in Figure 5.4. Geographic regions acronyms: BG (Beaufort Gyre); EB (Eurasian Basin–Amundsen and Nansen basins); LS (Laptev Sea); LSS (Laptev Sea Shelf–Lena river influenced); TPD (Transpolar Drift)..... **106**
- Table 5.3.** Environmental parameters for the geographic clusters based on hyperspectral measurements. Averaged values \pm standard deviation of geophysical parameters for each of the clusters presented in Figure 5.5.... **108**
- Table 5.4.** Evaluation of empirical ocean color algorithms. Regression statistics for retrieved Chl-*a* from *in situ* R_{rs} using the correspondent algorithms versus *in situ* measured parameters. r^2 and Slope were calculated using log-transformed data for each of the correspondent parameters..... **110**
- Table 5.5.** Evaluation of Chl-*a* retrievals from empirical ocean color algorithms, for low $a_{CDOM}(443)$ sites. Same as Table 5.4 but for the low $a_{CDOM}(443)$ stations..... **112**
- Table 5.6.** Evaluation of the semi-analytical ocean color algorithms. Regression statistics for modeled geophysical parameters calculated used *in situ* R_{rs} versus *in situ* measured parameters. r^2 and Slope were calculated using log-transformed data for each of the correspondent parameters..... **113**

Chapter 1

Introduction

1. Introduction

1.1. Motivation and objectives of the thesis

With the climate change pressure on the environment, the scientific community has sought a more comprehensive understanding on the carbon cycle, its reservoirs and the processes governing their dynamics. Aquatic systems play an important role for the carbon cycle, for instance, as provision of a large pool of carbon (stored as dissolved and particulate organic and inorganic carbon), important sink (by uptake of atmospheric CO_2 and carbon burial in the sediments) and turnover of organic carbon (by microbial activity) (Figure 1.1). As a consequence, increasing effort has been devoted to study aquatic environments and processes governing the distribution and behavior of both, organic and inorganic carbon. With more studies on the characterization of stocks, sources, reactivity and fate of both organic and inorganic carbon, a more comprehensive understanding of the carbon cycle would be reached, which is of great importance for improving forecasts of future climate scenarios.

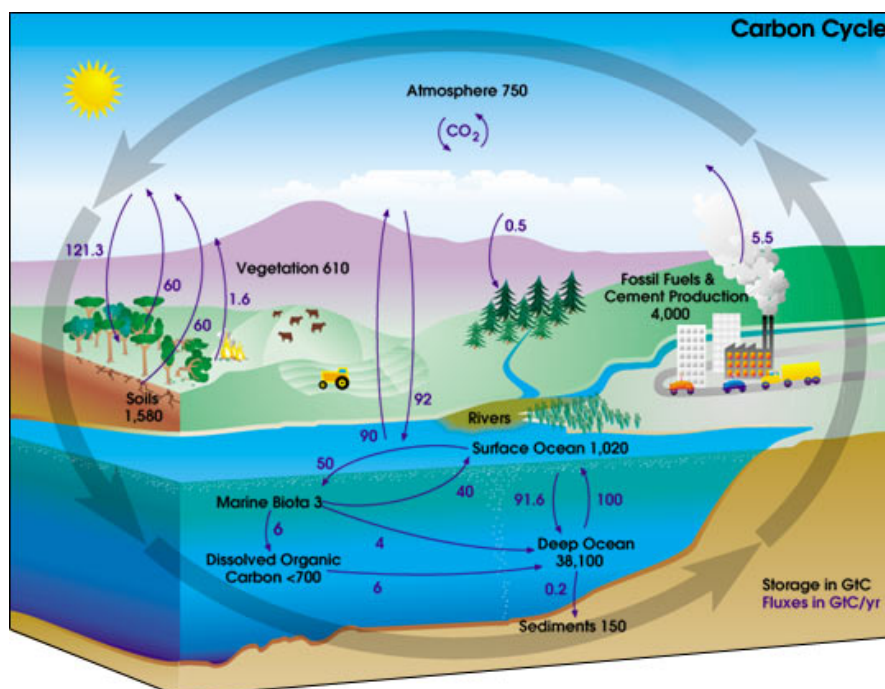


Figure 1.1. The global carbon cycle. The diagram shows the storage and annual exchange of carbon between the atmosphere, hydrosphere and geosphere in gigatons of Carbon (GtC). Credit: NASA Earth Observatory.

Non-living organic matter is present in aquatic systems as particles, colloids and dissolved molecules. The dissolved fraction of organic matter

(DOM) is operationally defined by filtration with specific pore size, with 0.45 μm being the most accepted limit [Steinberg, 2003]. The DOM fraction encompasses a wide range of compounds with variable molecular complexity, and consists of a large active organic carbon reservoir [Hedges, 1992]. The DOM-pool is most frequently composed by amino acids, carbohydrates, lipids, pigments, lignins, tannins and proteins, whose relative contribution varies in different environments, depending on its origin. For instance, the lignins, which are formed exclusively in the cell walls of vascular plants, contain large amounts of carbon in the form of aromatic carbons and phenols [Lebo *et al.*, 2000], and therefore is a good tracer of terrestrial DOM. Microbially derived amino acids and proteins, on the other hand, contain a lower aromatic and phenolic content in relation to terrestrial sourced DOM [Geider and La Roche, 2002]. These non-humic components of marine DOM are related to autochthonous production, primarily from microbial community, rather than to a terrestrial source [Coble, 2007].

The Arctic Ocean is of great importance for climate regulation and carbon sequestration, contributing 5–14% to the global balance of CO₂ sinks and sources [Bates and Mathis, 2009]. This uptake is highly influenced by physical and biological processes such as seasonal phytoplankton primary production, temperature effects (both cooling and warming), shelf-basin exchanges and formation of dense winter waters, and river inputs of freshwater and carbon. As the only pole-located ocean basin on Earth, the Arctic is also important for the global overturning circulation [Broecker, 1991]. The formation of the dense North Atlantic Deep Water is related to the advection of cold waters from the Arctic Basin and to the deep convection system in the Labrador Sea [Carmack and Aagaard, 1973; Clarke and Gascard, 1983]. Furthermore, the Arctic plays a significant role on human life and economy, given its importance for global fisheries [Chapin *et al.*, 2005] and shipping [Lasserre and Pelletier, 2011], with the possibility of opening the targeted North-West passage.

Phytoplankton can attain high biomass not only in open waters and marginal ice zones of the Arctic Ocean, but also in melt ponds and in the ice itself (as sea-ice algae), reaching high primary production rates [Arrigo *et al.*, 2012; Fernández-Méndez *et al.*, 2015]. Such primary production can sustain relatively high zooplankton biomass and production [Auel and Hagen, 2002; Olli *et al.*, 2007; Nöthig *et al.*, 2015], leading to increase in biogenic carbon export from the surface layer in those areas [Lalande *et al.*, 2014]. Besides, the Arctic Ocean receives ~11% of global river runoff and represents only ~1.3% of world's ocean by volume [Shiklomanov *et al.*, 2000], making it a globally important region for freshwater storage [Rabe *et al.*, 2014]. Together with the vast amount of freshwater, high loads of both dissolved and particulate matter are brought into the Arctic, through the estuaries, continental shelves and finally to the pelagic domain.

The Arctic Ocean receives ca. 18–26 Tg C year⁻¹ of dissolved- and 4–6 Tg C year⁻¹ of particulate organic carbon (DOC and POC, respectively) via riverine outflow. As a result the majority of organic carbon introduced in the Arctic Ocean is dissolved. Furthermore, the DOM in the Arctic Rivers and Ocean has a strong terrestrial character, being primarily dominated by compounds with visible wavelength (VIS) fluorescence [Walker *et al.*, 2013; Guéguen *et al.*, 2015], which are associated to lignin [Mann *et al.*, 2016]. Such a strong terrestrial characteristic can be easily detected in the absorption spectra of DOM and can be further used to trace the freshwater in the surface of the Arctic Ocean [Stedmon and Markager, 2001; Granskog *et al.*, 2012; Stedmon *et al.*, 2015]. Although advances have been made on determining the composition and spectral characterization of DOM and several studies have addressed this issue in the Arctic rivers and seas [Stedmon and Markager, 2001; Walker *et al.*, 2013; Jørgensen *et al.*, 2014; Guéguen *et al.*, 2015; Fichot *et al.*, 2016; Mann *et al.*, 2016], the fate of the terrestrial DOM in the Arctic Ocean is still under debate. While some studies point to a conservative mixing along the shelf [Dittmar and Kattner, 2003; Semiletov *et al.*, 2013], some studies have observed strong and rapid removal of DOM [Alling *et al.*, 2010; Letscher *et al.*, 2011].

A fraction of the total DOM-pool is colored (CDOM) and therefore absorbs light, primarily in the ultra-violet (UV) and VIS ranges; and a fraction of CDOM is further able to emit light through fluorescence (FDOM) (Figure 1.2). Given the interactions between CDOM molecules and light, especially in the VIS range, it imparts a yellowish–brownish color to the water (Figure 1.3), easily detectable by ocean color remote sensing. In short, the latter uses algorithms to convert reflectance from the sea surface into inherent optical properties (IOPs) of seawater. IOPs, e.g. absorption and scattering, are properties of the medium and do not depend on the ambient light field. Those properties can be further converted into biogeochemical parameters such as chlorophyll-*a* (Chl-*a*) and POC concentration, CDOM absorption coefficients, among others. Two kinds of algorithms are most commonly employed to perform those retrievals: empirical and semi-analytical [IOCCG, 2006]. The former uses simple remote sensing reflectance (R_{rs}) band ratios to derive absorption coefficients by empirical relationships. Semi-analytical ocean color algorithms, on the other hand, apply nonlinear statistical inversion methods to retrieve IOPs from R_{rs} . These algorithms account for fundamental relationships between IOPs of the non-water absorbers (e.g., phytoplankton, CDOM and non-algal particles), as well as for their spectral shapes, among other properties. From the IOPs, finally, the quantities (e.g. Chl-*a* concentration) of the optical constituents are derived.

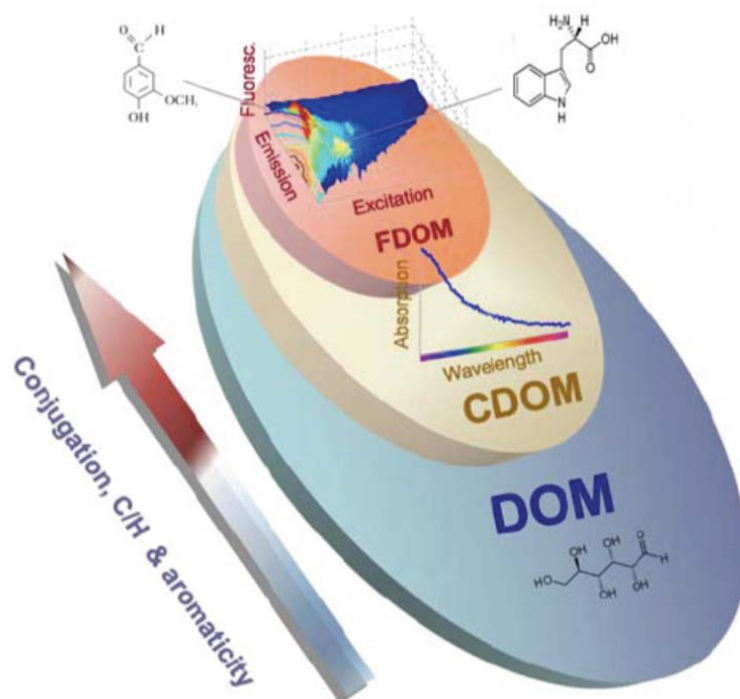


Figure 1.2. Schematic diagram of the total DOM-pool with respect to the chromophoric (CDOM) and fluorescent (FDOM) fractions. Examples of CDOM absorption spectra and excitation-emission matrices are shown over the CDOM and FDOM domains, respectively. Structure of tryptophan, a natural amino acid, and vanillin, a constituent of lignin, are shown as examples of fluorescent CDOM. The grey lines indicate the position of their respective fluorescence excitation-emission peaks. Taken from *Stedmon and Álvarez-Salgado* [2011].

Ocean color remote sensing has been frequently applied to monitor biogeochemical processes in the global oceans. In the Arctic Ocean, it has been primarily employed in studies concerning changes in Chl-*a* and primary production [*Pabi et al.*, 2008; *Arrigo and van Dijken*, 2011; *Cherkasheva*, 2014; *Cherkasheva et al.*, 2014; *Nöthig et al.*, 2015], and also for monitoring CDOM variability [*Matsuoka et al.*, 2013; *Heim et al.*, 2014]. A recent study using CDOM and salinity satellite data showed the applicability of those products for determining water masses end-members, especially with respect to river water [*Matsuoka et al.*, 2016]. Thus, with an improved spatial and temporal resolution one can provide more insights into the freshwater and carbon export from the Arctic Ocean.



Figure 1.3. The brownish waters of the Lena River Plume. Surface waters in the southern Laptev Sea during the Lena Expedition (September 2013). The brownish color of the water denotes the strong influence of the Lena River waters, with high loads of terrestrial organic matter (*Photo: Rafael Gonçalves-Araujo*).

Although ocean color remote sensing is a powerful tool for synoptically monitoring the Arctic Ocean, the global empirical algorithms perform poor at estimating Chl-*a* in the western Arctic [*Cota et al.*, 2004; *Matsuoka et al.*, 2007; *Ben Mustapha et al.*, 2012]. Regional tuned algorithms showed improved performance related to global algorithms in that region [*Cota et al.*, 2004; *Ben Mustapha et al.*, 2012]. The semi-analytical algorithms, on the other hand, provide better retrievals of Chl-*a*, as well as reliable estimates of CDOM and phytoplankton absorption [*Matsuoka et al.*, 2013, 2014; *Chaves et al.*, 2015]. However, those studies are constrained to the western Arctic Ocean [*JOCCG*, 2015], while such studies are limited in the eastern and central Arctic, mainly due to logistic challenges to reach especially the Siberian shelves.

Whilst providing high-resolution spatial and temporal biogeochemical data, ocean color remote sensing in the Arctic is very limited due to the sea-ice and cloud coverage, and winter polar night. In this sense, alternative autonomous platforms, such as ice-tethered profilers (ITPs), automated underwater vehicles (AUVs), gliders, Argo floats, etc. would not only increase the amount of data available, but also provide more information about the biogeochemical conditions under sea-ice and also during the polar night, with no ocean color remote sensing data available.

Considering the abovementioned facts and the current gaps and uncertainties related to dissolved organic matter in the Arctic Ocean, this work primarily aims to complement and extend the existing knowledge on the field through four main objectives:

1. to quantify, characterize and assess the distribution and transformation of dissolved organic matter in the river-ocean transition and, thus, provide insights into the fate of Arctic riverine DOM;
2. to assess the potential of DOM, especially FDOM, as a tracer of freshwater in the surface layers in the Arctic Ocean;
3. to characterize the non-water absorption in the surface central and eastern Arctic Ocean and further test whether bio-optical properties (such as absorption and reflectance) can reproduce hydrographical variability;
4. to evaluate the performance of ocean color algorithms frequently applied for studies in the Arctic Ocean using novel data from a central-eastern Arctic cruise.

1.2. Thesis outline and author's contribution

Chapter 2 is sub-divided into two sections. In the first section the Arctic Ocean and its main aspects such as circulation, biogeochemistry and climate change effects are introduced. In the second section a mini review published in the proceedings of the *YOUMARES 7 Conference* [Gonçalves-Araujo, 2016] briefly presents the state-of-art regarding analysis of DOM as well as its applications as an environmental tracer.

Chapter 3 presents results from the expedition conducted in the Lena Delta region (southern Laptev Sea) in September 2013 published in *Frontiers in Marine Science* [Gonçalves-Araujo et al., 2015b]. In this study, DOM was quantified and characterized based on its optical properties (e.g., absorption and fluorescence) and its behavior along the river-sea transition was examined. For this study, the thesis' author collected and analyzed the samples and data, and wrote the manuscript.

Chapter 4 consists of a study published in *Scientific Reports* with existing samples from expeditions in the Fram and Davis Straits in late summer 2012/2013 [Gonçalves-Araujo et al., 2016]. This study investigates the potential of using the spectral properties of visible wavelength range fluorescence of DOM (VIS-FDOM) to trace and distinguish the origin of Arctic surface waters, with focus on the freshwater export. Additionally, it addresses the use of VIS-FDOM as a biogeochemical tracer in the Davis Strait. The author of the thesis performed the data analyses and synthesis of results, and prepared the manuscript.

Chapter 5 investigates the spatial variability in light absorption in the surface waters of the central and eastern Arctic Ocean based on existing data from an expedition carried out in August–October 2011. In this study non-water absorbers were partitioned and further related to hydrographical conditions, to evaluate whether bio-optical properties can reproduce

hydrographical variability. Moreover, ocean color remote sensing algorithms frequently applied in the global and Arctic Oceans were evaluated for their performance in the central and eastern Arctic. This chapter consists of a manuscript written by the author of the thesis, which is in preparation for submission. The author performed the analyses of samples and data; performed the calculations and compilation of results and elaborated the manuscript.

Chapter 6 presents a summary of the main findings of the thesis along with the outlook for future research.

In Chapter 7 the literature cited in this thesis is provided. And, finally, in Chapter 8 the reprints of published manuscripts incorporated to this thesis are presented.

Chapter 2

Scientific background

2. Scientific Background

2.1. The Arctic Ocean

The Arctic Ocean, located above the Arctic Circle (66° 34' N), is the smallest ($\sim 14 \times 10^6$ km²) and shallowest (average of 1038 m and maximum of 5450 m) ocean basin on Earth. It is surrounded by land and has limited exchanges with its adjacent basins, the Atlantic and Pacific. The Arctic Basin is connected to the Pacific Ocean by the Bering Strait, and to the Atlantic Basin by the Fram Strait and Canadian Archipelago. Furthermore, the Arctic seas, especially in the eastern sector, exhibit shallow and wide continental shelves (reaching up to 800 km of extension), with an average depth of 100 m, which cover approximately 50% of total Arctic Ocean's extent. The central Arctic basin is divided into two main deep basins, the Eurasian and the Amerasian Basins (Figures 2.1 and 2.2). Those basins are separated by the Lomonosov Ridge, rising up to 3700 m above the sea floor. The Amerasian is the most shallow of the two basins and the Alpha Ridge divides it into two basins, the Canada and the Markarov Basins. The Eurasian basin can be further divided by another but smaller ridge, the Nansen Gakkel Ridge, into two other basins, the Amundsen and the Nansen Basins. Finally, the Arctic Ocean can be further divided into six major marginal seas: Barents Sea, Kara Sea, Laptev Sea, East Siberian Sea, Chuckchi Sea, and Beaufort Sea.

As mentioned above, the Arctic Basin has limited exchanges with its adjacent basins, the Pacific and the Atlantic. Those two basins are the main responsible for the inflow of warm waters from sub-polar regions into the Arctic. The waters advected from the North Pacific enter the Arctic Ocean through the shallow (45 m) and narrow (50 km) Bering Strait and the majority of this relatively low inflow becomes trapped in the Beaufort Gyre [Rudels, 2009]. The major inflow of warm waters occurs through the Fram Strait with the advection of waters from the North Atlantic. When entering the Arctic Ocean, warm Atlantic waters encounter sea-ice and melt it. With that, while transforming the Atlantic waters, a less dense mixed surface layer, the Polar Mixed Layer (PML), is generated. The modified Atlantic Waters occupy the layers immediately below the PML, forming the Atlantic Halocline Waters with the Atlantic Water Layer underneath [Schauer *et al.*, 2002; Rudels, 2009, 2012] (Figure 2.2.). The PML is also affected by heat fluxes with the atmosphere and by the great volume of low salinity waters from river runoff, resulting in near freezing temperatures and relatively low salinity, intrinsic to the waters occupying that layer [Rudels, 2009]. The huge amount of freshwater introduced in the Arctic Ocean by the riverine outflow stays in the PML and is transported (and also modified) along the central Arctic Basin, where low salinity values are observed in the surface waters within the halocline waters [Rudels, 2009, 2012]. Furthermore, during summer a

pycnocline is observed in the PML in the shelf seas, mainly due to the riverine discharge. During winter, with the remarkable reduction in the freshwater export from the Arctic rivers, such stratification is absent and a well-mixed surface layer is observed. The Atlantic and Pacific modified waters incoming the Arctic Ocean are mixed with the low salinity shelf waters and are further transported throughout the central Arctic Ocean by the Transpolar Drift. However, due to variability in the atmospheric forcing over the Arctic Ocean, changes in the character of surface waters transported within the Transpolar Drift due to strong and weak states of the Beaufort Gyre may be observed [Mauritzen, 2012]. In the western Arctic Ocean, the Beaufort Gyre is the dominant feature in the surface circulation. It consists of an anticyclonic current system, which encompasses the largest freshwater storage area in the Arctic Ocean [Proshutinsky et al., 2002, 2009a, 2009b], presenting the lowest salinity, in comparison to the Eurasian Basin (Figure 2.2). Most of the water occupying the surface layers of the Arctic Ocean are exported to the Atlantic Basin via the Fram Strait and Canadian Archipelago, with the major export observed in the Fram Strait, with a freshwater export of up to $3160 \text{ km}^3 \text{ yr}^{-1}$ [Rabe et al., 2009, 2013].

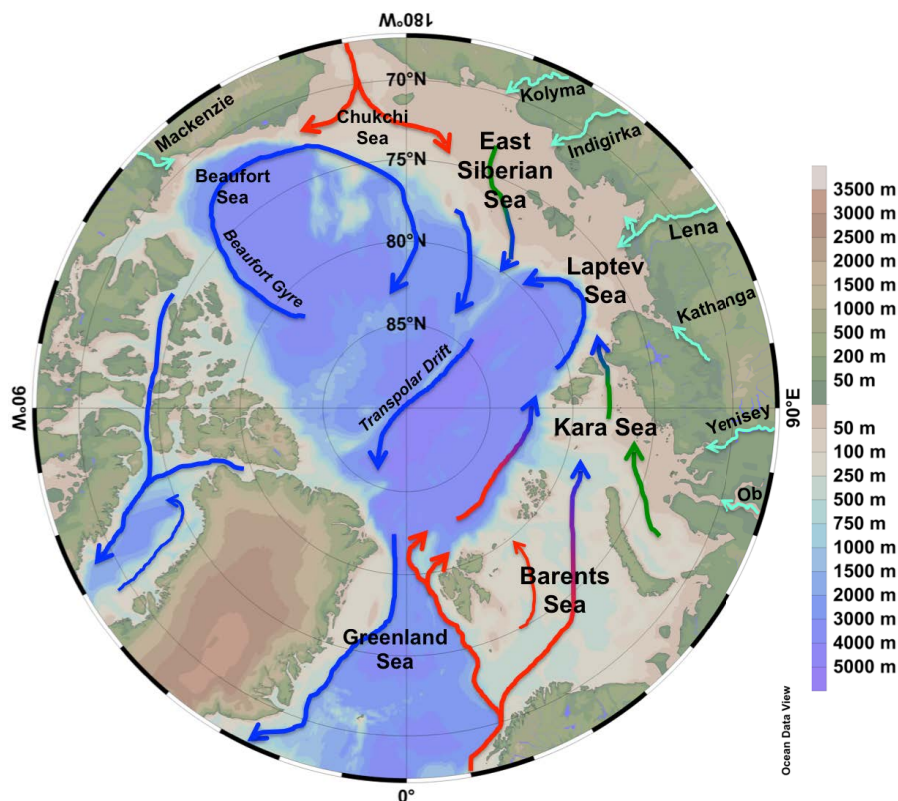


Figure 2.1. The Arctic seas and surface circulation. Arrows represent the main surface circulation patterns in the Arctic Ocean [Rudels, 2009] colored as follows: major rivers (light green); riverine runoff (dark green) inflowing currents (red); out flowing currents (blue). Produced with Ocean Data View [Schlitzer, 2015].

Sea-ice reaches its maximum extent in March reaching up to 19.0 million km² on average [IOCCG, 2015] almost permanently covering the central Arctic Ocean (north of 78 °N). Its minimum is reached in September, when an average of 6.4 million km² is observed covering only part of the Arctic. Sea-ice formation at the surface during winter (first year ice – FYI) leads to brine formation (high salinity, with temperature just above freezing point). The release and sinking of dense brines from sea-ice contribute to the halocline layer [Aagaard *et al.*, 1985; Rudels, 2009]. In summer, sea-ice melt freshens the surface layer and a stratified surface mixed layer is established [Korhonen *et al.*, 2013]. Concomitantly, sea-ice and snow cover melt from above, leading to the formation of the so-called melt ponds [Fetterer and Untersteiner, 1998; Polashenski *et al.*, 2012], commonly observed in the Arctic sea-ice [Rösel *et al.*, 2012].

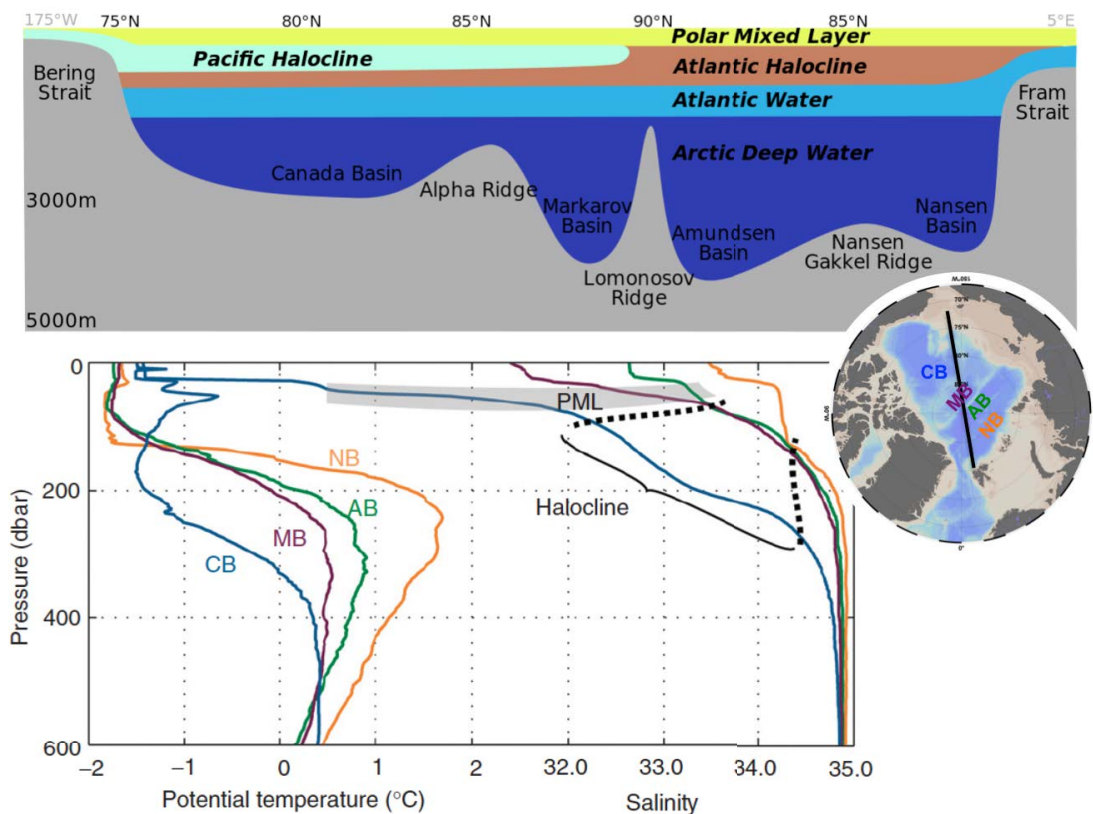


Figure 2.2. Hydrography of the Arctic Ocean. Schematic vertical distribution of the major water masses in the Arctic Ocean based on a hypothetical transect from 175°W to 5°E (black line in the map) [adapated from Aagaard and Carmack, 1989] (top). Typical vertical distribution of potential temperature (°C) and salinity for Nansen Basin (NB), Amundsen Basin (AB), Markarov Basin (MB) and Canada (CB). PML indicates Polar Mixed Layer [Rudels, 2009] (bottom).

Despite of the significant input from terrestrial sources, the supply of nutrients from Arctic rivers is low [Dittmar and Kattner, 2003]. The sustained stratification of surface waters limits vertical fluxes of nutrients, and nitrogen is the main limiting nutrient for primary production [Tremblay and Gagnon, 2009; Codispoti et al., 2013]. Sea-ice strongly affects the establishment and development of spring and summer phytoplankton and sea-ice algae blooms (and primary production) in the Arctic Ocean by influencing light and nutrient availability through vertical fluxes [Sakshaug et al., 2004; Arrigo, 2014; Fernández-Méndez et al., 2015]. Apart from the nutrient limitation, light is the primary factor limiting primary production in the Arctic surface layer, resulting in the highest primary production being observed in the ice-free areas. Therefore, given the coupling between primary production and biogenic carbon export [Lalande et al., 2009], higher values of the latter are observed in ice-free areas [Lalande et al., 2014]. Additionally, primary production also differs between the two major Arctic Basins, with the highest production associated to the Eurasian basin [Sakshaug et al., 2004; Codispoti et al., 2013]. Besides strongly influencing primary production in the surface, sea-ice also influences the fluxes between ocean and atmosphere. For instance, greenhouse gases exchange rates with the atmosphere differ with varying sea-ice extent [Parmentier et al., 2013].

Parallel to the primary production and vertical biogenic carbon export, the dissolved and the particulate organic carbon (DOC and POC, respectively) exert strong impact in the Arctic carbon cycle. High loads of DOC and POC are introduced in the Arctic Ocean from the rivers and most of this material is of dissolved character [Alling et al., 2010; Sánchez-García et al., 2011]. In the Laptev and Eastern Siberian Seas the POC-pool has significant inputs of lignin-phenols, mainly from woody gymnosperm and non-woody angiosperm sources [Winterfeld et al., 2015]. Furthermore, it has a non-conservative behavior along the river-sea transition, and a considerable removal of POC is observed at low salinity [Sánchez-García et al., 2011]. DOC (or DOM), similarly to POC, has a high terrestrial character in the Arctic waters, being highly correlated to lignin-phenol concentrations [Alling et al., 2010; Fichot et al., 2016]. Furthermore, whilst early reports showed DOM to behave conservatively through its transition to the ocean [Cauwet and Sidorov, 1996; Kattner et al., 1999], recent studies point to a non-conservative mixing, with strong removal at low salinity [Alling et al., 2010; Letscher et al., 2011]. However, DOM signal from the Arctic rivers is still detectable in polar waters exiting to the North Atlantic through the Fram Strait [Amon et al., 2003; Granskog et al., 2012; Pavlov et al., 2015; Stedmon et al., 2015]. Recent estimates showed that, together with the freshwater, almost half of the terrigenous CDOM input from the Arctic rivers is exported through the Fram Strait, with a net flux of $24.9 \cdot 10^{12} \text{ m}^2 \text{ yr}^{-1}$ [Granskog et al., 2012].

The mean temperature on Earth has increased, on average, by 0.89 °C since the beginning of the anthropogenic release of CO₂ to the atmosphere [IPCC, 2013]. Such an increase in temperature is even higher in the Arctic (two- or three-fold the global average rate), and it is called the “Arctic amplification”. The consequences of those effects have already been observed in the Arctic, which registered the lowest summer sea-ice minimum extent in the last years [Comiso *et al.*, 2008; Parkinson and Comiso, 2013], with a reduction of about 45% in the past 30 years [Arrigo, 2014]. If CO₂ emissions continue to increase, a summer ice-free Arctic Ocean is predicted in the next 30 years [Wang and Overland, 2012]. Such changes would imply in drastic changes in dense water formation in the Arctic basin during winter due to the warming and freshening of the surface layer [Serreze *et al.*, 2007; Yamamoto-Kawai *et al.*, 2009], as well as changes in primary productivity in the surface layer. As already demonstrated, sea-ice shrinking in the Arctic Ocean implies in increased primary production [Arrigo and van Dijken, 2011] and changes in the composition of phytoplankton communities [Li *et al.*, 2009]. Furthermore, high atmospheric CO₂ concentrations lead to increase in the *p*CO₂ in the seawater and subsequent ocean acidification. Increase in both acidification levels and temperature would drastically impact the Arctic ecosystem and trophic chain as seen in organisms occupying the first levels of the Arctic food web such as phytoplankton [Riebesell and Tortell, 2011] and zooplankton [Hildebrandt *et al.*, 2014; Boersma *et al.*, 2016].

Apart from the direct impacts it exerts in the Arctic Ocean waters and sea-ice, global warming also affects the Arctic terrestrial environment with regards to glacier melt [Sapiano *et al.*, 1998] and permafrost thaw [Schuur *et al.*, 2008, 2013]. That, in turn, leads to an increase in river discharge and fresh water export to the Arctic seas [Frey and McClelland, 2009] and increased coastal erosion is observed [Solomon, 2005; Obu *et al.*, 2015]. The latter is responsible for the release of significant amounts of DOC to the coastal Beaufort Sea from the Yukon coasts [Tanski *et al.*, 2016]. Along with that, thawing permafrost does not only increase the fresh water discharge; it also increases the export of dissolved organic matter [Frey and McClelland, 2009] and the release of ancient organic carbon [Vonk *et al.*, 2012; Aiken *et al.*, 2014; Dubinenkov *et al.*, 2015a]. Most of DOM in Arctic Rivers during the spring and summer freshet is fresh, and with vegetation and fresh litter from boreal forests as the dominant source of riverine DOM [Amon *et al.*, 2012]. However a recent report suggested that ancient carbon is released especially during spring and summer in the Yukon River and its tributaries, related to permafrost thaw, and an increased contribution of older DOM in those waters is expected in the coming decades [Aiken *et al.*, 2014]. Furthermore, permafrost and sediments around the Arctic Ocean contain great amount of methane (CH₄), which is a greenhouse gas four times more potent than CO₂, and is released upon warming [Shakhova *et al.*, 2010; Hayes *et al.*, 2014].

Finally, a recent study pointed out that degradation of terrestrial organic matter and discharge of Arctic river water with elevated CO₂ concentrations drive the acidification of waters in the East Siberian Arctic Shelf [*Semiletov et al.*, 2016]. Therefore, studies on DOM in the region are of great importance for improving the current knowledge on the characterization, stocks and fate of DOM. Moreover, the development of equipment and techniques for autonomously monitoring DOM is extremely required given the difficulty to access the Arctic Oceans and a more accurate evaluation of the Arctic carbon cycle can be reached.

2.2. Tools for assessing content, speciation and origin of DOM in aquatic systems

Rafael Gonçalves-Araujo^{1,2}

¹Alfred Wegener Institute Helmholtz Centre for Polar and Marine Research, Climate Sciences Division, Physical Oceanography of Polar Seas, PHYTOOPTICS Group, Bussestraße 24, 27570 Bremerhaven, Germany

²University of Bremen, Faculty of Biology, PO Box 330440, 28334 Bremen, Germany

Manuscript published in the proceedings of YOUMARES 7 (2016)

Abstract

Dissolved organic matter (DOM) is a major component of the carbon-pool in aquatic systems and thus represents an important pathway on the carbon cycle, especially in marine environments. For instance, studies have used DOM to assess drinking water quality, its importance on biogeochemical cycles, its usefulness as an environmental tracer, etc. This article discusses some of the current methods used to assess the amount and composition of DOM, and applications of DOM as an environmental tracer in aquatic systems. Different techniques varying from molecular, optical and chemical analyses to satellite remote sensing have been employed to identify, characterize and quantify DOM and to assess its distribution, composition and dynamics in distinct aquatic environments. Those approaches however, focus only on specific fractions of the total DOM-pool. Hence, recent studies have attempted to link the results provided by such complimentary methods to reach a more comprehensive understanding on the total DOM-pool in aquatic systems. Additionally, DOM spectroscopic measurements (e.g. absorbance and fluorescence) are cost-effective tools and can be sampled with high resolution by autonomous devices such as fluorometers. Furthermore, the optical properties of DOM have been shown to be reliable proxies for monitoring water quality and for tracing fresh water along the Arctic Ocean. With the climate change pressure on Arctic environments and the expected increase in fresh water and ancient carbon export from the continent to the ocean, optical analyses of DOM can be an easy-to-measure and affordable parameters for assessing and monitoring these effects in the Arctic environment.

Keywords: dissolved organic matter, CDOM, FDOM, optical indices, environmental assessment

2.2.1. Objectives

Given the huge variety in DOM composition and the wide panel of different approaches employed to analyze it, this article provides a brief review on some of the current methods applied to assess the amount and composition of DOM. Secondly, an overview on the applications of DOM properties as environmental tracers in aquatic systems is presented, with focus on the Arctic marine environment.

2.2.2. Quantitative and qualitative methods for DOM assessment

Different methods have been applied for performing chemical analyses of DOM. In general, those methods can be classified into two groups according to the preparation of the sample for analysis: the analyses involving purification and/or pre-concentration and the analyses performed in filtered original water (Figure 2.3). The purification and pre-concentration are employed to avoid interference of inorganic ions, which can affect highly to sensitive analyses. However, those methods can have analytical errors embedded in their analysis such as oxidation of only a part of DOM and increase in DOM concentration during drying of samples [*Bolan et al.*, 1996]. A wide range of methods have been developed using such techniques, for instance, solid phase extraction (SPE), ultrafiltration, nanofiltration, reverse osmosis, or electrodialysis. Although those methods have been widely applied in DOM studies, this article focuses on the approaches using filtered original water, which are here further divided into molecular and bulk analyses. The methods for DOM analysis using filtered original water can vary significantly with regards to the analytical procedure, including elemental analysis, isotopic analysis, chromatography and mass spectrometry.

2.2.2.1. Molecular analysis

By molecular analysis, this article refers to the quantification of an essentially pure type of organic compound or compound class. Two major groups of methods are applied in molecular analysis of DOM, the targeted and the non-targeted (Figure 2.4). Targeted methods are focused on analyzing specific organic compounds, which structure is well defined in the literature. In DOM research, such molecules are usually referred to as biomarkers. Non-targeted methods are used to detect the analytical signal (or superposition of signals) from multiple molecular components with the DOM mixture. In addition, non-targeted methods can also be employed for the characterization of bulk DOM, since they can provide information on the carbon content in a water sample.

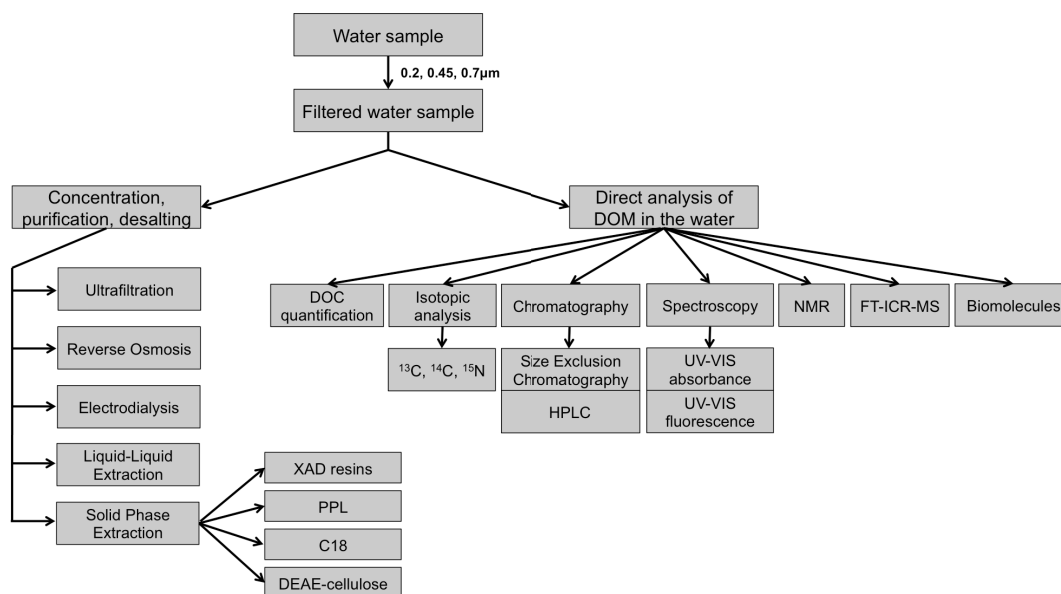


Figure 2.3. Strategies in the chemical analyses of DOM with respect to the pre-processing of samples [addapted from *Dubinenkov, 2015*].

Targeted molecules

The analysis of targeted molecules consists of quantifying a specific compound based on its extraction from the water samples. Examples for targeted biomolecules are lignin phenols, proteins and amino acids, sugars, amino-sugars and lipids. Such molecules can be analyzed by applying different techniques. For example, most proteinogenic amino acids can be retained and separated by high-performance liquid chromatography (HPLC; *Mopper and Lindroth, 1982*) whereas some phenols can be separated using both gas chromatography [*Benner and Opsahl, 2001*] and HPLC.

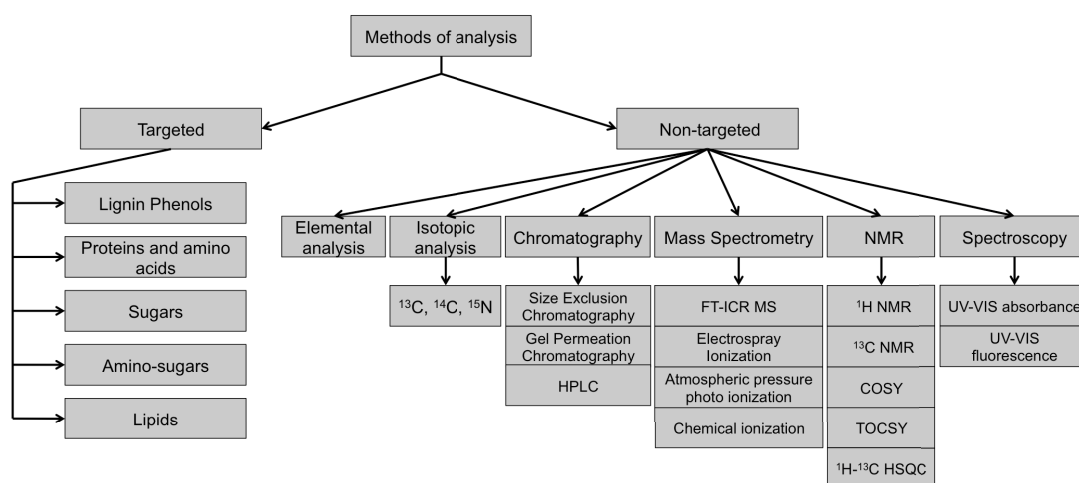


Figure 2.4. Strategies in the chemical analyses of DOM regarding the methods of analysis [addapted from *Dubinenkov, 2015*].

Non-targeted molecules

Non-targeted approaches focus on the simultaneous detection of multiple molecular components. However, such methods can also provide bulk estimates of DOM. Among the several non-targeted methods for analysis of DOM, the nuclear magnetic resonance (NMR) and the Fourier transform ion cyclotron resonance mass spectrometry (FT-ICR MS) have been applied in many studies focusing on molecular characterization of DOM in the last decades. Despite of the wide application of both methods, this subsection focuses on the FT-ICR MS method, given the significant increase in the number of studies using that method to chemically characterize DOM.

The FT-ICR MS provides a detailed characterization of the diversity of molecular formulas contained in the analyzed DOM samples [Koch and Dittmar, 2006]. Three distinct ways are used to analyze DOM with mass spectrometry, nevertheless all involving preliminary purification and concentration of samples: hyphenation with HPLC [Dittmar *et al.*, 2007], direct injection of samples extracts [Kim *et al.*, 2003] and chromatographic fractions [Koch *et al.*, 2008]. The FT-ICR MS determines the mass-to-charge ratio (m/z) of ions based on their cyclotron frequency in a fixed magnetic field [Marshall and Hendrickson, 2002]. Given the high accuracy and sensitivity of the method, thousands of different mass peaks of DOM can be resolved and their respective molecular formulas can be assigned [Koch *et al.*, 2005]. Several different approaches have been applied for visualizing the molecular information provided by the FT-ICR MS. Among them, the van Krevelen diagram is the most popular method applied [van Krevelen, 1950; Schmidt *et al.*, 2009]. The diagram is constructed based on the atomic ratios of carbon compounds and is obtained from the hydrogen index (hydrogen:carbon) as a function of the oxygen index (oxygen:carbon).

2.2.2.2. Bulk analyses

Bulk analyses to quantify and characterize DOM samples can be subdivided into elemental, isotopic and spectroscopic methods. The most common quantitative representation of DOM in natural waters is dissolved organic carbon (DOC) concentration. It is usually quantified via high temperature catalytic oxidation to CO_2 [Sugimura and Suzuki, 1988]. Carbon isotopic measurements (e.g. ^{13}C and ^{14}C) can also provide information on bulk DOM in aquatic systems. Furthermore, such measurements can provide information on both mass and age of DOM [Williams and Druffel, 1987; Druffel and Bauer, 2000]. Studies have shown that DOC in deep waters presented $\Delta^{14}\text{C}$ values reaching -502‰ (i.e., 5600 years) in the Southern Ocean [Druffel and Bauer, 2000] and -540‰ (i.e., 6240 years) in the central North Pacific Ocean [Williams and Druffel, 1987]. However, this article focuses on the spectroscopic methods, such as absorbance (section 2.2.2.1) and

fluorescence (section 2.2.2.2) spectra. These parameters can be monitored with *in situ* autonomous platforms and ocean color remote sensing [Cooper et al., 2005; Siegel et al., 2005; Heim et al., 2014], and the derived optical indices (section 2.2.2.3) used to characterize and evaluate the transformation and reactivity of DOM.

Chromophoric dissolved organic matter

Spectral analyses of DOM have been applied to assess the optically active fraction of DOM, the colored (or chromophoric) and fluorescent DOM (CDOM and FDOM, respectively). CDOM is the DOM fraction that absorbs light in the ultraviolet (UV) and visible wavelength ranges [Siegel et al., 2002], whereas a fraction of CDOM is able to fluoresce, characterizing the FDOM fraction. From the absorbance spectra obtained with spectrophotometers, the Napierian absorption coefficient of CDOM (a) at each wavelength (λ) is obtained from the given equation: $a_{\lambda}(\text{m}^{-1})=(2.303 \times A_{\lambda})/L$, where A_{λ} is the absorbance at specific wavelength and L is the cuvette path length in meters. That coefficient is adopted as an index of CDOM amount and different wavelengths have been chosen to determine a . Studies focusing on ocean color remote sensing previously presented results on absorption in the visible wavelength range, a_{440} or a_{443} [Siegel et al., 2002, 2005; Heim et al., 2014]. Other studies, on the other hand, used the absorption in the UV range (e.g. a_{325} and a_{350}) because of its correlations with DOC and lignin concentration [Spencer et al., 2009; Stedmon et al., 2011], and also because CDOM is the most important optically active constituent of water in the open ocean with regards to absorption in the UV wavelength range [Nelson and Siegel, 2013]. Moreover, DOC has been shown to be strongly correlated with both CDOM and FDOM in the Arctic Ocean [Walker et al., 2013]. Therefore optically active fractions of DOM can be a proxy for the total DOM-pool (based on DOC measurements) in the Arctic environment.

Fluorescent dissolved organic matter

FDOM has also been used as an index of DOM amount [Benner et al., 2005; Cooper et al., 2005]. Furthermore, it can provide information on the origin, mixing, and removal of different fractions of DOM [Yamashita and Tanoue, 2003b; Chari et al., 2013; Fukuzaki et al., 2014]. By acquiring the excitation-emission-matrices (EEMs), a qualitative evaluation of the different compounds of bulk DOM from spectroscopy can be performed [Coble, 1996]. With the adaptation of the Parallel Factor Analysis (PARAFAC) for the analysis of DOM, a more holistic differentiation of underlying independent DOM components was possible [Stedmon et al., 2003; Stedmon and Bro, 2008]. The PARAFAC is a multi-way analysis that can be applied to

decompose trilinear data arrays such as EEMs. Furthermore, EEMs must be corrected for inner-filter effects and for the Raman and Rayleigh scattering prior to PARAFAC modeling [Murphy *et al.*, 2013]. Recent studies attempted to associate molecular groups and PARAFAC-derived DOM components [Stubbins *et al.*, 2014; Kellerman *et al.*, 2015; Wagner *et al.*, 2015]. They found significant correlations between the humic-like fluorescent peak A [e.g., Coble, 2007] and high molecular weight compounds with little nitrogen, between the protein-like fluorescent peak T and low molecular weight aromatic compounds (such as amino acids) and between the humic-like fluorescent peak C and lignin-derived phenols. Moreover, a recent study pointed out that some PARAFAC-derived components from the OpenFluor database [Murphy *et al.*, 2014] have been shown to match with fluorescence of specific organic compounds, such as salicylic acid, tyrosine, tryptophan and *p*-cresol [Wünsch *et al.*, 2015]. Finally, the fluorescence quantum yield (Φ) of a pure fluorophore represents the probability of it to fluoresce after being excited by light [Lakowicz, 2006]. However, given that CDOM in a natural sample represents a complex mixture of different molecules, some of those molecules are not able to fluoresce. Hence, the CDOM fluorescence efficiency of a given water sample is the result of the combination of those signals. Thus, studies for analysis of DOM in natural water samples have expressed their results by means of the apparent fluorescence quantum yield (AQY), which represents Φ for a mixture of fluorophores [Green and Blough, 1994; Del Vecchio and Blough, 2004; Wünsch *et al.*, 2015]. AQY has been pointed out as a good proxy to assess the effects of microbial turnover of DOM [Catalá *et al.*, 2015b].

Optical indices for DOM modification

The information contained in the spectral analysis of both CDOM and FDOM cannot only determine the amount and composition of DOM components, but it can also give insights into DOM origin and transformation. For that purpose, several optical indices have been developed. The spectral slope of absorption spectra (S) is obtained by applying an exponential function to the UV-VIS spectral range. It has been shown to be inversely correlated with the molecular weight of DOM and it can also be related to photobleaching [Helms *et al.*, 2008]. The choice of each spectral range for assessment of the spectral slope varies among different studies and sampling regions. For instance, S values acquired in the UV region (e.g., 275–295 nm) can differ from results expressed by means of the VIS region (e.g., 350–400 nm) reflecting differences regarding the origin of DOM, as from terrestrial or marine character [Helms *et al.*, 2008]. Other studies obtained S values considering the full UV-VIS regions, deriving S from the range between 300–650 nm [Stedmon and Markager, 2001]. A recent study showed that nitrate

and cytochrome C exert strong influence on CDOM absorption spectra, given their absorbance peaks at 302 and 405 nm, respectively [Catalá *et al.*, 2016]. Furthermore, that same study showed that those two chromophores can lead $S_{275-295}$ and $S_{350-400}$ to an overestimation by $13.3 \pm 6.0\%$ and $14.8 \pm 10.6\%$, respectively. The slope ratio (S_R) is obtained from the ratio between UV and VIS absorption spectral slope (275–295 and 350–400 nm, respectively) and provides strong differentiation between open ocean waters from those of near-shore coastal or estuarine origin [Helms *et al.*, 2008]. The specific UV absorbance (SUVA) index is obtained as a function of the UV absorbance (at 254 nm) and DOC concentration, and it is used to trace the degree of aromaticity in CDOM samples [Weishaar *et al.*, 2003], which is in turn correlated to the molecular weight [Helms *et al.*, 2008].

Fluorescence is widely used to assess the degree of humification of bulk DOM, and thus to provide insights into the origin of DOM. The fluorescence index (FI) can be applied to distinguish sources of isolated aquatic fulvic acids. It is determined based on the ratio of the emission intensity at a wavelength of 450 nm to that at 500 nm, obtained with an excitation of 370 nm [Mcknight *et al.*, 2001]. The humification index (HIX) estimates the degree of maturation of DOM [Zsolnay *et al.*, 1999; Zsolnay, 2003], considering that humification is associated with an increase in the C/H ratio [Stevenson, 1994] and is thus reflected in emissions at longer wavelengths [Senesi *et al.*, 1991]. This index is obtained from the ratio of the areas of two spectral wavelength regions (435-480 nm versus 300-345 nm) in the emission spectra for an excitation at 254 nm [Zsolnay *et al.*, 1999]. An increase in the degree of aromaticity (humification) leads to a red shift in the emission spectrum, which results in higher HIX values. The biological/autochthonous index (BIX) is used to assess the biological modification of DOM based on UV fluorescence. The BIX index is obtained by calculating the ratio of the emission at 380 and 430 nm, excited at 310 nm [Huguet *et al.*, 2009]. High BIX values correspond to autochthonous origin of DOM, i.e., freshly released DOM, whereas low BIX values indicate allochthonous DOM [Huguet *et al.*, 2009].

A recent study investigated the correlations between optical indices and molecular families derived from FT-ICR-MS measurements [Wagner *et al.*, 2015]. The authors found that SUVA and HIX are effective in tracking terrestrially-derived groups of highly aromatic compounds with low N, P and S content, which have been previously pointed out by other studies to be photolabile [Gonsior *et al.*, 2009; Stubbins *et al.*, 2010]. FI and BIX indices have been shown, on the other hand, to be associated to bio-labile aliphatic formulae [Wagner *et al.*, 2015].

2.2.3. DOM as an environmental tracer

DOM has been shown to be a useful tool in a wide range of applications, from scientific to management interests. Studies have shown that FDOM measurements provide a fast and sensitive way to monitor the qualitative and quantitative variation of DOM in drinking water, and during the sewage treatment and also recycling water processes [Guo *et al.*, 2010; Hambly *et al.*, 2010; Murphy *et al.*, 2011]. PARAFAC-derived protein-like components (and their relative contribution compared to humic-like components) were suggested to be a reliable tracer to monitor the relative amount of raw or treated sewage in China [Guo *et al.*, 2010]. Another study, conducted with samples from municipal water systems, highlighted the dominance of the terrestrial humic-like PARAFAC-derived component, which has also been identified in other studies performed on engineered, wastewater impact environments [Murphy *et al.*, 2011].

Besides its potential use to monitor water quality and sewage and wastewater treatment, DOM has been shown to be a water mass tracer, especially the fresh water fractions [Stedmon and Markager, 2001; Stedmon *et al.*, 2015]. Strong correlations between CDOM and the fraction of meteoric water, which is a tracer of continental fresh water input [Dodd *et al.*, 2012], can be used as a proxy to monitor the fresh water export from the Arctic to the Atlantic basins, given the high DOM concentrations in those waters. Furthermore, other optical parameters of DOM can be applied to trace the fraction of meteoric water in the Arctic Ocean. Studies have used the correlation between S and a_{375} to detect the fractions of meteoric water [Granskog *et al.*, 2012; Stedmon *et al.*, 2015] by applying the model proposed by Stedmon and Markager [2001]. Such information has potential for supporting the design of *in situ* DOM fluorometers as a low-cost mechanism to provide high spatial and temporal resolution data for tracing the freshwater origins and decipher water mass mixing dynamics in the region, given the concern regarding the effects of climate change over the Arctic Ocean.

Given that CDOM absorbs light in both the UV and visible wavelength ranges, it can play an important role in the biogeochemical cycles in coastal and inner-shelf waters, being one of the dominant components interacting with the underwater light field in those environments [Siegel *et al.*, 2002; Nelson and Siegel, 2013]. Furthermore, it can act as a shield for the aquatic biota from harmful UV radiation [Arrigo and Brown, 1996]. As a result of its UV absorbing properties, CDOM is susceptible to photo-degradation, which either induces direct mineralization or produces microbiologically labile low molecular weight compounds, which are subsequently utilized by bacteria [Mopper and Kieber, 2002]. CDOM does not only absorb UV-radiation, it also absorbs heat, thus influencing the light and heat penetration in surface waters [Granskog *et al.*, 2015], especially in coastal and inner-shelf regions.

2.2.4. Conclusions

DOM has been shown to play an important role on the carbon cycle, acting as a link between terrestrial and aquatic systems. Furthermore, it is an easy-to-measure and affordable tool for monitoring water quality and sewage treatment. DOM is subject to several processes that affect its composition, amount and reactivity. However, the effects of such processes on different compounds, as well as the fate of DOM in aquatic systems are still under debate. With the ongoing climate change over the environment, more effort has been devoted to understand the role and fate of DOM in aquatic systems. A variety of new techniques have emerged in the last decades and better qualitative and quantitative assessment of the DOM is possible. However, there are still unresolved questions and unmet capabilities that need attention in the coming years. For instance, a more comprehensive understanding on the processes governing DOM dynamics, such as photo-oxidation, microbial turnover, adsorption/flocculation, etc. is needed for a better estimation of DOM production rates as well as the rates of DOM transformation. A recent special issue gathered several papers linking the chemical and optical properties of DOM (*“Linking optical and chemical properties of dissolved organic matter in natural waters”*, *Frontiers in Journal, Section Marine Biogeochemistry*). Such studies can provide, for instance, a more consistent interpretation of optical indices of DOM modification and PARAFAC-derived fluorescent components. Finally, it is clear that implementation of new observing systems including new ocean color sensors and ocean observing systems, as well as the deployment of autonomous platforms with DOM-fluorometers, will be responsible for much of the future collection of data. Therefore, advances on the analysis and interpretation of the optical properties of DOM are required to improve the sensitivity and specificity of sensors deployable on these platforms.

2.2.5. Acknowledgements

The author thanks to Prof. Dr. Astrid Bracher and Lumi Haraguchi for their valuable comments and discussions. Rafael Gonçalves-Araujo is supported by a PhD fellowship from the Coordination for the Improvement of Higher Level Personnel (CAPES-Brazil, Grant 12362/12-3) in collaboration with the German Academic Exchange Service (DAAD).

Chapter 3

From fresh to marine waters: characterization and fate of dissolved organic matter in the Lena River Delta region, Siberia

Manuscript published in *Frontiers in Marine Science* (2015)

3. From fresh to marine waters: characterization and fate of dissolved organic matter in the Lena River delta region, Siberia

Rafael Gonçalves-Araujo^{1,2*}, Colin A. Stedmon³, Birgit Heim⁴, Ivan Dubinenkov^{5,2}, Alexandra Kraberg⁶, Denis Moiseev⁷, Astrid Bracher^{1,8}

¹PHYTOOPTICS Group, Physical Oceanography of Polar Seas, Climate Sciences, Alfred Wegener Institute for Polar and Marine Research, Bremerhaven, Germany

²Faculty of Biology and Chemistry (FB-2), University of Bremen, Bremen, Germany

³Section for Marine Ecology and Oceanography, National Institute for Aquatic Resources, Technical University of Denmark, Charlottenlund, Denmark

⁴Periglacial Research, Geosciences, Alfred Wegener Institute for Polar and Marine Research, Potsdam, Germany

⁵Ecological Chemistry, Biosciences, Alfred Wegener Institute for Polar and Marine Research, Bremerhaven, Germany

⁶Biologische Anstalt Helgoland, Shelf Sea System Ecology, Biosciences, Alfred Wegener Institute for Polar and Marine Research, Helgoland, Germany

⁷Murmansk Marine Biological Institute of Kola Science Centre, Russian Academy of Sciences, Murmansk, Russia

⁸Institute of Environmental Physics, University of Bremen, Bremen, Germany

*Corresponding author: PHYTOOPTICS Group, Physical Oceanography of Polar Seas, Climate Sciences, Alfred Wegener Institute for Polar and Marine Research, Bussestraße 24, F402, 27570 Bremerhaven, Germany (rafael.goncalves.araujo@awi.de / rafaeldoncalvesaraujo@gmail.com)

Abstract

Connectivity between the terrestrial and marine environment in the Arctic is changing as a result of climate change, influencing both freshwater budgets and the supply of carbon to the sea. This study characterizes the optical properties of dissolved organic matter (DOM) within the Lena Delta region and evaluates the behavior of DOM across the fresh water-marine gradient. Six fluorescent components (four humic-like; one marine humic-like; one protein-like) were identified by Parallel Factor Analysis (PARAFAC) with a clear dominance of allochthonous humic-like signals. Colored DOM (CDOM) and dissolved organic carbon (DOC) were highly correlated and had their distribution coupled with hydrographical conditions. Higher DOM concentration and degree of humification were associated with the low salinity waters of the Lena River. Values decreased towards the higher salinity Laptev Sea shelf waters. Results demonstrate different responses of DOM mixing in relation to the vertical structure of the water column, as reflecting the hydrographical dynamics in the region. Two mixing curves for DOM were apparent. In surface waters above the pycnocline there was a sharper decrease in DOM concentration in relation to salinity indicating removal. In the bottom water layer the DOM decrease within salinity was less. We propose there is a removal of DOM occurring primarily at the surface layer, which is likely driven by photodegradation and flocculation.

Keywords: DOC, CDOM, FDOM, PARAFAC, optical indices, hydrography, Laptev Sea, Arctic

3.1. Introduction

Colored or chromophoric dissolved organic matter (CDOM) is the fraction of DOM that absorbs light and it is one of the dominant components influencing the underwater light field in coastal and inner-shelf waters [Siegel *et al.*, 2002; Nelson and Siegel, 2013]. CDOM absorbs light in the ultraviolet (UV) and visible wavelength ranges and thus it is able to shield aquatic biota from harmful UV radiation [Arrigo and Brown, 1996] and can be detected by ocean color remote sensing [Siegel *et al.*, 2002, 2005]. As a result of its UV absorbing properties, CDOM is susceptible to photodegradation, which either induces direct mineralization or produces microbiologically labile low molecular weight compounds, which are subsequently utilized by bacteria [Mopper and Kieber, 2002]. Fluorescent DOM (FDOM), which is the part of CDOM able to fluoresce, can be used to trace the supply, mixing and removal of different fractions of DOM [Yamashita and Tanoue, 2003a, 2004; Coble, 2007; Chari *et al.*, 2013; Fukuzaki *et al.*, 2014]. With the recent adaptation of the Parallel Factor Analysis (PARAFAC) for analysis of DOM, a more holistic analysis of excitation-emission matrices (EEMs) allows for the differentiation

of wider range of underlying DOM components [Stedmon and Bro, 2008]. A recent study showed significant associations between molecular groups and PARAFAC-derived DOM components [Stubbins *et al.*, 2014]. For instance, the humic-like fluorescent peak A [e.g. Coble, 2007] is associated with high molecular weight compounds with little nitrogen, whereas the humic-like peak C correlated to lignin-derived phenols and the amino acid-like peak T was associated to low molecular weight and aromatic content compounds, such as hydrolysable amino acids [Stubbins *et al.*, 2014].

By applying the EEMs/PARAFAC technique, the distribution and dynamics of fluorescent DOM have been studied in a wide range of environments varying from lakes [Zhang *et al.*, 2009], estuaries [Stedmon and Markager, 2005; Singh *et al.*, 2010], coastal and shelf [Murphy *et al.*, 2008; Kowalczyk *et al.*, 2010; Para *et al.*, 2010] to pelagic waters [Yamashita *et al.*, 2010; Jørgensen *et al.*, 2011; Kowalczyk *et al.*, 2013]. In coastal regions, especially in areas close to river outflows, the riverine input and its mixing with marine waters are the major factors controlling the distribution and composition of DOM [Stedmon and Markager, 2003; Guo *et al.*, 2007; Alling *et al.*, 2010]. In these waters processes such as photobleaching [Opsahl and Benner, 1998; Stubbins *et al.*, 2006; Helms *et al.*, 2008, 2014, Porcal *et al.*, 2013, 2015], sorption to sediments, flocculation [Uher *et al.*, 2001; Shank *et al.*, 2005; Guo *et al.*, 2007; von Wachenfeldt *et al.*, 2008; Asmala *et al.*, 2014], biological uptake [Boyd and Osburn, 2004], biological release [Romera-Castillo *et al.*, 2010] and photo-production of DOM [Helms *et al.*, 2014] can also play a crucial role in controlling the amount, composition and reactivity of DOM in these environments.

The Arctic Ocean receives considerable input of terrigenous carbon mobilized from high latitude carbon-rich soils and peatlands [Opsahl *et al.*, 1999; Benner *et al.*, 2004]. This terrigenous material is supplied by Arctic rivers, which account for more than 10% of the total riverine and terrestrial organic carbon into the global ocean waters [Opsahl *et al.*, 1999; Benner *et al.*, 2004]. Among those rivers, the Lena River (eastern Siberia) accounts for the highest annual DOM discharge into the Arctic Ocean [Raymond *et al.*, 2007; Stedmon *et al.*, 2011], with a peak discharge in June [Amon *et al.*, 2012; Fedorova *et al.*, 2015]. It contributes approximately 20% to the total fresh water discharge into the Arctic Ocean through its delta into the Laptev Sea [Cauwet and Sidorov, 1996]. The Lena Delta and the Laptev Sea inner shelf encompass a large, shallow environment characterized by pronounced physical-chemical gradients [Bauch *et al.*, 2009; Fofonova *et al.*, 2014] and considerable amounts of sediments, dissolved and particulate organic matter over the water column [Semiletov *et al.*, 2011; Vonk *et al.*, 2012, 2014; Wegner *et al.*, 2013; Heim *et al.*, 2014; Sánchez-García *et al.*, 2014]. Eastern Siberia (including the Lena River and its delta) is known to be affected by global warming with a thawing permafrost [Yang *et al.*, 2002; Schuur *et al.*,

2008], which subsequently affects the fresh water discharge, the production of DOM in river catchments and the riverine transport of organic material input into the shelf seas [Frey and McClelland, 2009; Lyon and Destouni, 2010; Semiletov et al., 2012, 2013, Vonk et al., 2012, 2014; Sánchez-García et al., 2014; Fedorova et al., 2015].

The Lena Delta region and Laptev Sea have high DOC concentrations (>500 μM) and high CDOM associated with low salinity waters [Alling et al., 2010; Stedmon et al., 2011; Semiletov et al., 2013; Walker et al., 2013; Heim et al., 2014; Dubinenkov et al., 2015a], decreasing towards higher salinities through conservative mixing [Cauwet and Sidorov, 1996; Kattner et al., 1999]. This is a characteristic also thought to be shared by other Arctic rivers [Dittmar and Kattner, 2003]. However, a recent study has indicated non-conservative mixing of DOC within the Lena Delta region, with average losses of 30–50% during mixing along the shelf [Alling et al., 2010]. These authors also identified additional sources of DOC in the region (such as primary production and coastal erosion), and pointed out photodegradation, flocculation, sedimentation, and microbial activity as possible processes to be responsible for the removal of DOC and humic substances, although currently poorly resolved. Rectifying this is difficult due to not only the remoteness of the location but also because there is a lack of information on the composition, amount, reactivity and fate of DOM in these waters. Despite the recent techniques applied for DOM analysis and the advances in the knowledge of the dynamics and composition of DOM in some aquatic environments, there is still a considerable lack of information on this important component of the global carbon pool. This is particularly compounded when accounting for the composition and processes modulating the distribution and reactivity of DOM in the Arctic regions. Hence, further studies addressing these issues are essential for a better understanding of the role of DOM in the carbon cycle within the aquatic environments, especially the Arctic Ocean.

In this study DOM characteristics within the Lena Delta region based on fluorescent properties was investigated. The distribution and transformation of the DOM along the fresh water-marine gradient were investigated, using samples collected in September 2013 at the Lena Delta region in the southern Laptev Sea. The findings provide an insight into the fate of Arctic riverine DOM while it is mixed at the shelf with the waters from the Laptev Sea.

3.2. Material and methods

3.2.1. Sampling

The Lena Expedition was conducted in late summer 2013 (1–7 September) on board the Russian R/V “Dalnie Zelentsy” of the Murmansk Marine Biological Institute, in the surrounding areas of the Lena River Delta

region, Laptev Sea, Siberia. A total of 18 oceanographic stations were occupied and split into 4 transects (Figure 3.1a). The hydrographic characteristics of the water column were assessed from vertical profiles acquired with a CTD-profiler SEACAT SBE 19+. Prior to the cruise, temperature, conductivity and pressure sensors were calibrated at laboratories of the All-Russia D. I. Mendeleev Scientific and Research Institute for Metrology. Water samples were taken using Niskin bottles at surface and discrete depths chosen based on CTD profiles. The amount of samples per profile and station varied according to the local depth, ranging from 2 samples at shallow water (<5 m) and 6 samples at deeper water stations (e.g. 20–35 m). The full data set used to compose this work is available online in two published datasets [Dubinenkov *et al.*, 2015b; Gonçalves-Araujo *et al.*, 2015a].

3.2.2. Water column structure assessment

To assess the structure of the water column, vertical profiles of temperature and salinity from the CTD casts were used to obtain potential water density (ρ) profiles. The depth where variations in density were equal or greater than 0.125 kg m^{-3} over a 5-m depth interval was considered the upper mixed layer depth (UMLD), as adapted from Levitus [Levitus, 1982] and Kara *et al.* [Kara *et al.*, 2000a]. The bottom depth was adopted as UMLD for inner shelf stations with vertically mixed profiles. The water column stability parameter (E) was obtained from vertical density variations assessed by the buoyancy or Brunt-Väisälä frequency (N^2), which is defined by $N^2 = \frac{g}{\rho} \frac{\partial \rho}{\partial z}$ ($\text{rad}^2 \text{ s}^{-2}$) leading to $E = \frac{N^2}{g}$ ($10^{-8} \text{ rad}^2 \text{ m}^{-1}$), where g is gravity. The maximum stability immediately below the UMLD was considered to represent the strength of the pycnocline/stratification [Gonçalves-Araujo *et al.*, 2015b and references therein].

3.2.3. DOC and DOM sample processing and data analysis

Water samples for DOC analysis were filtered through $0.7 \mu\text{m}$ GF/F filters (Whatman, pre-combusted, 4 h, $450 \text{ }^\circ\text{C}$) and dark stored in a freezer until further analysis in the laboratory. DOC concentrations were measured using high temperature catalytic oxidation (TOC-VCPN, Shimadzu). For external calibration of the instrument potassium hydrogen phthalate (KHP, Merck) was used. All samples were acidified (0.1 M HCl suprapur, Merck) and purged with O_2 for >5 min. Performance of the instrument was recorded by daily analysis of in-lab KHP standard solutions and reference samples (deep sea reference, DSR, Hansell research lab). The instrument blank was $\sim 2 \mu\text{M C}$ and quality of

analysis was monitored continuously based on results of DSR reference samples.

The samples for CDOM analysis were immediately syringe- filtered after sampling with Whatman Spartan 13 filters (0.2 μm) and then stored in amber glass bottles (100 mL) and kept cooled in the fridge (4 $^{\circ}\text{C}$) until further analysis. Before analysis, the samples were mixed and filtered once more through Whatman Spartan 13 syringe filters (0.2 μm). Fluorescence EEMs were collected using an Aqualog® fluorescence spectrometer (HORIBA Jobin Yvon, Germany). Freshly produced Milli-Q water was used as reference. Fluorescence intensity was measured across emission wavelengths 220–620 nm (resolution 1.77 nm, 4 pixel) at excitation wavelengths from 240 to 600 nm with 3 nm increments, and an integration time of 2 s. The blank-corrected absorbance spectra was converted into Napierian absorption coefficient (a) at each wavelength (λ), using the given equation: $a_{\lambda}(\text{m}^{-1})=(2.303 \times A_{\lambda})/L$, where A_{λ} is the absorbance at specific wavelength and L is the cuvette path length in meters. The absorption coefficients in the visible (440 nm— a_{440}) and UV (350 nm— a_{350}) bands are generally adopted as indicators of CDOM magnitude. Although many studies have presented their results using the absorption coefficient at 440 nm (a_{440}) due to its application to ocean color remote sensing [e.g., *Siegel et al.*, 2005; *Heim et al.*, 2014], in this study we determined the absorption coefficients in both visible (a_{440}) and UV (a_{350}) ranges. Nevertheless, we focus our results and discussions on the a_{350} coefficient because of its correlations to DOC and lignin concentrations and to permit comparison with earlier results [*Spencer et al.*, 2009; *Stedmon et al.*, 2011; *Walker et al.*, 2013]. The raw EEMs acquired with Aqualog® were corrected for inner-filter effects and for the Raman and Rayleigh scattering (*Murphy et al.*, 2013). The different fluorescent components of DOM were isolated from combined signal by PARAFAC modeling using the “drEEM Toolbox” and following the recommendation of *Murphy et al.* [2013]. The DOM components derived from PARAFAC modeling were compared with PARAFAC components from other studies through the OpenFluor database [*Murphy et al.*, 2014]. The complete absorption and emission spectra of the fluorescent components derived from PARAFAC are available on the OpenFluor database after publication (<http://www.openfluor.org>). We have estimated the hypothetical conservative mixing of DOM (i.e., a_{350} , DOC, and fluorescence intensity of each of the PARAFAC components) by considering the average of two values of the respective parameter at the highest and at the lowest salinity extremities, respectively, as the end points of the conservative line.

3.2.4. DOM modification indices, statistical analyses, and graphical tools

Besides the determination of the magnitude and characterization of DOM components, the optical characteristics of CDOM and FDOM can also be used to assess the origin and degree of transformation of DOM through the calculation of optical indices. By applying an exponential function to the 275–295 nm spectral range it is possible to derive the spectral slope of absorption spectra (S_{CDOM} , in μm^{-1}) that varies in relation to the source of CDOM. It has also been shown to be inversely correlated with the molecular weight of DOM and can be related to photobleaching [Helms *et al.*, 2008; Fichot and Benner, 2012; Fichot *et al.*, 2013]. The specific UV absorbance (SUVA) is used as a proxy for the degree of aromaticity in CDOM samples [Weishaar *et al.*, 2003] and it is defined by $\text{SUVA} = A_{254}/[\text{DOC}]$, where A_{254} is the absorbance at 254 nm and the concentration of DOC, [DOC], is measured in mg CL^{-1} . Due to the high absorption of aromatic compounds in the UV-visible, higher SUVA values indicate higher aromaticity from allochthonous input (e.g., humic compounds), while lower SUVA values are associated to more autochthonous or modified terrestrial CDOM with lower aromaticity [Weishaar *et al.*, 2003].

Two optical indices, that take FDOM into account, were also used to investigate both the degree of humification and biological degradation of the DOM. The humification index (HIX) estimates the degree of maturation of DOM [Zsolnay *et al.*, 1999; Zsolnay, 2003], considering that humification is associated with an increase in the C/H ratio [Stevenson, 1982] and is thus reflected in emissions at longer wavelengths [Senesi *et al.*, 1991]. The HIX index is the ratio of the areas of two spectral wavelength regions in the emission spectra for an excitation at 254 nm and it is obtained as: $\text{HIX} = H/L$, where H is the area between 435 and 480 nm in the emission spectra and L is the area in the emission spectra between 300 and 345 nm [Zsolnay *et al.*, 1999]. An increase in the degree of aromaticity (humification) leads to a red shift in the emission spectrum, which will be associated with higher HIX values. The biological/autochthonous index (BIX) is used to assess the biological modification of DOM based on UV fluorescence. The BIX index is obtained by calculating the ratio of the emission at 380 and 430 nm, excited at 310 nm: $\text{BIX} = I_{\text{Em}380}/I_{\text{Em}430}$ [Huguet *et al.*, 2009]. High BIX values correspond to autochthonous origin of DOM, i.e., freshly released DOM, whereas low BIX values indicate allochthonous DOM [Huguet *et al.*, 2009]. The relationships between all pairs of variables were investigated using Spearman correlation coefficients. To compare the variables among themselves or among different groups of samples, Kruskal–Wallis H tests were applied, after performing normality tests. Furthermore, the relationship between each pair of variables was determined based on linear regressions.

3.3. Results

3.3.1. Hydrography and water column structure

Pronounced environmental variability was observed within the studied region, with sampling varying from fresh to marine waters, as demonstrated by the noticeable hydrographical gradients in the T-S diagram (Figure 3.1c). Salinity varied between 0.90 and 32.63, with the lowest values associated with fresh water input from the Lena River and plume (Figures 3.1b and 3.1c). Temperature ranged from -1.2 to 10.3 °C, with higher values related to the warmer and fresher Lena river plume and the lowest values attributed to the presence of the colder and saltier Laptev Sea shelf waters. In addition, a strong horizontal frontal zone was found within the NW portion of the study area, with the isohaline of 10 depicting the surface limit between two hydrographic provinces observed: the sites under direct influence of fresher Lena River plume and the sites under influence of the saltier waters from the Laptev Sea shelf (Figures 3.1a and 3.1b), hereafter named as plume- and marine-influenced stations. Note that, although named marine-influenced stations, those sites were still under influence of the continental fresh water input, however less than the plume-influenced ones, given the still low salinity observed at surface (varying from 13.21 to 25.60; Figure 3.1b).

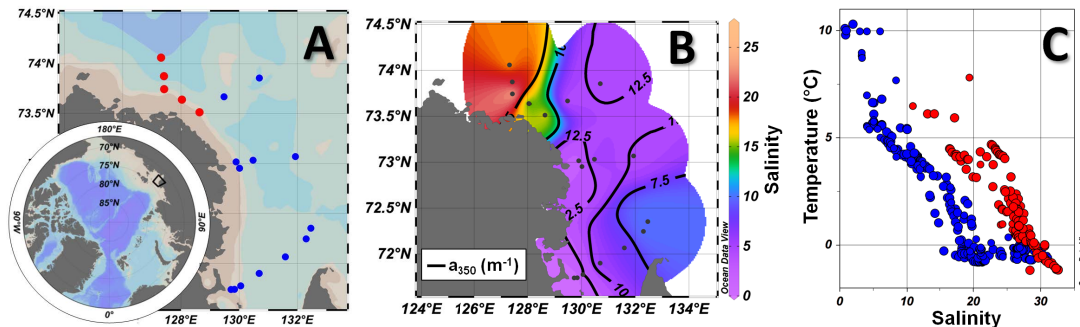


Figure 3.1. A) View of the Northern Hemisphere with the coverage of the sampled area in the black box, which is zoomed in highlighting the Lena delta region and southern Laptev Sea, as well as oceanographic stations and transects occupied during the Lena Expedition 2013. B) Surface distribution of salinity (colorbar) and a_{350} (m^{-1} ; solid black lines). C) T-S- a_{350} diagram for all the stations, with the plume-influenced and marine-influenced stations displayed in blue and red, respectively. Marine-influenced stations (surface salinity >10) are displayed in red in (A) and in the transects. Produced with Ocean Data View [Schlitzer, 2015].

A low salinity surface layer generated by the influence of the fresh waters from the Lena River was observed along the entire sampled area (Figure 3.1). The occupation of the surface layer by the river plume leads to the establishment of an upper mixed layer of ~10 m and a pronounced vertical gradient of density. Nevertheless, a few shallower stations (<5 m deep) close

to the main outflows of the Lena River (Bykovskaya and Trofimovskaya) were characterized by vertically mixed profiles with very low salinity (<3) waters from the Lena plume. The stability parameter (E) was obtained for all the stations where a vertical stratification was observed. The strength of the pycnocline was inversely related to the surface salinity ($r^2=0.82$; $p<0.01$). Thus, the plume-influenced stations exhibited a greater stratification in comparison to the marine-influenced ones, with averaged E values of about $7.01 \pm 2.84 \times 10^{-8}$, $4.32 \pm 1.79 \times 10^{-8} \text{ rad}^2 \text{ m}^{-1}$ and $3.98 \pm 1.80 \times 10^{-8} \text{ rad}^2 \text{ m}^{-1}$ for stations located at the inner-plume (surface salinity<5), outer-plume ($5<\text{surface salinity}<10$) and marine-influenced stations (surface salinity>10), respectively).

3.3.2. CDOM and DOC spatial variability

CDOM displayed a distribution tightly coupled with salinity (see Figures 3.1b and 3.2). a_{350} ranged from 0.9 to 15.7 m^{-1} (Figure 3.2) and showed a significant negative correlation with salinity [$a_{350} = -0.377(\text{salinity}) + 12.774$; $r^2=0.96$; $p<0.0001$]. The highest a_{350} values were observed within the fresher waters under the influence of the Lena plume with a decrease in a_{350} towards the saltier waters from the Laptev Sea. DOC ranged from 110 to $732 \mu\text{M}$ and was highly correlated to a_{350} [$\text{DOC} = 38.529(a_{350}) + 106.889$; $r^2=0.99$; $p<0.0001$], exhibiting a very similar behavior as CDOM across the salinity gradient [$\text{DOC} = -14.878(\text{salinity}) + 605.236$; $r^2=0.96$; $p<0.0001$] (Figure 3.2). Additionally, a_{440} varied between 0.12 and 2.97 m^{-1} and it was significantly highly correlated to a_{350} [$a_{350} = 5.188(a_{440}) + 0.361$; $r^2=0.99$; $p<0.0001$] and DOC [$\text{DOC} = 199.057(a_{440}) + 121.760$; $r^2=0.98$; $p<0.0001$].

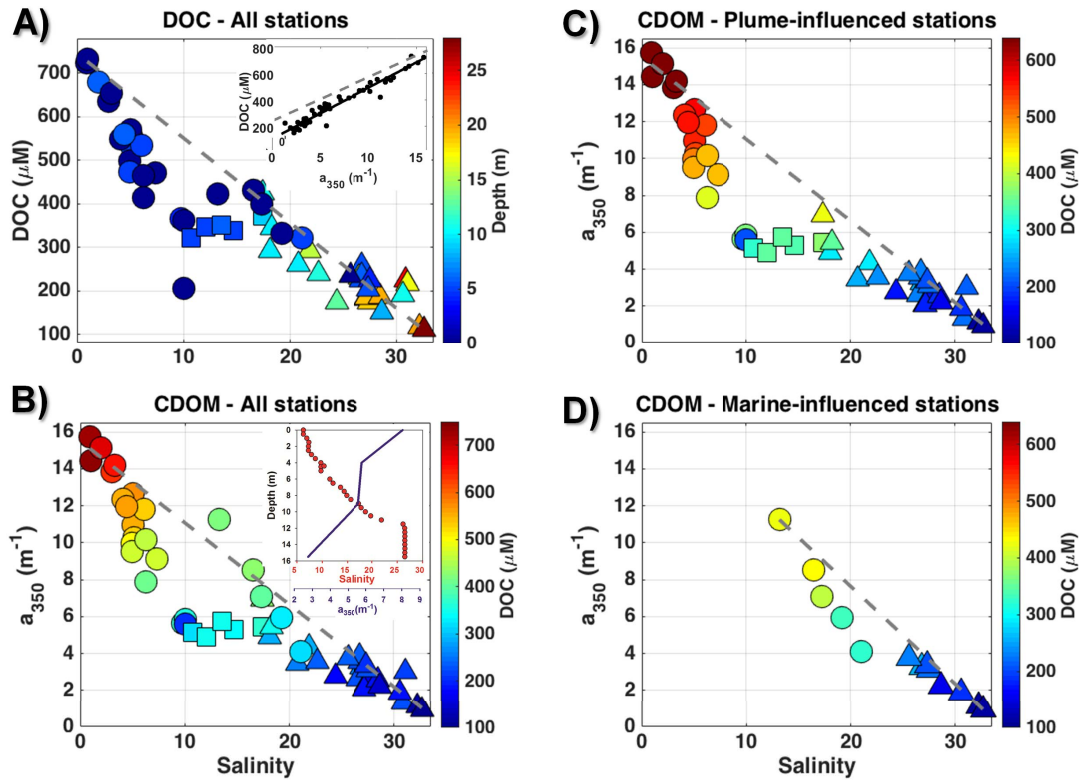


Figure 3.2. A) DOC (μM) against salinity and depth for all the samples related to this study (m; colorbar). B) a_{350} (m^{-1}) against salinity and DOC for the entire dataset used in this study (μM ; colorbar), which was split into two subsets regard to the hydrographical conditions: the plume-influenced stations (C) and the marine-influenced stations (D) that are plotted against salinity and DOC (μM ; colorbar). In all the plots, samples above the pycnocline are displayed as circles, samples at the pycnocline as squares, and samples below the pycnocline are displayed as triangles. Gray dashed-lines indicate the hypothetical conservative mixing line between DOM (or DOC) and salinity. Inset graph in (A) shows the relationship between a_{350} (m^{-1}) and DOC (μM) and the dashed line shows the fit exhibited for the coastal Canadian Arctic [Walker et al., 2009]. Inset graph in (B) exhibits vertical distribution of salinity (red dots) and a_{350} (m^{-1} ; blue line) for one typical plume-influenced station.

When taking into account the relationship between DOM and salinity for each of the hydrographic provinces separately, some features/patterns become clear (Figures 3.2 and 3.3): a higher DOM amount is associated to the plume-influenced sites; a steeper curve is exhibited by samples above the pycnocline in relation to the samples below it; and there is low variability in DOM along the pycnocline itself. In addition, the a_{350} versus salinity curve above the pycnocline displayed by the plume-influenced sites was even steeper than the same curve for the marine-influenced sites (Figure 3.3). Overall, a non-conservative behavior is observed in the low salinity, surface layer (given the deviation in relation to the hypothetical conservative mixing line) with an indication of removal of DOM (deviating up to 56% from the

hypothetical conservative mixing line). That deviation decreases at the underlying layer, suggesting a conservative mixing of DOM in those waters (see Figures 3.2 and 3.3).

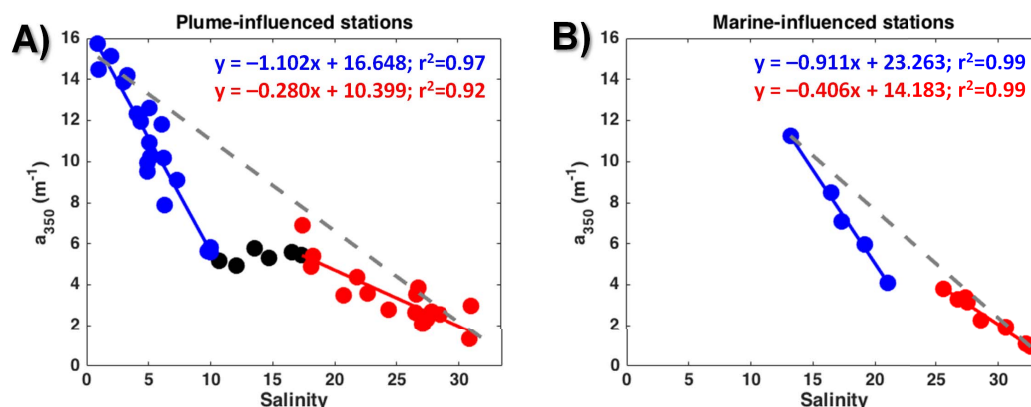


Figure 3.3. a_{350} against salinity plot with for the Plume-influenced (A) and Marine-influenced (B) stations. Samples above the pycnocline are displayed in blue whereas the ones below it are presented in red. Samples located in the pycnocline are displayed in black. All the fits presented in this figure are significant ($p < 0.0001$). Gray dashed-lines indicate the hypothetical conservative mixing line between DOM and salinity for each of the plots.

3.3.3. FDOM components by PARAFAC

Six fluorescent components (C1-C6) were identified by the PARAFAC model (Figure 3.4). Four components had broad emission and excitation spectra, with emission maxima at visible wavelengths typical of humic-like material (C1, C2, C4 and C5). C3 and C6 had comparably narrow UVA emission maxima. The fluorescence intensity of the components differed greatly, with C1 having the greatest values (reaching up to 2.08 nm^{-1}) and C6 the lowest (up to 0.18 nm^{-1}) (Figure 3.4). The humic-like components C1 and C2 were the dominant fluorescent signals, accounting for more than 50% of total FDOM in all the samples. The humic-like contribution to total FDOM reached up to 86% at low salinity (see colorbar in Figure 3.5), and was inversely related to salinity ($p < 0.0001$). C1, C2, C3 and C4 presented a similar scattered pattern in relation to salinity. A steeper curve at low salinity (< 10) suggests removal in that layer, whereas a less steep curve fit at high salinity (> 10) indicates the presence of a conservative mixing (Figure 3.4, right panel). Although being likewise inversely correlated with salinity, C5 and C6 presented distinct patterns when compared to the other components (Figure 3.4). Both components exhibited a non-conservative mixing, however with indication of release/production during the transit from the river to the outer shelf (Figure 3.4, right panel).

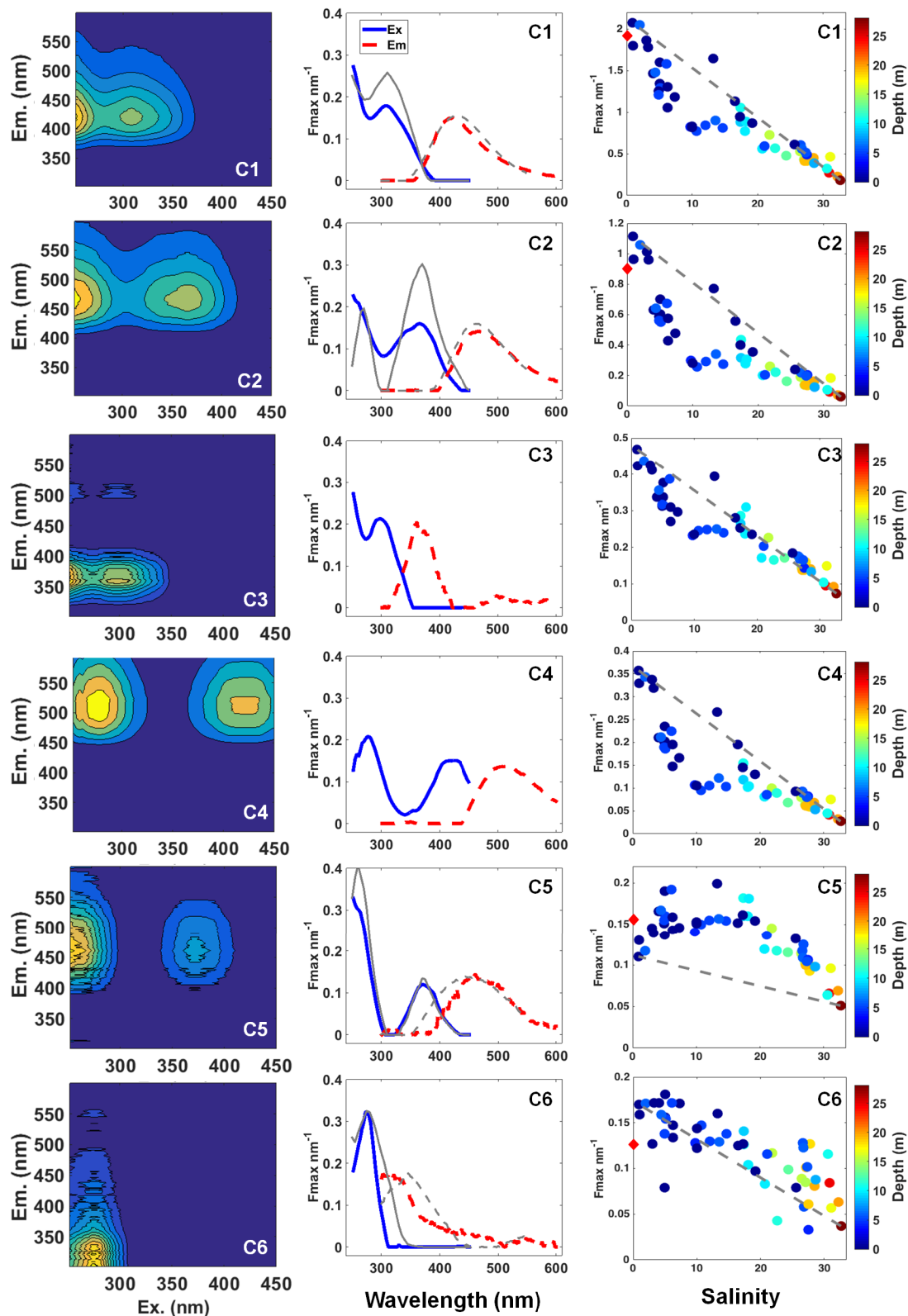


Figure 3.4. Three-dimensional fluorescence landscapes (left), the excitation (solid line) and emission (dashed line) spectra (center) and F_{max} (nm⁻¹) against salinity and depth (m) (right) for each of the six fluorescent components identified by PARAFAC model for all the samples. Gray lines displayed in components spectra graphs (center) show the spectra for components previously found in the major Arctic Rivers [Walker et al., 2013].

Gray dashed-lines in F_{\max} against salinity plots (right) indicate the hypothetical conservative mixing line between each of the components and salinity. Red diamonds in y-axis indicate averaged F_{\max} values for similar components found in the Lena River during periods of peak discharge (for C1 and C2) and mid flow (for C5 and C6) [Walker *et al.*, 2013].

3.3.4. Optical indices of DOM modification

Different optical indices including S_{CDOM} , SUVA, HIX and BIX indices (in Figure 3.5 shown in relation to salinity), as well as the slope ratio (S_{Ratio}) [Helms *et al.*, 2008] and the fluorescence index (FI) [Mcknight *et al.*, 2001] (not shown) were evaluated within all samples. All indices, except S_{Ratio} ($p > 0.05$), were significantly correlated with salinity, a_{350} , DOC and FDOM, and by that also to each other ($p < 0.0001$). Although it was not significantly correlated to salinity ($p > 0.05$), the S_{Ratio} indicated a dominance of terrigenous signal over the entire sample area, given that most of the samples (~93%) presented S_{Ratio} values below 1 (Figure 3.5e). In addition, the lack of significance between S_{Ratio} and salinity might be due to an increase in the signal-to-noise ratio for the absorbance spectra at wavelengths longer than 350 nm observed in samples at higher salinity that, in turn, presented the greatest variability in S_{Ratio} values. S_{CDOM} ranged from 15.5 to 21.4 μm^{-1} and was directly related to salinity (Figure 3.5a), suggesting a decrease in the molecular weight with increased salinity [Helms *et al.*, 2008]. The values observed for the SUVA index were high, ranging from 1.33 to 4.80 $\text{m}^2 \text{g}^{-1}$, and was inversely related to salinity ($p < 0.0001$), evidencing a decrease in the aromaticity of the molecules towards high salinity (Figure 3.5b). The HIX index values ranged from 3.4 to 16.6, and the BIX index values were lower than 0.73 (Figure 3.5c and d, respectively), indicating a high degree of humification and low autochthonous contribution within our sample set, respectively. Moreover, HIX and BIX showed a decrease (increase) in the degree of humification (DOM from biological activity) with increase in salinity, given the significant relationship ($p < 0.0001$) displayed by those indices and salinity (Figure 3.5c and d). FI presented values below 1.3 and was inversely related ($p < 0.0001$) to salinity (not shown), indicating a consistent predominance of terrestrial sources of DOM to the region.

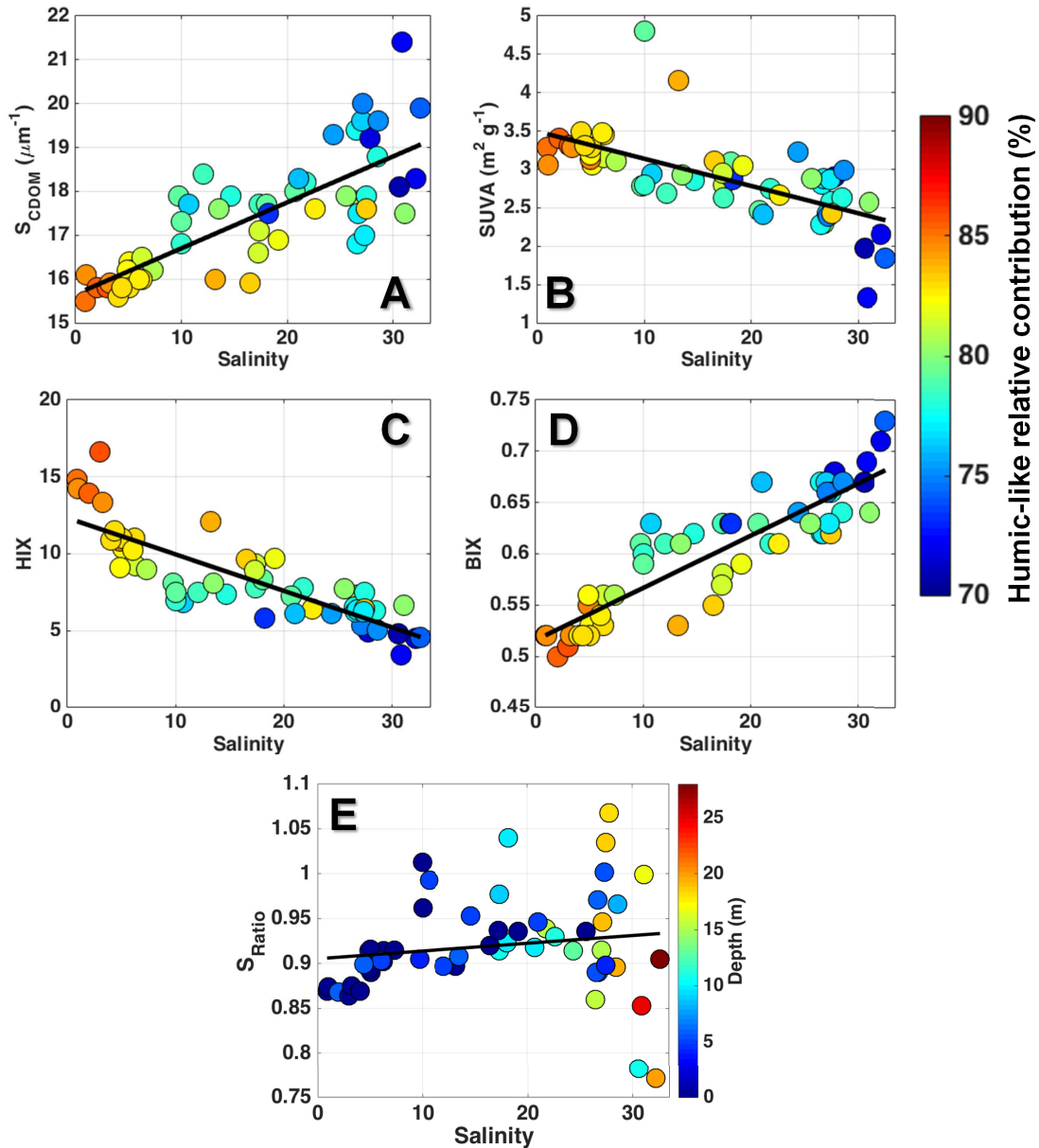


Figure 3.5. The relationship between the optical indices of DOM modification and salinity for all the samples: S_{CDOM} (μm^{-1}) (A); SUVA ($m^2 g^{-1}$) (B); HIX (C); BIX (D); S_{Ratio} (E). Colorbar indicates the relative contribution (%) of the humic-like signal (C1+C2+C4+C5) to the total FDOM (A-D) and depth (m; E). Black lines indicate the regression lines between each parameter and salinity.

3.4. Discussion

3.4.1. Characterization and transformation of DOM

The results characterize the DOM composition (here using the EEM/PAFARAC approach and optical indices of DOM modification) along the fresh water-marine gradient within the Lena delta region and Laptev Sea. Four of the six fluorescent components identified by PARAFAC analysis, three humic-like (C1, C2 and C5) and one protein-like (C6) (see Figure 3.4-center),

were already reported in the Lena River and in other large Arctic rivers [Walker *et al.*, 2013]. In addition, a recent study reported the presence of three of those components (C1, C2 and C6) in the Amerasian basin [Guéguen *et al.*, 2015], which seem to be common components of the Arctic DOM pool. Although our sampling was carried out during a period of mid discharge flow [Stedmon *et al.*, 2011], C1 and C2 presented similar fluorescence intensities to the average observed for the Lena River during the discharge peak (~ 1.6 and 0.9 nm^{-1} , respectively) [Walker *et al.*, 2013]. C5 and C6, on the other hand, presented intensities close to the average observed in the Lena during the mid discharge flow (see Figure 3.4-right column) [Walker *et al.*, 2013]. Our results demonstrate that the FDOM composition in the Lena Delta region was mainly characterized by the dominance of riverine humic-like compounds. This is evidenced by the high contribution of the allochthonous humic-like components with fluorescence in the visible range (C1, C2, C4 and C5) observed in relation to the total FDOM (Figure 3.4), as well as by the optical indices of DOM modification (Figure 3.5). A recent study has identified PARAFAC components similar to our humic-like C1 (also referred in the literature as the classical peak C) and C4, which presented strong correlation to lignin phenol concentrations [Yamashita *et al.*, 2015]. Dominance of humic-like compounds has been already reported in the Lena Delta in late summer 1995, when high concentrations of lignin, and high contribution of terrigenous DOC (about 60% of total DOC) were observed [Kattner *et al.*, 1999]. The humic-like component 1 is a dominant component of the FDOM signal not only in the Lena River and Delta, but it has also been found to be dominant in other Arctic rivers such as Mackenzie, Kolyma, Ob and Yenisei [Walker *et al.*, 2009, 2013], in the Amerasian basin [Guéguen *et al.*, 2015] and in shelf waters in the North Atlantic [Kowalczyk *et al.*, 2009; Yamashita *et al.*, 2013]. In accordance to the results obtained with the EEM/PARAFAC approach, the optical indices of DOM modification have also pointed to a dominance of humic-like compounds within the samples (see Figure 3.5).

Despite the dominance of allochthonous humic-like components over the entire sampled area, autochthonous components (such as the marine-humic like C3 and the protein-like C6) have their relative contribution (to total FDOM signal) enhanced towards high salinity (see colorbar in Figure 3.5). Increased relative contribution of C6 was also observed during the base flow of the Lena River, when the terrestrial input is reduced [Walker *et al.*, 2013]. In addition, the component C6, also referred in other studies as tryptophan-like, seems to be a useful indicator of bioavailability of DOM, given the strong correlation showed by it and total dissolved amino acids concentrations [Yamashita *et al.*, 2015]. The increase observed in the relative contribution of autochthonous compounds towards the high salinity waters of the Laptev Sea shelf region was also evident when observing the ranges presented by the optical indices of DOM modification (see Figure 3.5). Furthermore, those indices can provide

more information on the transformation of the DOM during the transit from the river to the outer shelf. The use of optical indices has been successfully applied to assess the transformation of DOM along wide salinity ranges in some estuary regions worldwide [Benner and Opsahl, 2001; Helms *et al.*, 2008, 2014; Huguet *et al.*, 2009; Asmala *et al.*, 2014]. The values obtained for the optical indices at low salinity in our study are in agreement with previous studies conducted in the Lena River. For instance, those studies have reported S_{CDOM} , SUVA and BIX values around $16 \mu\text{m}^{-1}$, $2.8 \text{ m}^2 \text{ g}^{-1}$ and 0.52, respectively [Stedmon *et al.*, 2011; Walker *et al.*, 2013]. All the optical indices taken into account in this study demonstrated that the DOM in the Lena delta region experiences an evident transformation along the riverine-marine transition. This is supported by the reduction on the molecular weight, aromaticity and humification degree of DOM observed towards high salinity, with the more photochemically reactive compounds associated to the surface (with lower salinity) layer and components with more refractory character being associated to the high salinity-Laptev Sea shelf waters (Figure 3.5). The possible mechanisms driving the observed transformation in DOM are discussed in the following section.

3.4.2. Dynamics and fate of DOM in the Lena delta region

The hydrographic observations during our campaign revealed strong gradients, with noticeable northward propagation of the Lena River plume along the study region. This generated a shallow, low salinity surface mixed layer with strong stratification, which separates the surface layer from the underlying high salinity layer with Laptev Sea shelf water (see Figure 3.1). The propagation of the plume along the Laptev Sea shelf has also induced the establishment of a strong frontal system in the NW part of our study area (see Figure 3.1). Such hydrographic characteristics were previously described as offshore wind conditions, when the predominant winds from the continent drive the offshore propagation of the Lena waters generating a strong stratification and a frontal system NW of the Lena Delta region [Bauch *et al.*, 2009; Wegner *et al.*, 2013]. Thus, we have identified the presence of two hydrographic provinces within the sampled area: the plume- and marine-influenced sites (see Figure 3.1).

The noticeable variability in hydrographic conditions due to the dynamics between fresh water input from the Lena River and the Laptev Sea shelf waters were also reflected in the striking differences of the amount and composition of DOM (Figures 3.2 and 3.3). The association of the highest DOM concentrations with the low salinity waters of the Lena outflow decreasing towards the high salinity Laptev Sea shelf waters (see Figure 3.2) re-emphasizes the importance of the Lena River as a major source of DOM to the Laptev Sea. Such inverse relationship has previously been indicated for

this region [Cauwet and Sidorov, 1996; Kattner et al., 1999; Alling et al., 2010; Semiletov et al., 2013; Heim et al., 2014] and it is the case for many other estuary regions [Benner and Opsahl, 2001; Guo et al., 2007; Huguet et al., 2009]. Both CDOM and DOC were highly correlated, displaying a similar relationship as found for the coastal Canadian Arctic [Walker et al., 2009] (see Figure 3.2), although with a higher a_{350} relative to DOC in the Lena delta waters. The presented values are comparable to other studies previously conducted in this region, with a_{350} (a_{440}) values of about 15 m^{-1} (2.9 m^{-1}) at low salinity and DOC concentrations ranging from 500-700 to $100 \mu\text{M}$ at low and high salinity, respectively [Alling et al., 2010; Stedmon et al., 2011; Semiletov et al., 2013; Walker et al., 2013; Heim et al., 2014; Dubinenkov et al., 2015a].

Our results show a coupled relationship between DOM and the two hydrographic provinces identified in this work. Plume-influenced stations presented higher DOM concentrations at surface as compared to marine-influenced stations ($p < 0.001$; see Figure 3.1). Despite these differences within the surface layers, both hydrographic provinces exhibited similar patterns regarding the relationship between DOM and salinity. Distinct DOM mixing patterns (in relation to salinity) were observed for samples above and below the pycnocline, i.e. the low and high salinity layers, respectively (Figure 3.6). The mixing curves derived from samples above the pycnocline exhibited higher slope than the ones below it (see Figures 3.2, 3.3 and 3.6). The same pattern is observed when looking at the results from an expedition conducted at the Lena Delta region in September 2005 [see Figure 9 in Semiletov et al., 2013]; however, the possible causes of this pattern were not addressed in that study. We suggest that such an increase in the slope of the relationship can be interpreted as a non-conservative decrease in DOM concentration along with the surface layer. This DOM removal in the surface (lower salinity) layer occurred despite the short residence time (of about 2 months) the Lena River plume waters in the Laptev Sea [Alling et al., 2010]. Release/production of the components C5 and C6 was observed along the entire riverine-marine transition (see Figure 3.4, right panel). The autochthonous protein-like C6 is known to be released by microbial metabolism [Romera-Castillo et al., 2010; Fukuzaki et al., 2014] and its release in our sampling area can be related to the microbial community presented within the region. On the other hand, the humic-like C5 could have had its release associated with photoproduction, given that some humic-like components, such as alkyl, have been shown to be produced via that process [Helms et al., 2014]. Although the components C5 and C6 presented indication of release/production along the riverine-marine transition, the contribution of those components to the total fluorescence signal was small (less than 20%). Thus, the overall DOM mixing curve mirrored the curves displayed by C1-C4 (accounting for more than 80% of the total FDOM signal), with a removal of DOM at low salinities and a conservative mixing behavior related to the saltier Laptev Sea shelf waters.

Non-conservative mixing characterized by removal at low salinities seems to be a characteristic shared by other estuarine regions in the Baltic Sea [Kowalczyk *et al.*, 2010; Asmala *et al.*, 2014].

Given the strong stratification observed within the sampled area, we assume that exchanges between surface and underneath layer are limited [Kara *et al.*, 2000b] compared to well-mixed conditions. As a result, the humic-like-dominated, highly photo-reactive DOM [Helms *et al.*, 2014; Timko *et al.*, 2015] is exposed longer to photochemical degradation [Fichot and Miller, 2010]. This process is evidenced by the relationship between S_{Ratio} and salinity (Figure 3.5e), with high S_{Ratio} values (>0.95) observed in intermediate salinity (10-20). Furthermore, the influence of particulate matter and sediments in coastal and shelf environments has to be taken into account given their influence on DOM removal through the process of sorption and flocculation [Uher *et al.*, 2001; Shank *et al.*, 2005; Guo *et al.*, 2007; Asmala *et al.*, 2014]. The flocculation process, in turn, can be increased either due to the presence of the salt in the marine water [Asmala *et al.*, 2014, and references therein] and to the exposition to high light intensities that, together with photochemical processes, can synergistically enhance the DOM removal from the dissolved phase [von Wachenfeldt *et al.*, 2008; Porcal *et al.*, 2013, 2015]. A sharp decrease in POC concentrations at low salinity has been reported in the Lena delta region and was attributed to sinking of particles [Cauwet and Sidorov, 1996]. We speculate that the main drivers on the apparent removal of highly humic content DOM observed within the surface layer are the photodegradation and flocculation, given the high susceptibility of those aromatic carbons to those processes [von Wachenfeldt *et al.*, 2008; Porcal *et al.*, 2013, 2015; Asmala *et al.*, 2014; Helms *et al.*, 2014]. Those processes have also been indicated to modulate the non-conservative mixing behavior in other estuaries such as the Mississippi delta [Benner and Opsahl, 2001]. Our findings from late summer 2013 corroborate the indication of DOM removal within the region as observed in late summer 2008 [Alling *et al.*, 2010]; however, with a more refined spatial coverage, we have demonstrated that the removal of DOM occurs mostly in the low salinity surface layer (Figure 3.6).

Considering that the impact of temperature increases to the Arctic and Siberian environments, an increase in permafrost thawing rates, changes in the freshwater budget, catchment vegetation and hydrology and subsequent DOM discharge into the Arctic Ocean are expected [Peterson *et al.*, 2002; McClelland *et al.*, 2004; Frey and McClelland, 2009]. As a consequence, changes in concentration and composition of DOM are expected, given the release of ancient DOM trapped in the permafrost layer due to its thaw [Aiken *et al.*, 2014; O'Donnell *et al.*, 2014], and given the variability of DOM composition in response to variations in river discharge [Walker *et al.*, 2013]. Subsequently, with an enhanced input of DOM (especially CDOM) into the

Arctic Ocean, changes in the radiant heating in the upper meters of the ocean as well as a possible increase in the sea-ice melt rates might be foreseen [Granskog *et al.*, 2015]. Furthermore, the characteristics of DOM have been shown to be a powerful proxy for tracing organic substances with permafrost origin [Aiken *et al.*, 2014; O'Donnell *et al.*, 2014; Dubinenkov *et al.*, 2015a]. Moreover, long-term studies concerning the quantification, composition and dynamics of DOM, from fresh to marine waters in the main rivers flowing into the Arctic Ocean, are needed to improve the understanding of DOM dynamics, its role in the carbon cycle pathways. Thus, a better comprehension of DOM composition and its fate, as presented in this study, can be used as baseline for further monitoring of the sources, biogeochemical implications and export of riverine DOM with regard to climate change effects in northern Siberian environments and Arctic Ocean.

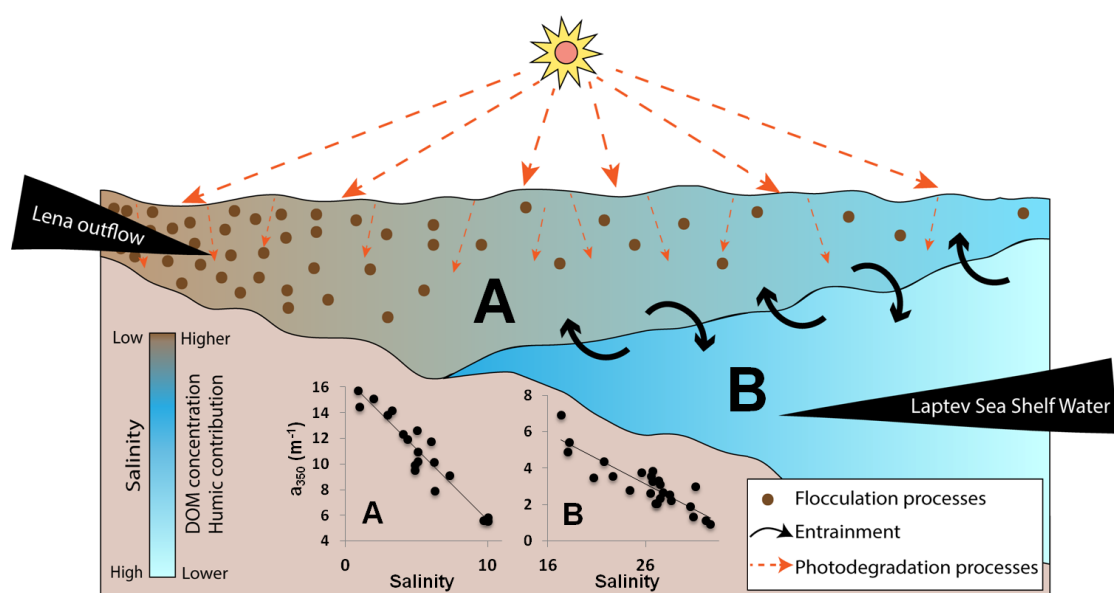


Figure 3.6. Schematic diagram showing the complex interactions occurring in the Laptev Sea continental shelf, close to the Lena River delta region. The vertical distribution of the two water masses found within the region (Lena River plume and Laptev Sea Shelf waters) is presented. A strong gradient between the two water masses with limited exchanges between them is depicted. Salinity, DOM concentration and the humic-like contribution are shown in the colorbar. The main removal processes within the surface layer (photodegradation and flocculation) are demonstrated by the symbols presented in the inset legend. Inset graphs show the DOM (a_{350} ; m^{-1}) against salinity plots for the Lena plume (A) and Laptev Sea shelf Waters (B).

3.5. Summary

This study brings new insights on the composition, transformation and fate of DOM in the Lena Delta region. DOM composition evaluated through

PARAFAC modeling showed dominance of strong humic-like signal over the entire sampled area. We have demonstrated that the dynamics between the Lena River outflow and Laptev Sea shelf waters is the main driver controlling the hydrographical conditions and, consequently, the DOM behavior within the region. Higher DOM concentrations (also with higher humic-like content) were associated to the low salinity waters of the Lena River that showed to be the main DOM source for the region. The concentration of DOM, as well as its humic-like content and reactivity, decreased along the fresh water-marine gradient towards high salinity. Although being limited by sampling within a synoptic scale, we have identified different mixing behaviors of DOM coupled with the dynamics between the Lena River plume and the Laptev Sea shelf waters, which were expressed through the vertical structure of the water column: a sharper decrease in DOM concentration in relation to salinity is observed in waters above the pycnocline, under influence of the low salinity waters from the continental runoff. This indicates that different processes modulating the distribution, composition and reactivity of DOM occur within the two layers and that there is evidence of removal of DOM in the surface mixed layer. Thus, we suggest photodegradation and flocculation as the main drivers on modulating the removal of highly humified DOM within the surface layer of the Lena Delta region.

3.6. Acknowledgements

The authors acknowledge the Captain and the crew of the R/V “Dalnie Zelentsy” and the researchers E. Druzhkova and K. Bobrov for their assistance during the field sampling. We are thankful to the logistics department of the Alfred Wegener Institute (AWI) particularly Waldemar Schneider for the support, and to Sonja Wiegmann for the work in the laboratory. This work was funded by the Helmholtz Impulse Fond (HGF Young Investigators Group Phytooptics), and by the Presidium of Russian Academy of Sciences program "Prospecting fundamental research in the interest of the Russian Arctic Zone development in 2014-2015" through the project "Biological resources of the Russian Arctic Seas: current state, influence of natural changes and anthropogenic impacts, scientific principles and perspectives of use". R.G.-A. is funded by a PhD fellowship from the Coordination for the Improvement of Higher Level Personnel (CAPES - Brazil) in collaboration with the German Academic Exchange Service (DAAD), and a visiting fellowship from the Helmholtz Graduate School for Polar and Marine Research (POLMAR - AWI). C.S. acknowledges funding from Danish Research Council for Independent Research (DFF 1323- 00336). B.H. acknowledges grants from the German Science Foundation (DFG 4575) and the Helmholtz Climate Initiative REKLIM.

Chapter 4

Using fluorescent dissolved organic matter to trace and distinguish the origin of Arctic surface waters

Manuscript published in Scientific Reports (2016)

4. Using fluorescent dissolved organic matter to trace and distinguish the origin of Arctic surface waters

Rafael **Gonçalves-Araujo**^{1,2,3*}, Mats A. **Granskog**⁴, Astrid **Bracher**^{1,5},
Kumiko **Azetsu-Scott**⁶, Paul A. **Dodd**⁴, and Colin A. **Stedmon**^{3**}

¹Alfred Wegener Institute Helmholtz Centre for Polar and Marine Research (AWI), Climate Sciences Division, Physical Oceanography of Polar Seas, Bussestraße 24, 27570 Bremerhaven, Germany

²University of Bremen, Faculty of Biology and Chemistry (FB2) - PO Box 330440, 28334 Bremen, Germany

³Technical University of Denmark, National Institute for Aquatic Resources, Section for Marine Ecology and Oceanography, Kavalergården 6, 2920 Charlottenlund, Denmark

⁴Norwegian Polar Institute, Fram Centre, Postbox 6606 Langnes, 9296 Tromsø, Norway

⁵University of Bremen, Institute of Environmental Physics, PO Box 330440, 28334 Bremen, Germany

⁶Fisheries and Ocean, Canada, Bedford Institute of Oceanography, PO Box 1006, Dartmouth, Nova Scotia, BY2 4A2 Canada

***Corresponding author:** rafael.goncalves.araujo@awi.de

****Corresponding author:** cost@aqua.dtu.dk

Abstract

Climate change affects the Arctic with regards to permafrost thaw, sea-ice melt, alterations to the freshwater budget and increased export of terrestrial material to the Arctic Ocean. The Fram and Davis Straits represent the major gateways connecting the Arctic and Atlantic. Oceanographic surveys were performed in the Fram and Davis Straits, and on the east Greenland Shelf (EGS), in late summer 2012/2013. Meteoric (f_{mw}), sea-ice melt, Atlantic and Pacific water fractions were determined and the fluorescence properties of dissolved organic matter (FDOM) were characterized. In Fram Strait and EGS, a robust correlation between visible wavelength fluorescence and f_{mw} was apparent, suggesting it as a reliable tracer of polar waters. However, a pattern was observed which linked the organic matter characteristics to the origin of polar waters. At depth in Davis Strait, visible wavelength FDOM was correlated to apparent oxygen utilization (AOU) and traced deep-water DOM turnover. In surface waters FDOM characteristics could distinguish between surface waters from eastern (Atlantic+modified polar waters) and western (Canada-basin polar waters) Arctic sectors. The findings highlight the potential of designing *in situ* multi-channel DOM fluorometers to trace the freshwater origins and decipher water mass mixing dynamics in the region without laborious samples analyses.

4.1. Introduction

Arctic rivers supply high loads of freshwater and dissolved organic matter (DOM) to the Arctic Ocean [Dittmar and Kattner, 2003; Cooper *et al.*, 2005; Stedmon *et al.*, 2011]. A major fraction of this DOM, which is mobilized from high latitude carbon-rich soils and peatlands [Opsahl *et al.*, 1999; Benner *et al.*, 2004], is transported across shelf seas [Fichot *et al.*, 2013] and is widely distributed across the surface waters of the Arctic Ocean. This makes the Arctic Ocean globally unique being highly impacted by both freshwater and terrestrial organic carbon compared to other ocean basins [Opsahl *et al.*, 1999]. With the expected permafrost thaw due to the effects of global warming over the Arctic [Schuur *et al.*, 2013], changes in freshwater export, production of DOM in river catchments and riverine transport of organic material into the shelf seas are foreseen [Frey and McClelland, 2009; Vonk *et al.*, 2012].

The strong relationship between riverine DOM and freshwater in the Arctic Ocean presents the opportunity of using DOM measurements to isolate and trace the contribution of Arctic riverine freshwater to the Arctic surface waters [Stedmon *et al.*, 2015]. Inflow from the Pacific Ocean through the Bering Strait is also an important component of the Arctic Ocean freshwater budget due to its lower salinity [Jones *et al.*, 1998; Beszczynska-Möller *et al.*, 2012]. In addition to regional input from North American and East Siberian rivers the

high productivity of the Chukchi shelf results in these waters also having a high DOM signal although less terrestrial in nature [Stedmon *et al.*, 2011]. Initial studies have indicated that the optical properties of DOM in surface and halocline (polar) waters of the Eurasian and Canada basin differ [Stedmon *et al.*, 2011] and suggest that there may be potential to utilize this to trace the contribution of these two freshwater sources to water exiting the Arctic Ocean into the North Atlantic through the two major gateways; Fram Strait and the Canadian Arctic Archipelago (CAA)/Davis Strait. It is important to understand the fate and any changes in the export of Arctic freshwater as two major sites of meridional overturning circulation bottom water formation lie directly in recipient waters; the Nordic Seas and the Labrador Sea [Aagaard and Carmack, 1989].

The Fram Strait is characterized by two main currents: to the west, the Arctic outflow carrying the cold polar waters, and to the east the Atlantic inflow [Rabe *et al.*, 2009; Beszczynska-Möller *et al.*, 2012]. Additionally, it has been demonstrated that there is recirculation of Atlantic water within the region [Hattermann *et al.*, 2016]. During summer, the polar waters are characterized by a shallow surface layer influenced by high fractions of seasonal sea-ice melt forming a low salinity surface layer over the underlying polar waters with brine excess and high fractions of meteoric water (a combination of river water, precipitation and glacial melt) [Jones *et al.*, 2008; Dodd *et al.*, 2012]. After passing through the Fram Strait, the polar waters are transported along the east Greenland shelf by the East Greenland Current (EGC). On the eastern side of Fram Strait, the Atlantic inflow is primarily characterized by warm and saline Atlantic water with little or no influence from meteoric waters [Rabe *et al.*, 2009; Beszczynska-Möller *et al.*, 2012; Dodd *et al.*, 2012].

The Davis Strait, at approximately 67 °N between Canada and Greenland, represents a transition from Arctic to North Atlantic environments. In the western Davis Strait, the Baffin Island Current (BIC) transports polar waters southwards, towards the Labrador Sea [Tang *et al.*, 2004; Curry *et al.*, 2014]. These waters have similar characteristics to their equivalent in Fram Strait: relatively low salinity, near freezing temperatures, high meteoric water fractions and brine excess [Alkire *et al.*, 2010; Azetsu-Scott *et al.*, 2012]. The surface waters of eastern Davis Strait are mainly characterized by the presence of the West Greenland Shelf Water (WGSW) and the West Greenland Irminger Water (WGIW). The WGSW originates from the EGC after it turns northward at the southern tip of Greenland, and continues as the West Greenland Current (WGC) [Tang *et al.*, 2004; Curry *et al.*, 2014]. The WGIW is of Atlantic origin (high temperature and salinity) and is transported northward along the western Greenland slope by the West Greenland Slope Current (WGSC), parallel to WGC [Tang *et al.*, 2004; Curry *et al.*, 2014].

A fraction of DOM is colored (CDOM) absorbing light (especially in the ultraviolet – UV – range), and in the Arctic this influences light and heat penetration in surface waters [Granskog *et al.*, 2015; Pavlov *et al.*, 2015]. When present in high concentrations CDOM imparts a brown color to water easily visible by eye or in satellite ocean color measurements near the mouths of Arctic rivers [Fichot *et al.*, 2013]. Despite considerable dilution the color signal from Arctic riverine CDOM can be easily traced across the Arctic. In addition the spectral properties of the absorption spectrum can be used to differentiate between contrasting CDOM sources such as marine productivity and rivers [Stedmon *et al.*, 2011]. A fraction of CDOM also emits a fluorescence signal (hereafter FDOM) which provides not only quantitative information on DOM, but also qualitative information regarding the composition and origin [Coble, 2007]. Fluorescence measurements are well suited for *in situ* sensors and studies have shown that visible wavelength DOM fluorescence (VIS-FDOM) can be linked to Arctic upper halocline waters [Amon *et al.*, 2003; Cooper *et al.*, 2005] and used to map DOM distribution at higher resolution. Detailed measurement and characterization of DOM fluorescence properties offers the potential to optimize the design and use of these *in situ* fluorometers, which typically measure at single excitation and emission wavelength pairs. Laboratory-based spectroscopic analysis of DOM results in an excitation-emission-matrix (EEM), which maps the UV-visible fluorescence properties. These EEMs represent a combined quantitative and qualitative measure of different signals present in FDOM, which can subsequently be separated into independent underlying DOM components using Parallel Factor Analysis (PARAFAC). Some of those components have been shown to match with fluorescence of specific organic compounds [Wünsch *et al.*, 2015] and are related to some DOM molecular species [Stubbins *et al.*, 2014; Wagner *et al.*, 2015]. PARAFAC characterization of FDOM has been recently used to assess DOM variability in the Arctic Ocean [Dainard *et al.*, 2015; Gonçalves-Araujo *et al.*, 2015b; Guéguen *et al.*, 2015], and here we seek to build on this and link the distribution of different FDOM components to bulk water fractions and mixing. Although having a less sensitive signal in comparison to FDOM [Blough and Del Vecchio, 2002; Coble, 2007], CDOM has shown to be a robust proxy for halocline (polar) waters [Granskog *et al.*, 2012; Stedmon *et al.*, 2015]. Based on that this study aims primarily to assess the potential of FDOM, especially VIS-FDOM, as a tracer of polar waters along two important export pathways of Arctic waters: Fram Strait (as well as the eastern Greenland shelf) and Davis Strait. Secondly the biogeochemical dynamics of FDOM was evaluated in Davis Strait. The results here can be further applied on the development of *in situ* profilers, as well as autonomous platforms (such as ROVs and AUVs), focusing on monitoring the freshwater fluxes exiting the Arctic Ocean. Moreover, it would increase the sampling resolution and accelerate the data processing, given that waters samples (especially $\delta^{18}\text{O}$, alkalinity and nutrient

analysis) would be taken only for calibration purposes and lab work time would be reduced.

4.2. Methods

4.2.1. Sampling strategy

Samples for salinity, dissolved organic matter fluorescence (FDOM), dissolved inorganic nutrients (nitrate and phosphate) and $\delta^{18}\text{O}$ were collected during several cruises around Greenland (Figure 4.1a). Two cruises were along a section in the Fram Strait at 78°55'N in Aug/Sep of 2012 and 2013 onboard *R/V Lance*, hereafter referred to as Fram2012 and Fram2013, respectively. A cruise onboard *R/V Dana* (September 2012, hereafter EGC2012) collected samples in the Denmark Strait region, Iceland Sea and along a number of sections across the EGC. Data from Fram2012 and EGC2012 cruises (including hydrography, water fractions and CDOM absorption) are also presented in other study [Stedmon *et al.*, 2015]. In addition, samples were collected across the Davis Strait onboard *R/V Knorr* (September 2013, hereafter Davis2013). During all cruises temperature and salinity profiles were acquired with a CTD attached to a rosette system at all the stations, which was calibrated with salinity from water samples.

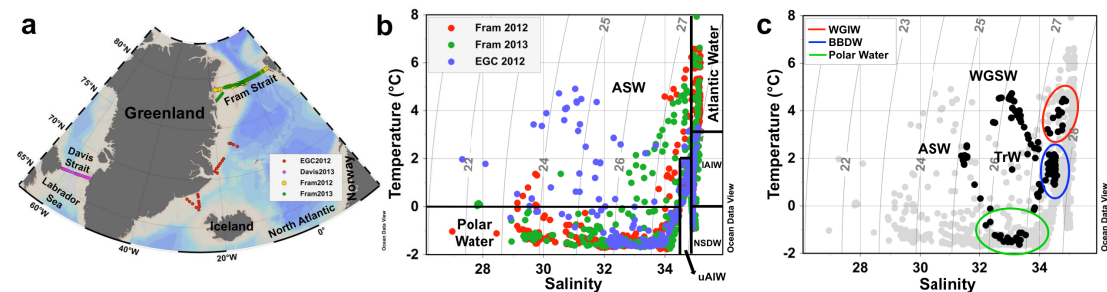


Figure 4.1. Study area and water masses. (a) Map of the study area and sampling stations in 2012 and 2013. **(b)** T-S diagram for all the oceanographic stations (except Davis2013) considered for this study with the identified water masses [Swift and Aagaard, 1981; Pavlov *et al.*, 2015] (Table S1): Atlantic Water, Polar Water, Arctic Surface Water (ASW), upper Arctic Intermediate Water (uAIW), lower Arctic Intermediate Water (IAIW) and Norwegian Sea Deep Water (NSDW). **(c)** T-S diagram showing the eastern Greenland cruises (gray) and Davis2013 (black) with the identified water masses for the latter region (adapted from Tang *et al.* [Tang *et al.*, 2004], Azetsu-Scott *et al.* [Azetsu-Scott *et al.*, 2012], Curry *et al.* [Curry *et al.*, 2014]): West Greenland Shelf Water (WGSW), West Greenland Irminger Water (WGIW), Polar Water, Arctic Surface Water (ASW), Baffin Bay Deep Water (BBDW) and Transitional Water (TrW). Isopycnals [potential density (σ , kg m^{-3})] are indicated as gray lines in (b) and (c). Produced with Ocean Data View [Schlitzer, 2015].

4.2.2. Analyses of salinity, dissolved inorganic nutrients, dissolved oxygen and $\delta^{18}\text{O}$

For calibration of the CTD, salinity samples were collected in glass bottles and analyzed using a Guildline 8410A Portasal salinometer (Fram and EGC). For the Fram2012, Fram2013 and EGC2012 cruises, nutrient samples were collected directly into acid-washed polyethylene bottles and frozen immediately after collection, and were kept at $-20\text{ }^{\circ}\text{C}$ until analysis. Nutrient analyses were conducted at Aarhus University (Roskilde, Denmark) using an autoanalyzer (Skalar) [Hansen and Koroleff, 1999]. For those cruises, $\delta^{18}\text{O}$ samples were collected in 40 mL glass vials that were filled completely, closed tightly and sealed with Parafilm, and were analyzed by equilibration with carbon dioxide. Measurements were carried out with isotope ratio mass spectrometers at the G.G. Hatch Stable Isotope Laboratory, University of Ottawa, Canada (Thermo Delta Plus XP).

For the Davis2013 cruise nutrient samples were frozen and later analyzed at Bedford Institute of Oceanography, Canada, following the World Ocean Circulation Experiment (WOCE) protocols using a Technicon Autoanalyzer with the precision of 0.19 mmol kg^{-1} for nitrate and nitrite ($\text{NO}_3 + \text{NO}_2$), and 0.04 mmol kg^{-1} for phosphate (PO_4). Oxygen isotope samples were collected in 60 mL Amber Boston Rounds with Poly-Seal-Lined caps secured with electrical tape, stored at room temperature. They were analyzed with a FISIONS PRISM III with a Micromass multiprep automatic equilibration system at Lamont-Doherty Earth Observatory, USA. Two-milliliter subsamples were equilibrated with CO_2 gas (8 h at $35\text{ }^{\circ}\text{C}$). Data are reported with respect to standard mean ocean water (SMOW) with the $\delta^{18}\text{O}$ notation. The external precision based on replicates and standards is $\pm 0.033\text{‰}$. Additionally, 293 samples for dissolved oxygen were collected only in the Davis2013 cruise and analyzed using Winkler titration (with precision of 0.5%), to calibrate oxygen sensors on CTD.

4.2.3. DOM samples processing

Water samples for DOM analysis (CDOM and FDOM) were collected through pre-rinsed $0.2\text{ }\mu\text{m}$ Millipore Opticap XL filter capsules, except on the EGC2012 cruise precombusted GF/F filters (nominal pore size $0.7\text{ }\mu\text{m}$) were used. The samples were stored in pre-combusted amber glass vials in dark at $4\text{ }^{\circ}\text{C}$ until analysis at the Technical University of Denmark, within two months of collection (Fram and Davis Straits) or analyzed immediately onboard (EGC2012). It should be noted that the optimal situation would be to have all samples $0.2\text{ }\mu\text{m}$ filtered (removing bacteria and colloids) and analyzed immediately onboard however, logistical constraints and practicalities of collaborative sampling hindered this. An analysis of histograms of the fluorescence properties of DOM from the Fram Strait (sterile filtered and

stored) and the EGC (GFF and analyses immediately) indicated no clear systematic bias resulting from the two approaches.

4.2.4. Spectroscopic measurements and PARAFAC modeling

CDOM absorbance was measured across the spectral range from 250 to 700 nm using a Shimadzu UV–2401PC spectrophotometer and 100 mm quartz cells with ultrapure water as reference [Stedmon and Markager, 2001]. Absorbance was used to correct fluorescence EEMs.

Fluorescence EEMs were collected using an Aqualog fluorescence spectrometer (HORIBA Jobin Yvon, Germany). Fluorescence intensity was measured across emission wavelengths 300–600 nm (resolution 1.64 nm) at excitation wavelengths from 250 to 450 nm, with 3 nm increments, and an integration time of 8 s. EEMs were corrected for inner-filter effects and for Raman and Rayleigh scattering [Murphy *et al.*, 2013] (Figure 5, top panel). The underlying fluorescent components of DOM in the EEMs were isolated by applying PARAFAC modeling using the “drEEM Toolbox” [Murphy *et al.*, 2013]. In this study different PARAFAC model fits were explored. At first, individual PARAFAC models were derived and split-half validated for each cruise individually. The split-half analysis consists in producing identical models from independent subsamples (halves) of the dataset, generally randomly generated. Similar PARAFAC components were identified (Figure 5, bottom panel) and these results were then compared to a model derived on the combined dataset (1022 samples). The fluorescent components derived from PARAFAC modeling were compared with PARAFAC components from other studies using the OpenFluor database [Murphy *et al.*, 2014].

4.2.5. Water masses fractionation

The fractions of meteoric water (f_{mw}), sea-ice melt water (f_{sim}), Pacific seawater (f_{pw}) and Atlantic seawater (f_{aw}) in discrete water samples were derived using a combination of procedures established by Östlund and Hut [Östlund and Hut, 1984] and Jones *et al.* [Jones *et al.*, 1998] as described in Dodd *et al.* [Dodd *et al.*, 2012]. The details behind the choice of end-member values and for the sensitivity of the estimates of freshwater fractions to variations in the end-member composition can be found in Jones *et al.* [Jones *et al.*, 2008], Dodd *et al.* [Dodd *et al.*, 2012] and Hansen *et al.* [Hansen *et al.*, 2012]. In brief, the contribution from Atlantic water, Pacific water, meteoric water, and sea-ice melt was carried out with the following equations:

$$P_{pw} = 0.065N + 0.94, \quad (4.1)$$

$$P_{aw} = 0.060N + 0.120, \quad (4.2)$$

$$f_{mw} + f_{sim} + f_{pw} + f_{aw} = 1 \quad (4.3)$$

$$f_{mw}S_{mw} + f_{sim}S_{sim} + f_{pw}S_{pw} + f_{aw}S_{aw} = S, \quad (4.4)$$

$$f_{mw}\delta^{18}O_{mw} + f_{sim}\delta^{18}O_{sim} + f_{pw}\delta^{18}O_{pw} + f_{aw}\delta^{18}O_{aw} = \delta^{18}O, \quad (4.5)$$

$$f_{mw}P_{mw} + f_{sim}P_{sim} + f_{pw}P_{pw} + f_{aw}P_{aw} = P, \quad (4.6)$$

N and P in the equations above correspond to the nitrate and phosphate concentrations, respectively (Figure S1a). The salinity (S) of meteoric water, sea-ice melt, Pacific water, and Atlantic water were 0, 4, 32.0, and 34.9, respectively, and the $\delta^{18}O$ end-members -18.4 , 0.5 , -1.3 , and 0.3 , respectively [Dodd *et al.*, 2012].

4.3. Results

4.3.1. Water mass distribution

Six water masses were identified in Fram Strait, on east Greenland shelf and Iceland Sea, based on published thermohaline characteristics [Swift and Aagaard, 1981; Pavlov *et al.*, 2015] (Table S4.1), as shown on the T-S diagram (Figure 4.1b): Atlantic Water, Polar Water and Arctic Surface Water (ASW) in the surface layer ($< \sim 200$ m); and upper and lower Arctic Intermediate Water (uAIW and lAIW, respectively) and Norwegian Sea Deep Water (NSDW) in the deep layers. In Davis Strait a similar pattern for the temperature versus salinity relation was observed, however with lower salinity values (Figure 4.1c). For Davis Strait the following water masses were observed: West Greenland Shelf Water (WGSW), West Greenland Irminger Water (WGIW), Polar Water, Arctic Surface Water (ASW), Transitional Water (TrW) at depth > 300 m and Baffin Bay Deep Water (BBDW) at depth > 900 m (adapted from Tang *et al.* [Tang *et al.*, 2004], Azetsu-Scott *et al.* [Azetsu-Scott *et al.*, 2012], Curry *et al.* [Curry *et al.*, 2014]). In cruises east of Greenland temperature ranged from -1.77 °C to 7.92 °C with the highest values associated with Atlantic Water in eastern Fram Strait (Figures 4.1b, 4.2a and 4.3a). In Davis Strait the highest temperatures (> 3 °C) were associated with WGSW and WGIW (in eastern Davis Strait) whereas the lowest values (down to -1.63 °C) were found within the Polar Water in the western Davis Strait (Figures 4.1c and 4.4a). Salinity in Fram Strait and east Greenland shelf varied typically between 28 and 35 with highest salinity associated with Atlantic Water and the deeper waters ($> \sim 500$ m; lAIW and NSDW), while the lowest values were observed in surface waters in central Fram Strait and inner Greenland shelf (Figures 4.1b, 4.2b and 4.3b). In Davis Strait, salinity ranged from 31.40 to 34.87, with highest salinity in warm subsurface waters of WGIW and TrW (Figures 4.1c and 4.4b). BBDW occupied the deepest parts of the Davis Strait section (> 750 m) and had lower temperatures than the layer above it, characterized by TrW. The distribution of apparent oxygen utilization (AOU) in Davis Strait showed a clear pattern with lowest values (< 60 $\mu\text{mol kg}^{-1}$) in western Greenland and surface waters, whereas these

values increase toward the bottom layer reaching up to $216 \mu\text{mol kg}^{-1}$ within BBDW (Figure 4.4i). Although we have sampled for temperature and salinity over the entire water column, in Fram Strait we hereafter focus our results on the surface layer (300 m).

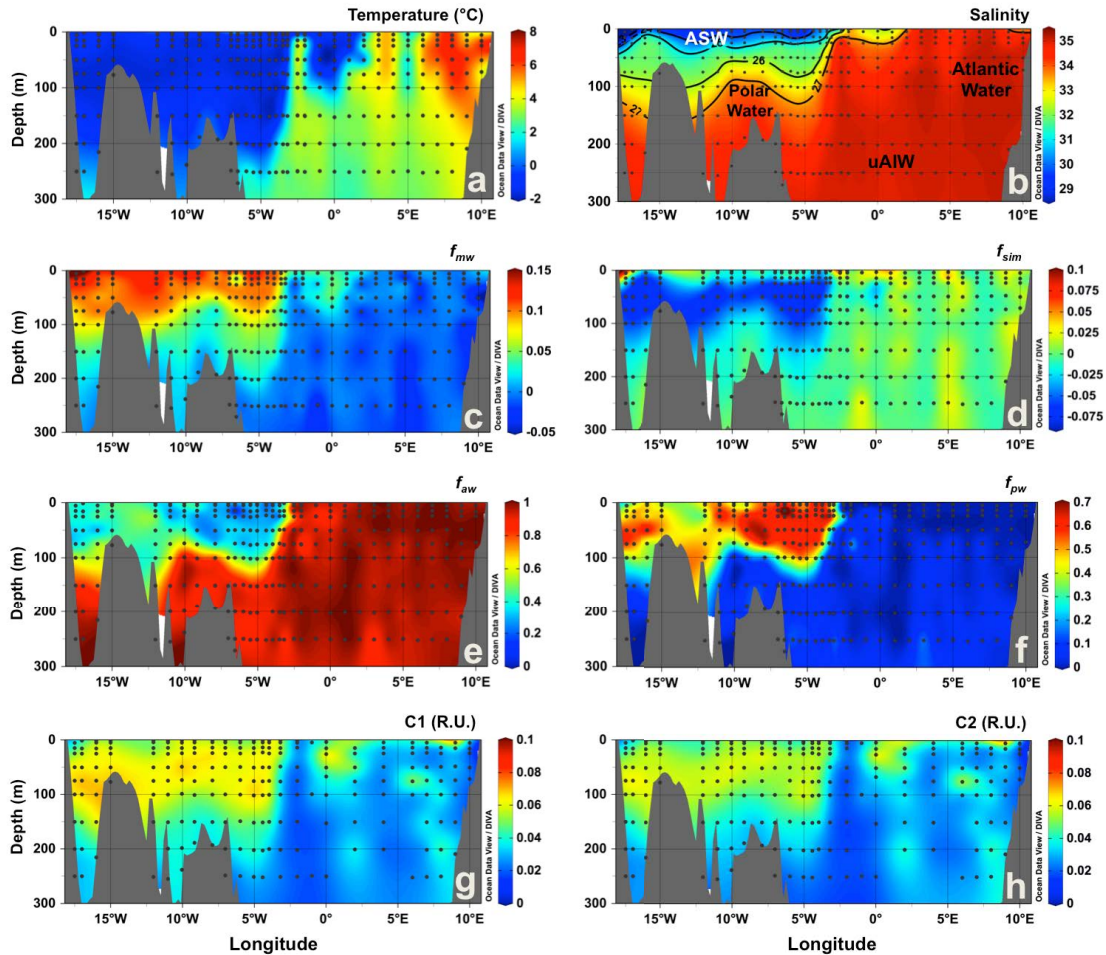


Figure 4.2. Vertical sections across the surface layer of Fram Strait in September 2012. (a) temperature ($^{\circ}\text{C}$), (b) salinity, fractions of (c) meteoric water (f_{mw}), (d) sea-ice melt (f_{sim}), (e) Atlantic water (f_{aw}), and (f) Pacific water (f_{pw}), (g) C1 (R.U.) and (h) C2 (R.U.). In (b) black lines indicate the potential density (σ , kg m^{-3}) and the abbreviations indicate the position of the water masses defined based on T-S diagrams (Figure 1). Produced with Ocean Data View [Schlitzer, 2015].

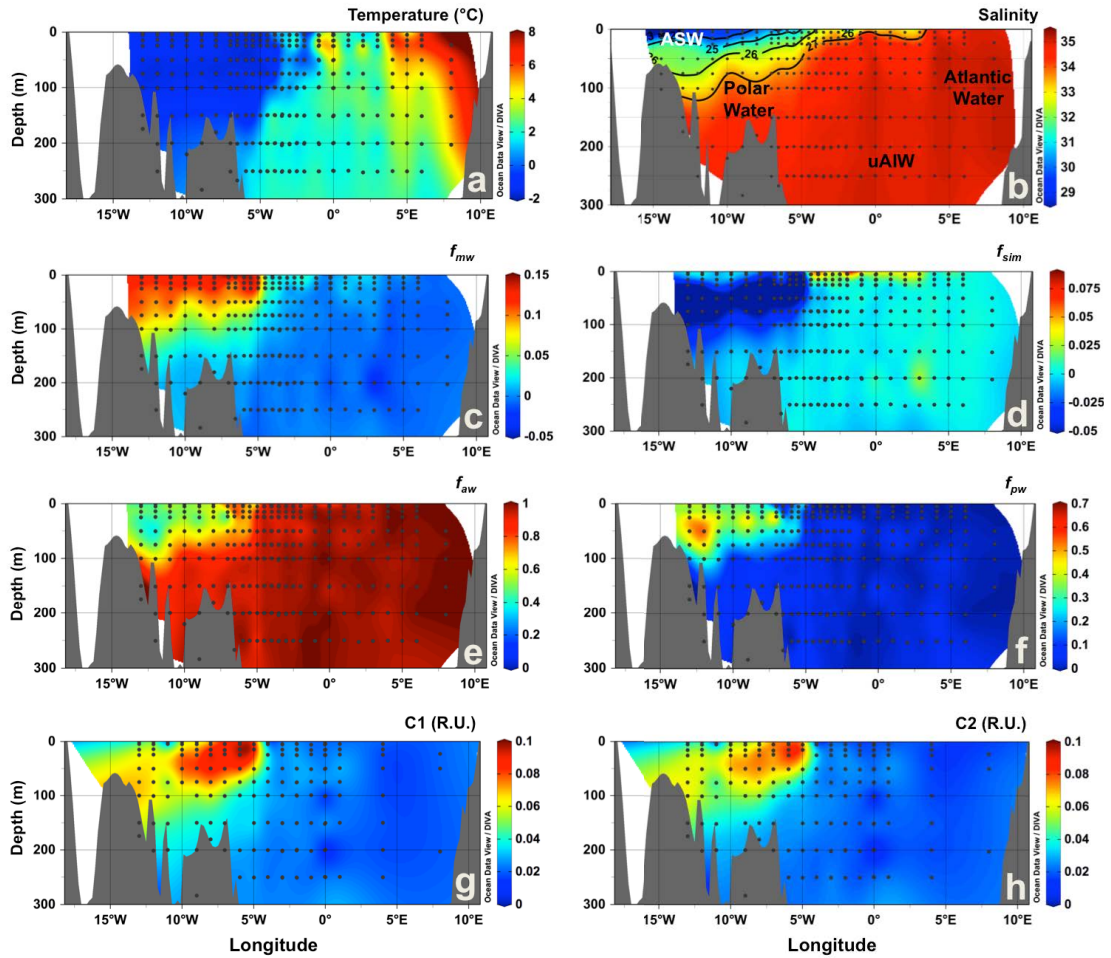


Figure 4.3. Vertical sections across the surface layer of Fram Strait in September 2013. (a) temperature ($^{\circ}\text{C}$), (b) salinity, fractions of (c) meteoric water (f_{mw}), (d) sea-ice melt (f_{sim}), (e) Atlantic water (f_{aw}) and (f) Pacific water (f_{pw}), (g) C1 (R.U.) and (h) C2 (R.U.). In (b) black lines indicate the potential density (σ , kg m^{-3}) and the abbreviations indicate the position of the water masses defined based on T-S diagrams (Figure 1). Produced with Ocean Data View [Schlitzer, 2015].

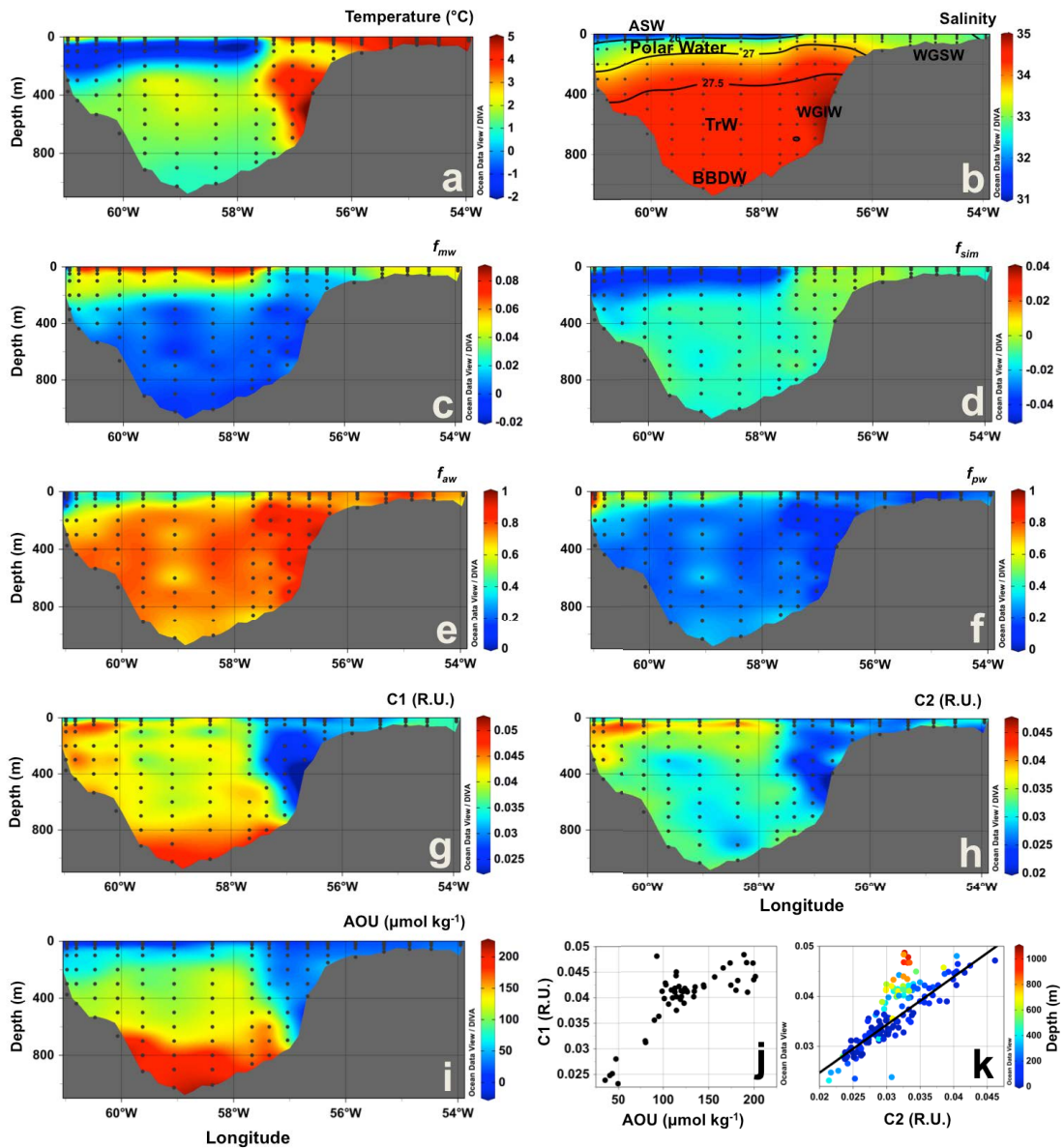


Figure 4.4. Vertical sections across Davis Strait in September 2013. (a) temperature ($^{\circ}\text{C}$), (b) salinity, fractions of (c) meteoric water (f_{mw}), (d) sea-ice melt (f_{sim}), (e) Atlantic water (f_{aw}) and (f) Pacific water (f_{pw}), (g) C1 (R.U.), (h) C2 (R.U.) and (i) apparent oxygen utilization (AOU, $\mu\text{mol kg}^{-1}$). (j) AOU ($\mu\text{mol kg}^{-1}$) vs. C1 (R.U.) for samples under influence of TrW and BBDW (below 300 m). (k) C2 vs. C1 plots for all the samples collected in the Davis Strait 2013, with colorbar indicating depth (m). In (b) black lines indicate the potential density (σ , kg m^{-3}) and the abbreviations indicate the position of the water masses defined based on T-S diagrams (Figure 1). Produced with Ocean Data View [Schlitzer, 2015].

4.3.2. Dissolved organic matter fluorescence characterization

Three fluorescent components (C1–C3) were identified during the different PARAFAC runs. C1 and C2 had broad emission and excitation spectra, with emission maxima at visible wavelengths, whereas C3 had an

emission maximum at ultraviolet-A wavelengths (UV-A) (Figure 4.5, bottom panel). The fluorescence intensities of C1 and C2 ranged from 0 to 0.1 and to 0.09 R.U., respectively, with highest values observed in the polar waters in Fram Strait (Figures 4.2g-h and 4.3g-h). In Davis Strait, C1 and C2 fluorescence values were notably lower, only reaching 0.05 and 0.04 R.U., respectively (Figure 4.4g-h). In surface waters (depth <300 m) C1 and C2 were significantly correlated ($C1 = 1.109 * C2 + 0.001$; $r^2=0.99$; $p<0.0001$), however, this correlation was not apparent in Davis Strait deep waters (Figure 4.4k). There was a clear addition of C1 in TrW and BBDW, without a proportional increase in C2.

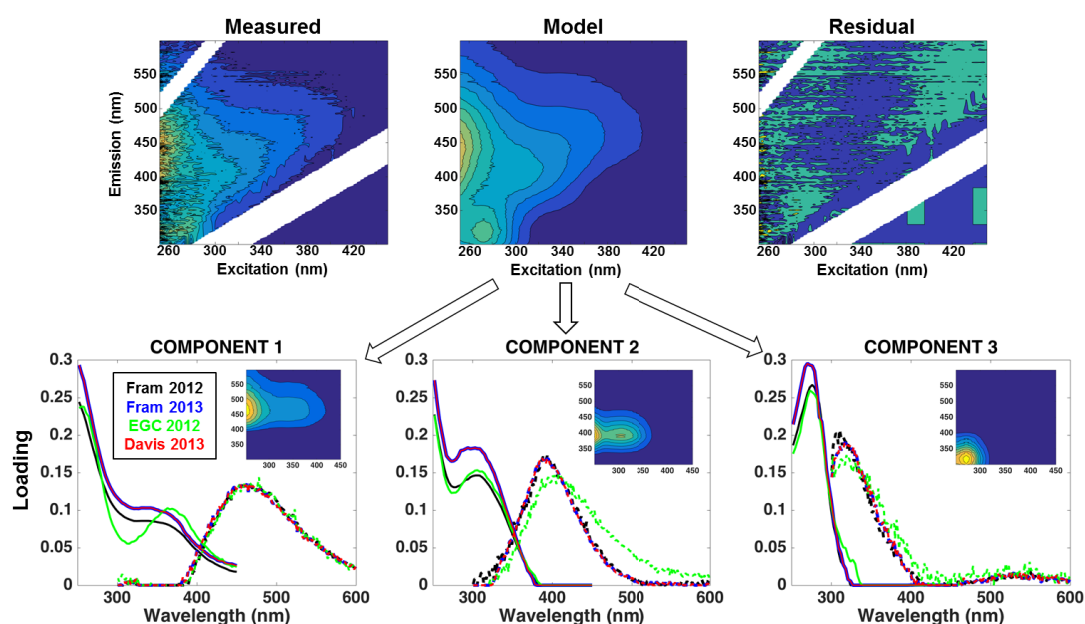


Figure 4.5. PARAFAC model and isolated components. (top) Three-dimensional fluorescence landscapes example of the measured, modeled and residual EEMs of the PARAFAC analysis. **(bottom)** The excitation (solid line) and emission (dashed line) spectra for the three fluorescent components identified by PARAFAC model for each of the cruises. Inset plots show the three-dimensional fluorescence landscapes for each of the final PARAFAC-derived component used in this work (with all cruises merged into one dataset).

The UV-A fluorescence signal of C3 ranged typically from 0 to 0.04 R.U. and was independent of C1 or C2. Its fluorescence was linked to productivity in surface waters, rather than water mass distribution, as evident from the significant correlation between C3 and chlorophyll-a fluorescence ($r^2=0.65$, $p<0.0001$; Figure S4.2c). Across the region fluorescence intensities of C3 were generally higher in surface waters (Figure S4.2b) and profiles often exhibited maxima at or just below phytoplankton chlorophyll fluorescence maxima (Figure S4.2a).

4.3.3. Distribution of water fractions

In Fram Strait and on east Greenland shelf f_{mw} and f_{pw} followed the distribution patterns of C1. The highest values for f_{mw} and f_{pw} were observed on the Greenland shelf, associated with the cold, high DOM, polar waters exiting the Arctic (Figures 4.2c, 4.2f, 4.3c and 4.3f). These waters also had negative f_{sim} values indicating the fact that freshwater has been lost to sea-ice formation and they have experienced brine accumulation in the Arctic Basin (Figures 4.2d and 4.3d). In surface waters f_{sim} was generally less negative or even positive representing the contribution of freshwater from seasonal sea-ice melt. Warmer waters off the Greenland shelf and further east were largely of Atlantic origin with high f_{aw} (Figures 4.2e and 4.3e). Pacific water contribution (f_{pw}) to the polar waters on the Greenland Shelf in Fram Strait was significantly higher in 2012 than in 2013 ($p < 0.001$) (Figures 4.2f and 4.3f).

Some similarities in the distribution of the waters masses in Fram Strait could be observed in Davis Strait (Figure 4.4c-f). In western Davis Strait, cold polar waters occupied the sub-surface layer, characterized by sub-zero temperatures and high contribution of f_{mw} (Figure 4.4c). Similarly the highest f_{sim} values were at the very surface (0-30 m), indicating sea-ice melt, and the lowest (negative values) were associated with the polar waters in western Davis Strait (Figure 4.4d). The f_{aw} was the most dominant fraction on the west Greenland shelf and in deeper waters (Figure 4.4e). The contribution of Pacific water (f_{pw}) was associated with the cold polar waters exported from the Arctic (Figure 4.4f).

4.3.4. Linking visible organic matter fluorescence to water fractions

The T-S diagram (Figure 4.6a) shows a clear distinction of polar waters exiting the Arctic, with respect to C1. Highest C1 fluorescence was associated with polar waters and ASW. The latter had comparatively lower values, indicating the dilution of surface waters by sea-ice melt and precipitation (glacial input and snow). The correlation of C1 with both temperature (not shown) and salinity (Figure 4.6b-d) presented a very similar, however tighter, pattern than portrayed by absorption alone [Granskog *et al.*, 2012; Stedmon *et al.*, 2015]. When considering the salinity versus C1 relation for each cruise individually (except for Davis Strait), two distinct mixing curves for the dilution of polar waters are apparent (Figure 4.6). C1 was also strongly inversely correlated to f_{sim} (Figure S4.3) linking the high DOM signal to brine. In Davis Strait, different patterns were observed. The relationships C1 and C2 vs. salinity indicate two mixing curves (Figure 4.7) in agreement with the mixing curves visible on the T-S diagram (Figure 4.7a-b), where a clear separation of stations from eastern and western Davis Strait is apparent. The correlation between C1 and C2 in the East Greenland data could be harnessed tested if

the FDOM in the Davis Strait had the same characteristics (relative proportions of C1 and C2) and hence similar origins. A regression was derived for C1 fluorescence based on C2 considering all the surface data (<200 m). This was then applied to the Davis Strait data to predict expected C1 fluorescence, C1*, for the surface layer in Davis Strait. The difference between measured and predicted C1 fluorescence, C1–C1*, is plotted against C2 (Figure 4.7d) and indicates significant differences ($p < 0.05$) between eastern and western Davis Strait DOM. Samples in eastern Davis Strait have similar properties to those from the Fram Strait, whereas on the Canadian side of the strait the DOM has comparatively less C1. Finally for Davis Strait deep waters (>300 m), C1 was highly correlated with AOU, with the highest values of both parameters in BBDW (Figures 4.4g and 4.4i). C2 showed no indication of elevated values at depth (Figure 4.4h).

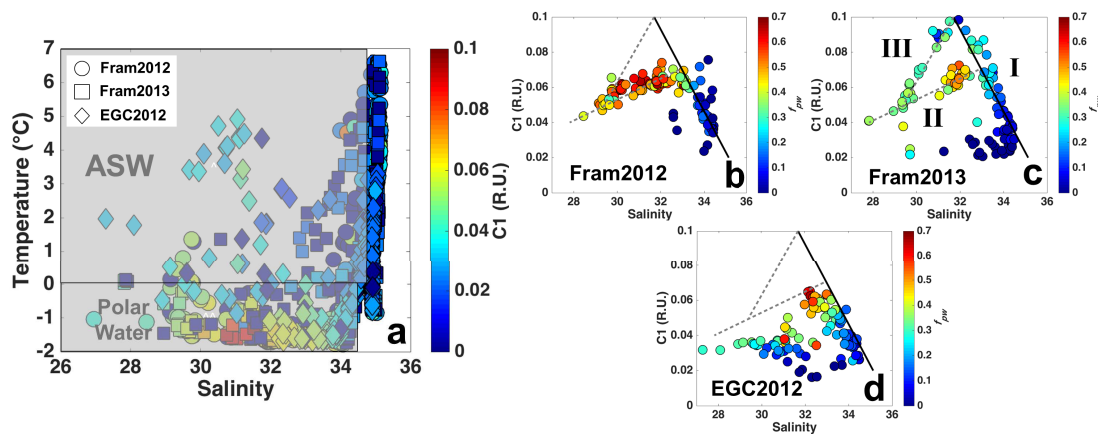


Figure 4.6. T-S diagram and correlations between salinity and C1 in the east of Greenland. (a) Temperature (°C) vs. salinity with colorbar indicating C1 (R.U.) for all the samples collected in the eastern Greenland cruises. (b-d) Salinity vs. C1 (R.U.) and f_{pw} as colorbar for polar waters and ASW for each of the eastern Greenland cruises. Black solid line (I) indicates the mixing curve for the polar waters (based on Fram 2012 and 2013 datasets). Gray dashed lines (II and III) indicate the two distinct mixing curves of polar waters over the Greenland shelf. The regressions were obtained by combining the three datasets. (I) $y = -0.02 * (\text{Sal}) + 0.723$, $r^2 = 0.90$, $p < 0.0001$, $n = 240$. (II) $y = 0.0042 * (\text{Sal}) - 0.0698$, $r^2 = 0.90$, $p < 0.0001$, $n = 126$. (III) $y = 0.0183 * (\text{Sal}) - 0.4816$, $r^2 = 0.98$, $p < 0.0001$, $n = 18$.

4.4. Discussion

The distribution of the water fractions in the surface layer (0–300 m) of the Fram Strait followed the overall patterns and values reported for the region [Dodd *et al.*, 2012; Granskog *et al.*, 2012; Rabe *et al.*, 2013] (Figures 4.2c-f and 4.3c-f). Similar hydrographic features were also observed in the distributions of temperature and salinity (Figures 4.2ab, 4.3ab), agreeing with previous reports [Rabe *et al.*, 2009; Beszczynska-Möller *et al.*, 2012; Pavlov

et al., 2015]. f_{mw} was related to the Arctic outflow through the EGC and the highest values (up to 0.15) were observed in the western section and aligned with earlier reports [Rabe et al., 2009; Dodd et al., 2012; Granskog et al., 2012; Stedmon et al., 2015]. Evidence for sea-ice melt was apparent in the surface layer with generally more positive f_{sim} values than immediately below. f_{sim} and f_{mw} were inversely correlated in polar waters indicating the origins from brine rejection during sea ice formation on coastal waters influenced by riverine inputs [Bauch et al., 2011b; Dodd et al., 2012; Stedmon et al., 2015]. The f_{pw} was associated with polar waters with values up to 0.7, and within the range reported in previous multi-year analysis conducted in the region [Dodd et al., 2012]. Interannual variability in the contributions of f_{pw} to polar waters exiting the Arctic Ocean in the Fram Strait is related to variability in atmospheric forcing, and consequently ocean surface circulation, over the Arctic [Falck et al., 2005; Rabe et al., 2013].

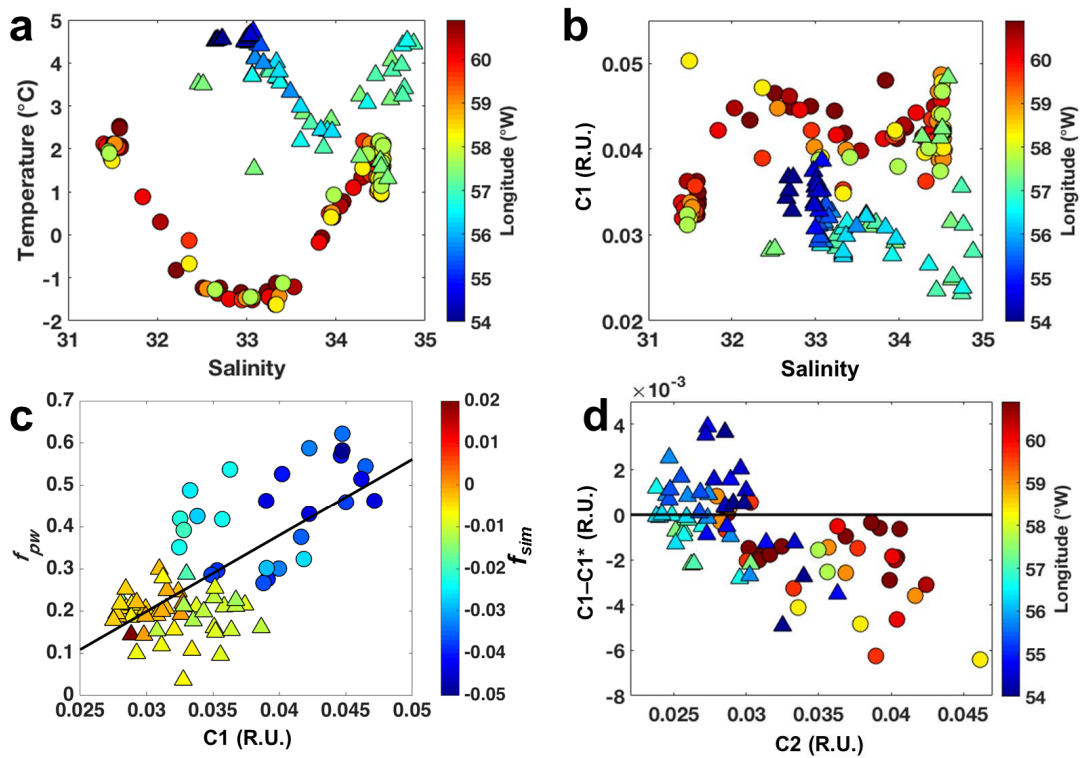


Figure 4.7. VIS-FDOM as a water mass tracer in the Davis Strait. Plots for the Davis2013 cruise. **(a)** T-S diagram with longitude (°W) as colorbar.. **(b)** Salinity vs. C1 (R.U.), with colorbar indicating longitude (°W). **(c)** C1 (R.U.) vs. f_{pw} for the surface layer (<300 m) and f_{sim} as colorbar. **(d)** C2 (R.U.) vs. C1–C1* (R.U.) for the surface layer (<300 m), with longitude (°W) as colorbar. Triangles indicate the samples within the eastern part of Davis Strait, whereas circles refer to samples located in the western sector (separated by the 57.5 °W longitude). Black line in (c) indicates the best fit.

The three fluorescent components identified by PARAFAC modeling (Figure 4.5) are similar to fluorescent components identified in previous studies conducted in Fram and Davis Straits [Guéguen *et al.*, 2014; Jørgensen *et al.*, 2014, 2015], but also in other regions of the Arctic Ocean [Guéguen *et al.*, 2011; Dainard *et al.*, 2015]. The visible wavelength fluorescence character of C1 and C2 has been linked to aromatic, high molecular weight organic matter (humic-like) with terrestrial character [Stubbins *et al.*, 2014; Wagner *et al.*, 2015] and correlated to lignin phenol concentrations [Amon *et al.*, 2003]. However, the precise chemical origin of those signals is currently unknown and the subject of much research. In Fram Strait, these components (C1 and C2; Figures 4.2g-h and 4.3g-h) presented similar distribution as CDOM (a_{350}) [Granskog *et al.*, 2012; Pavlov *et al.*, 2015; Stedmon *et al.*, 2015]. Their fluorescence intensities were highly correlated and both had their maximum associated with the relatively low salinity polar waters and ASW (Figure 4.6a) in agreement with previous *in situ* VIS-FDOM measurements (Ex: 350-460 nm; Em: 550 nm) in the region [Amon *et al.*, 2003].

The UV-A FDOM signal (C3) is associated with compounds with lower aromaticity, such as dissolved and combined amino acids [Yamashita and Tanoue, 2003a] and is often linked to aquatic productivity [Romera-Castillo *et al.*, 2010; Jørgensen *et al.*, 2011, 2014, 2015; Catalá *et al.*, 2015a]. As can therefore be expected C3 fluorescence in this study was not correlated to polar waters; but rather linked to phytoplankton productivity in surface waters (Figure S4.2). In support of this C3 fluorescence in Greenland shelf waters are correlated to amino acid concentrations [Jørgensen & Stedmon, *unpublished data*].

In Davis Strait the distributions of temperature and salinity followed previous reports [Tang *et al.*, 2004; Azetsu-Scott *et al.*, 2010, 2012; Curry *et al.*, 2014] (Figures 4.4a-b). The surface layer in western Davis Strait was occupied by sub-zero temperature polar waters, characterizing the Arctic outflow with the BIC. Similarly to the Fram Strait, the impact of freshening by seasonal sea-ice melt was observed in a shallow surface layer (~40 m) [Azetsu-Scott *et al.*, 2012; Curry *et al.*, 2014]. The bottom layer was characterized by the presence of BBDW [Azetsu-Scott *et al.*, 2012]. While the origin of this water mass is still under debate [Tang *et al.*, 2004] the high AOU values (over 220 $\mu\text{mol kg}^{-1}$) associated with it (Figure 4.4i-j) are comparable to AOU values observed for very old deep ocean waters and waters beneath productive upwelling regions [Jørgensen *et al.*, 2011].

The distribution and contribution of water fractions in Davis Strait were in agreement with previous studies applying different approaches [Alkire *et al.*, 2010; Azetsu-Scott *et al.*, 2010, 2012] (Figure 4.4c-f). As in Fram Strait, polar waters were found in the western sector, with the highest values of f_{mw} and f_{pw}

[Alkire *et al.*, 2010; Azetsu-Scott *et al.*, 2010, 2012]. However, f_{pw} contributions were greater than the ones found in Fram Strait, with values for polar waters varying between 0.5 and 1, indicating a great contribution of polar waters originating from the Canada basin. The lowest values of f_{sim} were associated with the polar waters, reflecting the fact that they have been modified by sea-ice formation. This layer was underneath a thin surface layer highly influenced by sea-ice melt [Alkire *et al.*, 2010; Azetsu-Scott *et al.*, 2010, 2012]. The contribution of f_{aw} was highest in the eastern Davis Strait, associated with the WGC [Azetsu-Scott *et al.*, 2012].

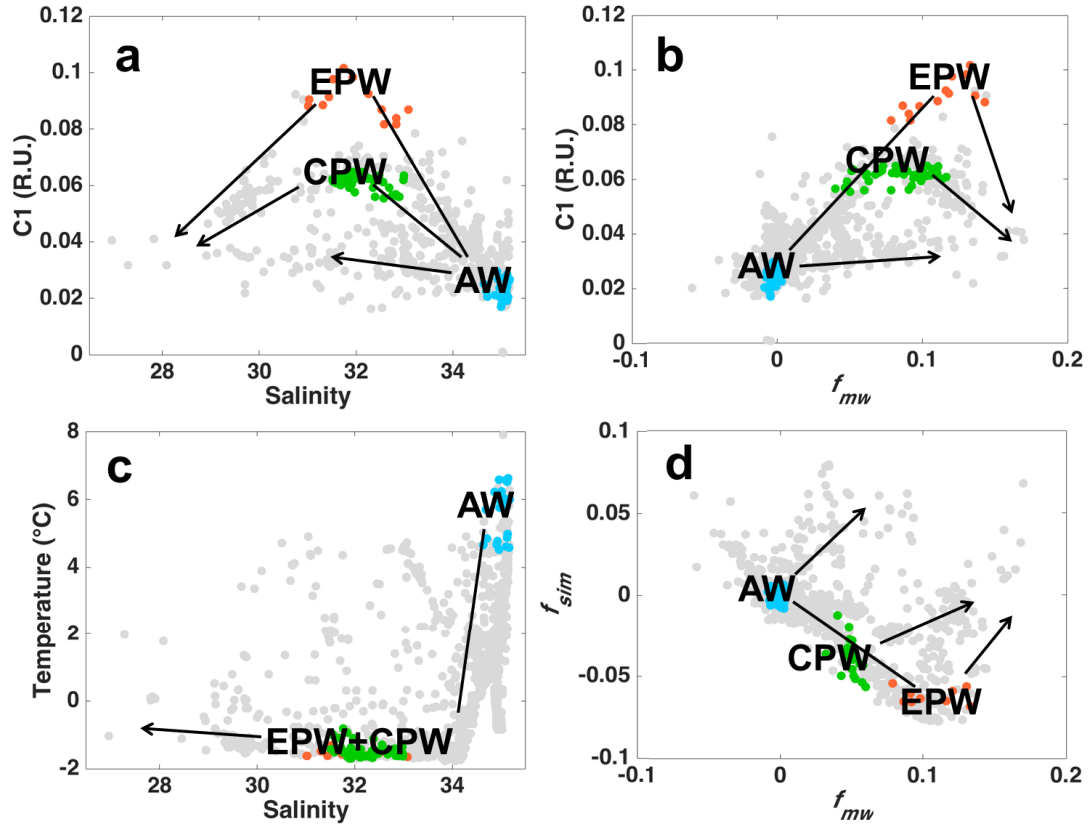
The distribution of the components C1 and C2 in Davis Strait surface waters resembled the general hydrographic conditions in the region [Azetsu-Scott *et al.*, 2010, 2012; Curry *et al.*, 2014] with the highest fluorescence intensities associated with polar outflow to the west, as portrayed in the Fram Strait. Those components were, however, found in lower concentrations than in Fram Strait polar waters. This can be due to either a greater dilution of polar waters from Canada basin passing through the CAA and Baffin Bay [Guéguen *et al.*, 2014] or an indication of lower FDOM levels in the source Canada basin polar waters relative to Eurasian Basin polar waters. The elevated levels of C1 and C2 observed on the west Greenland shelf likely originates from the diluted, reminiscent FDOM signal from polar waters transported through Fram Strait, with the EGC and subsequently the WGC (see discussion later). Although there is a detectable input of meteoric water from eastern Greenland to the EGC, there is little terrestrial DOM contribution from Greenland to shelf waters [Stedmon *et al.*, 2015].

The fluorescence intensities of C1 and C2 were highly correlated in the whole dataset; however, there were two clear exceptions. In Davis Strait deep waters there had an excess C1 relative to C2. Organic matter with these spectral characteristics has previously been linked to bacterial biomass [Rochelle-Newall and Fisher, 2002; Shimotori *et al.*, 2009], microbial respiration and degradation of organic material [Yamashita and Tanoue, 2008; Catalá *et al.*, 2015a]. Earlier studies have linked the generation of visible wavelength FDOM to AOU in ocean bottom waters [Yamashita and Tanoue, 2008; Jørgensen *et al.*, 2011], which was also proven by incubation experiments [Jørgensen *et al.*, 2014]. A similar correlation is apparent in the deep layer of the Baffin Bay for C1 vs. AOU (Figure 4.4j). Since ~90% of the oxygen consumption in the deep ocean is due to particle remineralization [Aristegui *et al.*, 2002], our results thus suggest that the observed increase in C1 at the bottom layer is likely derived from the turnover of sinking particulate organic matter. This is supported by the fact that waters from the deeper layers of Davis Strait have a relatively long residence time [Punshon *et al.*, 2014] where such a signature from the microbial production of bio-refractory material would persist and be easily detectable.

The second exception to the correlation between C1 and C2 was in the surface waters of the western Davis Strait (Figure 4.4k). If the DOM fluorescence signal in polar waters present in Davis Strait and Fram Strait would have common origins one would expect all data to lie on one relationship as dilution would influence both C1 and C2 in the same fashion. The fact that the DOM in the WGC has the same proportions of C1 and C2 as that found in polar waters of the EGC (Figure 4.7d) strongly suggests that it represents here the same material transported along the Greenland shelf and gradually diluted. In contrast, the lower levels of C1 relative to C2 in polar waters in the western Davis Strait suggest a different DOM source (Figure 4.7d). This could be reflecting the documented differences in DOM in polar waters originating from the Canada and Eurasian Basins, marine production and terrestrial material, respectively [Stedmon *et al.*, 2011]. This is supported by the correlation of C1 fluorescence to f_{pw} in Davis Strait (Figure 4.7c) and to f_{mw} in Fram Strait (Figure 4.8b).

In Fram Strait Pacific water contribution varied between 2012 and 2013. Although the Davis Strait results discussed above suggest that visible wavelength DOM fluorescence might distinguish between polar waters from Eurasian and Canada basins, there were no such systematic deviations in Fram Strait C1 vs. C2 relationship, which could be linked to Pacific water contribution. However, plots of C1 fluorescence against salinity and f_{mw} clearly reveal a segregation into three groups where polar waters highly influenced by f_{pw} (waters from Canada basin) have lower C1 fluorescence than those of Eurasian origin which have a C1 fluorescence greater than 0.08 R.U. (Figures 4.6 and 4.8). Such clear distinction between the origins of polar waters is not apparent for CDOM (a_{350}) [Granskog *et al.*, 2012; Stedmon *et al.*, 2015], most likely due to the lesser sensitivity of this bulk measurement.

Freshening of polar waters at the very surface layer (<40 m) was clearly detected in the relationship between f_{mw} and f_{sim} (Figure 4.8d), where dilution of both Atlantic and polar waters by sea-ice melt at the surface layer is apparent [Granskog *et al.*, 2012; Bauch *et al.*, 2013; Stedmon *et al.*, 2015]. Dilution of CDOM absorption (a_{350}) was observed in previous studies where samples deviating from the correlation line (to f_{mw}) indicated the dilution by sea-ice melt and/or precipitation (at the very surface layer) [Granskog *et al.*, 2012; Stedmon *et al.*, 2015]. However, the correlations observed for fluorescence in this study had a better fit than the ones for a_{350} . This can again be expected due to the general higher sensitivity of fluorescence measurements in comparison to absorbance spectroscopy [Blough and Del Vecchio, 2002]. Thus, we surmise VIS-FDOM is a more reliable tracer of polar waters and the mixing processes associated to those waters (sea-ice melt and sea-ice formation). This result holds great promise for further developments in the use of DOM visible wavelength fluorescence in tracer studies in the Arctic and warrants further investigation.



	Water mass	Temperature (°C)	Salinity	f_{mw}	f_{sim}	f_{pw}	C1 (R.U.)
AW	Atlantic Water	4.5 – 6.6 (5.6)	34.6 – 35.2 (35.0)	0	-0.01 – 0.01 (0)	0 – 0.06 (0.01)	0.02 – 0.03 (0.02)
EPW	Eurasian polar water	-1.7 – -1.3 (-1.5)	31.5 – 33.5 (32.0)	0.08 – 0.15 (0.11)	-0.07 – -0.04 (-0.06)	0.04 – 0.36 (0.24)	0.08 – 0.10 (0.09)
CPW	Canada basin polar water	-1.7 – -0.8 (-1.46)	31.5 – 33.5 (32.1)	0.04 – 0.11 (0.08)	-0.08 – -0.01 (-0.06)	0.15 – 0.67 (0.51)	0.05 – 0.06 (0.06)

Figure 4.8. Schematic graphs for eastern Greenland. Schematic graphs showing the behavior during mixing of distinct waters defined in the text (Atlantic water, Eurasian and Canada basin polar waters, whose end members in this study are colored accordingly): for (a) C1 and salinity, (b) C1 and f_{mw} , (c) temperature and salinity, (d) f_{sim} and f_{mw} . All data used in this study is shown with gray dots. Lines indicate the mixing between different waters, whose end-members for this study are tabulated below. Arrows represent the approximate direction of the deviation expected by dilution with sea-ice melt and precipitation (including glacial melt). The table shows information (range and average) on some parameters for the end members of each water type identified in this study.

4.5. Summary

The visible wavelength DOM fluorescence components identified by PARAFAC modeling were correlated to the fraction of meteoric and Pacific water determined using established techniques [Bauch et al., 2011a; Dodd et al., 2012]. The ratio of the two fluorescence signals was linked to the dominant organic matter sources in polar waters exiting the Arctic from the

Canada and Eurasian basins. In 2012 a greater fraction of Pacific waters in the Fram Strait suggests greater contribution of waters from the Canada basin which is reflected in organic matter fluorescence intensities. Such changes were not detectable from CDOM absorption measurements [Granskog *et al.*, 2012; Stedmon *et al.*, 2015]. Our results demonstrate that Eurasian polar waters have higher visible wavelength DOM fluorescence signal than waters from the Canada basin. The result also show that the organic matter exported through the Davis and Fram straits differ in quality reflecting the contrasting dominant sources of DOM in polar waters from the two basins. In addition, in deep waters of the Davis Strait there was a production of bio-refractory organic matter fluorescence signal linked to microbial respiration driven by degradation of sinking particulate matter.

The results presented here provide an indication of which wavelength regions of DOM fluorescence carry information on DOM source and mixing. As fluorescence is well suited for use *in situ* instrumentation, these measurements can aid the design of new multi-channel fluorometers for different platforms. These can provide additional insight into the physical oceanography of the region and complement current hydrographic measurements focused on monitoring freshwater fluxes and circulation.

4.6. Acknowledgements

The authors thank the captain, crew and scientists onboard *R/V Lance*, *R/V Dana* and *R/V Knorr* for their assistance during the campaigns. Study was supported by the Danish Strategic Research Council for the NAACOS project (grant 10–093903), the Danish Center for Marine Research (grant 2012-01), the Danish Research Council for Independent Research (DFF 1323- 00336). The funding for Davis Strait program comes from the U.S. National Science Foundation (ARC1022472) and the International Governance Strategy (IGS) fund for the Fisheries and Oceans, Canada. The authors acknowledge the “Fram Strait Arctic Outflow Observatory” for providing data from the Fram Strait. Authors also acknowledge the chief scientist and lead of the Davis Strait program, Dr. Craig Lee of University of Washington. R.G.-A. was supported by a PhD fellowship from the Coordination for the Improvement of Higher Level Personnel (CAPES-Brazil, Grant 12362/12-3) in collaboration with the German Academic Exchange Service (DAAD), and by an impulsive grant from the University of Bremen. M.A.G. was supported by the Polish–Norwegian Research Program operated by the National Centre for Research and Development under the Norwegian Financial Mechanism 2009–2014 in the frame of Project Contract Pol-Nor/197511/40/2013, CDOM-HEAT and the Fram Centre Ocean Acidification Flagship programme. M.A.G. and P.A.D. were supported by the Centre for Ice, Climate and Ecosystems (ICE) at the Norwegian Polar Institute.

4.7. Supplementary material

Table S4.1. Water masses classification. Thermohaline ranges used to characterize the water masses in the Fram Strait and east Greenland [Swift and Aagaard, 1981; Pavlov et al., 2015].

Water Mass	Temperature	Salinity
Atlantic Water (AW)	> 3 °C	> 34.9
Arctic Surface Water (ASW)	> 0 °C > 2 °C	< 34.4 < 34.9
Polar Water (PW)	< 0 °C	< 34.4
Upper Arctic Intermediate Water (uAIW)	< 2 °C	34.4–34.9
Lower Arctic Intermediate Water (lAIW)	0–3 °C	> 34.9
Norwegian Sea Deep Water (NSDW)	< 0 °C	> 34.9

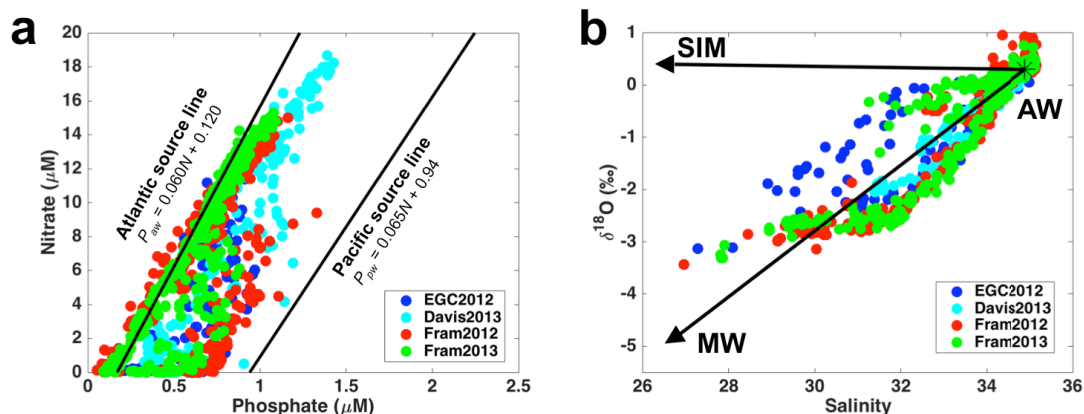


Figure S4.1. Water fractionation. (a) Phosphate (μM) vs. nitrate (μM) with the equations and source lines for the Atlantic and Pacific waters [Dodd et al., 2012]. (b) Salinity vs. $\delta^{18}\text{O}$ (‰) with the end members for Atlantic Water (AW), Meteoric Water (MW) and Sea-ice melt (SIM) and corresponding conservative mixing lines [Dodd et al., 2012].

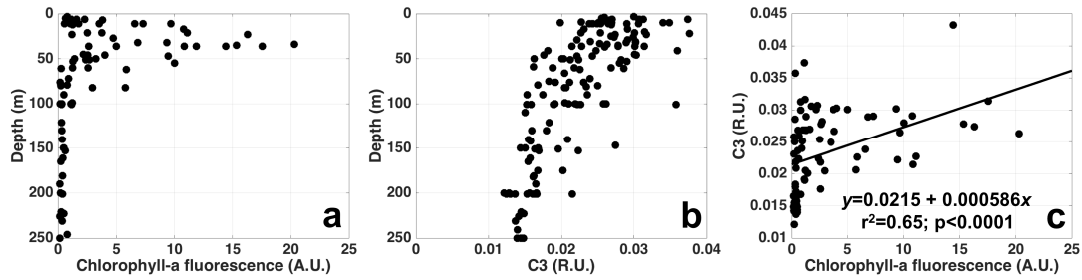


Figure S4.2. Vertical distribution of Chlorophyll-a and UV-FDOM for the EGC2012 cruise. Vertical distribution of (a) chlorophyll-a fluorescence (A.U.) and (b) C3 (R.U.) for the EGC2012 cruise, and (c) the correlation between chlorophyll-a fluorescence (A.U.) and C3 (R.U.).

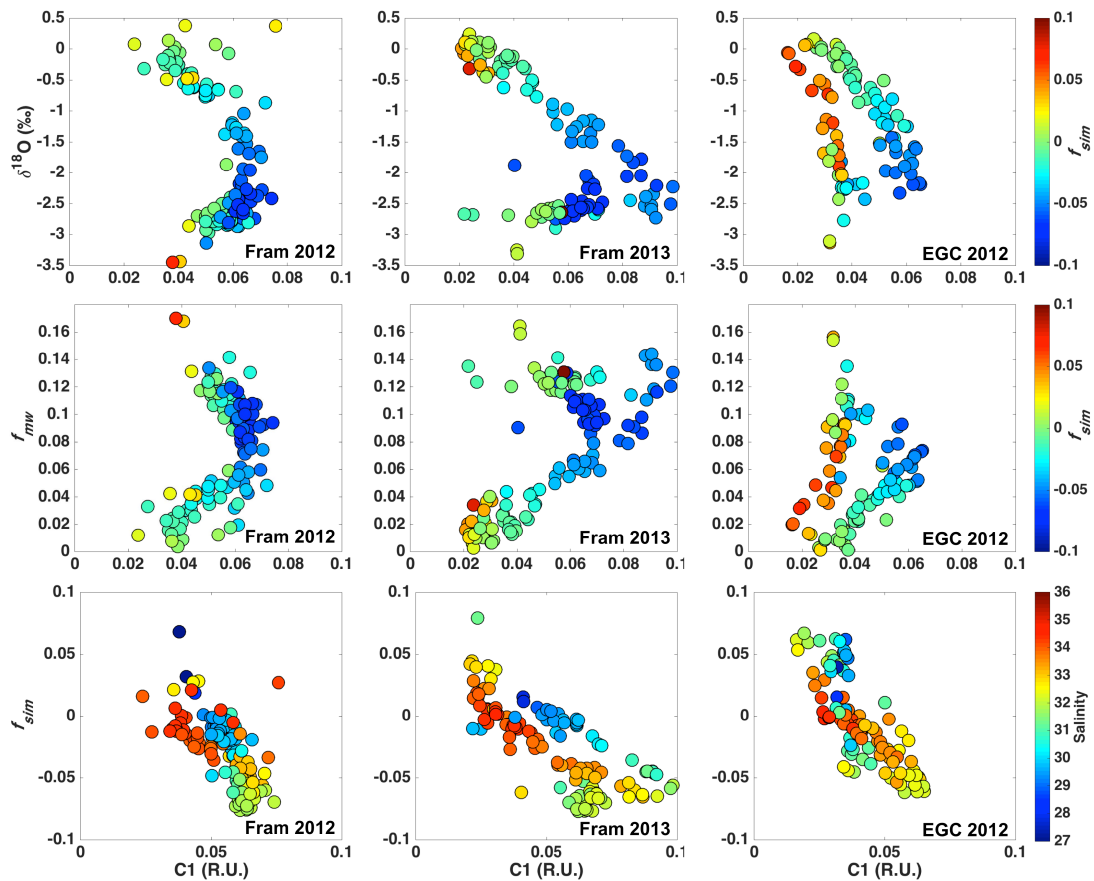


Figure S4.3. Scatter plots each of the cruises performed in the eastern Greenland, considering only PW and ASW (salinity<34.3). (top panel) C1 (R.U.) vs. $\delta^{18}\text{O}$ (‰) vs. f_{sim} . (middle panel) C1 (R.U.) vs. f_{mw} vs. f_{sim} . (bottom panel) C1 (R.U.) vs. f_{sim} vs. salinity.

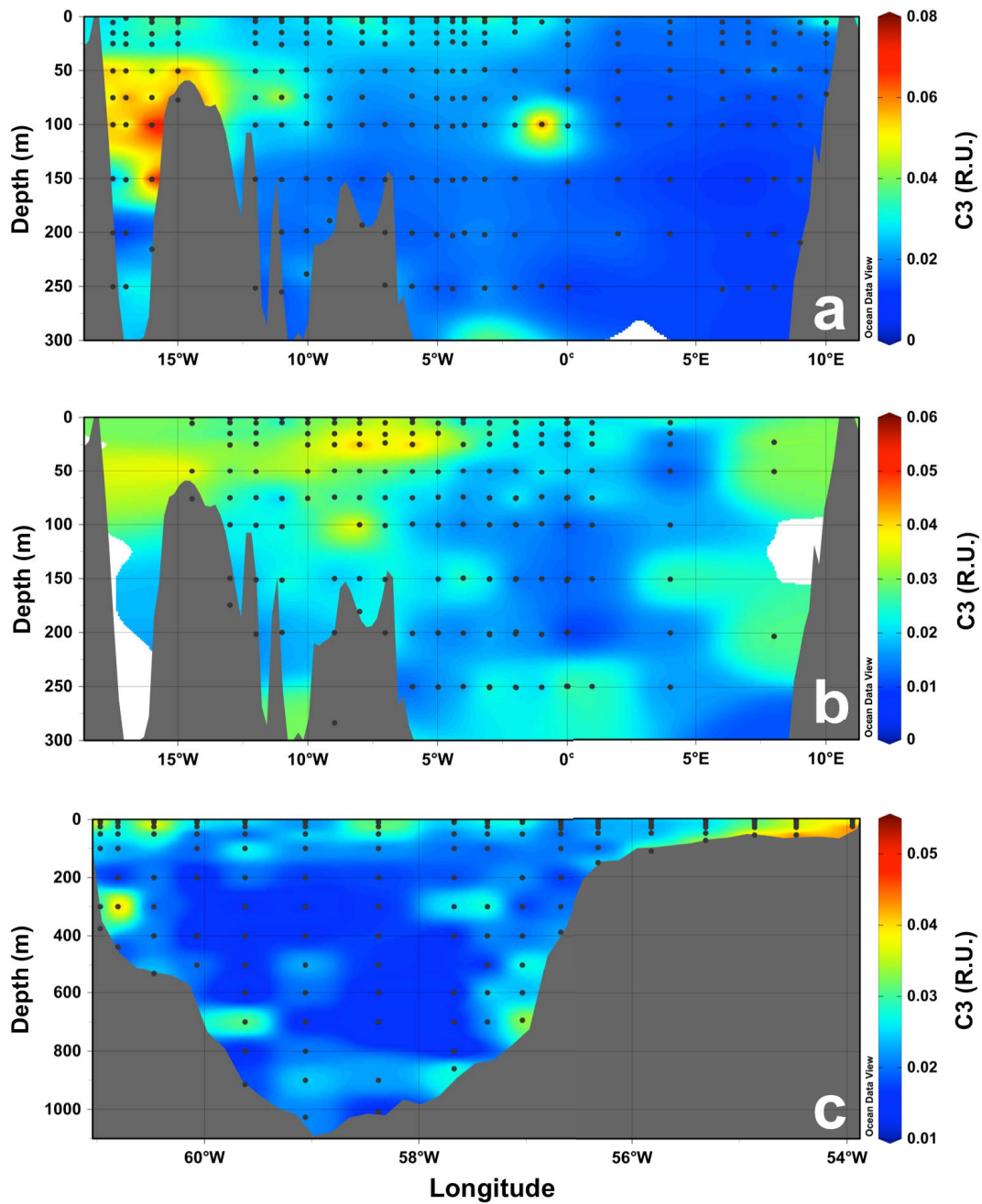


Figure S4.4. Vertical distribution of UV-fluorescent C3 (R.U.) along the transects. (a) Fram2012, (b) Fram2013 and (c) Davis2013. Note the differences in color bar ranges for the cruises. Produced with Ocean Data View [Schlitzer, 2015].

Chapter 5

High colored dissolved organic matter (CDOM) absorption by waters of central-eastern Arctic Ocean: implications for biogeochemistry and ocean color algorithms

Manuscript to be submitted

5. High colored dissolved organic matter (CDOM) absorption by waters of central-eastern Arctic Ocean: implications for biogeochemistry ocean color algorithms

Rafael Gonçalves-Araujo*^{1,2}
Benjamin Rabe³
Ilka Peeken⁴
Astrid Bracher^{1,5}

¹Phytooptics Group, Physical Oceanography of Polar Seas, Climate Sciences Division, Alfred Wegener Institute Helmholtz Centre for Polar and Marine Research, Bussestraße 24, 27570 Bremerhaven, Germany

²Faculty of Biology and Chemistry (FB-2), University of Bremen, PO Box 330440, 28334 Bremen, Germany

³Physical Oceanography of Polar Seas, Climate Sciences Division, Alfred Wegener Institute Helmholtz Centre for Polar and Marine Research, Bussestraße 24, 27570 Bremerhaven, Germany

⁴Polar Biological Oceanography, Biosciences Division, Alfred Wegener Institute Helmholtz Centre for Polar and Marine Research, Am Handelshafen 12, 27570 Bremerhaven, Germany

⁵Institute of Environmental Physics, University of Bremen, PO Box 330440, 28334 Bremen, Germany

*Corresponding author: rafael.goncalves.araujo@awi.de - rafaelgoncalvesaraujo@gmail.com

Key-words: dissolved organic matter, particulate matter absorption, spectroscopy, radiometry, remote sensing reflectance, ocean color algorithm

Highlights:

- Bio-optical parameters were analyzed in the central and eastern Arctic Ocean
- Light absorption in surface waters was strongly dominated by CDOM
- Non-water absorption water coupled to hydrography, drawing biogeographic units
- Empirical ocean color algorithms poorly estimate Chl-a, with clear CDOM bias
- Only semi-analytical algorithm performed reasonable, but with relatively high error

Abstract

The consequences of global warming are already seen in the Arctic environment with regards to sea-ice shrinking, permafrost thaw and changes in fresh water and terrestrial material export as well as in light penetration and primary production. Biogeochemical and physical parameters require to be extensively monitored to reach a better understanding of the current status of the Arctic region and more accurately provide forecasts of these parameters. In this sense, bio-optical properties, for instance absorption and remote sensing reflectance (R_{rs}), are useful to be measured due to the applicability of optical instrumentation to autonomous platforms, including satellites. This study brings novel results on the characterization of non-water absorbers in the surface waters of the central and eastern Arctic Ocean and their coupling to hydrographic conditions. A second aim is to evaluate current empirical and semi-analytical algorithms commonly applied in the Arctic Ocean. Colored dissolved organic matter (CDOM) dominated the light absorption in surface waters over the entire sampled area. The distribution of CDOM, phytoplankton and non-algal particles were compared to regional hydrographic conditions. We suggest the subdivision of the region into five major bio-optical provinces: Laptev Sea Shelf, Laptev Sea, Central Arctic/Transpolar Drift, Beaufort Gyre and Eurasian/Nansen Basin. We found that bio-optical measurements reproduce hydrographic variability in these regions of the Arctic Ocean. In accordance to other regions studies in the Arctic Ocean, empirical ocean color algorithms provided poor chlorophyll-*a* (Chl-*a*) estimates, and even regional tuned empirical algorithms did not produce reliable results. Opposed to that, the semi-analytical algorithm Generalized Inherent Optical Property model (GIOP) using the settings as in Chaves et al. [2015] provided robust Chl-*a* estimates and on absorption by colored matter. Also the semi-analytical algorithm GSM with modifications by Matsuoka et al. [2013] produced reliable data on the absorption by colored matter and specifically by CDOM. These findings highlight that only the semi-analytical ocean color algorithms provided robust retrievals in the Arctic Ocean, where CDOM dominated the bio-optical properties. Besides, those algorithms also allows the determination of other parameters such as the absorption coefficients of phytoplankton, bulk colored matter and CDOM.

5.1. Introduction

The Arctic Ocean basin is the most continentally influenced on Earth, receiving the largest amount of freshwater relative to its volume – 11% of the global freshwater input with its volume representing only 1% of the global ocean [Shiklomanov, 1993]. Together with the fresh water, high loads of terrestrial material (organic and inorganic; dissolved, colloidal and particulate) are introduced in the basin, in particular, through the wide continental Siberian

shelves (e.g., Alling et al., 2010; Fichot et al., 2013; Lalande et al., 2014; Sánchez-García et al., 2011; Walker et al., 2013). This makes the Arctic Ocean a large carbon reservoir, playing an important role in the planet's carbon cycle. Besides, the Arctic environment has been experiencing the effects of ongoing global warming regarding permafrost thaw [Schuur et al., 2013], changes in fresh water export [Rabe et al., 2013, 2014] and decline of sea-ice extent [Serreze et al., 2007; Stroeve et al., 2012] and volume [Polyakov et al., 2012]. The permanent loss of sea-ice may lead to an increase in light penetration in the Arctic surface layer [Nicolaus et al., 2012], changes in the composition of phytoplankton assemblages [Li et al., 2009] and in the overall primary production in the Arctic Ocean [Pabi et al., 2008; Arrigo and van Dijken, 2011], as well as degradation of terrestrial material transported to that basin [Hansell et al., 2004; Bélanger et al., 2006], whose fate is still under research.

Recent studies have pointed out regional differences within the different Arctic regions with respect to biogeochemical parameters. For instance, shelf and open Arctic seas have shown to differ regarding the fluxes of biogenic matter [Lalande et al., 2014] and export of terrigenous material [Fichot et al., 2013]. Furthermore, while varying between shelf and open water in the Arctic [Fichot et al., 2013; Matsuoka et al., 2013] colored and fluorescent dissolved organic matter (CDOM and FDOM, respectively) content differs between the western and eastern Arctic seas [Stedmon et al., 2011; Walker et al., 2013; Matsuoka et al., 2014; Granskog et al., 2015; Gonçalves-Araujo et al., 2016]. Similarly, geographical differences in primary [Codispoti et al., 2013; Fernández-Méndez et al., 2015] and net community production [Ulfsbo et al., 2014], as well as in phytoplankton (e.g., dinoflagellates) and protist distribution [Okolodkov and Dodge, 1996; Kiliyas et al., 2014] in the various basins of the Central Arctic Ocean have been observed. Such biogeographic patterns are likely related to hydrographic and sea-ice conditions [Kiliyas et al., 2014; Metfies et al., 2016] within the region, denoting a strong coupling between physical and biogeochemical processes within the surface layers in the Arctic Ocean.

With the aforementioned effects of global warming and its impacts on the Arctic environment, improved monitoring and understanding of the current situation and changes in the biogeochemical parameters are necessary. The optical properties of dissolved organic matter are reliable water mass tracers in the Arctic Ocean according to reports based on *in situ* [Stedmon et al., 2015; Gonçalves-Araujo et al., 2016] and remote sensing data [Matsuoka et al., 2016]. Biogeochemical parameters such as chlorophyll-*a* (Chl-*a*), primary production and CDOM can be detected (and estimated, for primary production) in surface waters by ocean color remote sensing. Furthermore, the Arctic Ocean is a unique ocean where the non-water light absorption in the surface layer is dominated by CDOM even in pelagic waters [Matsuoka et

al., 2014] and it does not covary with Chl-*a*, as assumed by empirical ocean color algorithms. Hence, these algorithms lead to an overall overestimation of Chl-*a* [Matsuoka *et al.*, 2007; Ben Mustapha *et al.*, 2012; Chaves *et al.*, 2015]. Improvement of algorithms for the Arctic Ocean is challenging given the difficulties to sample in those waters, in particular, on the remote Siberian shelves [IOCCG, 2015]. Empirical ocean color algorithms perform poorly while estimating Chl-*a* in the Arctic [Reynolds *et al.*, 2015]. However, regional tuned algorithms provided improved estimates related to global algorithms in the western Arctic [Cota *et al.*, 2004; Ben Mustapha *et al.*, 2012]. In addition, semi-analytical algorithms have provided better estimates of Chl-*a* in the Arctic in comparison to empirical algorithms in the western Arctic [Matsuoka *et al.*, 2014; Chaves *et al.*, 2015]. Besides the good estimates of Chl-*a*, semi-analytical algorithms can also retrieve fairly good estimates of CDOM in that region [Matsuoka *et al.*, 2013, 2014; Chaves *et al.*, 2015]. Several studies have addressed the quality of the estimates from ocean color algorithms in the western Arctic ocean [Cota *et al.*, 2004; Matsuoka *et al.*, 2007, 2013, 2014; Bélanger *et al.*, 2008; Ben Mustapha *et al.*, 2012; Chaves *et al.*, 2015]. Although the optical characteristics of surface waters in the central and eastern Arctic have been assessed via satellite remote sensing [Matsuoka *et al.*, 2014], *in situ* bio-optical measurements so far have been limited to photosynthetic active radiation (PAR) [Lund-Hansen *et al.*, 2015] or to the shallow shelf regions of the Laptev Sea [Heim *et al.*, 2014].

The objectives of this study are twofold and the results presented here benefit the understanding on the applications of optical measurements for biogeochemical studies in the Arctic Ocean: first, we aim to obtain a broad characterization of the non-water absorption constituents in the surface waters in the Central-Eastern Arctic. Those properties were tested whether they reproduce hydrographic and geographic patterns (or units). As a second main objective, we evaluate empirical and semi-analytical ocean color algorithms commonly applied to studies in the Arctic Ocean and compare their performances. Given the novelty of the results presented in this study, it contributes to the growing Arctic remote sensing research, which has been so far mostly devoted to the western Arctic Ocean. Moreover, as already pointed out [IOCCG, 2015], the sampling effort for the Arctic Ocean is still very low compared to other ocean basins and more studies are required to improve the ocean color estimates for that basin. Finally, it is important to stress that whilst ocean color sensors are not able to monitor under very low (or no) illumination and cloudy conditions and ice covered regions, *in situ* bio-optical measurements in those regions are crucial for improving biogeochemical models; however such measurements are very scarce in the central and eastern Arctic Ocean. Furthermore, results on bio-optical and biogeochemical monitoring are important for calibration of sensors coupled to autonomous platforms. In the future, those platforms will measure *in situ* biogeochemical

properties and will provide much improved spatially and temporally resolved data (e.g., ITPs [Krishfield et al., 2008; Toole et al., 2011; Laney et al., 2014]).

5.2. Methods

5.2.1. Sampling

The ARK XXVI-3 (PS-78) cruise was conducted in shelf and open waters through the central-eastern Arctic Ocean from 5th August to 6th October 2011 onboard the *R/V Polarstern*. Temperature and salinity profiles were acquired with a CTD attached to a rosette system at 110 oceanographic stations [Schauer et al., 2012] (Figure 5.1c). Surface water samples for analysis of dissolved organic matter, particulate matter and chlorophyll-*a* (Chl-*a*) were taken using Niskin bottles attached to the rosette system in 62 stations (Figure 5.1d).

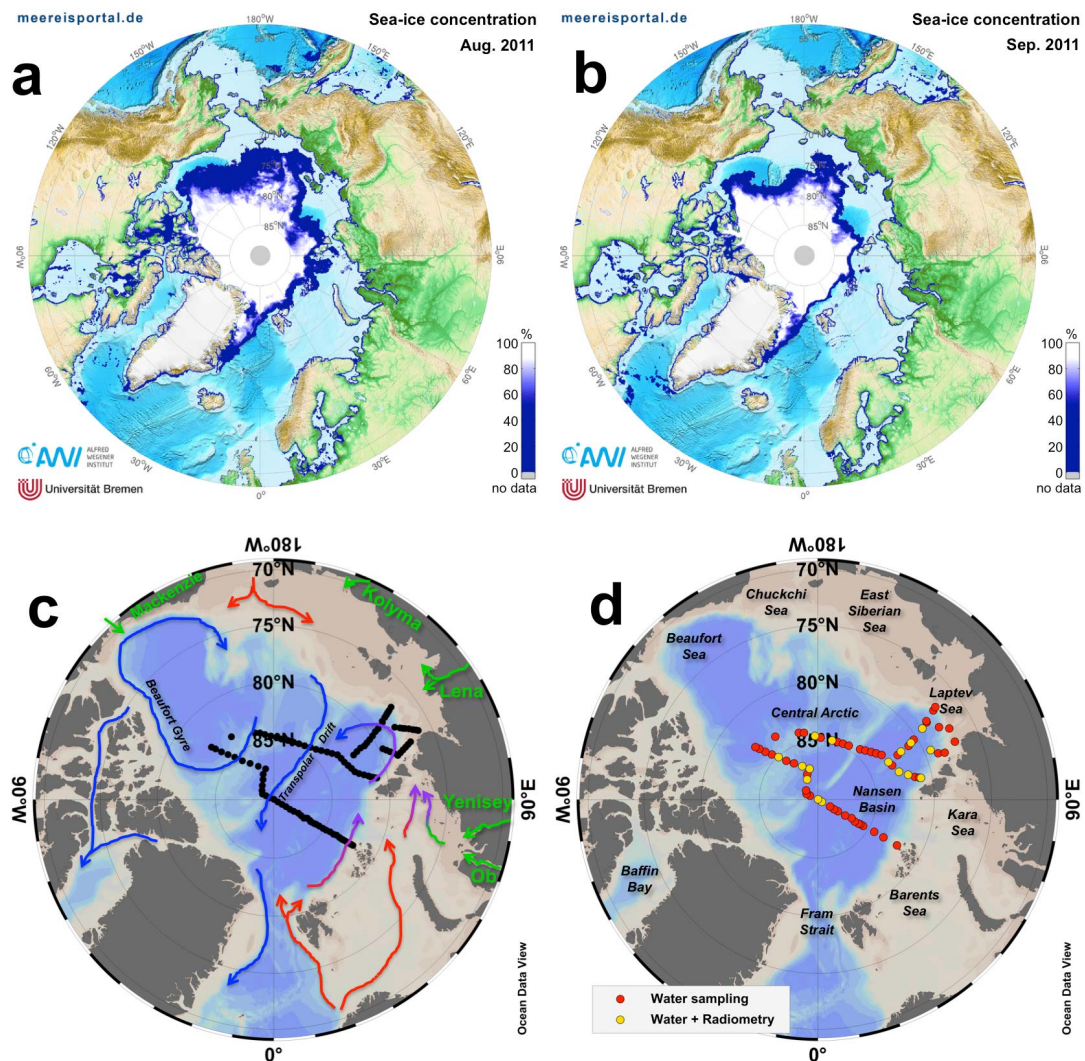


Figure 5.1. Study region and sea-ice conditions. AMRSR-2 sea-ice concentration (<http://meereisportal.de>) for August (a) and September (b) 2011. ODV maps [Schlitzer, 2015] showing the sampling stations occupied during the ARK-XXVI/3 (PS-78) cruise where CTD casts (c), water sampling and hyperspectral radiometric measurements (d) were performed. Arrows in (c) represent the main surface circulation patterns in the Arctic Ocean colored as follows: major rivers (green); inflowing currents (red); out flowing currents (blue) [Rudels, 2009].

5.2.2. Particulate absorption analysis

Water samples for particulate absorption analysis were filtered on GF/F filters (0.7 μm pore size), shock-frozen in liquid nitrogen and stored at $-80\text{ }^{\circ}\text{C}$ until laboratory analysis at the Alfred Wegener Institute Helmholtz Centre for Polar and Marine Research. Measurements were carried out on a dual-beam UV/VIS spectrophotometer (Cary 4000, Varian Inc.) equipped with a 150 mm integrating sphere (external DRA-900, Varian, Inc. and Labsphere Inc., made from SpectralonTM) using a quantitative filterpad technique [Simis *et al.*, 2005]. The filters were placed in the center of the integrating sphere using a center-mount filter holder perpendicular to the light beam. A wavelength scan from 300 to 850 nm with a resolution of 1 nm (slit width 2 nm, scan rate 150 nm min^{-1}) was performed, when the reflectance ports were covered with SpectralonTM reflectance standards. The baseline was recorded beforehand with a clean, dry filter, and a filter, which was soaked for more than 30 min in freshly produced Milli-Q water, was taken as a reference. The absorption coefficient was calculated from the transmittance [$T(\lambda)$], which is derived from the optical density (OD) measurements, using a path length amplification factor of 4.5 ($\beta = 1/4.5$) [Röttgers and Gehnke, 2012] following the equation:

$$a(\lambda) [\text{m}^{-1}] = -\ln [T(\lambda) \times A \times \beta \times V^{-1}], \quad (5.1)$$

$$T(\lambda) = \exp [-OD(\lambda)], \quad (5.2)$$

where V is the filtrated sample volume in m^3 and A the filter clearance area in m^2 . Results from the original filter gave total particulate absorption, a_p . To determine the absorption by non-algal particles (a_{NAP}), the algal pigments were bleached with NaOCl [Tassan and Ferrari, 1995; Ferrari and Tassan, 1999]. The bleached filters were measured following the procedure described above. The particulate absorption of phytoplankton at each wavelength (λ) [$a_{\text{ph}}(\lambda)$] was obtained by subtracting a_{NAP} from a_p .

5.2.3. Dissolved Organic Matter absorption analysis

Immediately after sampling water samples for DOM analysis were filtered through prerinsed 0.2 μm filters and stored in amber glass vials in dark at $4\text{ }^{\circ}\text{C}$ until analysis in laboratory at the Alfred Wegener Institute Helmholtz

Centre for Polar and Marine Research after the cruise. CDOM and FDOM were analyzed with an Aqualog® fluorescence spectrometer (HORIBA Jobin Yvon, Germany) using freshly produced Milli-Q water as reference. CDOM absorbance spectra measurements (260-600 nm) were blank-corrected and further converted into Napierian absorption coefficient [$a(\lambda)$], obtained from the given equation:

$$a(\lambda) [\text{m}^{-1}] = [2.303 \times A(\lambda)] \times L^{-1}, \quad (5.3)$$

where $A(\lambda)$ is the absorbance at specific wavelength and L is the cuvette path length in meters. a is generally adopted as a proxy for assessing the CDOM content in a given water sample and in this study it is presented in the visible (440 nm— a_{440}) and UV (350 nm— a_{350}) bands. a_{440} was chosen given its application to ocean color remote sensing (e.g., Heim et al., 2014; Siegel et al., 2005) and to make it comparable with the particulate matter absorption coefficients [*Prieur and Sathyendranath*, 1981]. The UV band a_{350} was determined in this study due to its correlations to DOC and lignin concentrations and to permit comparison with earlier results [*Stedmon et al.*, 2011; *Walker et al.*, 2013; *Gonçalves-Araujo et al.*, 2015b].

5.2.4. Chlorophyll-a analysis

For measuring the photosynthetic pigment Chl-a one liter of seawater samples were taken from Niskin bottles and the samples were immediately filtered on GF/F filters, frozen in liquid nitrogen, and stored at -80°C until further analyses by high-performance liquid chromatography (HPLC) at the home laboratory of the Alfred Wegener Institute Helmholtz Centre for Polar and Marine Research after the cruise. The samples were measured using a Waters 600 controller equipped with an auto sampler (717 plus), a photodiode array detector (2996) and the EMPOWER software. Chl-a was analyzed by reverse-phase HPLC using a VARIAN Microsorb-MV3 C8 column (4.6 3 100 mm) and HPLC-grade solvents (Merck). The solvents gradient and routine of analysis are fully described in Taylor et al. [2011]. Chl-a concentrations were quantified based on peak area of the external standard, which was spectrophotometrically calibrated using extinction coefficients published in *Jeffrey et al.* [1997].

5.2.5. Radiometric measurements

Underwater optical light fields were assessed through radiance and irradiance profiles obtained with hyperspectral radiometers (RAMSES ARC-VIS and ACC-VIS, respectively, TriOS GmbH, Germany). The instruments cover a wavelength range of 320 nm to 950 nm with an optical resolution of 3.3 nm and a spectral accuracy of 0.3 nm. Measurements were collected with sensor-specific automatically adjusted integration times (between 4 ms and 8

s). 16 radiometric profiles (Figure 1d) were collected simultaneously with the CTD profiles down to a maximum depth of 100 m. At each profile, measurements of upwelling radiance (L_u) and downwelling irradiance (E_d) were performed. One of the in-water sensors was equipped with inclination and pressure sensors. To avoid ship shadow, the ship was oriented such that the sun was illuminating the side where the measurements have taken place.

The radiometric measurements were performed during clear sky or nearly clear sky conditions and out of the ship's shadow. For the in-water data, the inclination in either dimensions was smaller than 14° [Matsuoka *et al.*, 2007]. During the acquisition of the profiles, stops (varying from 30 to 60 s) were performed within a 10 m depth interval. The radiance and irradiance profiles were corrected for incident sunlight using simultaneously obtained E_d at 490 nm [Smith *et al.*, 1986], measured above surface without ship's shading with another hyperspectral radiometer (RAMSES ACC-VIS, TriOS GmbH, Germany). These data were then averaged in discrete intervals of 10 m and interpolated to intervals of 5 m from depth between 0-30 m and were processed following the NASA protocols [Mueller *et al.*, 2003]. As surface waves strongly affect measurements in the upper few meters, deeper measurements that are more reliable to be used can be further extrapolated to the sea surface [Mueller *et al.*, 2003]. Analogously to Stramski *et al.* (2008) a depth interval was defined ($z' = 10$ to 30 m) to calculate the vertical attenuation coefficients for downwelling irradiance and upwelling radiance, [i.e. $K_d(\lambda, z')$ and $K_u(\lambda, z')$, respectively]. With $K_d(\lambda, z')$ and $K_u(\lambda, z')$, the subsurface irradiance $E_d^-(\lambda, 0 \text{ m})$ and radiance $L_u^-(\lambda, 0 \text{ m})$ were extrapolated from the profiles of $E_d(\lambda, z)$ and $L_u(\lambda, z)$.

For the calculation of the remote sensing reflectance [$R_{rs}(\lambda)$], the subsurface $L_u^-(\lambda, 0 \text{ m})$ was propagated through the water-air interface by applying a transfer coefficient of 0.5425 [Stramski *et al.*, 2008]. $R_{rs}(\lambda)$ was therefore calculated using the above-water reference downwelling irradiance $E_d^+(\lambda)$:

$$R_{rs}(\lambda) = [0.5425 \times L_u^-(\lambda, 0 \text{ m})]/E_d^+(\lambda). \quad (5.4)$$

5.2.6. Ocean color algorithms

In this study we evaluated the performance of ocean color algorithms to derive Chl-*a*, a_{dg} and a_{ph} . Firstly, we tested different empirical algorithms, which are used to derive Chl-*a* from band ratios of R_{rs} . These algorithms are frequently applied to the Arctic Ocean. Here their Chl-*a* retrievals were obtained using R_{rs} from the 16 stations as input and then compared with *in situ* measured Chl-*a*. The MODIS OC3M is a global algorithm, which is determined as a function of three R_{rs} band ratios [O'Reilly *et al.*, 2000]. The global SeaWiFS OC4V6 [O'Reilly *et al.*, 1998, 2000] and the regional Arctic

OC4L [Cota *et al.*, 2004] algorithms, nevertheless, use a four-band ratio approach. These algorithms are expressed as follows:

$$\begin{aligned} \text{Chl(OC3M)} &= 10^{(a + bR' + cR'^2 + dR'^3 + eR'^4)} \\ R' &= \log[R_{rs}(443 > 488 / 551)] \\ a &= 0.2830, b = -2.753, c = 1.457, d = 0.659, e = -1.403, \end{aligned} \quad (5.5)$$

$$\begin{aligned} \text{Chl(OC4V6)} &= 10^{(a_1 + b_1R + c_1R^2 + d_1R^3 + e_1R^4)} \\ R &= \log[R_{rs}(443 > 490 > 510 / 555)] \\ a_1 &= 0.366, b_1 = -3.067, c_1 = 1.930, d_1 = 0.649, e_1 = -1.532, \end{aligned} \quad (5.6)$$

$$\begin{aligned} \text{Chl(OC4L)} &= 10^{(a_2 + b_2R)} \\ R &= \log[R_{rs}(443 > 490 > 510 / 555)] \\ a_2 &= 0.592, b_2 = -3.607, \end{aligned} \quad (5.7)$$

where R is the the base 10 logarithm of the maximum band ratio, whichever is the greatest of $R_{rs}(443)/R_{rs}(555)$, $R_{rs}(490)/R_{rs}(555)$, and $R_{rs}(510)/R_{rs}(555)$; R' is the same as R but it considers the greater of the two band ratios $R_{rs}(443)/R_{rs}(551)$ and $R_{rs}(488)/R_{rs}(551)$; and the coefficients a , b , c , d , e , a_1 , b_1 , c_1 , d_1 , e_1 , a_2 , and b_2 are empirically derived values. Additionally, the performance of modifications to the global OC3M and OC4V6 algorithms developed for the western Arctic Ocean [Ben Mustapha *et al.*, 2012] hereafter OC3M-mod and OC4V6-mod, respectively, was evaluated. The coefficients for those regional algorithms are given below:

- OC3M-mod: $a_3 = -0.32$, $b_3 = -2.33$, $c_3 = 4.02$, $d_3 = -31.64$, $e_3 = 48.54$;
- OC4V6-mod: $a_4 = -0.35$, $b_4 = -1.52$, $c_4 = -2.44$, $d_4 = -12.80$, $e_4 = 30.48$.

Apart from the empirical ocean color algorithms, two semi-analytical algorithms (SAA) were tested. Firstly, we used the Generalized Inherent Optical Property model (GIOP) [Werdell *et al.*, 2013a, 2013b], for simplicity further named GIOP, using settings applied for the western Arctic [Chaves *et al.*, 2015] to allow comparison with the results from that study. In short, GIOP is a spectral matching inversion model, which applies non-linear least square methods to retrieve three eigenvalues [$a_{ph}(443)$, $a_{dg}(443)$ and the particles spectral backscattering coefficient – $b_{bp}(555)$]. GIOP can also estimate Chl- a from $a_{ph}(443)$, by using the factor 0.055. As in Chaves *et al.* (2015), we used the GIOP applied to *in situ* $R_{rs}(\lambda)$ at the SeaWiFS operational wavelengths

(412, 443, 490, 510, 555 and 670 nm). Besides the GIOP, a modification of the Garver-Siegel-Maritorena (GSM) SAA [Garver and Siegel, 1997; Maritorena et al., 2002] for retrieving $a_{\text{CDOM}}(\lambda)$ in the Arctic Ocean [Matsuoka et al., 2013] was used. This algorithm was developed based on a parametrization of absorption properties using data from the western Arctic. In short, it enables the separation of $a_{\text{NAP}}(\lambda)$, and therefore $a_{\text{CDOM}}(\lambda)$, from $a_{\text{dg}}(\lambda)$ by applying the parametrization of $a_{\text{NAP}}(\lambda)$ related to the particle backscatter at 555 nm [$b_{\text{bp}}(555)$] [Matsuoka et al., 2007].

To summarize, in this study we evaluate the following retrievals from ocean color algorithms:

- Chl- a_{OC3M} [O'Reilly et al., 2000];
- Chl- a_{OC4V6} [O'Reilly et al., 1998, 2000];
- Chl- $a_{\text{OC3M-mod}}$ and Chl- $a_{\text{OC4V6-mod}}$ [Ben Mustapha et al., 2012];
- Chl- a_{OC4L} [Cota et al., 2004];
- $a_{\text{ph}}(\lambda)_{\text{GIOP}}$, $a_{\text{dg}}(\lambda)_{\text{GIOP}}$, and Chl- a_{GIOP} [Werdell et al., 2013a, 2013b];
- $a_{\text{dg}}(\lambda)_{\text{Mat}}$ and $a_{\text{CDOM}}(\lambda)_{\text{Mat}}$ [Matsuoka et al., 2013].

5.2.7. Statistical analysis

Hierarchical cluster analysis using simple average linkage and Euclidean distance method was applied to classify both, a matrix containing environmental and bio-optical bulk properties (hereafter environmental matrix) and a matrix consisting of hyperspectral apparent optical properties, into coherent groups [Clarke and Warwick, 1994]. The environmental matrix consisted of surface measurements of temperature, salinity, $a_{\text{CDOM}}(443)$, $a_{\text{NAP}}(443)$ and $a_{\text{ph}}(443)$, which were normalized prior to analysis, by subtracting the mean value and then dividing by the standard deviation. The hyperspectral matrix consisted of the second derivative of $R_{\text{rs}}(\lambda)/R_{\text{rs}}(555)$. For that, R_{rs} spectra were interpolated to the optimal range for band separation (435–510 nm), and a smoothing filter window of 27 nm was used for the derivative calculations [Torrecilla et al., 2011]. Given that bio-optical parameters are generally log-normally distributed in natural environments [Campbell, 1995], power functions were applied to evaluate the correlation between pairs of bio-optical parameters [Bricaud et al., 1995, 1998].

Kruskal-Wallis H tests were applied to compare variables between pairs of clusters, after being normality-tested with the Kolmogorov-Smirnov test. To evaluate the performance of the ocean color algorithms, r^2 , slope, intercept and root mean square error (RMSE) for each pair of variables were determined. The RMSE was calculated as follows:

$$RMSE = \sqrt{\frac{\sum_{n=1}^N [\log_{10} Y - \log_{10} X]^2}{N}}, \quad (5.8)$$

where Y is the retrieved parameter (e.g. Chl- a , a_{dg} , a_{ph}) and X is the correspondent *in situ* measured parameter.

5.3. Results and Discussion

5.3.1. Hydrography

Five water masses were identified within the surface layer (0–200 m) of the sampled area, based on temperature and salinity profiles, and were in agreement with previous studies in the region [Rudels, 2009; Bauch et al., 2016]: Upper Halocline Water (UHW), Barents Sea Branch Water (BSBW) and Laptev Sea Shelf Water (LSSW) at the surface; and Lower Halocline Water (LHW) and Atlantic Water (AW) in the beneath layer (Figure 5.2a). Surface waters of the central Arctic were occupied by the UHW, whereas BSBW and LSSW were observed at surface in pelagic and shelf waters in the Laptev Sea, respectively. Most of the Arctic surface waters (or Halocline Water) are of Atlantic origin and are progressively modified at high latitudes by heat fluxes to the atmosphere, river runoff, melt water in summer and by salt rejection in winter [Jones et al., 1990]. The UHW was observed within the upper polar mixed layer (PML, ~40 m) and it was characterized by subzero temperatures and a thin upper mixed layer (10–20 m) characterized by dilution from sea-ice melt. This water mass can be further divided into two origins, given differences in the salinity ranges [Rudels, 2009]: the UHW from the Canadian Basin with the Beaufort Gyre (cUHW, with salinity <32.5), and the UHW from the Eurasian Basin (eUHW, with salinity between 32 and 34). The BSBW observed in the surface waters of the Laptev Sea are transported from the Kara Sea through the Vilkitsky Strait by the Vilkitsky Strait Current [Harms and Karcher, 1999; Janout et al., 2015; Bauch et al., 2016]. High temperatures and low salinity characterize the LSSW, and it is strongly influenced by the Lena River outflow [Bauch et al., 2009]. The highest temperature (3.67 °C) and lowest salinity (23.8) values were observed within LSSW. The lowest temperature (–1.86 °C), on the other hand, was associated with Lower Halocline Water whereas the highest salinity (34.9) was observed within AW located in the deepest sampled layer, generally below 100 m (Figure 5.2bc).

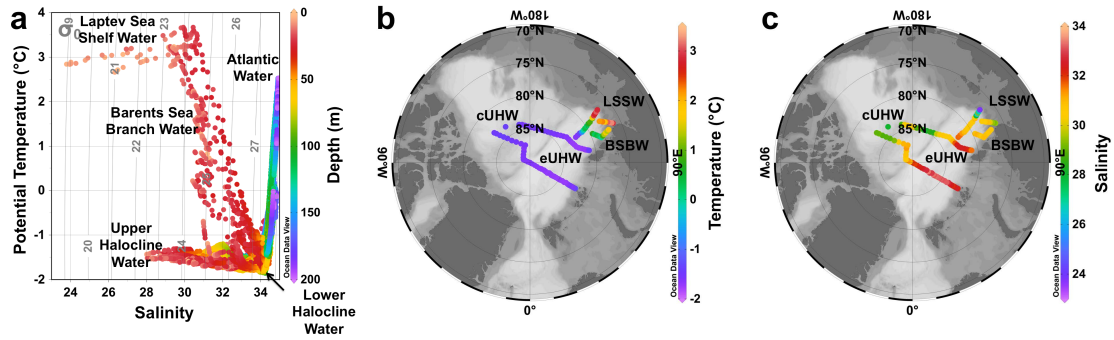


Figure 5.2. Hydrography in the surface Central and Eastern Arctic Ocean. (a) T-S diagram with depth (m) as color bar. **(b)** Surface distribution of temperature (°C) and salinity **(c)** with the approximate occupation of the water masses with the PML within the study region. Produced with Ocean Data View [Schlitzer, 2015].

5.3.2. Absorption coefficients of phytoplankton, NAP, and CDOM

Phytoplankton absorption coefficients [$a_{ph}(443)$] were highly correlated with the absorption coefficients of NAP [$a_{NAP}(443)$] ($r^2=0.95$; $p<0.0001$; $n=62$). $a_{ph}(443)$ ranged from 0.01 to 0.06 m^{-1} whereas the $a_{NAP}(443)$ varied between 0.0004 and 0.04 m^{-1} . The highest $a_{NAP}(443)$ values were associated to sites close to the shelf break, denoting the continent as its main source, reaching its maximum within the LSSW, in similar ranges as previously reported [Matsuoka *et al.*, 2014]. Relatively high values of $a_{ph}(443)$ were observed close to the Laptev Sea shelf break, as for $a_{NAP}(443)$, however, the highest $a_{ph}(443)$ values were obtained for the Nansen Basin. Further discussion on the spatial variability of those parameters is presented in Section 5.3.3.

To investigate the correlation of $a_{ph}(443)$ and $a_p(443)$ with Chl-*a* a power function was applied [Bricaud *et al.*, 1995, 1998]. Both $a_{ph}(443)$ (Figure 3d) and $a_p(443)$ were highly correlated to Chl-*a*, however the correlations for a_{ph} were higher. The power functions for $a_{ph}(443)$ and $a_p(443)$ in relation to Chl-*a* concentration obtained in this study are given below:

$$a_{ph}(443) = 0.0513 [\text{Chl-}a]^{0.6675} (r^2=0.85), \quad (5.9)$$

$$a_p(443) = 0.0595 [\text{Chl-}a]^{0.5603} (r^2=0.73). \quad (5.10)$$

As shown in Figure 3d, the correlation between $a_{ph}(443)$ and Chl-*a* was comparable to the one found by Bricaud *et al.* (1998), and to a recent expedition (R/V Polarstern – PS 93.2) conducted in the Fram Strait (Yangyang Liu and Astrid Bracher–AWI, *unpublished data*). The consistency between these results thus, reiterates the applicability of such absorption measurements in the VIS-range as a proxy to retrieve Chl-*a* concentrations. The correlation between $a_{ph}(443)$ and Chl-*a* observed in this study presents, in turn, a slight deviation from the trends observed in the Canadian Basin [Matsuoka *et al.*, 2007]. Those authors, however, pointed out that the

deviations in their study would be likely due to different pigment packaging effect in their specific region.

CDOM absorption coefficients in the visible and UV wavelength ranges [$a_{\text{CDOM}}(443)$ and $a_{\text{CDOM}}(350)$, respectively] were highly correlated ($r^2=0.99$, $p<0.0001$) and ranged from 0.02 and 0.19 m^{-1} to 1.14 and 4.42 m^{-1} , respectively (Figure 5.3a). The highest a_{CDOM} values [$a_{\text{CDOM}}(443)>1 \text{ m}^{-1}$] were observed in the Laptev Sea associated to the LSSW, with values in similar ranges as previously reported for those waters [Heim *et al.*, 2014; Matsuoka *et al.*, 2014; Gonçalves-Araujo *et al.*, 2015b]. High a_{CDOM} values [$\sim 0.5 \text{ m}^{-1}$ for $a_{\text{CDOM}}(443)$] were observed in the central Arctic, which have been shown to have a high terrestrial signal [Lund-Hansen *et al.*, 2015], likely associated to transport of high-DOM Siberian Shelf waters [Alling *et al.*, 2010] along the Transpolar Drift. That high-DOM signal can be traced even after significant removal during the transport of those waters to the central Arctic [Stedmon *et al.*, 2011] and in the Fram Strait [Granskog *et al.*, 2012, 2015; Pavlov *et al.*, 2015; Stedmon *et al.*, 2015; Gonçalves-Araujo *et al.*, 2016]. The lowest a_{CDOM} values [$<0.2 \text{ m}^{-1}$ for $a_{\text{CDOM}}(443)$] were observed in the Beaufort Gyre and Amundsen and Nansen basins. The low a_{CDOM} in the Amundsen and Nansen basins is related to the influence of waters from the Norwegian and Barents Sea [Rudels, 2009] that have a very low DOM content (e.g., Børsheim and Myklestad, 1997; Granskog *et al.*, 2012). The low a_{CDOM} observed in the Beaufort Gyre corroborates the well-known DOM decrease towards the center of oligotrophic oceanic basins and gyres, where a_{CDOM} values tend to be close to zero [Siegel *et al.*, 2002; Nelson and Siegel, 2013]. Furthermore, a_{CDOM} differed significantly ($p<0.001$) between pelagic samples from the Central Arctic and Beaufort Gyre. Likewise, a recent study reported higher $a_{\text{CDOM}}(443)$ values in shelf waters of Eurasian basin in comparison to the Canadian basin [Matsuoka *et al.*, 2014]. Such a difference in the DOM background between the Canadian and Eurasian basins is likely a reflection of the higher loads of DOM from Siberian Rivers [Stedmon *et al.*, 2011; Walker *et al.*, 2013]. Moreover, the differences between DOM from Eurasian and Canadian basins can be also detected in the intensity of visible DOM fluorescence, which can further distinguish the origins of fresh water exiting the Arctic Ocean [Gonçalves-Araujo *et al.*, 2016].

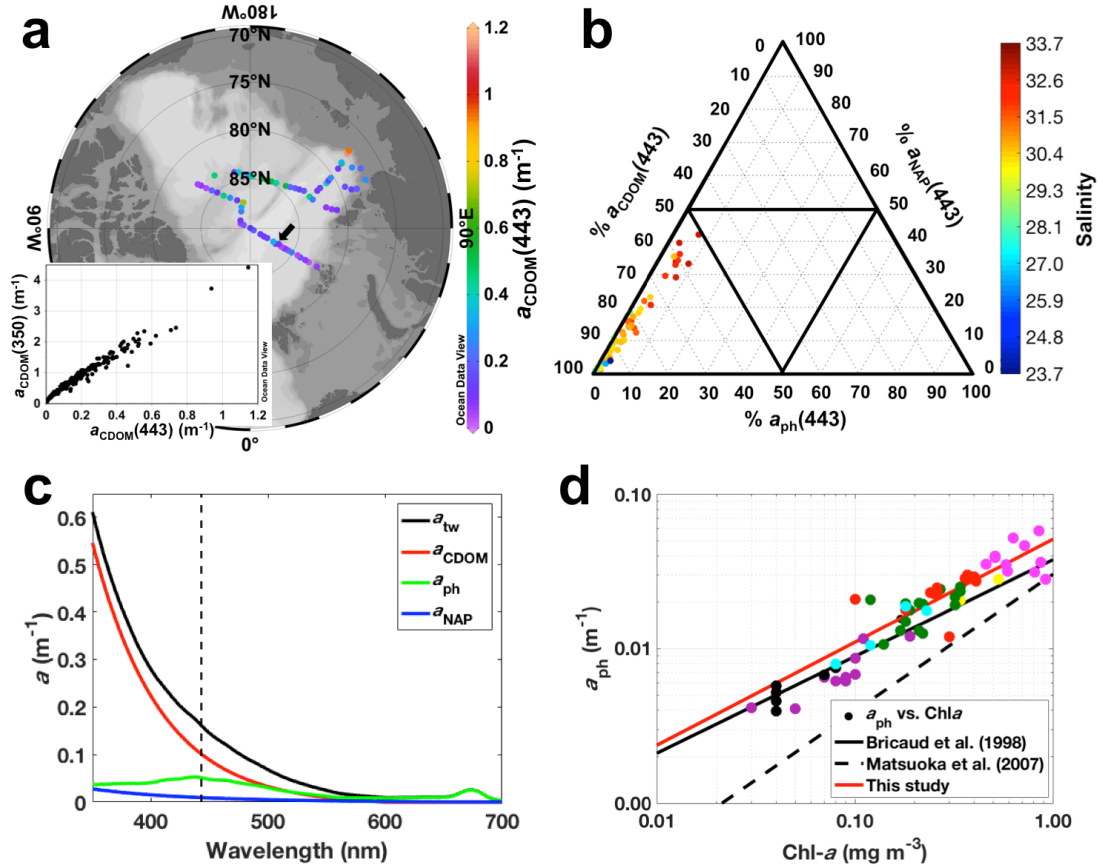


Figure 5.3. Absorption coefficients in the surface waters of Central and Eastern Arctic Ocean. (a) Surface distribution of $a_{\text{CDOM}}(443)$ (m^{-1}) and correlation between $a_{\text{CDOM}}(443)$ and $a_{\text{CDOM}}(350)$ (inset graph); produced with Ocean Data View [Schlitzer, 2015]. (b) Ternary plot denoting the contribution of the non-water absorbers (a_{CDOM} , a_{ph} , a_{NAP}) to total non-water absorption (a_{tw}) at surface; colorbar indicates salinity. (c) Station 207 (indicated by the arrow in a) as example of a_{CDM} , a_{CDOM} , a_{ph} and a_{NAP} spectra (m^{-1}). Dashed line indicates the position of 443 nm. (d) Correlation between Chl-*a* (mg m^{-3}) and $a_{\text{ph}}(443)$ (m^{-1}); for the colors, please refer to Figure 5.4.

We computed the total non-water coefficient absorption spectra [$a_{\text{CDM}}(\lambda)$] as follows:

$$a_{\text{tw}}(\lambda) = a_{\text{ph}}(\lambda) + a_{\text{NAP}}(\lambda) + a_{\text{CDOM}}(\lambda). \quad (5.11)$$

a_{tw} was strongly correlated with a_{CDOM} ($p < 0.0001$) in the UV and VIS (violet-blue, mostly) wavelength ranges, suggesting CDOM as the major absorber component of the surface waters in that spectral regions through the entire sampling region (Figure 5.3c). Such dominance of CDOM is also clear when looking at the relative proportion of the non-water absorbers (a_{ph} , a_{NAP} and a_{CDOM}) to a_{tw} (Figure 5.3b), which shows that all sampled stations are classified as CDOM-dominated [Prieur and Sathyendranath, 1981]. The proportion of CDOM at 443 nm was high (Table 5.1), with it contributing to over 50% at all sampled station, reaching a maximum contribution of 99% to

a_{tw} . Similar averaged values (0.85 ± 0.07) for the $a_{CDOM}(443)$ contribution to $a_{tw}(443)$ was observed in a recent study conducted in the Eurasian Basin [Matsuoka et al., 2014]. Nearly as, high contributions of CDOM were also reported in the Canadian Basin (Chukchi Sea: 0.74 ± 0.14 ; Western Arctic: 0.76 ± 0.11) in that same study [Matsuoka et al., 2014]. This shows that CDOM is the major non-water absorber not only in the western Arctic and shelf seas of the eastern Arctic [Matsuoka et al., 2007, 2014], it also strongly dominates the non-water absorption in the central Arctic, as reported by our study. Dominance of CDOM to the total non-water absorption has been primarily reported to coastal environments, classified as “Case-2 waters” because CDOM (and NAP) does not covary with Chl-*a* [Morel and Prieur, 1977; Antoine et al., 2014]. Oligotrophic pelagic systems (as the Central Arctic), on the other hand, are generally characterized as “Case-1 waters”, where Chl-*a* is thought to be the dominant absorber and covaries with CDOM [Morel and Prieur, 1977; Antoine et al., 2014]. That assumption, however, is not applicable to the pelagic Arctic Ocean, whose non-water absorption is clearly dominated by CDOM that, in turn, does not covary with Chl-*a* ($r^2=0.01$). Such an absence of covariance between CDOM and Chl-*a* has been already reported for the Labrador Sea [Cota et al., 2003] and Western Arctic Ocean [Wang et al., 2005; Matsuoka et al., 2007]. The correlation observed in this study ($r^2=0.01$) was, nevertheless, the weakest observed for the entire Arctic Ocean, and could be related to the greater contribution and variability of CDOM to the total non-water absorption in those waters. Hence, this would affect estimates of Chl-*a* and, consequently, of primary productivity from standard products of ocean color remote sensing [Arrigo and van Dijken, 2011; Arrigo et al., 2015; Reynolds et al., 2015]. Finally, $a_{NAP}(443)$ contribution to $a_{tw}(443)$ was the lowest found for the Arctic waters, being likely negligible compared to $a_{CDOM}(443)$ contributions (Table 5.1).

Table 5.1. Relative absorption of non-water absorbers. Averaged contribution of the absorption coefficients for each of the non-water absorbers to a_{tw} in this and other studies carried out in different regions.

Study	Sampling area	Layer	$\frac{a_{ph}(443)}{a_{tw}(443)}$	$\frac{a_{NAP}(443)}{a_{tw}(443)}$	$\frac{a_{CDOM}(443)}{a_{tw}(443)}$	N
This study	Central & E Arctic	surface	0.12 ± 0.11	0.03 ± 0.02	0.85 ± 0.13	62
Matsuoka et al. [2014]	East Siberian and Laptev Seas	euphotic layer	0.08 ± 0.04	0.08 ± 0.02	0.85 ± 0.07	18
Matsuoka et al. [2014]	Chukchi Sea	euphotic layer	0.18 ± 0.12	0.08 ± 0.05	0.74 ± 0.14	179
Matsuoka et al. [2007]	Beaufort and Chukchi Seas	<90 m	0.16 ± 0.09	0.08 ± 0.03	0.76 ± 0.11	94
Babin et al., [2003]	Coastal Europe	surface	0.36 ± 0.14	0.22 ± 0.14	0.41 ± 0.14	317

5.3.3. Geographic clustering

Hierarchical cluster analysis was applied to the environmental matrix [temperature, salinity, $a_{\text{CDOM}}(443)$, $a_{\text{NAP}}(443)$ and $a_{\text{ph}}(443)$] to classify the sampling sites according to coherent groups with respect to hydrography and non-water absorption. A total of seven major clusters were identified and those could be used to divide the study area into five distinct geographic zones (Figure 5.4): Laptev Sea Shelf, Laptev Sea (pelagic), Central Arctic/Transpolar Drift, Beaufort Gyre and Nansen Basin. Those zones were easily discriminated based on the surface values of the environmental matrix. The average and standard deviation of the analyzed parameters for each cluster are presented in Table 5.2. In short, cluster 1 characterized the surface Laptev Sea shelf waters, influenced by the Lena River outflow, with high temperature, low salinity, moderate a_{ph} and the highest values of CDOM and NAP, in agreement with previous reports for that region [Alling *et al.*, 2010; Sánchez-García *et al.*, 2011; Semiletov *et al.*, 2013; Matsuoka *et al.*, 2014; Gonçalves-Araujo *et al.*, 2015b]. Cluster 6 was composed of stations located in the pelagic and western domain of the Laptev Sea, with influence of shelf waters from the Kara Sea [Harms and Karcher, 1999; Janout *et al.*, 2015]. Those waters presented high temperatures, relatively low salinity and moderate values of a_{CDOM} , a_{ph} and a_{NAP} . Clusters 2 and 5 united the stations located in the Central Arctic, over the Transpolar Drift stream (e.g., Rudels, 2009), where the Arctic shelf waters with relatively low salinity and high a_{CDOM} are being transported along the Arctic Basin [Stedmon *et al.*, 2011]; however cluster 5 seems to be a transitional zone, with less influence of Arctic shelf waters, exhibiting lower a_{CDOM} and higher a_{ph} compared to cluster 2. Cluster 3 grouped the stations located in the Beaufort Gyre. Those lower salinity waters [Proshutinsky *et al.*, 2009a] presented near freezing temperature and very low non-water absorption was observed, with $a_{\text{CDOM}}(443)$ and $a_{\text{ph}}(443)$ exhibiting the lowest values among the seven clusters. These results corroborates previous studies showing Canadian Basin water with low Chl-*a* and primary production [Pabi *et al.*, 2008; Codispoti *et al.*, 2013], as well as lower DOM content [Stedmon *et al.*, 2011; Walker *et al.*, 2013; Matsuoka *et al.*, 2014; Gonçalves-Araujo *et al.*, 2016], in comparison to the Eurasian Basin. Finally, the clusters 4 and 7 grouped the stations located in the Nansen and Amundsen basins, with influence of waters advected from the North Atlantic Ocean and Norwegian Sea. Those waters were characterized by the lowest temperatures, the highest salinity, low a_{CDOM} and a_{NAP} , as reported for the waters of the Atlantic inflow to the Arctic in the Fram Strait [Pavlov *et al.*, 2015]. On the other hand, a_{ph} (and Chl-*a*) values within that cluster were the highest, likely explained by the advection of nutrient rich Atlantic water [Bluhm *et al.*, 2015]. Clusters 4 and 7 differed from each other only regarding the a_{ph} (and Chl-*a*) values, with the highest values being observed in cluster 7. High a_{ph} (and Chl-*a*) observed in the Nansen and Amundsen basins can be

attributed to the high transmittance of light in those waters primarily due to the development of melt ponds in the sea-ice [Nicolaus et al., 2012], which increases primary production in those areas [Fernández-Méndez et al., 2015].

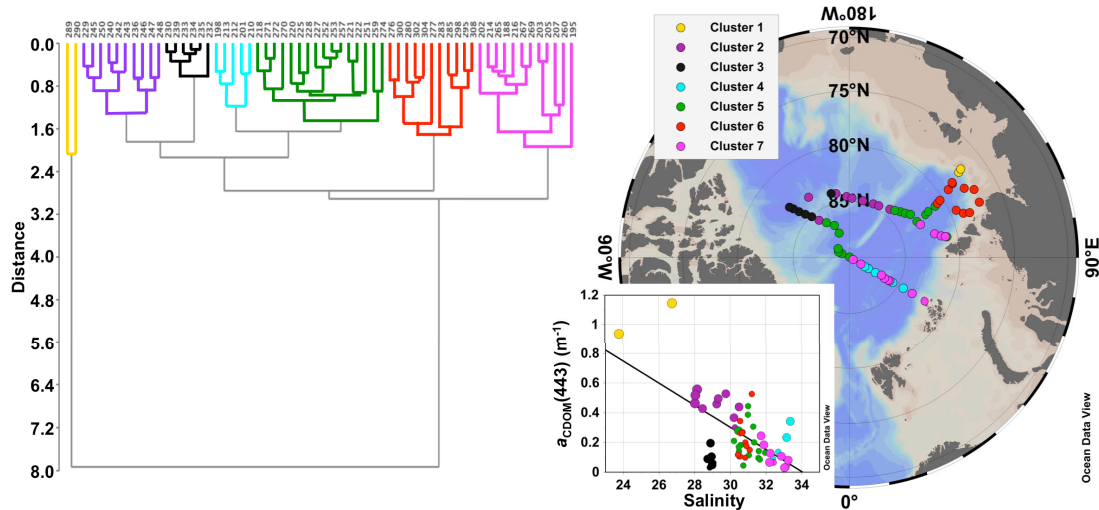


Figure 5.4. Environmental clustering. (left) Dendrogram (cophenetic correlation coefficient: $c=0.91$) for sampling stations based on surface normalized values of an environmental matrix containing environmental and bio-optical parameters: temperature, salinity, $a_{\text{CDOM}}(443)$, $a_{\text{NAP}}(443)$ and $a_{\text{ph}}(443)$. (right) ODV map [Schlitzer, 2015] showing the position of each station according to the classification based on the hierarchical clustering. Inset graph shows the correlation between $a_{\text{CDOM}}(443)$ and salinity colored with respect to the clusters; black line indicates the best fit ($p < 0.01$).

Table 5.2. Environmental parameters for the geographic clusters based on the environmental matrix. Averaged values \pm standard deviation of environmental/bio-optical parameters and geographic region for each of the clusters presented in Figure 5.4. Geographic regions acronyms: BG (Beaufort Gyre); EB (Eurasian Basin–Amundsen and Nansen basins); LS (Laptev Sea); LSS (Laptev Sea Shelf–Lena river influenced); TPD (Transpolar Drift).

Cluster	Temperature (°C)	Salinity	$a_{\text{CDOM}}(443)$ (m^{-1})	$a_{\text{NAP}}(443)$ (m^{-1})	$a_{\text{ph}}(443)$ (m^{-1})	n	Area
1	2.95 ± 0.15	25.2 ± 2.1	1.04 ± 0.15	0.04 ± 0.0001	0.02 ± 0.001	2	LSS
2	-1.54 ± 0.05	29.2 ± 1.0	0.45 ± 0.08	0.03 ± 0.002	0.01 ± 0.002	10	TPD
3	-1.47 ± 0.03	28.9 ± 0.1	0.09 ± 0.05	0.002 ± 0.0004	0.006 ± 0.001	6	BG
4	-1.71 ± 0.03	32.9 ± 0.4	0.16 ± 0.12	0.001 ± 0.001	0.01 ± 0.004	5	EB
5	-1.55 ± 0.23	31.0 ± 0.5	0.19 ± 0.11	0.005 ± 0.002	0.02 ± 0.004	16	TPD
6	0.99 ± 0.80	30.7 ± 0.2	0.23 ± 0.13	0.01 ± 0.003	0.02 ± 0.005	11	LS
7	-1.66 ± 0.14	32.4 ± 0.5	0.09 ± 0.06	0.005 ± 0.003	0.04 ± 0.01	12	EB

To test whether hyperspectral remote sensing information is capable of detecting hydrographic/bio-optical variability we have also applied hierarchical cluster analysis to hyperspectral R_{rs} [in this case, the 2nd derivative of $R_{\text{rs}}(\lambda)/R_{\text{rs}}(555)$; see section 5.2.7]. Despite the low number of sampled

stations ($n=16$), the analysis yielded satisfactory results (cophenetic correlation coefficient: $c=0.87$) and two main clusters were isolated (Figure 5.5). The partition based on hyperspectral data shows some similarities with the one provided by clustering the environmental data (see Figure 4). Cluster I comprised the R_{rs} spectra (i.e. stations) with lower $a_{CDOM}(443)$, located mainly the Nansen and Amundsen basins and North Laptev Sea, under influence of waters from the North Atlantic, Norwegian Sea and also from Kara Sea. This cluster can be correlated to the clusters 7 and 6 displayed in Figure 5.4, with relatively low $a_{CDOM}(443)$ and influence of waters advected from the abovementioned regions. Additionally, the only station from the Beaufort Gyre, which also presented low $a_{CDOM}(443)$, was included in this same cluster 1. Here we speculate that given the low number of stations performed, the multivariate analysis may not be able to solve such variability and grouped all the low CDOM spectra into one unique cluster. However, with an increased number of sampling stations, such variability would be easier to be detected in R_{rs} spectra. Cluster II isolated R_{rs} spectra from stations with high $a_{CDOM}(443)$ and lower R_{rs} (Figure 5.5 and Table 5.3), located in the central Arctic and close to the Laptev Sea shelf (Figure 5.5). Its corresponding environmental clusters are mainly the clusters 2 and 5, which were under influence of the shelf waters transported within the Transpolar Drift (e.g., Rudels, 2009).

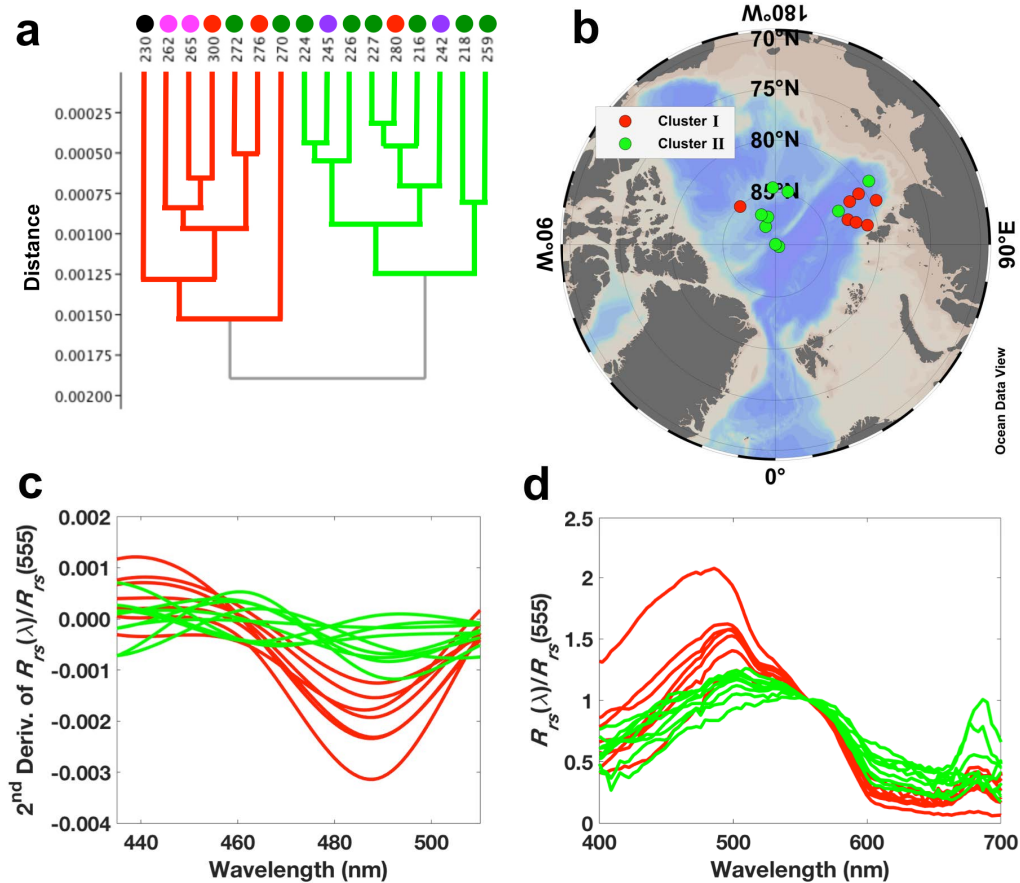


Figure 5.5. Hyperspectral clustering. (a) Dendrogram (cophenetic correlation coefficient: $c=0.87$) for sampling stations based on hierarchical cluster analysis applied to the 2nd derivative of $R_{rs}(\lambda)/R_{rs}(555)$ (following Torrecilla et al., 2011). (b) ODV map [Schlitzer, 2015] showing the position of each station according to the classification based on the hierarchical clustering. (c) 2nd derivative of normalized hyperspectral remote sensing reflectance, $R_{rs}(\lambda)/R_{rs}(555)$, with respect to the wavelength range of 435–510 nm (following Torrecilla et al., 2011). (d) Normalized hyperspectral remote sensing reflectance, $R_{rs}(\lambda)/R_{rs}(555)$ in the visible wavelength range. Colored circles in (a) refer to the environmental clusters presented in Figure 5.4. Colors in (c) and (d) are in accordance with the clusters presented in (a) and (b).

Table 5.3. Environmental parameters for the geographic clusters based on hyperspectral measurements. Averaged values \pm standard deviation of geophysical parameters for each of the clusters presented in Figure 5.5.

Cluster	Temperature (°C)	Salinity	$a_{CDOM}(443)$ (m^{-1})	$a_{NAP}(443)$ (m^{-1})	$a_{ph}(443)$ (m^{-1})	n
I	-1.03 ± 0.86	31.1 ± 1.2	0.11 ± 0.03	0.01 ± 0.0002	0.02 ± 0.01	7
II	-1.30 ± 0.88	30.9 ± 0.9	0.31 ± 0.19	0.01 ± 0.003	0.02 ± 0.01	9

5.3.4. Arctic bio-optical provinces

The results provided in this study by hierarchical cluster analyses (see Figures 5.4 and 5.5 and Tables 5.2 and 5.3) show that hydrographic data and non-water absorption, but also hyperspectral apparent optical properties (e.g. R_{rs} spectra) are applicable tools for characterizing surface waters (geographic zones) with differing bio-optical properties, even in waters where non-water absorption is strongly dominated by CDOM, such as the Arctic Ocean [Matsuoka et al., 2014]. Similarly, a recent study applied hierarchical cluster analysis to the spectral particulate backscattering-to-absorption ratio in the western Arctic allowing the partitioning of optically-distinct clusters of particles assemblages, which, in turn, reflect difference in the characteristics of particle concentration, composition, and phytoplankton taxonomic composition and size [Neukermans et al., 2016]. Furthermore, given the coupling between hydrographic and bio-optical properties, one can further suggest those clusters as bio-optical units or provinces. Bio-optical provinces have been shown to be reliable descriptors of Longhurst provinces [Longhurst, 2007] in the Atlantic Ocean [Taylor et al., 2011]. On the other hand, almost the entire Arctic Ocean is classified as a unique ecological province, the Boreal Polar Province (BPLR), within the Polar Biome [Longhurst, 2007]. That same author suggested that there might be spatial variability between shelf and pelagic ecosystems (as well as in the marginal ice zones) within the BPLR, however it is very difficult to sustain an adequate description of smaller units, given the difficulty to access the northern seas. Along with that, differences among the

Arctic Seas have been already reported, for instance, with respect to export of biogenic matter [Lalande *et al.*, 2014], number of dinoflagellates species [Okolodkov and Dodge, 1996], protist diversity [Kiliyas *et al.*, 2014; Metfies *et al.*, 2016], and primary production [Codispoti *et al.*, 2013; Arrigo *et al.*, 2015; Fernández-Méndez *et al.*, 2015]. Those studies, therefore, reinforce the existence of distinct biogeographic units in the Arctic Ocean and further implementation of a biogeographic characterization in the region is of great importance to improve the current understanding about the Arctic environment. The determination of such biogeographic zones would guide future strategies for Arctic monitoring and ecosystem modeling, leading to a more accurate understanding of the ecosystem functioning and biogeochemical stocks, as well as on the prediction of future scenarios with regards to climate change. Finally, to build on that, based on the results presented by our quasi-synoptic sampling through the central-eastern Arctic Ocean, we therefore propose an overall classification of the sampling sites into five major bio-optical provinces, as follows:

1. Laptev Sea Shelf: strongly influenced by the Lena River outflow, is primarily characterized by low salinity, high temperature and a_{NAP} , moderate a_{ph} , Chl-*a* and very high a_{CDOM} ;
2. Laptev Sea: low influence of Lena River outflow, however with contributions of waters advected from the Kara Sea; presents relatively low salinity, relatively high temperature and moderate levels of a_{CDOM} , a_{ph} , Chl-*a* and a_{NAP} ;
3. Central Arctic/Transpolar Drift: characterized by shelf waters transported within the Transpolar Drift, it has very low temperatures and relatively low salinity, a_{ph} and Chl-*a*; however with high a_{CDOM} and very low a_{NAP} ;
4. Beaufort Gyre: the waters with lower non-water absorption; they present low temperature and salinity, together with very low values of a_{CDOM} , a_{ph} , Chl-*a* and a_{NAP} ;
5. Eurasian/Nansen Basin: region influenced by waters advected from the Atlantic Ocean and Norwegian Sea, those waters present the highest salinity and near freezing temperature, with very low a_{CDOM} and a_{NAP} , and the highest a_{ph} and Chl-*a* levels due to high transmittance through sea-ice.

5.3.5. Evaluation of ocean color algorithms

Figure 5.6 shows the evaluation of the current global empirical ocean color algorithms OC3M and OC4V6 (and their regional adaptations for the western Arctic, OC3M-mod and OC4V6-mod) frequently applied to the Arctic Ocean, as well as the Arctic OC4L algorithm, which is designed to be

applicable to high northern latitudes. When considering all sampled stations, the five empirical algorithms failed in retrieving Chl-*a* from R_{rs} bands, and a general inverse correlation with *in situ* Chl-*a* was observed (Figure 5.6 and Table 5.4). While OC3M and OC4V6 tended to overestimate Chl-*a*, Arctic OC4L underestimated it. The best performances (RMSE=0.12 and 0.13), although still inversely correlated with *in situ* Chl-*a*, were performed by OC4V6-mod and OC3M-mod, respectively. Those algorithms provided better retrievals than the ones observed for the western Arctic (RMSE=0.26 and 0.27 for OC4V6-mod and OC3M-mod, respectively) [Ben Mustapha et al., 2012]. It is worth to recall that although the Arctic regional OC4V6-mod and OC3M-mod significantly improved performance (i.e., lower RMSE) related to OC4V6, OC3M and Arctic OC4L, the overall correlation is negative and low ($r^2=0.14$), and the observations tend to considerably deviate from the 1:1 line. Furthermore, despite the relatively low RMSE observed for OC4V6-mod and OC3M-mod, all the band-ratio algorithms applied in this study appeared to attribute CDOM absorption to phytoplankton absorption (Figure 5.6d and Table 5.4). Such CDOM-biased retrievals from empirical Chl-*a* ocean color algorithms have already been reported for the western Arctic [Matsuoka et al., 2007; Ben Mustapha et al., 2012; Chaves et al., 2015]. This is attributed to the fact that CDOM is the greatest absorber at 443 nm over the entire sampled region (see Figure 5.3 and Table 5.1). As pointed out by Chaves et al. (2015), excess $a_{CDOM}(\lambda)$ –that is assumed to covary with Chl-*a*– produces lower maximum band ratios [$R_{rs}(443>490>510/555)$], thus resulting in overestimation of Chl-*a* (see Figure 5.6c).

Table 5.4. Evaluation of empirical ocean color algorithms. Regression statistics for retrieved Chl-*a* from *in situ* R_{rs} using the correspondent algorithms versus *in situ* measured parameters. r^2 and Slope were calculated using log-transformed data for each of the correspondent parameters.

Retrieved Chl- <i>a</i> vs. <i>in situ</i> Chl- <i>a</i>				
Algorithm	<i>N</i>	r^2	Slope	RMSE
OC3M	16	0.45	-0.14	0.62
OC4V6	16	0.38	-0.09	0.49
Arctic OC4L	16	0.29	-0.18	1.18
OC3M-mod	16	0.14	-0.01	0.13
OC4V6-mod	16	0.14	-0.01	0.12
Retrieved Chl- <i>a</i> vs. $a_{CDOM}(443)$				
Algorithm	<i>N</i>	r^2	Slope	RMSE
OC3M	15	0.83	0.49	0.49
OC4V6	15	0.82	0.44	0.36
Arctic OC4L	15	0.80	1.48	1.00
OC3M-mod	15	0.77	0.40	0.10
OC4V6-mod	15	0.78	0.44	0.09

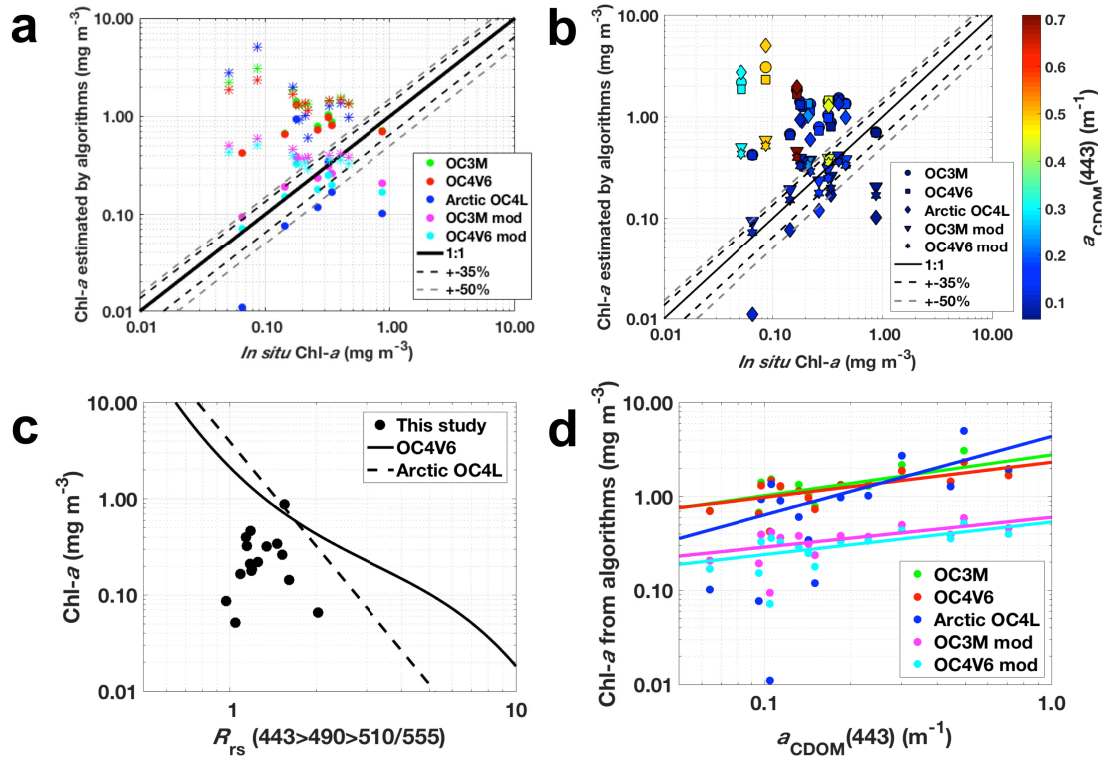


Figure 5.6. Evaluation of empirical ocean color algorithms frequently applied to the Arctic Ocean. (a) Chl-*a* estimated by empirical algorithms (mg m⁻³; indicated by different colors) versus *in situ* Chl-*a* (mg m⁻³). Stations belonging to the low a_{CDOM} cluster (Cluster 1) are presented as circles, whereas stars represent stations grouped in the high a_{CDOM} cluster (Cluster 2; Figure 5.5). (b) Chl-*a* estimated by empirical algorithms (mg m⁻³; indicated by different symbols) versus *in situ* Chl-*a* (mg m⁻³), with $a_{\text{CDOM}}(443)$ (m⁻¹) as colorbar. (c) *In situ* Chl-*a* (mg m⁻³) versus maximum band ratio [MBR; $R_{\text{rs}}(443>490>510/555)$]. (d) Chl-*a* estimated by empirical algorithms (mg m⁻³; indicated by different colors) versus $a_{\text{CDOM}}(443)$ (m⁻¹). Information on the fits displayed in (d) is given in Table 5.4.

Although not covarying with CDOM, Chl-*a* has still been well retrieved by empirical ocean color algorithms (especially the Arctic OC4L) applied to *in situ* R_{rs} measurements in CDOM dominated waters in the western Arctic (RMSE=0.13), when turbid waters [$R_{\text{rs}}(676)>0.00042$] were excluded [Matsuoka *et al.*, 2007]. This could be one of the reasons attributed to the poor performance of those algorithms in our study, given that all the sampling stations were classified as turbid. This is supported by the fact that the most overestimated Chl-*a* retrievals were especially related to the high CDOM cluster (see Figure 5.6). When looking only at the stations grouped in Cluster I, i.e. with lower a_{CDOM} (although still with relatively high turbidity), the retrievals were significantly improved and positively correlated to *in situ* Chl-*a* (Table 5.5). Furthermore, a better performance was observed for all the five empirical algorithms (strong reduction in RMSE), primarily for OC4V6-mod and OC3M-mod (RMSE=0.08 and 0.10, respectively), and the estimates were

less variable ($r^2 > 0.62$) compared to previously reported for the western Arctic (e.g., Matsuoka et al., 2007). This reiterates the need for developing or tuning regional algorithms for the Arctic, especially accounting for the high CDOM absorption in those waters and its non-covariance with Chl-*a*, which would classify those waters, although being pelagic, as “Case 2” waters instead.

Table 5.5. Evaluation of Chl-*a* retrievals from empirical ocean color algorithms, for low $a_{\text{CDOM}}(443)$ sites. Same as Table 5.4 but for the low $a_{\text{CDOM}}(443)$ stations.

Retrieved Chl- <i>a</i> vs. <i>in situ</i> Chl- <i>a</i>				
Algorithm	<i>N</i>	r^2	Slope	RMSE
OC3M	7	0.62	0.18	0.34
OC4V6	7	0.62	0.17	0.30
Arctic OC4L	7	0.66	0.75	0.35
OC3M-mod	7	0.70	0.28	0.10
OC4V6-mod	7	0.70	0.29	0.08

Besides, GIOP was also applied to retrieve Chl-*a*, as well as a_{ph} and a_{dg} , and provided robust estimates for the entire sampling area (Table 5.6 and Figure 5.7). Such an improvement is due to the fact that GIOP, like other SAAs, does not assume Chl-*a* and CDOM absorption as covariant. Even better estimates from GIOP were obtained for $a_{\text{ph}}(443)$ (Figure 5.7 and Table 5.6) which is probably due to that GIOP uses the spectral shape of Chl-*a*-specific absorption coefficient from Bricaud et al. (1998) as basis vector. As pointed out before (Figure 5.3) our dataset exhibited similar spectral shape for $a_{\text{ph}}(\lambda)$ and correlations between Chl-*a* and $a_{\text{ph}}(443)$ as observed in that study. Moreover, the performance of GIOP to retrieve $a_{\text{ph}}(443)$ in our study was much better than recently observed in the western Arctic ($r^2=0.85$; Slope=1.18; RMSE=0.20) [Chaves et al., 2015]. With regards to Chl-*a*, that same study reported fairly similar results ($r^2=0.72$; Slope=0.73; overestimation of Chl-*a*), however with better performance (RMSE=0.24) in comparison to our results (see Table 5.6). Our results clearly show that GIOP provides much more reliable Chl-*a* estimates when compared to global, but also to regional tuned, empirical ocean color algorithms evaluated in this study. Additionally, other semi-analytical algorithm, the GSM [Garver and Siegel, 1997; Maritorena et al., 2002], showed improved Chl-*a* retrievals in relation to the global empirical algorithms in the Arctic Ocean; however, fairly similar performance was observed by GSM retrievals compared to the regional adaptations OC3M-mod and OC4V6-mod [Ben Mustapha et al., 2012]. Hence, regional tuned algorithms such as the OC3M-mod and OC4V6-mod [Ben Mustapha et al., 2012] seem to significantly improve Chl-*a* estimates in lower CDOM Arctic waters and further studies would facilitate improvement of Arctic ocean color algorithms, given the high CDOM bias in phytoplankton absorption.

Finally, $a_{dg}(443)$ was also retrieved in this study using GIOP and GSM-Matsuoka. Here we assume that $a_{dg}(443)$ would be a direct estimation of $a_{CDOM}(443)$, given the very low contribution of $a_{NAP}(443)$ to total non-water absorption (generally <1%) in comparison to $a_{CDOM}(443)$ (Figure 5.3). In general, GIOP and GSM-Matsuoka retrievals were very similar and provided relatively good retrievals of $a_{dg}(443)$, with most of the data points located within the 50% error intervals (Figure 5.7 and Table 5.6). Although with similar performance (RMSE=0.08), GIOP seems to provide more reliable (Slope=1.05) and less variable ($r^2=0.91$) $a_{dg}(443)$ estimates for the western Arctic, as observed for $a_{ph}(443)$ [Chaves *et al.*, 2015]. As being highly correlated to $a_{dg}(443)$, $a_{CDOM}(443)$ retrieved with GSM-Matsuoka provided very similar statistics related to $a_{dg}(443)$ using that same model, thus resembling the observed with our *in situ* sampling (see Table 5.1). Better performance ($r^2=0.87$; Slope=0.97; RMSE=0.07) for retrieving $a_{CDOM}(443)$ using the GSM-Matsuoka model was reported for the western Arctic using a much larger dataset related to our study [Matsuoka *et al.*, 2014]. That model was then applied to MODIS monthly-averaged climatology of $R_{rs}(\lambda)$ and results were reported consistent with *in situ* measurements. Although the $a_{CDOM}(443)$ GSM-Matsuoka retrievals were not as good in our study, the results shows that SAAs in general have a high potential for obtaining reliable Chl-*a* estimates than empirical algorithms, besides the advantage of also providing other reliable retrievals such as $a_{dg}(\lambda)$, $a_{ph}(\lambda)$ and $a_{CDOM}(\lambda)$. Thus, products from SAAs are more suitable for application to biogeochemical studies in the Arctic Ocean, although improvement of the current algorithms is still requested, given the persistence of embedded errors to those retrievals, as demonstrated in this study.

Table 5.6. Evaluation of the semi-analytical ocean color algorithms. Regression statistics for modeled geophysical parameters calculated used *in situ* R_{rs} versus *in situ* measured parameters. r^2 and Slope were calculated using log-transformed data for each of the correspondent parameters.

GIOP				
Parameter	N	r^2	Slope	RMSE
$a_{ph}(443)$	11	0.86	0.89	0.02
Chl- <i>a</i>	12	0.79	0.64	0.40
$a_{dg}(443)$	15	0.56	0.25	0.08
GSM-Matsuoka				
Parameter	N	r^2	Slope	RMSE
$a_{dg}(443)$	15	0.59	0.29	0.09
$a_{CDOM}(443)$	15	0.57	0.29	0.09

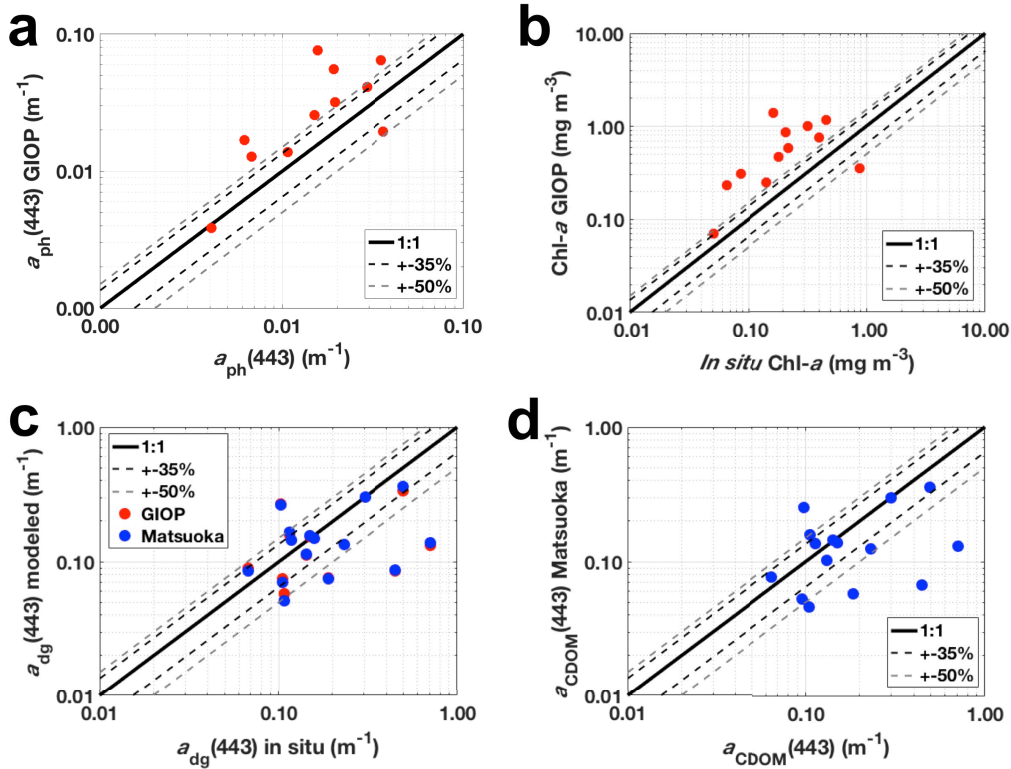


Figure 5.7. Evaluation of the semi-analytical algorithms. Modeled geophysical parameters calculated using *in situ* R_{rs} versus *in situ* measured parameters: $a_{ph}(443)$ (a); Chl-*a* (b); $a_{dg}(443)$ (c) and $a_{CDOM}(443)$ (d). Red points refer to the GIOP [Werdell *et al.*, 2013a, 2013b] retrievals, whereas blue points to the retrievals from the GSM model adapted to the Arctic [Matsuoka *et al.*, 2013].

5.4. Summary and scope

Based on a quasi-synoptic sampling strategy over the surface Central-Eastern Arctic Ocean we reiterate the dominance of CDOM related to total non-water absorption through the entire region under study. As CDOM and DOC are strongly correlated in the Arctic Ocean (e.g., Gonçalves-Araujo *et al.*, 2015; Stedmon *et al.*, 2011; Walker *et al.*, 2013), one can assume CDOM as a very reliable proxy for retrieving carbon concentrations in that basin. This can further provide insights on the Arctic biogeochemical cycles. Furthermore, our results show that $a_{CDOM}(443)$ and $a_{ph}(443)$, together with temperature and salinity, are useful parameters for distinguishing hydrographical regimes within the Central Arctic. Although with reduced number of sampling sites, hyperspectral measurements [$R_{rs}(\lambda)$] were able to reproduce the major bio-optical features at surface. As demonstrated for the Eastern Atlantic [Taylor *et al.*, 2011], bio-optical provinces efficiently reflect the ecosystem variability/biogeography proposed by Longhurst [Longhurst, 2007] and thus are a valuable tool for biogeochemical modeling. However, currently, practically the entire Arctic Ocean is still classified by this author as

a unique ecosystem unit, despite the reports of clear geographic patterns in different aspects (e.g., Arrigo et al., 2015; Fernández-Méndez et al., 2015; Lalande et al., 2014; Rutgers van der Loeff et al., 2014). Moreover, to our understanding, no study has proposed such a sub-division of the Boreal Polar Province (BPLR) into bio-optical units. Based on our findings we, therefore, propose a geographic characterization of the sampling regions into bio-optical provinces, which reflect hydrographic characteristics of the region with regards to the non-water absorption: Laptev Sea Shelf, Laptev Sea, Central Arctic/Transpolar Drift, Beaufort Gyre, and Eurasian/Nansen Basin. Moreover, it becomes clear that the characterization of provinces, in particular, in the highly seasonal variable Arctic Ocean, cannot hold true for every season and every year. Thus, although here we present a primary, simple bio-optical classification, we recall that such variability has been observed along the Arctic and integrative biogeochemical studies would benefit from the advances in Arctic Ecosystem monitoring and management by improving the delimitation of such geographic units. Future perspectives using automated platforms (e.g., floats, ice tethered profilers–ITPs, gliders) with bio-optical (e.g., Chl-*a* and DOM fluorescence, hyperspectral radiometry) and salinity sensors will allow to monitor the spatial and temporal variability within those biogeographic provinces.

The evaluation of empirical ocean color algorithms applied to our *in situ* $R_{rs}(\lambda)$ measurements showed that the evaluated algorithms are inappropriate to estimate Chl-*a* in the Central-Eastern Arctic Ocean, exhibiting an overall inverse correlation with *in situ* Chl-*a*. Even the regionally tuned OC3M-mod and OC4V6-mod only performed slightly better than the global algorithms, with great part of the retrievals staying within the 50% error interval. However, the retrievals were still inversely correlated to *in situ* Chl-*a*. Whilst better estimates have been obtained by applying those algorithms in the western Arctic (e.g., Cota et al., 2004; Matsuoka et al., 2014, 2007; Mustapha et al., 2012), our results show that those retrievals are strongly influenced by the high CDOM absorption in our study, leading to an overestimation of Chl-*a*. The empirical estimates were improved when removing stations with high $a_{CDOM}(443)$, reinforcing the existence of a persuasive positive bias by CDOM absorption on empirical Chl-*a* estimates for the Arctic Ocean. The semi-analytical ocean color algorithm GIOP, on the other hand, retrieved reliable Chl-*a* estimates related to the empirical algorithms, as well as considerably well estimates of $a_{ph}(443)$ and $a_{dg}(443)$, as previously reported to the western Arctic [Chaves et al., 2015]. Fairly similar retrievals were obtained within the GSM model with the modifications for the Arctic Ocean [Matsuoka et al., 2013] for $a_{dg}(443)$. The better performance by SAAs is mainly attributed to the fact that these algorithms do not consider Chl-*a* and CDOM as covariant.

Finally, with the ongoing pressure of climate change over the Arctic environment, a better understanding on the dynamics of carbon stocks has

been sought. Ocean color remote sensing appears to be a key tool on improving both the spatial and temporal monitoring these stocks. However, accurate ocean color retrievals are required to get to a real estimate of stocks and processes involving organic and inorganic carbon in the Arctic Ocean. We acknowledge the initiatives for developing regional tuned algorithms for the Arctic Ocean [Cota *et al.*, 2004; Bélanger *et al.*, 2008; Ben Mustapha *et al.*, 2012], which show the potential of those algorithms to provide better Chl-*a* estimates in the region. However, the positive bias between estimated Chl-*a* and CDOM absorption is still not resolved by those algorithms that keep the assumption of covariance between both parameters. Thus, we recall that additional spectral bands would improve the performance of such algorithms, as demonstrated for the GIOP in the western Arctic [Chaves *et al.*, 2015]. In addition, the coverage of ocean color remote sensing data in the polar regions needs to be increased by investing in developing efficient atmospheric correction for adjacency effects and low illumination conditions.

5.5. Acknowledgements

We thank the captain and crew of the RV Polarstern for their support during the ARKXXVI/3 cruise and to the chief scientist Dr. Ursula Schauer. We acknowledge for AWI Prof. Dr. Antje Boetius, Dr. Alexandra Cherkasheva, Dr. Estelle Kiliass and Olivia Serdeczny for RAMSES radiometric operation, water sampling and filtration during the cruise and Dr. Eva-Maria Nöthig, Christiane Lorenzen and Sonja Wiegmann (AWI) for their assistance in the preparation of the cruise. Sonja Wiegmann and Sandra Murawski for measurements of particulate absorption and pigment samples, respectively. Funding for the cruise was supplied partly by the Helmholtz Innovation Fund via the project Phytooptics (VH-NG-300). R.G.-A. was supported by a PhD fellowship from the Coordination for the Improvement of Higher Level Personnel (CAPES-Brazil, Grant 12362/12-3) in collaboration with the German Academic Exchange Service (DAAD).

Chapter 6

Synthesis and major outcomes

6. Synthesis and major outcomes

The Arctic environment is changing and the effects of these changes have already been observed in the Arctic Ocean. With an increase in the atmospheric temperature by 3 °C and 4 °C during summer and winter, respectively, since the 1950's [Przybylak, 2007], the Arctic sea-ice has reached its summer minimum records in 2007 and 2012 [Comiso *et al.*, 2008; Parkinson and Comiso, 2013]. In response to that, changes in the hydrological and biogeochemical cycles have already been reported [Peterson *et al.*, 2002; Bates and Mathis, 2009; Lalande *et al.*, 2009; Li *et al.*, 2009; Morison *et al.*, 2012; Parmentier *et al.*, 2013].

The Arctic Ocean basin receives the largest amount of freshwater relative to its volume compared to other oceans [Shiklomanov *et al.*, 2000] and with increased temperatures and consequent glacier melt [Sapiano *et al.*, 1998] and permafrost thaw [Schuur *et al.*, 2008, 2013], the export of freshwater has increased. For instance, the six largest Eurasian rivers had their average annual discharge increased by 7% from 1936 to 1999 [Peterson *et al.*, 2002]. Changes in the circulation due to the Arctic Oscillation index [Thompson and Wallace, 1998] exerts direct influence on the strength of the Beaufort Gyre and therefore is another factor modulating the variability in freshwater export relative to Canadian and Eurasian basins [Morison *et al.*, 2012]. Alongside, sea-ice melt introduces freshwater to the surface layer, which becomes warmer and less dense leading to stronger stratification of the surface layer [Serreze *et al.*, 2007; Yamamoto-Kawai *et al.*, 2009].

Changes in temperature, sea-ice coverage and freshwater export from the rivers implies drastic consequences to the Arctic biogeochemical cycles with respect to changes in primary production, greenhouse gases exchanges between ocean and atmosphere, and terrestrial carbon export and consequent carbon export to the deep layers. Studies have shown that both primary production [Arrigo and van Dijken, 2011] and carbon export from surface layers [Lalande *et al.*, 2009, 2014] increase as the sea-ice shrinks. At the same time, the abovementioned changes in the surface layer of the Arctic Ocean drive changes in the size structure of phytoplankton communities. With a stronger stratification and limited input of nutrients from the underneath layers smaller organisms (picophytoplankton, with a surface-area-to-volume ratio that provides effective acquisition of nutrient solutes and photons) outcompete over nanophytoplankton [Li *et al.*, 2009]. With increases in phytoplankton growth rates, increase in atmospheric CO₂ uptake in the Arctic Ocean surface waters is expected to happen [Bates *et al.*, 2006; Bates and Mathis, 2009]; however projections of future scenarios are still under debate and not yet fully understood. Although it has been postulated that an ice-free condition in the Arctic Ocean would increase the CO₂ uptake from the

atmosphere [Bates *et al.*, 2006; Bates and Mathis, 2009], recent predictions show that the Arctic Ocean will not become a large atmospheric CO₂ sink under ice-free condition [Cai *et al.*, 2010].

Permafrost is widely distributed along the Arctic environment [Schuur *et al.*, 2008] and it is susceptible to thawing when exposed to increased temperatures. It has been reported that permafrost thaw releases to the environment significant amounts of freshwater, organic matter and CH₄. The latter is a powerful greenhouse gas which can potentiate the effects of global warming over the Arctic [Hayes *et al.*, 2014]. The input of freshwater from the glacier melt together with the release of freshwater and organic carbon trapped in the permafrost increase significantly the freshwater and terrestrial organic carbon export to the Arctic Ocean [Peterson *et al.*, 2002; Schuur *et al.*, 2008, 2013]. In this sense, the Arctic Rivers play important role on these processes by draining both freshwater and terrestrial organic carbon into the Arctic Seas.

Among those rivers, the Lena River although having the third largest catchment ($\sim 2.4 \times 10^6$ km²) and the second highest freshwater discharge (about 600×10^9 m³ year⁻¹) accounts for the highest annual DOM discharge into the Arctic Ocean [Raymond *et al.*, 2007; Stedmon *et al.*, 2011]. Estimates for the annual discharge of DOC range between ~ 4 – 6 Tg C year⁻¹ [Opsahl *et al.*, 1999; Dittmar and Kattner, 2003; Raymond *et al.*, 2007], whereas POC contributes significantly less with an annual discharge of 0.38 Tg C year⁻¹ [Semiletov *et al.*, 2011]. It has been shown that most of the DOM input from the Lena River is of humic-like character and is highly correlated to lignin-phenol concentrations [Alling *et al.*, 2010; Walker *et al.*, 2013; Dubinenkov *et al.*, 2015a]. Former studies identified a conservative mixing of DOM along the transition river-ocean, suggesting that no processes other than pure dilution were modulating DOM mixing along the shelf [Cauwet and Sidorov, 1996; Kattner *et al.*, 1999]. However, it has been recently suggested that, in fact, a non-conservative DOM mixing takes place in the Laptev Sea, with strong removal of DOM (30–50%) possibly driven by photodegradation, flocculation, sedimentation, and microbial activity [Alling *et al.*, 2010]. Another factor leading to the dilution of DOM, primarily in coastal regions, is the sea-ice melt induced by the massive discharge of relatively warm river waters [Amon *et al.*, 2012].

In the study presented in Chapter 3 [Gonçalves-Araujo *et al.*, 2015b] a classification and relative contribution of fluorescent dissolved organic compounds (e.g., terrestrial vs. marine) were assessed along the mixing of the waters from the Lena River along the Laptev Sea shelf. It shows that UV-FDOM (generally associated to humic-like acids such as lignin-phenols) is the dominant FDOM fraction along the entire sampled region, with salinity ranging from 0.9 to 32.6. Furthermore, distinct mixing behaviors were observed with

respect to the DOM composition (terrestrial vs. marine) and water mass influence. Therefore, waters directly influenced by the Lena River plume (surface salinity <10) experienced strong removal of DOM, which in turn, was less for the high-salinity adjoining waters. It has also been shown that the strong removal at low salinity occurs preferably over terrestrial, humic-like compounds, while marine compounds seemed to be introduced in the environment by bacterial activity, leading to the quasi-conservative mixing observed for those components. Such a strong removal of terrestrially-derived compounds at low salinity was likely driven by photodegradation, adsorption, and flocculation, which was reinforced by analysis of the optical indices of DOM transformation. The study also showed that after removal at lower salinities, DOM presents a conservative behavior, with values close to the hypothetical conservative mixing lines. This suggests that after reaching high salinities DOM does not seem to suffer significant transformation or degradation else than pure dilution. The results and conclusions presented in this study gives insights on the composition and transformation of DOM in the transition river-sea and elucidates a more comprehensive understanding on the behavior of DOM through the mixing along the Laptev Sea shelf. Furthermore, although sea-ice melt and formation can affect the DOM amount, only a few studies have addressed this issue [e.g., *Amon et al.*, 2012; *Stedmon et al.*, 2015]. Therefore, sampling for analysis of the fractions of sea-ice melt and formation (i.e., $\delta^{18}\text{O}$) is crucial for DOM studies in the Arctic Ocean to achieve a more precise evaluation of the effects of sea-ice on DOM and estimation of reasonable estimation of DOM end-members. In addition, more studies addressing the spatial (and also temporal) variability of DOM in the Arctic shelves are required to reach a better comprehension on the DOM dynamics on a basin scale. Such a task is challenging given that in the Laptev Sea and most of the Arctic Ocean, oceanographic expeditions are mostly limited to late spring and summer seasons, due to the difficulties to access the Arctic Seas.

Although DOM is strongly removed in the Arctic shelves [*Alling et al.*, 2010; *Letscher et al.*, 2011; *Gonçalves-Araujo et al.*, 2015b], its signal is still strong enough to be detected in the Arctic surface waters exiting to the North Atlantic through the Fram Strait [*Amon et al.*, 2003; *Granskog et al.*, 2012; *Pavlov et al.*, 2015; *Stedmon et al.*, 2015]. It has been estimated that approximately 50% of the terrigenous CDOM input from the Arctic rivers is transported through the Fram Strait [*Granskog et al.*, 2012]. Therefore, studies have linked the spectral properties of CDOM (i.e., spectral slope vs. absorption coefficients) to trace the fresh water (estimated by means of riverine/meteoric water fraction) in the surface of the Arctic Ocean [*Stedmon and Markager*, 2001; *Granskog et al.*, 2012; *Stedmon et al.*, 2015]. However, although having a more sensitive signal than CDOM [*Blough and Del Vecchio*, 2002; *Coble*, 2007] and providing insights into the composition of DOM

[Coble, 1996; Stedmon *et al.*, 2003], the potential of FDOM as a tracer of freshwater has been applied considering the fluorescence only for specific, selected wavelength bands [Cooper *et al.*, 2005].

Given that most of the DOM in the surface waters exiting the Fram Strait is of terrestrial character [Granskog *et al.*, 2012; Stedmon *et al.*, 2015], the study presented in Chapter 4 [Gonçalves-Araujo *et al.*, 2016] presents the potential of using visible wavelength range fluorescence of DOM (VIS-FDOM) to trace the Arctic surface waters. This fraction of DOM, the VIS-FDOM, is strongly correlated to lignin-phenol (characteristic of terrestrial vascular plants) [Amon *et al.*, 2003]. The study showed that the VIS-FDOM is strongly correlated to the fraction of meteoric water (f_{mw} ; derived from riverine and atmospheric sources, such as glacier melt and precipitation) and, therefore, is a reliable tracer of the Arctic surface waters (responsible for the freshwater export to the North Atlantic). Additionally, with the variability observed in the contributions of the fractions of Atlantic and Pacific waters between the sampling years (f_{aw} and f_{pw} , respectively) a direct response was observed in VIS-FDOM, which was not detected by classical analysis of T-S diagrams. In the year with high contributions of f_{aw} , denoting greater contributions from Eurasian runoff, VIS-FDOM was higher than in the year with increased contribution of waters from the Canadian basin. Such differences in the background of Eurasian and Canadian waters related to DOM content are already known, with Eurasian waters presenting higher contribution of DOM related to waters from the Canadian basin [Stedmon *et al.*, 2011; Matsuoka *et al.*, 2014]. Finally, in the Davis Strait, VIS-FDOM detected turnover of DOM in the deep layers, which was not detected by absorption measurements. In those layers (>800 m) increased apparent oxygen utilization (AOU) was followed by increase in VIS-FDOM, suggesting a production of VIS-FDOM, linked to bacterial activity (respiration), in those waters. Thus, the study highlighted the potential of VIS-FDOM not only as a reliable tracer of the origin of Arctic surface waters, but also as a biogeochemical tracer, by detecting deep water turnover of DOM.

The VIS-FDOM wavelength fingerprints determined in the study [Gonçalves-Araujo *et al.*, 2016] showed which wavelength bands carry information on the source and mixing of DOM. Those components were in agreement with other studies conducted in the Arctic seas [Guéguen *et al.*, 2014; Dainard *et al.*, 2015; Jørgensen *et al.*, 2015]. Interestingly, the same three components isolated by the PARAFAC model in the referred study were also identified in cruises conducted along the central Arctic and Fram Strait [Rafael Gonçalves-Araujo and Astrid Bracher, unpublished data]. This suggests that the DOM along the pelagic waters of the Arctic Ocean has similar spectral characteristics, however with differing fluorescence intensities. Therefore, the spectral characteristics of the VIS-FDOM components isolated in this study provides information that will support the designing of new

technologies such as *in situ* multi-channel DOM fluorometers to trace the freshwater origins and decipher the water mass mixing dynamics in the region. Another advantage is the relatively cost effectiveness of the method, given that laborious samples will be taken only for calibration purposes. Finally, although using a dataset composed by only two summer samplings, the study showed that VIS-FDOM was highly correlated to f_{mw} what makes it a reliable tracer of Arctic freshwater. Thus, based on the potential exhibited by VIS-FDOM as a water mass tracer with an increased temporal resolution, it might be possible to determine a reverse model using VIS-FDOM fluorescence to retrieve river water fractions, and their respective exports to the North Atlantic. This would improve the sampling resolution, given that VIS-FDOM can be measured by *in situ* fluorometers, and those can be coupled to rosette systems as well as to autonomous platforms.

Because a fraction of DOM interacts with light via absorption (especially in the UV-VIS wavelength range), it has potential to be monitored by *in situ* bio-optical measurements and ocean color remote sensing. For instance, variability in R_{rs} spectra in the western Atlantic grouped similar spectra into bio-optical units that reproduced the biogeographical provinces defined by Longhurst [Longhurst, 2007] for that region [Taylor et al., 2011]. Additionally, a recent study used salinity data acquired with the MIRAS radiometer onboard the SMOS satellite, and derived $a_{\text{CDOM}}(443)$ from MODIS $R_{\text{rs}}(\lambda)$ products to waters in the western Arctic [Matsuoka et al., 2016]. Those authors identified the end-members of three major water masses through the correlations between $a_{\text{CDOM}}(443)$ and salinity: sea water, sea-ice melt water and river water. The last manuscript composing this thesis, presented in Chapter 5, shows that the surface waters in central and eastern Arctic Ocean have their non-water absorption extremely dominated by CDOM, which represented 99% of the total non-water absorption in some regions. Furthermore, by analyzing the absorption by non-water constituents (phytoplankton, CDOM and non-algal particles) together with hydrographical data (temperature and salinity) the division of five Arctic bio-optical provinces, with respect to spatial variability in those parameters, was suggested. The variability presented within those bio-optical provinces was reflected in R_{rs} spectra. Those provinces were classified as follows: (1) the Laptev Sea shelf, strongly influenced by the Lena River waters; (2) the Laptev Sea, with low contribution from the Lena runoff, however with contribution of waters advected from the Kara Sea; (3) the Central Arctic/Transpolar Drift, characterized by shelf waters transported through the central Arctic Basin; (4) the Beaufort Gyre, under influence of waters from the Canadian Basin; and (5) the Eurasian/Nansen Basin, characterized by the influence of Atlantic Waters entering the Arctic Ocean.

Those results reinforce the applicability of bio-optical information (e.g., absorption and R_{rs}) for detecting hydrographical and biogeochemical patterns

in the surface layers of the Arctic Ocean. Such variability led to the classification of the sampled region into bio-optical provinces. Those provinces showed different responses of non-water absorption to hydrographical variability and therefore, it suggests the existence of distinct geographical patterns in the Arctic carbon cycle. Studies have shown that microorganisms [Kilias *et al.*, 2014; Metfies *et al.*, 2016], biogenic carbon export from the surface layer [Lalande *et al.*, 2014] and primary production [Codispoti *et al.*, 2013; Fernández-Méndez *et al.*, 2015] have also presented geographically distinct distribution patterns. This emphasizes the need of the delimitation of Arctic biogeographical units based not only in bio-optical properties, but also taking into account the ecological aspects. Finally, the delimitation of biogeographic provinces in the Arctic Ocean would benefit not only the overall understanding of the ecological functioning and dynamics of carbon stocks in the region, it can also serve as a base for future strategies on Arctic environmental and resources awareness and management.

Whilst ocean color remote sensing provides data with improved spatial and temporal resolution, studies have shown that empirical ocean color algorithms perform poor for the Arctic Ocean [Cota *et al.*, 2004; Matsuoka *et al.*, 2007; Ben Mustapha *et al.*, 2012; IOCCG, 2015]. The most used ocean color remote sensing product, Chl-*a*, tend to be overestimated in the Arctic by those algorithms [Matsuoka *et al.*, 2007; IOCCG, 2015]. Such a poor performance by those algorithms is mainly to the CDOM absorption. Empirical ocean color algorithms applied to pelagic, oligotrophic waters assume CDOM and Chl-*a* to covary, what is not the case for the Arctic Ocean [Cota *et al.*, 2003; Wang *et al.*, 2005; Matsuoka *et al.*, 2007]. On the other hand, semi-analytical ocean color algorithms have performed better for retrieving Chl-*a* in the Arctic and they have the advantage of providing other biogeochemical products such as a_{ph} , a_{dg} , a_{NAP} and a_{CDOM} [Garver and Siegel, 1997; Maritorena *et al.*, 2002; Matsuoka *et al.*, 2013; Werdell *et al.*, 2013a, 2013b]. Although it is a powerful tool for biogeochemical monitoring of the Arctic Ocean, studies regarding the hyperspectral light variability in the water and evaluation of ocean color algorithms (as well as development of regional tuned ones) are limited to the western Arctic and, to our understanding, no such a study has been conducted in shelf and pelagic waters in the central and eastern Arctic Ocean. Regarding this lack of data, the second aim of the manuscript presented in Chapter 5 was to evaluate the performance of ocean color remote sensing algorithms from current missions that are frequently applied in the Arctic Ocean. For that purpose, those algorithms were applied to R_{rs} spectra measured *in situ* with hyperspectral radiometers, and the retrievals were then compared to the correspondent *in situ* measured parameters. The results demonstrated that the semi-analytical algorithms are more suitable for application in studies concerning biogeochemistry variability

in the Arctic Ocean in relation to empirical ocean color algorithms, given their better performance and providing reliable retrievals.

Finally, as previously pointed out in this thesis, ocean color remote sensing has strong limitations due to sea-ice and cloud coverage as well as the absence of data during the polar night. In this sense, optical sensors (such as multi-channel DOM fluorometers) appear as promising tools to fill those gaps and can increase the amount of biogeochemical data in the Arctic Ocean with reduced lab time. In the scope of the “*FRontiers in Arctic marine Monitoring*” initiative (FRAM Ocean Observing System-AWI), existing and next-generation sensors (e.g., multi-channel DOM fluorometers) are being designed with the aim to allow synchronous observation of relevant ocean variables, as well as the study of physical, chemical and biological processes in the water column and at the seafloor. Those sensors have potential to fill the sampling gaps from oceanographic expeditions and ocean color remote sensing in the Arctic Ocean when attached to autonomous platforms such as gliders, automated underwater vehicles (AUVs), ice-tethered profilers (ITPs), etc. For instance, ITPs can provide high-quality upper-ocean water-property observations for the Arctic Ocean [Krishfield *et al.*, 2008; Toole *et al.*, 2011]. Bio-optical measurements acquired with ITPs showed changes in bio-optical properties (e.g., CDOM fluorescence and particle backscatter) coupled with hydrographical variability [Laney *et al.*, 2014], stressing the applicability of bio-optical measurements to monitor water masses and biogeochemical dynamics and trends in the Arctic Ocean. Thus, autonomous profilers can provide a unique perspective into pelagic water column ecosystems, even in perennially ice-covered regions of the Arctic. In the future, with the development of more sophisticated and compact hyperspectral radiometers to incorporate to ITPs, those could be further used for optical inversion algorithms [Moline *et al.*, 2012].

Chapter 7

References

7. References

- Aagaard, K., and E. C. Carmack (1989), The role of sea ice and other fresh water in the Arctic circulation, *J. Geophys. Res.*, *94*(C10), 14485, doi:10.1029/JC094iC10p14485.
- Aagaard, K., J. H. Swift, and E. C. Carmack (1985), Thermohaline circulation in the Arctic Mediterranean Seas, *J. Geophys. Res.*, *90*(C3), 4833, doi:10.1029/JC090iC03p04833.
- Aiken, G. R., R. G. M. Spencer, R. G. Striegl, P. F. Schuster, and P. A. Raymond (2014), Influences of glacier melt and permafrost thaw on the age of dissolved organic carbon in the Yukon River basin, *Global Biogeochem. Cycles*, *28*(5), 525–537, doi:10.1002/2013GB004764.
- Alkire, M. B., K. K. Falkner, and T. Boyd (2010), Sea ice melt and meteoric water distribution in Nares Strait, Baffin Bay, and the Canadian Arctic Archipelago, *J. Mar.*, *68*(6), 767–798.
- Alling, V. et al. (2010), Nonconservative behavior of dissolved organic carbon across the Laptev and East Siberian seas, *Global Biogeochem. Cycles*, *24*(4), doi:10.1029/2010GB003834.
- Amon, R. M. W., G. Budéus, and B. Meon (2003), Dissolved organic carbon distribution and origin in the Nordic Seas: Exchanges with the Arctic Ocean and the North Atlantic, *J. Geophys. Res.*, *108*(C7), 3221, doi:10.1029/2002JC001594.
- Amon, R. M. W. et al. (2012), Dissolved organic matter sources in large Arctic rivers, *Geochim. Cosmochim. Acta*, *94*, 217–237, doi:10.1016/j.gca.2012.07.015.
- Antoine, D., M. Babin, J.-F. Berthon, A. Bricaud, B. Gentili, H. Loisel, S. Maritorena, and D. Stramski (2014), Shedding Light on the Sea: André Morel's Legacy to Optical Oceanography, *Ann. Rev. Mar. Sci.*, *6*(1), 1–21, doi:10.1146/annurev-marine-010213-135135.
- Aristegui, J., C. M. Duarte, S. Agustí, M. D. Doval, X. A. Álvarez-Salgado, and D. A. Hansell (2002), Dissolved Organic Carbon Support of Respiration in the Dark Ocean, *Science* (80-.), *298*, 1967–1967, doi:10.1126/science.1076746.
- Arrigo, K. R. (2014), Sea ice ecosystems, *Ann. Rev. Mar. Sci.*, *6*, 439–467, doi:10.1146/annurev-marine-010213-135103.
- Arrigo, K. R., and C. B. Brown (1996), Impact of chromophoric dissolved organic matter on UV inhibition of primary production in the sea, *Mar. Ecol. Progr. Ser.*, *140*, 207–216.
- Arrigo, K. R., and G. L. van Dijken (2011), Secular trends in Arctic Ocean net primary production, *J. Geophys. Res.*, *116*(C9), C09011, doi:10.1029/2011JC007151.
- Arrigo, K. R. et al. (2012), Massive Phytoplankton Blooms Under Arctic Sea Ice, *Science* (80-.), *336*(6087), 1408–1408,

doi:10.1126/science.1215065.

- Arrigo, K. R., V. Hill, S. Bélanger, B. G. Mitchell, T. Hirawake, and M. Babin (2015), *Estimates of Net Primary Production from Space-based Measurements, IOCCG Report 16: Ocean Colour Remote Sensing in Polar Seas*.
- Asmala, E., R. Autio, H. Kaartokallio, C. A. Stedmon, and D. N. Thomas (2014), Processing of humic-rich riverine dissolved organic matter by estuarine bacteria: effects of predegradation and inorganic nutrients, *Aquat. Sci.*, 76(3), 451–463, doi:10.1007/s00027-014-0346-7.
- Auel, H., and W. Hagen (2002), Mesozooplankton community structure, abundance and biomass in the central Arctic Ocean, *Mar. Biol.*, 140(5), 1013–1021, doi:10.1007/s00227-001-0775-4.
- Azetsu-Scott, K., A. Clarke, K. Falkner, J. Hamilton, E. P. Jones, C. Lee, B. Petrie, S. Prinsenberg, M. Starr, and P. Yeats (2010), Calcium carbonate saturation states in the waters of the Canadian Arctic Archipelago and the Labrador Sea, *J. Geophys. Res.*, 115(C11), C11021, doi:10.1029/2009JC005917.
- Azetsu-Scott, K., B. Petrie, P. Yeats, and C. Lee (2012), Composition and fluxes of freshwater through Davis Strait using multiple chemical tracers, *J. Geophys. Res. Ocean.*, 117(C12), n/a-n/a, doi:10.1029/2012JC008172.
- Babin, M., D. Stramski, G. M. Ferrari, H. Claustre, A. Bricaud, G. Obolensky, and N. Hoepffner (2003), Variations in the light absorption coefficients of phytoplankton, nonalgal particles, and dissolved organic matter in coastal waters around Europe, *J. Geophys. Res.*, 108(C7), 3211, doi:10.1029/2001JC000882.
- Bates, N. R., and J. T. Mathis (2009), The Arctic Ocean marine carbon cycle: evaluation of air-sea CO₂ exchanges, ocean acidification impacts and potential feedbacks, *Biogeosciences*, 6(4), 2433–2459, doi:10.5194/bg-6-6695-2009.
- Bates, N. R., S. B. Moran, D. A. Hansell, and J. T. Mathis (2006), An increasing CO₂ sink in the Arctic Ocean due to sea-ice loss, *Geophys. Res. Lett.*, 33(23), 1–7, doi:10.1029/2006GL027028.
- Bauch, D., I. Dmitrenko, S. Kirillov, C. Wegner, J. Hölemann, S. Pivovarov, L. Timokhov, and H. Kassens (2009), Eurasian Arctic shelf hydrography: Exchange and residence time of southern Laptev Sea waters, *Cont. Shelf Res.*, 29(15), 1815–1820, doi:10.1016/j.csr.2009.06.009.
- Bauch, D., M. Gröger, I. Dmitrenko, J. Hölemann, S. Kirillov, A. Mackensen, E. Taldenkova, and N. Andersen (2011a), Atmospheric controlled freshwater release at the Laptev Sea continental margin, *Polar Res.*, 30(SUPPL.1), 1–14, doi:10.3402/polar.v30i0.5858.
- Bauch, D., M. R. van der Loeff, N. Andersen, S. Torres-Valdes, K. Bakker, and E. P. Abrahamson (2011b), Origin of freshwater and polynya water in the Arctic Ocean halocline in summer 2007, *Prog. Oceanogr.*, 91(4), 482–495, doi:10.1016/j.pocean.2011.07.017.

- Bauch, D., J. a. Hölemann, A. Nikulina, C. Wegner, M. a. Janout, L. a. Timokhov, and H. Kassens (2013), Correlation of river water and local sea-ice melting on the Laptev Sea shelf (Siberian Arctic), *J. Geophys. Res. Ocean.*, *118*(1), 550–561, doi:10.1002/jgrc.20076.
- Bauch, D., E. Cherniavskaia, and L. Timokhov (2016), Shelf basin exchange along the Siberian continental margin: Modification of Atlantic Water and Lower Halocline Water, *Deep Sea Res. Part I Oceanogr. Res. Pap.*, *115*, 188–198, doi:10.1016/j.dsr.2016.06.008.
- Bélanger, S., H. Xie, N. Krotkov, P. Larouche, W. F. Vincent, and M. Babin (2006), Photomineralization of terrigenous dissolved organic matter in Arctic coastal waters from 1979 to 2003: Interannual variability and implications of climate change, *Global Biogeochem. Cycles*, *20*(4), n/a-n/a, doi:10.1029/2006GB002708.
- Bélanger, S., M. Babin, and P. Larouche (2008), An empirical ocean color algorithm for estimating the contribution of chromophoric dissolved organic matter to total light absorption in optically complex waters, *J. Geophys. Res.*, *113*(C4), C04027, doi:10.1029/2007JC004436.
- Benner, R., and S. Opsahl (2001), Molecular indicators of the sources and transformations of dissolved organic matter in the Mississippi river plume, *Org. Geochem.*, *32*, 597–611.
- Benner, R., B. Benitez-Nelson, K. Kaiser, and R. M. W. Amon (2004), Export of young terrigenous dissolved organic carbon from rivers to the Arctic Ocean, *Geophys. Res. Lett.*, *31*(5), doi:10.1029/2003GL019251.
- Benner, R., P. Louchouart, and R. M. W. Amon (2005), Terrigenous dissolved organic matter in the Arctic Ocean and its transport to surface and deep waters of the North Atlantic, *Global Biogeochem. Cycles*, *19*(2), n/a-n/a, doi:10.1029/2004GB002398.
- Beszczyńska-Möller, A., E. Fahrbach, U. Schauer, and E. Hansen (2012), Variability in Atlantic water temperature and transport at the entrance to the Arctic Ocean, 1997-2010, *ICES J. Mar. Sci.*, *69*(5), 852–863, doi:10.1093/icesjms/fss056.
- Blough, N. V., and R. Del Vecchio (2002), Chromophoric DOM in the coastal environment, in *Biogeochemistry of marine dissolved organic matter*, edited by D. A. Hansell and C. A. Carlson, pp. 509–546, Academic Press.
- Bluhm, B. A., K. N. Kosobokova, and E. C. Carmack (2015), A tale of two basins: An integrated physical and biological perspective of the deep Arctic Ocean, *Prog. Oceanogr.*, *139*(August), 89–121, doi:10.1016/j.pocean.2015.07.011.
- Boersma, M., K. A. Mathew, B. Niehoff, K. L. Schoo, R. M. Franco-Santos, and C. L. Meunier (2016), Temperature driven changes in the diet preference of omnivorous copepods: No more meat when it's hot?, *Ecol. Lett.*, *19*(1), 45–53, doi:10.1111/ele.12541.
- Bolan, N. S., S. Baskaran, and S. Thiagarajan (1996), An evaluation of the methods of measurement of dissolved organic carbon in soils, manures, sludges, and stream water, *Commun. Soil Sci. Plant Anal.*, *27*(13–14),

2723–2737, doi:10.1080/00103629609369735.

- Børsheim, K. Y., and S. M. Mykkestad (1997), Dynamics of DOC in the Norwegian Sea inferred from monthly profiles collected during 3 years at 66°N, 2°E, *Deep Sea Res. Part I Oceanogr. Res. Pap.*, 44(4), 593–601, doi:10.1016/S0967-0637(96)00106-9.
- Boyd, T. J., and C. L. Osburn (2004), Changes in CDOM fluorescence from allochthonous and autochthonous sources during tidal mixing and bacterial degradation in two coastal estuaries, *Mar. Chem.*, 89(1–4), 189–210, doi:10.1016/j.marchem.2004.02.012.
- Bricaud, A., M. Babin, A. Morel, and H. Claustre (1995), Variability in the chlorophyll-specific absorption coefficients of natural phytoplankton: Analysis and parametrization, *J. Geophys. Res.*, 100(C7), 13321–13332.
- Bricaud, A., A. Morel, M. Babin, K. Allali, and H. Claustre (1998), Variations of light absorption by suspended particles with chlorophyll a concentration in oceanic (case 1) waters: Analysis and implications for bio-optical models, *J. Geophys. Res. Ocean.*, 103(C13), 31033–31044, doi:10.1029/98JC02712.
- Broecker, W. (1991), The Great Ocean Conveyor, *Oceanography*, 4(2), 79–89, doi:10.5670/oceanog.1991.07.
- Cai, W.-J. et al. (2010), Decrease in the CO₂ Uptake Capacity in an Ice-Free Arctic Ocean Basin, *Science* (80-.), 329(5991), 556–559, doi:10.1126/science.1189338.
- Campbell, J. W. (1995), The lognormal distribution as a model for bio-optical variability in the sea, *J. Geophys. Res.*, 100(C7), 13237, doi:10.1029/95JC00458.
- Carmack, E., and K. Aagaard (1973), On the deep water of the Greenland Sea, *Deep Sea Res. Oceanogr. Abstr.*, 20(8), 687–715, doi:10.1016/0011-7471(73)90086-7.
- Catalá, T. S. et al. (2015a), Turnover time of fluorescent dissolved organic matter in the dark global ocean., *Nat. Commun.*, 6, 5986, doi:10.1038/ncomms6986.
- Catalá, T. S. et al. (2015b), Water mass age and aging driving chromophoric dissolved organic matter in the dark global ocean, *Global Biogeochem. Cycles*, 29(7), 917–934, doi:10.1002/2014GB005048.
- Catalá, T. S., I. Reche, C. L. Ramón, À. López-Sanz, M. Álvarez, E. Calvo, and X. A. Álvarez-Salgado (2016), Chromophoric signatures of microbial by-products in the dark ocean, *Geophys. Res. Lett.*, 43(14), 7639–7648, doi:10.1002/2016GL069878.
- Cauwet, G., and I. Sidorov (1996), The biogeochemistry of Lena River: Organic carbon and nutrients distribution, *Mar. Chem.*, 53(3–4), 211–227, doi:10.1016/0304-4203(95)00090-9.
- Chapin, F. S. et al. (2005), Ecosystems and human well-being. Volume 1: Current state and trends, in *Polar systems*, edited by R. Hassan, R. Scholes, and N. Ash, pp. 717–746, Island Press, Washington, Columbia.

- Chari, N. V. H. K., S. Keerthi, N. S. Sarma, S. R. Pandi, G. Chiranjeevulu, R. Kiran, and U. Koduru (2013), Fluorescence and absorption characteristics of dissolved organic matter excreted by phytoplankton species of western Bay of Bengal under axenic laboratory condition, *J. Exp. Mar. Bio. Ecol.*, *445*, 148–155, doi:10.1016/j.jembe.2013.03.015.
- Chaves, J. E., P. J. Werdell, C. W. Proctor, A. R. Neeley, S. A. Freeman, C. S. Thomas, and S. B. Hooker (2015), Assessment of ocean color data records from MODIS-Aqua in the western Arctic Ocean, *Deep Sea Res. Part II Top. Stud. Oceanogr.*, *118*, 32–43, doi:10.1016/j.dsr2.2015.02.011.
- Cherkasheva, A. (2014), Greenland Sea primary production with respect to changes in sea ice cover, University of Bremen.
- Cherkasheva, A., A. Bracher, C. Melsheimer, C. Köberle, R. Gerdes, E.-M. Nöthig, E. Bauerfeind, and A. Boetius (2014), Influence of the physical environment on polar phytoplankton blooms: A case study in the Fram Strait, *J. Mar. Syst.*, *132*, 196–207, doi:10.1016/j.jmarsys.2013.11.008.
- Clarke, K. R., and R. M. Warwick (1994), *Changes in Marine Communities: An approach to Statistical Analysis and Interpretation.*, Natural Environmental Research Council, Plymouth, UK.
- Clarke, R. A., and J.-C. Gascard (1983), The Formation of Labrador Sea Water. Part I: Large-Scale Processes, *J. Phys. Oceanogr.*, *13*(10), 1764–1778, doi:10.1175/1520-0485(1983)013<1764:TFOLSW>2.0.CO;2.
- Coble, P. G. (1996), Characterization of marine and terrestrial DOM in seawater using excitation-emission matrix spectroscopy, *Mar. Chem.*, *51*(4), 325–346, doi:10.1016/0304-4203(95)00062-3.
- Coble, P. G. (2007), Marine Optical Biogeochemistry: The Chemistry of Ocean Color, *Chem. Rev.*, *107*, 402–418.
- Codispoti, L. A., V. Kelly, A. Thessen, P. Matrai, S. Suttles, V. Hill, M. Steele, and B. Light (2013), Synthesis of primary production in the Arctic Ocean: III. Nitrate and phosphate based estimates of net community production, *Prog. Oceanogr.*, *110*(December 2012), 126–150, doi:10.1016/j.pocean.2012.11.006.
- Comiso, J. C., C. L. Parkinson, R. Gersten, and L. Stock (2008), Accelerated decline in the Arctic sea ice cover, *Geophys. Res. Lett.*, *35*(1), 1–6, doi:10.1029/2007GL031972.
- Cooper, L. W., R. Benner, J. W. McClelland, B. J. Peterson, R. M. Holmes, P. A. Raymond, D. A. Hansell, J. M. Grebmeier, and L. A. Codispoti (2005), Linkages among runoff, dissolved organic carbon, and the stable oxygen isotope composition of seawater and other water mass indicators in the Arctic Ocean, *J. Geophys. Res.*, *110*(G2), G02013, doi:10.1029/2005JG000031.
- Cota, G., J. Wang, and J. C. Comiso (2004), Transformation of global satellite chlorophyll retrievals with a regionally tuned algorithm, *Remote Sens. Environ.*, *90*(3), 373–377, doi:10.1016/j.rse.2004.01.005.
- Cota, G. F., W. G. Harrison, T. Platt, S. Sathyendranath, and V. Stuart (2003),

- Bio-optical properties of the Labrador Sea, *J. Geophys. Res.*, 108(C7), 3228, doi:10.1029/2000JC000597.
- Curry, B., C. M. Lee, B. Petrie, R. E. Moritz, and R. Kwok (2014), Multiyear Volume, Liquid Freshwater, and Sea Ice Transports through Davis Strait, 2004–10*, *J. Phys. Oceanogr.*, 44(4), 1244–1266, doi:10.1175/JPO-D-13-0177.1.
- Dainard, P. G., C. Guéguen, N. McDonald, and W. J. Williams (2015), Photobleaching of fluorescent dissolved organic matter in Beaufort Sea and North Atlantic Subtropical Gyre, *Mar. Chem.*, 177, 630–637, doi:10.1016/j.marchem.2015.10.004.
- Dittmar, T., and G. Kattner (2003), The biogeochemistry of the river and shelf ecosystem of the Arctic Ocean: a review, *Mar. Chem.*, 83(3–4), 103–120, doi:10.1016/S0304-4203(03)00105-1.
- Dittmar, T., K. Whitehead, E. C. Minor, and B. P. Koch (2007), Tracing terrigenous dissolved organic matter and its photochemical decay in the ocean by using liquid chromatography/mass spectrometry, *Mar. Chem.*, 107(3), 378–387, doi:10.1016/j.marchem.2007.04.006.
- Dodd, P. A., B. Rabe, E. Hansen, E. Falck, A. Mackensen, E. Rohling, C. Stedmon, and S. Kristiansen (2012), The freshwater composition of the Fram Strait outflow derived from a decade of tracer measurements, *J. Geophys. Res.*, 117(C11005), 1–26, doi:10.1029/2012JC008011.
- Druffel, E. R. M., and J. E. Bauer (2000), Radiocarbon distributions in Southern Ocean dissolved and particulate organic matter, *Geophys. Res. Lett.*, 27(10), 1495–1498, doi:10.1029/1999GL002398.
- Dubinenkov, I., R. Flerus, P. Schmitt-Kopplin, G. Kattner, and B. P. Koch (2015a), Origin-specific molecular signatures of dissolved organic matter in the Lena Delta, *Biogeochemistry*, 123(1–2), 1–14, doi:10.1007/s10533-014-0049-0.
- Dubinenkov, I., A. C. Kraberg, I. Bussmann, G. Kattner, and B. P. Koch (2015b), Physical Oceanography and Dissolved Organic Matter in the Coastal Laptev Sea in 2013, *PANGAEA*, doi:10.1594/PANGAEA.842221.
- Dubinenkov, I. V (2015), Molecular biogeochemistry of dissolved organic matter in the permafrost-influenced Lena delta, University of Bremen.
- Falck, E., G. Kattner, and G. Budéus (2005), Disappearance of Pacific Water in the northwestern Fram Strait, *Geophys. Res. Lett.*, 32(14), n/a-n/a, doi:10.1029/2005GL023400.
- Fedorova, I. et al. (2015), Lena Delta hydrology and geochemistry: long-term hydrological data and recent field observations, *Biogeosciences*, 12(2), 345–363, doi:10.5194/bg-12-345-2015.
- Fernández-Méndez, M., C. Katlein, B. Rabe, M. Nicolaus, I. Peeken, K. Bakker, H. Flores, and A. Boetius (2015), Photosynthetic production in the central Arctic Ocean during the record sea-ice minimum in 2012, *Biogeosciences*, 12, 3525–3549, doi:10.5194/bg-12-3525-2015.
- Ferrari, G. M., and S. Tassan (1999), A method using chemical oxidation to

- remove light absorption by phytoplankton pigments, *J. Phycol.*, 35(5), 1090–1098, doi:10.1046/j.1529-8817.1999.3551090.x.
- Fetterer, F., and N. Untersteiner (1998), Observations of melt ponds on Arctic sea ice, *J. Geophys. Res. Ocean.*, 103(C11), 24821–24835, doi:10.1029/98JC02034.
- Fichot, C. G., and R. Benner (2012), The spectral slope coefficient of chromophoric dissolved organic matter (S₂₇₅₋₂₉₅) as a tracer of terrigenous dissolved organic carbon in river-influenced ocean margins, *Limnol. Oceanogr.*, 57(5), 1453–1466, doi:10.4319/lo.2012.57.5.1453.
- Fichot, C. G., and W. L. Miller (2010), An approach to quantify depth-resolved marine photochemical fluxes using remote sensing: Application to carbon monoxide (CO) photoproduction, *Remote Sens. Environ.*, 114(7), 1363–1377, doi:10.1016/j.rse.2010.01.019.
- Fichot, C. G., K. Kaiser, S. B. Hooker, R. M. W. Amon, M. Babin, S. Bélanger, S. A. Walker, and R. Benner (2013), Pan-Arctic distributions of continental runoff in the Arctic Ocean, *Sci. Rep.*, 3, 1053, doi:10.1038/srep01053.
- Fichot, C. G., R. Benner, K. Kaiser, Y. Shen, R. M. W. Amon, H. Ogawa, and C.-J. Lu (2016), Predicting Dissolved Lignin Phenol Concentrations in the Coastal Ocean from Chromophoric Dissolved Organic Matter (CDOM) Absorption Coefficients, *Front. Mar. Sci.*, 3(February), 7, doi:10.3389/fmars.2016.00007.
- Fofonova, V., A. Androsov, S. Danilov, M. Janout, E. Sofina, and K. Wiltshire (2014), Semidiurnal tides in the Laptev Sea Shelf zone in the summer season, *Cont. Shelf Res.*, 73, 119–132, doi:10.1016/j.csr.2013.11.010.
- Frey, K. E., and J. W. McClelland (2009), Impacts of permafrost degradation on arctic river biogeochemistry, *Hydrol. Process.*, 23(1), 169–182, doi:10.1002/hyp.7196.
- Fukuzaki, K., I. Imai, K. Fukushima, K.-I. Ishii, S. Sawayama, and T. Yoshioka (2014), Fluorescent characteristics of dissolved organic matter produced by bloom-forming coastal phytoplankton, *J. Plankton Res.*, 36(3), 685–694, doi:10.1093/plankt/fbu015.
- Garver, S. A., and D. A. Siegel (1997), Inherent optical property inversion of ocean color spectra and its biogeochemical interpretation: 1. Time series from the Sargasso Sea, *J. Geophys. Res. Ocean.*, 102(C8), 18607–18625, doi:10.1029/96JC03243.
- Geider, R., and J. La Roche (2002), Redfield revisited: variability of C:N:P in marine microalgae and its biochemical basis, *Eur. J. Phycol.*, 37(1), 1–17, doi:10.1017/S0967026201003456.
- Gonçalves-Araujo, R. (2016), Tools for assessing content, speciation and origin of DOM in aquatic systems, in *Proceedings YOUMARES7*, pp. 32–42, YOUMARES 7 - Proceedings, Hamburg - Germany.
- Gonçalves-Araujo, R., C. A. Stedmon, B. Heim, I. Dubinenkov, A. C. Kraberg, D. Moiseev, and A. Bracher (2015a), Dissolved Organic Matter in the Lena River Delta Region, Siberia, Russia., *PANGAEA*,

doi:10.1594/PANGAEA.84492.

- Gonçalves-Araujo, R., C. A. Stedmon, B. Heim, I. Dubinenkov, A. Kraberg, D. Moiseev, and A. Bracher (2015b), From Fresh to Marine Waters: Characterization and Fate of Dissolved Organic Matter in the Lena River Delta Region, Siberia, *Front. Mar. Sci.*, *2*:108, 1–13, doi:10.3389/fmars.2015.00108.
- Gonçalves-Araujo, R., M. S. de Souza, V. M. Tavano, and C. A. E. Garcia (2015c), Influence of oceanographic features on spatial and interannual variability of phytoplankton in the Bransfield Strait, Antarctica, *J. Mar. Syst.*, *142*, 1–15, doi:10.1016/j.jmarsys.2014.09.007.
- Gonçalves-Araujo, R., M. A. Granskog, A. Bracher, K. Azetsu-Scott, P. A. Dodd, and C. A. Stedmon (2016), Using fluorescent dissolved organic matter to trace and distinguish the origin of Arctic surface waters, *Sci. Rep.*, *6*, 33978, doi:10.1038/srep33978.
- Gonsior, M., B. M. Peake, W. T. Cooper, D. Podgorski, J. D'Andrilli, and W. J. Cooper (2009), Photochemically Induced Changes in Dissolved Organic Matter Identified by Ultrahigh Resolution Fourier Transform Ion Cyclotron Resonance Mass Spectrometry, *Environ. Sci. Technol.*, *43*(3), 698–703, doi:10.1021/es8022804.
- Granskog, M. A., C. A. Stedmon, P. A. Dodd, R. M. W. Amon, A. K. Pavlov, L. de Steur, and E. Hansen (2012), Characteristics of colored dissolved organic matter (CDOM) in the Arctic outflow in the Fram Strait: Assessing the changes and fate of terrigenous CDOM in the Arctic Ocean, *J. Geophys. Res.*, *117*(C12), C12021, doi:10.1029/2012JC008075.
- Granskog, M. A., A. K. Pavlov, S. Sagan, P. Kowalczyk, A. Raczowska, and C. A. Stedmon (2015), Effect of sea-ice melt on inherent optical properties and vertical distribution of solar radiant heating in Arctic surface waters, *J. Geophys. Res. Ocean.*, *120*(10), 7028–7039, doi:10.1002/2015JC011087.
- Green, S. A., and N. V. Blough (1994), Optical absorption and fluorescence properties of chromophoric dissolved organic matter in natural waters, *Limnol. Oceanogr.*, *39*(8), 1903–1916, doi:10.4319/lo.1994.39.8.1903.
- Guéguen, C., M. A. Granskog, G. McCullough, and D. G. Barber (2011), Characterisation of colored dissolved organic matter in Hudson Bay and Hudson Strait using parallel factor analysis, *J. Mar. Syst.*, *88*(3), 423–433, doi:10.1016/j.jmarsys.2010.12.001.
- Guéguen, C., C. W. Cuss, C. J. Cassels, and E. C. Carmack (2014), Absorption and fluorescence of dissolved organic matter in the waters of the Canadian Arctic Archipelago, Baffin Bay, and the Labrador Sea, *J. Geophys. Res. Ocean.*, *119*(3), 2034–2047, doi:10.1002/2013JC009173.
- Guéguen, C., M. Itoh, T. Kikuchi, J. Eert, and W. J. Williams (2015), Variability in dissolved organic matter optical properties in surface waters in the Amerasian Basin, *Front. Mar. Sci.*, *2*:78, 1–9, doi:10.3389/fmars.2015.00078.
- Guo, W., C. A. Stedmon, Y. Han, F. Wu, X. Yu, and M. Hu (2007), The

- conservative and non-conservative behavior of chromophoric dissolved organic matter in Chinese estuarine waters, *Mar. Chem.*, 107(3), 357–366, doi:10.1016/j.marchem.2007.03.006.
- Guo, W., J. Xu, J. Wang, Y. Wen, J. Zhuo, and Y. Yan (2010), Characterization of dissolved organic matter in urban sewage using excitation emission matrix fluorescence spectroscopy and parallel factor analysis, *J. Environ. Sci.*, 22(11), 1728–1734, doi:10.1016/S1001-0742(09)60312-0.
- Hambly, A. C., R. K. Henderson, M. V. Storey, A. Baker, R. M. Stuetz, and S. J. Khan (2010), Fluorescence monitoring at a recycled water treatment plant and associated dual distribution system – Implications for cross-connection detection, *Water Res.*, 44(18), 5323–5333, doi:10.1016/j.watres.2010.06.003.
- Hansell, D. A., D. Kadko, and N. R. Bates (2004), Degradation of Terrigenous Dissolved Organic Carbon in the Western Arctic Ocean, *Science (80-.)*, 304(5672), 858–861, doi:10.1126/science.1096175.
- Hansen, H. P., and F. Koroleff (1999), Determination of nutrients, in *Methods of Seawater Analysis*, edited by K. Grasshoff, K. Kremling, and M. Ehrhardt, pp. 159–228, Wiley-VCH Verlag GmbH, Weinheim, Germany.
- Hansen, M. O., T. G. Nielsen, C. A. Stedmon, and P. Munk (2012), Oceanographic regime shift during 1997 in Disko Bay, Western Greenland, *Limnol. Oceanogr.*, 57(2), 634–644, doi:10.4319/lo.2012.57.2.0634.
- Harms, I. H., and M. J. Karcher (1999), Modeling the seasonal variability of hydrography and circulation in the Kara Sea, *J. Geophys. Res.*, 104(C6), 13431, doi:10.1029/1999JC900048.
- Hattermann, T., P. E. Isachsen, W.-J. von Appen, J. Albrechtsen, and A. Sundfjord (2016), Eddy-driven recirculation of Atlantic Water in Fram Strait, *Geophys. Res. Lett.*, 43(7), 3406–3414, doi:10.1002/2016GL068323.
- Hayes, D. J., D. W. Kicklighter, A. D. McGuire, M. Chen, Q. Zhuang, F. Yuan, J. M. Melillo, and S. D. Wullschleger (2014), The impacts of recent permafrost thaw on land–atmosphere greenhouse gas exchange, *Environ. Res. Lett.*, 9(4), 45005, doi:10.1088/1748-9326/9/4/045005.
- Hedges, J. I. (1992), Global biogeochemical cycles: progress and problems, *Mar. Chem.*, 39(1–3), 67–93, doi:10.1016/0304-4203(92)90096-S.
- Heim, B. et al. (2014), Ocean colour remote sensing in the southern Laptev Sea: evaluation and applications, *Biogeosciences*, 11(15), 4191–4210, doi:10.5194/bg-11-4191-2014.
- Helms, J. R., A. Stubbins, J. D. Ritchie, E. C. Minor, D. J. Kieber, and K. Mopper (2008), Absorption spectral slopes and slope ratios as indicators of molecular weight, source, and photobleaching of chromophoric dissolved organic matter, *Limnol. Oceanogr.*, 53(3), 955–969.
- Helms, J. R., J. Mao, A. Stubbins, K. Schmidt-Rohr, R. G. M. Spencer, P. J. Hernes, and K. Mopper (2014), Loss of optical and molecular indicators

- of terrigenous dissolved organic matter during long-term photobleaching, *Aquat. Sci.*, 76(3), 353–373, doi:10.1007/s00027-014-0340-0.
- Hildebrandt, N., B. Niehoff, and F. J. Sartoris (2014), Long-term effects of elevated CO₂ and temperature on the Arctic calanoid copepods *Calanus glacialis* and *C. hyperboreus*, *Mar. Pollut. Bull.*, 80(1–2), 59–70, doi:10.1016/j.marpolbul.2014.01.050.
- Huguet, A., L. Vacher, S. Relexans, S. Saubusse, J. M. Froidefond, and E. Parlanti (2009), Properties of fluorescent dissolved organic matter in the Gironde Estuary, *Org. Geochem.*, 40(6), 706–719, doi:10.1016/j.orggeochem.2009.03.002.
- IOCCG (2006), *IOCCG Report number 5: Remote Sensing of Inherent Optical Properties: Fundamentals, Tests of Algorithms, and Applications*.
- IOCCG (2015), *IOCCG Report number 16: Ocean Colour Remote Sensing in Polar Seas*.
- IPCC (2013), *Climate Change 2013: The Physical Science Basis. Contribution of working group I to the Fifth Assessment Report of the IPCC*.
- Janout, M. A. et al. (2015), Kara Sea freshwater transport through Vilkitsky Strait: Variability, forcing, and further pathways toward the western Arctic Ocean from a model and observations, *J. Geophys. Res. Ocean.*, 120(7), 4925–4944, doi:10.1002/2014JC010635.
- Jeffrey, S. W., R. F. C. Mantoura, and S. W. Wright (Eds.) (1997), *Phytoplankton pigments in Oceanography: Guideline to modern methods*, UNESCO Publishing.
- Jones, E. P., D. M. Nelson, and P. Treguer (1990), Chemical Oceanography, in *Polar Oceanography Part B: Chemistry, Biology, and Geology*, edited by W. O. Smith Jr, pp. 407–476, Elsevier Inc.
- Jones, E. P., L. G. Anderson, S. Jutterstro, L. Mintrop, and J. H. Swift (2008), Pacific freshwater, river water and sea ice meltwater across Arctic Ocean basins: Results from the 2005 Beringia Expedition, *J. Geophys. Res.*, 113(C08012), 1–10, doi:10.1029/2007JC004124.
- Jones, P. E., L. G. Anderson, and J. H. Swift (1998), Distribution of Atlantic and Pacific water in the upper Arctic Ocean: Implications for circulation, *Geophys. Res. Lett.*, 25(6), 765–768.
- Jørgensen, L., C. A. Stedmon, T. Kragh, S. Markager, M. Middelboe, and M. Søndergaard (2011), Global trends in the fluorescence characteristics and distribution of marine dissolved organic matter, *Mar. Chem.*, 126(1–4), 139–148, doi:10.1016/j.marchem.2011.05.002.
- Jørgensen, L., C. A. Stedmon, M. A. Granskog, and M. Middelboe (2014), Tracing the long-term microbial production of recalcitrant fluorescent dissolved organic matter in seawater, *Geophys. Res. Lett.*, 41(7), 2481–2488, doi:10.1002/2014GL059428.
- Jørgensen, L., C. A. Stedmon, H. Kaartokallio, M. Middelboe, and D. N. Thomas (2015), Changes in the composition and bioavailability of dissolved organic matter during sea ice formation, *Limnol. Oceanogr.*,

- 60(3), 817–830, doi:10.1002/lno.10058.
- Kara, A. B., P. A. Rochford, and H. E. Hurlburt (2000a), An optimal definition for ocean mixed layer depth, *J. Geophys. Res.*, *105*, 16803–18621.
- Kara, A. B., P. A. Rochford, and H. E. Hurlburt (2000b), Mixed layer depth variability and barrier layer formation over the North Pacific Ocean, *J. Geophys. Res. Ocean.*, *105*(C7), 16783–16801.
- Kattner, G., J. . Lobbes, H. . Fitznar, R. Engbrodt, E.-M. Nöthig, and R. . Lara (1999), Tracing dissolved organic substances and nutrients from the Lena River through Laptev Sea (Arctic), *Mar. Chem.*, *65*(1–2), 25–39, doi:10.1016/S0304-4203(99)00008-0.
- Kellerman, A. M., D. N. Kothawala, T. Dittmar, and L. J. Tranvik (2015), Persistence of dissolved organic matter in lakes related to its molecular characteristics, *Nat. Geosci.*, *8*(6), 454–457, doi:10.1038/geo2440.
- Kilias, E., G. Kattner, C. Wolf, S. Frickenhaus, and K. Metfies (2014), A molecular survey of protist diversity through the central Arctic Ocean, *Polar Biol.*, *37*(9), 1271–1287, doi:10.1007/s00300-014-1519-5.
- Kim, S., R. W. Kramer, and P. G. Hatcher (2003), Graphical Method for Analysis of Ultrahigh-Resolution Broadband Mass Spectra of Natural Organic Matter, the Van Krevelen Diagram, *Anal. Chem.*, *75*(20), 5336–5344, doi:10.1021/ac034415p.
- Koch, B. P., and T. Dittmar (2006), From mass to structure: an aromaticity index for high-resolution mass data of natural organic matter, *Rapid Commun. Mass Spectrom.*, *20*(5), 926–932, doi:10.1002/rcm.2386.
- Koch, B. P., M. Witt, R. Engbrodt, T. Dittmar, and G. Kattner (2005), Molecular formulae of marine and terrigenous dissolved organic matter detected by electrospray ionization Fourier transform ion cyclotron resonance mass spectrometry, *Geochim. Cosmochim. Acta*, *69*(13), 3299–3308, doi:10.1016/j.gca.2005.02.027.
- Koch, B. P., K.-U. Ludwichowski, G. Kattner, T. Dittmar, and M. Witt (2008), Advanced characterization of marine dissolved organic matter by combining reversed-phase liquid chromatography and FT-ICR-MS, *Mar. Chem.*, *111*(3–4), 233–241, doi:10.1016/j.marchem.2008.05.008.
- Korhonen, M., B. Rudels, M. Marnela, A. Wisotzki, and J. Zhao (2013), Time and space variability of freshwater content, heat content and seasonal ice melt in the Arctic Ocean from 1991 to 2011, *Ocean Sci.*, *9*(6), 1015–1055, doi:10.5194/os-9-1015-2013.
- Kowalczyk, P., M. J. Durako, H. Young, A. E. Kahn, W. J. Cooper, and M. Gonsior (2009), Characterization of dissolved organic matter fluorescence in the South Atlantic Bight with use of PARAFAC model: Interannual variability, *Mar. Chem.*, *113*(3–4), 182–196, doi:10.1016/j.marchem.2009.01.015.
- Kowalczyk, P., M. Zablocka, S. Sagan, and K. Kulinski (2010), Fluorescence measured in situ as a proxy of CDOM absorption and DOC concentration in the Baltic Sea, *Oceanologia*, *52*(3), 431–471.

- Kowalczyk, P., G. H. Tilstone, M. Zabłocka, R. Röttgers, and R. Thomas (2013), Composition of dissolved organic matter along an Atlantic Meridional Transect from fluorescence spectroscopy and Parallel Factor Analysis, *Mar. Chem.*, 157, 170–184, doi:10.1016/j.marchem.2013.10.004.
- van Krevelen, D. V (1950), Graphical-statistical method for the study of structure and reaction processes of coal, *Fuel*, 29, 269–284.
- Krishfield, R., J. Toole, A. Proshutinsky, and M. L. Timmermans (2008), Automated ice-tethered profilers for seawater observations under pack ice in all seasons, *J. Atmos. Ocean. Technol.*, 25(11), 2091–2105, doi:10.1175/2008JTECHO587.1.
- Lakowicz, J. R. (2006), *Principles of Fluorescence Spectroscopy*, edited by J. R. Lakowicz, Springer US, Boston, MA.
- Lalande, C., S. Bélanger, and L. Fortier (2009), Impact of a decreasing sea ice cover on the vertical export of particulate organic carbon in the northern Laptev Sea, Siberian Arctic Ocean, *Geophys. Res. Lett.*, 36(21), 1–5, doi:10.1029/2009GL040570.
- Lalande, C., E.-M. Nöthig, R. Somavilla, E. Bauerfeind, V. Shevchenko, and Y. Okolodkov (2014), Variability in under-ice export fluxes of biogenic matter in the Arctic Ocean, *Global Biogeochem. Cycles*, 28(5), 571–583, doi:10.1002/2013GB004735.
- Laney, S. R., R. A. Krishfield, J. M. Toole, T. R. Hammar, C. J. Ashjian, and M. L. Timmermans (2014), Assessing algal biomass and bio-optical distributions in perennially ice-covered polar ocean ecosystems, *Polar Sci.*, 8(2), 73–85, doi:10.1016/j.polar.2013.12.003.
- Lasserre, F., and S. Pelletier (2011), Polar super seaways? Maritime transport in the Arctic: an analysis of shipowners' intentions, *J. Transp. Geogr.*, 19(6), 1465–1473, doi:10.1016/j.jtrangeo.2011.08.006.
- Lebo, S. E., J. D. Gargulak, and T. J. McNally (2000), *Lignin, Kirk-Othmer Encyclopedia of Chemical Technology*, John Wiley & Sons, Inc.
- Letscher, R. T., D. A. Hansell, and D. Kadko (2011), Rapid removal of terrigenous dissolved organic carbon over the Eurasian shelves of the Arctic Ocean, *Mar. Chem.*, 123(1–4), 78–87, doi:10.1016/j.marchem.2010.10.002.
- Levitus, S. (1982), *Climatological atlas of the world ocean*, U.S. Govt. Print. Office, Washington.
- Li, W. K. W., F. A. McLaughlin, C. Lovejoy, and E. C. Carmack (2009), Smallest Algae Thrive As the Arctic Ocean Freshens, *Science* (80-.), 326(5952), 539–539, doi:10.1126/science.1179798.
- Longhurst, A. (2007), *Ecological geography of the sea*, 2nd ed., Elsevier Inc.
- Lund-Hansen, L. C., S. Markager, K. Hancke, T. Stratmann, S. Rysgaard, H. Ramløv, and B. K. Sorrell (2015), Effects of sea-ice light attenuation and CDOM absorption in the water below the Eurasian sector of central Arctic Ocean (>88°N), *Polar Res.*, 34(0), 1–12, doi:10.3402/polar.v34.23978.

- Lyon, S. W., and G. Destouni (2010), Changes in Catchment-Scale Recession Flow Properties in Response to Permafrost Thawing in the Yukon River Basin, *Int. J. Climatol.*, 30(14), 2138–2145, doi:10.1002/joc.1993.
- Mann, P. J., R. G. M. Spencer, P. J. Hernes, J. Six, G. R. Aiken, S. E. Tank, J. W. McClelland, K. D. Butler, R. Y. Dyda, and R. M. Holmes (2016), Pan-Arctic Trends in Terrestrial Dissolved Organic Matter from Optical Measurements, *Front. Earth Sci.*, 4(25), 1–18, doi:10.3389/feart.2016.00025.
- Maritorena, S., D. A. Siegel, and A. R. Peterson (2002), Optimization of a semianalytical ocean color model for global-scale applications, *Appl. Opt.*, 41(15), 2705, doi:10.1364/AO.41.002705.
- Marshall, A. G., and C. L. Hendrickson (2002), Fourier transform ion cyclotron resonance detection: principles and experimental configurations, , 215, 59–75.
- Matsuoka, A., Y. Huot, K. Shimada, S.-I. Saitoh, and M. Babin (2007), Bio-optical characteristics of the western Arctic Ocean: implications for ocean color algorithms, *Can. J. Remote Sens.*, 33(6), 503–518, doi:10.5589/m07-059.
- Matsuoka, A., S. B. Hooker, A. Bricaud, B. Gentili, and M. Babin (2013), Estimating absorption coefficients of colored dissolved organic matter (CDOM) using a semi-analytical algorithm for southern Beaufort Sea waters: application to deriving concentrations of dissolved organic carbon from space, *Biogeosciences*, 10(2), 917–927, doi:10.5194/bg-10-917-2013.
- Matsuoka, A., M. Babin, D. Doxaran, S. B. Hooker, B. G. Mitchell, S. Bélanger, and A. Bricaud (2014), A synthesis of light absorption properties of the Arctic Ocean: application to semianalytical estimates of dissolved organic carbon concentrations from space, *Biogeosciences*, 11(12), 3131–3147, doi:10.5194/bg-11-3131-2014.
- Matsuoka, A., M. Babin, and E. C. Devred (2016), A new algorithm for discriminating water sources from space: A case study for the southern Beaufort Sea using MODIS ocean color and SMOS salinity data, *Remote Sens. Environ.*, 184, 124–138, doi:10.1016/j.rse.2016.05.006.
- Mauritzen, C. (2012), Oceanography: Arctic freshwater, *Nat. Geosci.*, 5(3), 162–164, doi:10.1038/ngeo1409.
- McClelland, J. W., R. M. Holmes, B. J. Peterson, and M. Stieglitz (2004), Increasing river discharge in the Eurasian Arctic: Consideration of dams, permafrost thaw, and fires as potential agents of change, *J. Geophys. Res. Atmos.*, 109(18), 1–12, doi:10.1029/2004JD004583.
- Mcknight, D. M., E. W. Boyer, P. K. Westerhoff, P. T. Doran, T. Kulbe, and D. T. Andersen (2001), Spectrofluorometric characterization of dissolved organic matter for indication of precursor organic material and aromaticity, *Limnol. Oceanogr.*, 46(1), 38–48.
- Metfies, K., W. J. Von Appen, E. Kiliyas, A. Nicolaus, and E. M. Nöthig (2016),

- Biogeography and photosynthetic biomass of arctic marine pico-eukaryotes during summer of the record sea ice minimum 2012, *PLoS One*, 11(2), 1–20, doi:10.1371/journal.pone.0148512.
- Moline, M. A., I. Robbins, B. Zelenke, W. S. Pegau, and H. Wijesekera (2012), Evaluation of bio-optical inversion of spectral irradiance measured from an autonomous underwater vehicle, *J. Geophys. Res. Ocean.*, 117(1), 1–12, doi:10.1029/2011JC007352.
- Mopper, K., and D. J. Kieber (2002), Photochemistry and the cycling of carbon, sulfur, nitrogen and phosphorus, in *Biogeochemistry of Marine Dissolved Organic Matter*, edited by C. A. Carlson and D. A. Hansell, pp. 455–508, Academic Press, San Diego, CA.
- Mopper, K., and P. Lindroth (1982), Diel and depth variations in dissolved free amino acids and ammonium in the Baltic Sea determined by shipboard HPLC analysis, *Limnol. Oceanogr.*, 27(2), 336–347, doi:10.4319/lo.1982.27.2.0336.
- Morel, A., and L. Prieur (1977), Analysis of variations in ocean color, *Limnol. Oceanogr.*, 22(4), 709–722, doi:10.4319/lo.1977.22.4.0709.
- Morison, J., R. Kwok, C. Peralta-Ferriz, M. Alkire, I. Rigor, R. Andersen, and M. Steele (2012), Changing Arctic Ocean freshwater pathways, *Nature*, 481(7379), 66–70, doi:10.1038/nature10705.
- Mueller, J. L., G. S. Fargion, and C. R. McClain (2003), *Ocean Optics Protocols for Satellite Ocean Color Sensor Validation, Revision 4, Volume III: Radiometric Measurements and Data Analysis Protocols*, NASA/TM-2003-211621/Rev4-Vol. III, NASA Goddard Space Flight Center, Greenbelt, Maryland.
- Murphy, K. R., C. A. Stedmon, T. D. Waite, and G. M. Ruiz (2008), Distinguishing between terrestrial and autochthonous organic matter sources in marine environments using fluorescence spectroscopy, *Mar. Chem.*, 108(1–2), 40–58, doi:10.1016/j.marchem.2007.10.003.
- Murphy, K. R., A. Hambly, S. Singh, R. K. Henderson, A. Baker, R. Stuetz, and S. J. Khan (2011), Organic Matter Fluorescence in Municipal Water Recycling Schemes: Toward a Unified PARAFAC Model, *Environ. Sci. Technol.*, 45(7), 2909–2916, doi:10.1021/es103015e.
- Murphy, K. R., C. A. Stedmon, D. Graeber, and R. Bro (2013), Fluorescence spectroscopy and multi-way techniques. PARAFAC, *Anal. Methods*, 5(23), 6557, doi:10.1039/c3ay41160e.
- Murphy, K. R., C. A. Stedmon, P. Wenig, and R. Bro (2014), OpenFluor— an online spectral library of auto-fluorescence by organic compounds in the environment, *Anal. Methods*, 6(3), 658–661, doi:10.1039/C3AY41935E.
- Ben Mustapha, S., S. Bélanger, and P. Larouche (2012), Evaluation of ocean color algorithms in the southeastern Beaufort Sea, Canadian Arctic: New parameterization using SeaWiFS, MODIS, and MERIS spectral bands, *Can. J. Remote Sens.*, 38(5), 535–556, doi:10.5589/m12-045.
- Nelson, N. B., and D. A. Siegel (2013), The Global Distribution and Dynamics of Chromophoric Dissolved Organic Matter, *Ann. Rev. Mar. Sci.*, 5(1),

447–476, doi:10.1146/annurev-marine-120710-100751.

- Neukermans, G., R. A. Reynolds, and D. Stramski (2016), Optical classification and characterization of marine particle assemblages within the western Arctic Ocean, *Limnol. Oceanogr.*, 61(4), 1472–1494, doi:10.1002/lno.10316.
- Nicolaus, M., C. Katlein, J. Maslanik, and S. Hendricks (2012), Changes in Arctic sea ice result in increasing light transmittance and absorption, *Geophys. Res. Lett.*, 39(24), n/a-n/a, doi:10.1029/2012GL053738.
- Nöthig, E.-M. et al. (2015), Summertime plankton ecology in Fram Strait—a compilation of long- and short-term observations, *Polar Res.*, 34, 1–18, doi:10.3402/polar.v34.23349.
- O'Donnell, J. A., G. R. Aiken, M. A. Walvoord, P. A. Raymond, K. D. Butler, M. M. Dornblaser, and K. Heckman (2014), Using dissolved organic matter age and composition to detect permafrost thaw in boreal watersheds of interior Alaska, *J. Geophys. Res. Biogeosciences*, 119(11), 2155–2170, doi:10.1002/2014JG002695.
- O'Reilly, J. E., S. Maritorena, B. G. Mitchell, D. A. Siegel, K. L. Carder, S. A. Garver, M. Kahru, and C. McClain (1998), Ocean color chlorophyll algorithms for SeaWiFS, *J. Geophys. Res. Ocean.*, 103(C11), 24937–24953, doi:10.1029/98JC02160.
- O'Reilly, J. E. et al. (2000), SeaWiFS Postlaunch Calibration and Validation Analyses, Part 3, *SeaWiFS Postlaunch Tech. Rep. Ser.*, 11, 51pp.
- Obu, J., H. Lantuit, G. Grosse, F. Günther, T. Sachs, V. Helm, and M. Fritz (2015), Coastal erosion and mass wasting along the Canadian Beaufort Sea based on annual airborne LiDAR elevation data, *Geomorphology*, doi:10.1016/j.geomorph.2016.02.014.
- Okolodkov, Y. B., and J. D. Dodge (1996), Biodiversity and biogeography of planktonic dinoflagellates in the Arctic Ocean, *J. Exp. Mar. Bio. Ecol.*, 202(1), 19–27, doi:10.1016/0022-0981(96)00028-7.
- Olli, K. et al. (2007), The fate of production in the central Arctic Ocean – top-down regulation by zooplankton expatriates?, *Prog. Oceanogr.*, 72(1), 84–113, doi:10.1016/j.pocean.2006.08.002.
- Opsahl, S., and R. Benner (1998), Photochemical reactivity of dissolved lignin in river and ocean waters, *Limnol. Oceanogr.*, 43(6), 1297–1304.
- Opsahl, S., R. Benner, and R. M. W. Amon (1999), Major flux of terrigenous dissolved organic matter through the Arctic Ocean, *Limnol. Oceanogr.*, 44(8), 2017–2023, doi:10.4319/lno.1999.44.8.2017.
- Östlund, H. G., and G. Hut (1984), Arctic Ocean water mass balance from isotope data, *J. Geophys. Res.*, 89(C4), 6373–6381, doi:10.1029/JC089iC04p06373.
- Pabi, S., G. L. van Dijken, and K. R. Arrigo (2008), Primary production in the Arctic Ocean, 1998–2006, *J. Geophys. Res.*, 113(C8), C08005, doi:10.1029/2007JC004578.
- Para, J., P. G. Coble, B. Charrière, M. Tedetti, C. Fontana, and R. Sempéré

- (2010), Fluorescence and absorption properties of chromophoric dissolved organic matter (CDOM) in coastal surface waters of the Northwestern Mediterranean Sea (Bay of Marseilles, France), *Biogeosciences Discuss.*, 7(4), 5675–5718, doi:10.5194/bgd-7-5675-2010.
- Parkinson, C. L., and J. C. Comiso (2013), On the 2012 record low Arctic sea ice cover: Combined impact of preconditioning and an August storm, *Geophys. Res. Lett.*, 40(7), 1356–1361, doi:10.1002/grl.50349.
- Parmentier, F.-J. W., T. R. Christensen, L. L. Sørensen, S. Rysgaard, A. D. McGuire, P. A. Miller, and D. A. Walker (2013), The impact of lower sea-ice extent on Arctic greenhouse-gas exchange, *Nat. Clim. Chang.*, 3(3), 195–202, doi:10.1038/nclimate1784.
- Pavlov, A. K., M. A. Granskog, C. A. Stedmon, B. V. Ivanov, S. R. Hudson, and S. Falk-Petersen (2015), Contrasting optical properties of surface waters across the Fram Strait and its potential biological implications, *J. Mar. Syst.*, 143, 62–72, doi:10.1016/j.jmarsys.2014.11.001.
- Peterson, B. J., R. M. Holmes, J. W. McClelland, A. I. Vörösmarty, I. A. Shiklomanov, and S. Rahmstorf (2002), Increasing River Discharge to the Arctic Ocean, *Science* (80-.), 298(5601), 2171–2173, doi:10.1126/science.1077445.
- Polashenski, C., D. Perovich, and Z. Courville (2012), The mechanisms of sea ice melt pond formation and evolution, *J. Geophys. Res. Ocean.*, 117(1), 1–23, doi:10.1029/2011JC007231.
- Polyakov, I. V., J. E. Walsh, and R. Kwok (2012), Recent changes of Arctic multiyear sea ice coverage and the likely causes, *Bull. Am. Meteorol. Soc.*, 93(2), 145–151, doi:10.1175/BAMS-D-11-00070.1.
- Porcal, P., P. J. Dillon, and L. A. Molot (2013), Photochemical production and decomposition of particulate organic carbon in a freshwater stream, *Aquat. Sci.*, 75(4), 469–482, doi:10.1007/s00027-013-0293-8.
- Porcal, P., P. J. Dillon, and L. A. Molot (2015), Temperature Dependence of Photodegradation of Dissolved Organic Matter to Dissolved Inorganic Carbon and Particulate Organic Carbon, edited by A. Almeida, *PLoS One*, 10(6), e0128884, doi:10.1371/journal.pone.0128884.
- Prieur, L., and S. Sathyendranath (1981), An optical classification of coastal and oceanic waters based on the specific spectral absorption curves of phytoplankton pigments, dissolved organic matter, and other particulate materials¹, *Limnol. Oceanogr.*, 26(4), 671–689, doi:10.4319/lo.1981.26.4.0671.
- Proshutinsky, A., R. H. Bourke, and F. A. McLaughlin (2002), The role of the Beaufort Gyre in Arctic climate variability: Seasonal to decadal climate scales, *Geophys. Res. Lett.*, 29(23), 2100-, doi:10.1029/2002GL015847.
- Proshutinsky, A., R. Krishfield, M.-L. Timmermans, J. Toole, E. Carmack, F. McLaughlin, W. J. Williams, S. Zimmermann, M. Itoh, and K. Shimada (2009a), Beaufort Gyre freshwater reservoir: State and variability from observations, *J. Geophys. Res.*, 114, C00A10,

doi:10.1029/2008JC005104.

- Proshutinsky, A., R. Krishfield, and D. Barber (2009b), Preface to special section on Beaufort Gyre climate system exploration studies: Documenting key parameters to understand environmental variability, *J. Geophys. Res. Ocean.*, *114*(5), 6–11, doi:10.1029/2008JC005162.
- Przybylak, R. (2007), Recent air-temperature changes in the Arctic, *Ann. Glaciol.*, *46*(1), 316–324, doi:10.3189/172756407782871666.
- Punshon, S., K. Azetsu-Scott, and C. M. Lee (2014), On the distribution of dissolved methane in Davis Strait, North Atlantic Ocean, *Mar. Chem.*, *161*, 20–25, doi:10.1016/j.marchem.2014.02.004.
- Rabe, B., U. Schauer, A. Mackensen, M. Karcher, E. Hansen, and A. Beszczynska-Möller (2009), Freshwater components and transports in the Fram Strait – recent observations and changes since the late 1990s, *Ocean Sci.*, *5*(3), 219–233, doi:10.5194/os-5-219-2009.
- Rabe, B., P. A. Dodd, E. Hansen, E. Falck, U. Schauer, A. Mackensen, A. Beszczynska-Möller, G. Kattner, E. J. Rohling, and K. Cox (2013), Liquid export of Arctic freshwater components through the Fram Strait 1998 – 2011, *Ocean Sci.*, *9*, 91–109, doi:10.5194/os-9-91-2013.
- Rabe, B., M. Karcher, F. Kauker, U. Schauer, M. Toole, R. A. Krishfield, S. Pisarev, T. Kikuchi, and J. Su (2014), Arctic Ocean liquid freshwater storage trend 1992-2012, *Geophys. Res. Lett.*, *41*, 961–968, doi:10.1002/2013GL058121.
- Raymond, P. A., J. W. McClelland, R. M. Holmes, A. V. Zhulidov, K. Mull, B. J. Peterson, R. G. Striagl, G. R. Aiken, and T. Y. Gurtovaya (2007), Flux and age of dissolved organic carbon exported to the Arctic Ocean: A carbon isotopic study of the five largest arctic rivers, *Global Biogeochem. Cycles*, *21*(4), 1–9, doi:10.1029/2007GB002934.
- Reynolds, R., A. Matsuoka, T. Hirawake, and B. G. Mitchell (2015), *Ocean Colour algorithms and bio-optical relationships for polar seas, IOCCG Report 16*.
- Riebesell, U., and P. D. Tortell (2011), *Effects of ocean acidification on pelagic organisms and ecosystems*, edited by J. Gattuso and L. Hanson, Oxford University Press, Oxford.
- Rochelle-Newall, E. J., and T. R. Fisher (2002), Production of chromophoric dissolved organic matter fluorescence in marine and estuarine environments: an investigation into the role of phytoplankton, *Mar. Chem.*, *77*, 7–21.
- Romera-Castillo, C., H. Sarmiento, X. A. Álvarez-Salgado, J. M. Gasol, and C. Marrase (2010), Production of chromophoric dissolved organic matter by marine phytoplankton, *Limnol. Oceanogr.*, *55*(1), 446–454.
- Rösel, A., L. Kaleschke, and G. Birnbaum (2012), Melt ponds on Arctic sea ice determined from MODIS satellite data using an artificial neural network, *Cryosph.*, *6*(2), 431–446, doi:10.5194/tc-6-431-2012.
- Röttgers, R., and S. Gehnke (2012), Measurement of light absorption by

- aquatic particles: improvement of the quantitative filter technique by use of an integrating sphere approach, *Appl. Opt.*, 51(9), 1336, doi:10.1364/AO.51.001336.
- Rudels, B. (2009), Arctic Ocean Circulation, in *Ocean Currents: A Derivative of the Encyclopedia of Ocean Sciences*, edited by J. H. Steele, S. A. Thorpe, and K. K. Turekian, pp. 211–225.
- Rudels, B. (2012), Arctic Ocean circulation and variability – advection and external forcing encounter constraints and local processes, *Ocean Sci.*, 8(2), 261–286, doi:10.5194/os-8-261-2012.
- Rutgers van der Loeff, M. M., N. Cassar, M. Nicolaus, B. Rabe, and I. Stimac (2014), The influence of sea ice cover on air-sea gas exchange estimated with radon-222 profiles, *J. Geophys. Res. Ocean.*, 119(5), 2735–2751, doi:10.1002/2013JC009321.
- Sakshaug, E., R. Stein, and R. W. Macdonald (2004), Primary and secondary production in the Arctic Seas, in *The Organic Carbon Cycle in the Arctic Ocean*, edited by R. Stein and R. W. Macdonald, pp. 57–82, Springer.
- Sánchez-García, L., V. Alling, S. Pugach, J. Vonk, B. van Dongen, C. Humborg, O. Dudarev, I. Semiletov, and Ö. Gustafsson (2011), Inventories and behavior of particulate organic carbon in the Laptev and East Siberian seas, *Global Biogeochem. Cycles*, 25(2), n/a-n/a, doi:10.1029/2010GB003862.
- Sánchez-García, L., J. E. Vonk, A. N. Charkin, D. Kosmach, O. V. Dudarev, I. P. Semiletov, and Ö. Gustafsson (2014), Characterisation of Three Regimes of Collapsing Arctic Ice Complex Deposits on the SE Laptev Sea Coast using Biomarkers and Dual Carbon Isotopes, *Permafrost. Periglac. Process.*, 25(3), 172–183, doi:10.1002/ppp.1815.
- Sapiano, J. J., W. D. Harrison, and K. A. Echelmeyer (1998), Elevation, volume and terminus changes of nine glaciers in North America, *J. Glaciol.*, 44(146), 119–135, doi:10.3198/1998JoG44-146-119-135.
- Schauer, U., H. Loeng, B. Rudels, V. K. Ozhigin, and W. Dieck (2002), Atlantic Water flow through the Barents and Kara Seas, *Deep Sea Res. Part I Oceanogr. Res. Pap.*, 49(12), 2281–2298, doi:10.1016/S0967-0637(02)00125-5.
- Schauer, U., B. Rabe, and A. Wisotzki (2012), Physical oceanography during POLARSTERN cruise ARK-XXVI/3 (TransArc), *PANGAEA*, doi:10.1594/PANGAEA.774181.
- Schlitzer, R. (2015), Ocean Data View, Available from: <http://odv.awi.de>
- Schmidt, F., M. Elvert, B. P. Koch, M. Witt, and K. U. Hinrichs (2009), Molecular characterization of dissolved organic matter in pore water of continental shelf sediments, *Geochim. Cosmochim. Acta*, 73(11), 3337–3358, doi:10.1016/j.gca.2009.03.008.
- Schuur, E. A. G. et al. (2008), Vulnerability of Permafrost Carbon to Climate Change: Implications for the Global Carbon Cycle, *Bioscience*, 58(8), 701, doi:10.1641/B580807.

- Schuur, E. A. G. et al. (2013), Expert assessment of vulnerability of permafrost carbon to climate change, *Clim. Change*, 119(2), 359–374, doi:10.1007/s10584-013-0730-7.
- Semiletov, I. et al. (2016), Acidification of East Siberian Arctic Shelf waters through addition of freshwater and terrestrial carbon, *Nat. Geosci.*, 9(April), doi:10.1038/NEGO2695.
- Semiletov, I. P., I. I. Pipko, N. E. Shakhova, O. V. Dudarev, S. P. Pugach, A. N. Charkin, C. P. Mcroy, D. Kosmach, and Ö. Gustafsson (2011), Carbon transport by the Lena River from its headwaters to the Arctic Ocean, with emphasis on fluvial input of terrestrial particulate organic carbon vs. carbon transport by coastal erosion, *Biogeosciences*, 8(9), 2407–2426, doi:10.5194/bg-8-2407-2011.
- Semiletov, I. P., N. E. Shakhova, V. I. Sergienko, I. I. Pipko, and O. V. Dudarev (2012), On carbon transport and fate in the East Siberian Arctic land–shelf–atmosphere system, *Environ. Res. Lett.*, 7(1), 15201, doi:10.1088/1748-9326/7/1/015201.
- Semiletov, I. P., N. E. Shakhova, I. I. Pipko, S. P. Pugach, A. N. Charkin, O. V. Dudarev, D. a. Kosmach, and S. Nishino (2013), Space-time dynamics of carbon and environmental parameters related to carbon dioxide emissions in the Buor-Khaya Bay and adjacent part of the Laptev Sea, *Biogeosciences*, 10(9), 5977–5996, doi:10.5194/bg-10-5977-2013.
- Senesi, N., T. M. Miano, M. R. Provenzano, and G. Brunetti (1991), Characterization, differentiation and classification of humic substances by fluorescence spectroscopy, *Soil Sci.*, 152(4), 259–271, doi:10.1097/00010694-199110000-00004.
- Serreze, M. C., M. M. Holland, and J. Stroeve (2007), Perspectives on the Arctic's Shrinking Sea-Ice Cover, *Science (80-.)*, 315(5818), 1533–1536, doi:10.1126/science.1139426.
- Shakhova, N., I. Semiletov, A. Salyuk, V. Yusupov, D. Kosmach, and O. Gustafsson (2010), Extensive Methane Venting to the Atmosphere from Sediments of the East Siberian Arctic Shelf, *Science (80-.)*, 327(5970), 1246–1250, doi:10.1126/science.1182221.
- Shank, G. C., R. G. Zepp, R. F. Whitehead, and M. A. Moran (2005), Variations in the spectral properties of freshwater and estuarine CDOM caused by partitioning onto river and estuarine sediments, *Estuar. Coast. Shelf Sci.*, 65, 289–301, doi:10.1016/j.ecss.2005.06.009.
- Shiklomanov, I. (1993), World fresh water resources, in *Water in Crisis: A guide to the World's fresh water resources*, edited by P. H. Gleick, pp. 13–24, Oxford University Press, New York.
- Shiklomanov, I. A., A. I. Shiklomanov, R. B. Lammers, B. J. Peterson, and C. J. Vorosmarty (2000), The dynamics of river water inflow to the Arctic Ocean, in *The Freshwater Budget of the Arctic Ocean. NATO Science Series*, edited by E. Lewis, E. P. Jones, P. Lemke, T. Prowse, and P. Wadhams, pp. 281–296, Springer Netherlands.
- Shimotori, K., Y. Omori, and T. Hama (2009), Bacterial production of marine

- humic-like fluorescent dissolved organic matter and its biogeochemical importance, *Aquat. Microb. Ecol.*, *58*(1), 55–66, doi:10.3354/ame01350.
- Siegel, D. A., S. Maritorena, N. B. Nelson, D. A. Hansell, and M. Lorenzi-Kayser (2002), Global distribution and dynamics of colored dissolved and detrital organic materials, *J. Geophys. Res.*, *107*(C12), 3228, doi:10.1029/2001JC000965.
- Siegel, D. A., S. Maritorena, N. B. Nelson, M. J. Behrenfeld, and C. R. McClain (2005), Colored dissolved organic matter and its influence on the satellite-based characterization of the ocean biosphere, *Geophys. Res. Lett.*, *32*(20), L20605, doi:10.1029/2005GL024310.
- Simis, S. G. H., M. Tjidsens, H. L. Hoogveld, and H. J. Gons (2005), Optical changes associated with cyanobacterial bloom termination by viral lysis, *J. Plankton Res.*, *27*(9), 937–949, doi:10.1093/plankt/fbi068.
- Singh, S., E. J. D'Sa, and E. M. Swenson (2010), Chromophoric dissolved organic matter (CDOM) variability in Barataria Basin using excitation–emission matrix (EEM) fluorescence and parallel factor analysis (PARAFAC), *Sci. Total Environ.*, *408*(16), 3211–3222, doi:10.1016/j.scitotenv.2010.03.044.
- Smith, G. L., R. N. Green, E. Raschke, L. M. Avis, J. T. Suttles, B. A. Wielicki, and R. Davies (1986), Inversion methods for satellite studies of the Earth's Radiation Budget: Development of algorithms for the ERBE Mission, *Rev. Geophys.*, *24*(2), 407, doi:10.1029/RG024i002p00407.
- Solomon, S. M. (2005), Spatial and temporal variability of shoreline change in the Beaufort-Mackenzie region, northwest territories, Canada, *Geo-Marine Lett.*, *25*(2–3), 127–137, doi:10.1007/s00367-004-0194-x.
- Spencer, R. G. M., G. R. Aiken, K. D. Butler, M. M. Dornblaser, R. G. Striegl, and P. J. Hernes (2009), Utilizing chromophoric dissolved organic matter measurements to derive export and reactivity of dissolved organic carbon exported to the Arctic Ocean: A case study of the Yukon River, Alaska, *Geophys. Res. Lett.*, *36*(6), L06401, doi:10.1029/2008GL036831.
- Stedmon, C. A., and X. A. Álvarez-Salgado (2011), *Sheddin light on a black box: UV-Visible spectroscopic characterization of marine dissolved organic matter*, edited by N. Jiao, F. Azam, and S. Sanders, Science/AAAS.
- Stedmon, C. A., and R. Bro (2008), Characterizing dissolved organic matter fluorescence with parallel factor analysis: a tutorial, *Limnol. Oceanogr. Methods*, *6*, 1–6.
- Stedmon, C. A., and S. Markager (2001), The optics of chromophoric dissolved organic matter (CDOM) in the Greenland Sea : An algorithm for differentiation between marine and terrestrially derived organic matter, *Limnol. Oceanogr.*, *46*(8), 2087–2093.
- Stedmon, C. A., and S. Markager (2003), Behaviour of the optical properties of coloured dissolved organic matter under conservative mixing, *Estuar. Coast. Shelf Sci.*, *57*(5–6), 973–979, doi:10.1016/S0272-7714(03)00003-9.

- Stedmon, C. A., and S. Markager (2005), Resolving the variability in dissolved organic matter fluorescence in a temperate estuary and its catchment using PARAFAC analysis, *Limnol. Oceanogr.*, 50(2), 686–697.
- Stedmon, C. A., S. Markager, and R. Bro (2003), Tracing dissolved organic matter in aquatic environments using a new approach to fluorescence spectroscopy, *Mar. Chem.*, 82, 239–254, doi:10.1016/S0304-4203(03)00072-0.
- Stedmon, C. A., R. M. W. Amon, A. J. Rinehart, and S. A. Walker (2011), The supply and characteristics of colored dissolved organic matter (CDOM) in the Arctic Ocean: Pan Arctic trends and differences, *Mar. Chem.*, 124(1–4), 108–118, doi:10.1016/j.marchem.2010.12.007.
- Stedmon, C. A., M. A. Granskog, and P. A. Dodd (2015), An approach to estimate the freshwater contribution from glacial melt and precipitation in East Greenland shelf waters using colored dissolved organic matter (CDOM), *J. Geophys. Res. Ocean.*, 120(2), 1107–1117, doi:10.1002/2014JC010501.
- Steinberg, C. E. W. (2003), *Ecology of Humic Substances in Freshwaters*, Springer Berlin Heidelberg, Berlin, Heidelberg.
- Stevenson, F. J. (1982), *Humus Chemistry: Genesis, Composition, Reactions*, Wiley-Interscience, New York, NY.
- Stevenson, F. J. (1994), *Humus Chemistry: Genesis, Composition and reactions*, 2nd ed., Wiley-Interscience, New York, NY.
- Stramski, D. et al. (2008), Relationships between the surface concentration of particulate organic carbon and optical properties in the eastern South Pacific and eastern Atlantic Oceans, *Biogeosciences*, 5(1), 171–201, doi:10.5194/bg-5-171-2008.
- Stroeve, J. C., V. Kattsov, A. Barrett, M. Serreze, T. Pavlova, M. Holland, and W. N. Meier (2012), Trends in Arctic sea ice extent from CMIP5, CMIP3 and observations, *Geophys. Res. Lett.*, 39(16), 1–7, doi:10.1029/2012GL052676.
- Stubbins, A., G. Uher, C. S. Law, K. Mopper, C. Robinson, and R. C. Upstill-Goddard (2006), Open-ocean carbon monoxide photoproduction, *Deep. Res. Part II Top. Stud. Oceanogr.*, 53(14–16), 1695–1705, doi:10.1016/j.dsr2.2006.05.011.
- Stubbins, A., R. G. M. Spencer, H. Chen, P. G. Hatcher, K. Mopper, P. J. Hernes, V. L. Mwamba, A. M. Mangangu, J. N. Wabakanghanzi, and J. Six (2010), Illuminated darkness: Molecular signatures of Congo River dissolved organic matter and its photochemical alteration as revealed by ultrahigh precision mass spectrometry, *Limnol. Oceanogr.*, 55(4), 1467–1477, doi:10.4319/lo.2010.55.4.1467.
- Stubbins, A., J.-F. Lapierre, M. Berggren, Y. T. Prairie, T. Dittmar, and P. A. del Giorgio (2014), What's in an EEM? Molecular Signatures Associated with Dissolved Organic Fluorescence in Boreal Canada, *Environ. Sci. Technol.*, 48(18), 10598–10606, doi:10.1021/es502086e.
- Sugimura, Y., and Y. Suzuki (1988), A high-temperature catalytic oxidation

- method for the determination of non-volatile dissolved organic carbon in seawater by direct injection of a liquid sample, *Mar. Chem.*, 24(2), 105–131, doi:10.1016/0304-4203(88)90043-6.
- Swift, J. H., and K. Aagaard (1981), Seasonal transitions and water mass formation in the Iceland and Greenland seas, *Deep Sea Res. Part A. Oceanogr. Res. Pap.*, 28(10), 1107–1129, doi:10.1016/0198-0149(81)90050-9.
- Tang, C. C. ., C. K. Ross, T. Yao, B. Petrie, B. M. DeTracey, and E. Dunlap (2004), The circulation, water masses and sea-ice of Baffin Bay, *Prog. Oceanogr.*, 63(4), 183–228, doi:10.1016/j.pocean.2004.09.005.
- Tanski, G., N. Couture, H. Lantuit, A. Eulenburg, and M. Fritz (2016), Eroding permafrost coasts release low amounts of dissolved organic carbon (DOC) from ground ice into the nearshore zone of the Arctic Ocean, *Global Biogeochem. Cycles*, doi:10.1002/2015GB005337.
- Tassan, S., and G. M. Ferrari (1995), An alternative approach to absorption measurements of aquatic particles retained on filters, *Limnol. Oceanogr.*, 40(8), 1358–1368, doi:10.4319/lo.1995.40.8.1358.
- Taylor, B. B., E. Torrecilla, A. Bernhardt, M. H. Taylor, I. Peeken, R. Röttgers, J. Piera, and A. Bracher (2011), Bio-optical provinces in the eastern Atlantic Ocean and their biogeographical relevance, *Biogeosciences*, 8(12), 3609–3629, doi:10.5194/bg-8-3609-2011.
- Thompson, D. W. J., and J. M. Wallace (1998), The Arctic oscillation signature in the wintertime geopotential height and temperature fields, *Geophys. Res. Lett.*, 25(9), 1297, doi:10.1029/98GL00950.
- Timko, S. A., A. Maydanov, S. L. Pittelli, M. H. Conte, W. J. Cooper, B. P. Koch, P. Schmitt-Kopplin, and M. Gonsior (2015), Depth-dependent photodegradation of marine dissolved organic matter, *Front. Mar. Sci.*, 2(September), 1–13, doi:10.3389/fmars.2015.00066.
- Toole, J., R. Krishfield, M.-L. Timmermans, and A. Proshutinsky (2011), The Ice-Tethered Profiler: Argo of the Arctic, *Oceanography*, 24(3), 126–135, doi:10.5670/oceanog.2011.64.
- Torrecilla, E., D. Stramski, R. A. Reynolds, E. Millán-Núñez, and J. Piera (2011), Cluster analysis of hyperspectral optical data for discriminating phytoplankton pigment assemblages in the open ocean, *Remote Sens. Environ.*, 115(10), 2578–2593, doi:10.1016/j.rse.2011.05.014.
- Tremblay, J.-É., and J. Gagnon (2009), The effects of irradiance and nutrient supply on the productivity of Arctic waters: a perspective on climate change, in *Influence of climate change on the Changing Arctic and sub-Arctic conditions*, edited by J. Nihoul and A. Kostianoy, pp. 73–93, Springer.
- Uher, G., C. Hughes, G. Henry, and R. C. Upstill-Goddard (2001), Non-conservative mixing behavior of colored dissolved organic matter in a humic-rich, turbid estuary, *Geophys. Res. Lett.*, 28(17), 3309–3312.
- Ulfso, A., N. Cassar, M. Korhonen, S. van Heuven, M. Hoppema, G. Kattner, and L. G. Anderson (2014), Late summer net community production in

- the central Arctic Ocean using multiple approaches, *Global Biogeochem. Cycles*, 28(10), 1129–1148, doi:10.1002/2014GB004833.
- Del Vecchio, R., and N. V Blough (2004), On the Origin of the Optical Properties of Humic Substances, *Environ. Sci. Technol.*, 38(14), 3885–3891, doi:10.1021/es049912h.
- Vonk, J. E. et al. (2012), Activation of old carbon by erosion of coastal and subsea permafrost in Arctic Siberia, *Nature*, 489(7414), 137–140, doi:10.1038/nature11392.
- Vonk, J. E., I. P. Semiletov, O. V. Dudarev, T. I. Eglinton, A. Andersson, N. Shakhova, A. Charkin, B. Heim, and Ö. Gustafsson (2014), Preferential burial of permafrost-derived organic carbon in Siberian-Arctic shelf waters, *J. Geophys. Res. Ocean.*, 119(12), 8410–8421, doi:10.1002/2014JC010261.
- von Wachenfeldt, E., S. Sobek, D. Bastviken, and L. J. Tranvik (2008), Linking allochthonous dissolved organic matter and boreal lake sediment carbon sequestration: The role of light-mediated flocculation, *Limnol. Oceanogr.*, 53(6), 2416–2426.
- Wagner, S., R. Jaffé, K. Cawley, T. Dittmar, and A. Stubbins (2015), Associations Between the Molecular and Optical Properties of Dissolved Organic Matter in the Florida Everglades, a Model Coastal Wetland System, *Front. Chem.*, 3:66, 1–14, doi:10.3389/fchem.2015.00066.
- Walker, S. A., R. M. W. Amon, C. Stedmon, S. Duan, and P. Louchouart (2009), The use of PARAFAC modeling to trace terrestrial dissolved organic matter and fingerprint water masses in coastal Canadian Arctic surface waters, *J. Geophys. Res.*, 114, G00F06, doi:10.1029/2009JG000990.
- Walker, S. A., R. M. W. Amon, and C. A. Stedmon (2013), Variations in high-latitude riverine fluorescent dissolved organic matter: A comparison of large Arctic rivers, *J. Geophys. Res. Biogeosciences*, 118(4), 1689–1702, doi:10.1002/2013JG002320.
- Wang, J., G. F. Cota, and D. A. Ruble (2005), Absorption and backscattering in the Beaufort and Chukchi Seas, *J. Geophys. Res.*, 110(C4), C04014, doi:10.1029/2002JC001653.
- Wang, M., and J. E. Overland (2012), A sea ice free summer Arctic within 30 years: An update from CMIP5 models, *Geophys. Res. Lett.*, 39(17), 6–11, doi:10.1029/2012GL052868.
- Wegner, C., D. Bauch, J. a. Hölemann, M. a. Janout, B. Heim, a. Novikhin, H. Kassens, and L. Timokhov (2013), Interannual variability of surface and bottom sediment transport on the Laptev Sea shelf during summer, *Biogeosciences*, 10(2), 1117–1129, doi:10.5194/bg-10-1117-2013.
- Weishaar, J. L., G. R. Aiken, B. A. Bergamaschi, M. S. Fram, R. Fujii, and K. Mopper (2003), Evaluation of Specific Ultraviolet Absorbance as an Indicator of the Chemical Composition and Reactivity of Dissolved Organic Carbon, *Environ. Sci. Technol.*, 37(20), 4702–4708, doi:10.1021/es030360x.

- Werdell, P. J. et al. (2013a), Generalized ocean color inversion model for retrieving marine inherent optical properties, *Appl. Opt.*, 52(10), 2019–2037, doi:10.1364/AO.52.002019.
- Werdell, P. J., B. A. Franz, J. T. Lefler, W. D. Robinson, and E. Boss (2013b), Retrieving marine inherent optical properties from satellites using temperature and salinity-dependent backscattering by seawater, *Opt. Express*, 21(26), 32622, doi:10.1364/OE.21.032611.
- Williams, P. M., and E. R. M. Druffel (1987), Radiocarbon in dissolved organic matter in the central North Pacific Ocean, *Nature*, 330(6145), 246–248, doi:10.1038/330246a0.
- Winterfeld, M., M. A. Goñi, J. Just, J. Hefter, and G. Mollenhauer (2015), Characterization of particulate organic matter in the Lena River delta and adjacent nearshore zone, NE Siberia - Part 2: Lignin-derived phenol compositions, *Biogeosciences*, 12(7), 2261–2283, doi:10.5194/bg-12-2261-2015.
- Wünsch, U. J., K. R. Murphy, and C. A. Stedmon (2015), Fluorescence Quantum Yields of Natural Organic Matter and Organic Compounds: Implications for the Fluorescence-based Interpretation of Organic Matter Composition, *Front. Mar. Sci.*, 2:98, 1–15, doi:10.3389/fmars.2015.00098.
- Yamamoto-Kawai, M., F. A. McLaughlin, E. C. Carmack, S. Nishino, K. Shimada, and N. Kurita (2009), Surface freshening of the Canada Basin, 2003–2007: River runoff versus sea ice meltwater, *J. Geophys. Res. Ocean.*, 114(4), 2003–2007, doi:10.1029/2008JC005000.
- Yamashita, Y., and E. Tanoue (2003a), Chemical characterization of protein-like fluorophores in DOM in relation to aromatic amino acids, *Mar. Chem.*, 82(3–4), 255–271, doi:10.1016/S0304-4203(03)00073-2.
- Yamashita, Y., and E. Tanoue (2003b), Distribution and alteration of amino acids in bulk DOM along a transect from bay to oceanic waters, *Mar. Chem.*, 82(3–4), 145–160, doi:10.1016/S0304-4203(03)00049-5.
- Yamashita, Y., and E. Tanoue (2004), Chemical characteristics of amino acid-containing dissolved organic matter in seawater, *Org. Geochem.*, 35(6), 679–692, doi:10.1016/j.orggeochem.2004.02.007.
- Yamashita, Y., and E. Tanoue (2008), Production of bio-refractory fluorescent dissolved organic matter in the ocean interior, *Nat. Geosci.*, 1(9), 579–582, doi:10.1038/ngeo279.
- Yamashita, Y., R. M. Cory, J. Nishioka, K. Kuma, E. Tanoue, and R. Jaffé (2010), Fluorescence characteristics of dissolved organic matter in the deep waters of the Okhotsk Sea and the northwestern North Pacific Ocean, *Deep Sea Res. Part II Top. Stud. Oceanogr.*, 57(16), 1478–1485, doi:10.1016/j.dsr2.2010.02.016.
- Yamashita, Y., J. N. Boyer, and R. Jaffé (2013), Evaluating the distribution of terrestrial dissolved organic matter in a complex coastal ecosystem using fluorescence spectroscopy, *Cont. Shelf Res.*, 66, 136–144, doi:10.1016/j.csr.2013.06.010.

- Yamashita, Y., C. G. Fichot, Y. Shen, R. Jaffé, and R. Benner (2015), Linkages among fluorescent dissolved organic matter, dissolved amino acids and lignin-derived phenols in a river-influenced ocean margin, *Front. Mar. Sci.*, 2(November), 1–14, doi:10.3389/fmars.2015.00092.
- Yang, D., D. L. Kane, L. D. Hinzman, X. Zhang, T. Zhang, and H. Ye (2002), Siberian Lena River hydrologic regime and recent change, *J. Geophys. Res. Atmos.*, 107(23), 1–10, doi:10.1029/2002JD002542.
- Zhang, Y., M. A. van Dijk, M. Liu, G. Zhu, and B. Qin (2009), The contribution of phytoplankton degradation to chromophoric dissolved organic matter (CDOM) in eutrophic shallow lakes: Field and experimental evidence, *Water Res.*, 43(18), 4685–4697, doi:10.1016/j.watres.2009.07.024.
- Zsolnay, A., E. Baigar, M. Jimenez, B. Steinweg, and F. Saccomandi (1999), Differentiating with fluorescence spectroscopy the sources of dissolved organic matter in soils subjected to drying, *Chemosphere*, 38(1), 45–50, doi:10.1016/S0045-6535(98)00166-0.
- Zsolnay, Á. (2003), Dissolved organic matter: artefacts, definitions, and functions, *Geoderma*, 113, 187–209, doi:10.1016/S0016-7061(02)00361-0.

Chapter 8

Addendum

The addendum to this thesis contains the official reprints of published manuscripts presented in chapters 2, 3 and 4.

TOOLS FOR ASSESSING CONTENT, SPECIATION AND ORIGIN OF DOM IN AQUATIC SYSTEMS

RAFAEL GONÇALVES-ARAÚJO^{1,2*}

¹Alfred Wegener Institute Helmholtz Centre for Polar and Marine Research, Climate Sciences Division, Physical Oceanography of Polar Seas, PHYTOOPTICS Group, Bussestraße 24, 27570 Bremerhaven, Germany

²University of Bremen, Faculty of Biology, PO Box 330440, 28334 Bremen, Germany

*email: rafael.goncalves.araujo@awi.de

ABSTRACT

Dissolved organic matter (DOM) is a major component of the carbon-pool in aquatic systems and thus represents an important pathway on the carbon cycle, especially in marine environments. For instance, studies have used DOM to assess drinking water quality, its importance on biogeochemical cycles, its usefulness as an environmental tracer, etc. This article discusses some of the current methods used to assess the amount and composition of DOM, and applications of DOM as an environmental tracer in aquatic systems. Different techniques varying from molecular, optical, and chemical analyses to satellite remote sensing have been employed to identify, characterize and quantify DOM and to assess its distribution, composition and dynamics in distinct aquatic environments. Those approaches however, focus only on specific fractions of the total DOM-pool. Hence, recent studies have attempted to link the results provided by such complimentary methods to reach a more comprehensive understanding on the total DOM-pool in aquatic systems. Additionally, DOM spectroscopic measurements (e.g. absorbance and fluorescence) are cost-effective tools and can be sampled with high resolution by autonomous devices such as fluorimeters. Furthermore, the optical properties of DOM have been shown to be reliable proxies for monitoring water quality and for tracing fresh water along the Arctic Ocean. With the climate change pressure on Arctic environments and the expected increase in fresh water and ancient carbon export from the continent to the ocean, optical analyses of DOM can be an easy-to-measure and affordable parameters for assessing and monitoring these effects in the Arctic environment.

KEYWORDS: DISSOLVED ORGANIC MATTER, CDOM, FDOM, OPTICAL INDICES, ENVIRONMENTAL ASSESSMENT

1. Introduction

With the climate change pressure on the environment, the scientific community has sought a more comprehensive understanding on the carbon cycle, its reservoirs and the processes governing their dynamics. Aquatic systems play an important role for the carbon cycle, for instance, as provision of a large pool of carbon, important sink and turnover of organic carbon. As a consequence, increasing effort has been devoted to study aquatic environments and processes governing the dynamics of both, organic and inorganic carbon. With more studies on the characterization of stocks, sources, dynamics, and fate of

both organic and inorganic carbon, a more comprehensive understanding of the carbon cycle would be reached, which is of great importance for improving forecasts of future climate scenarios.

Non-living organic matter is present in aquatic systems as particles, colloids, and dissolved molecules. The dissolved fraction of organic matter (DOM) is operationally defined by filtration with specific pore size, with 0.45 μm being the most accepted limit [Steinberg, 2003]. The DOM fraction encompasses a wide range of organic compounds with variable molecular complexity

and is one of the largest carbon-pools on Earth [Hedges, 1992]. The most frequently observed compounds in the DOM-pool are amino acids, carbohydrates, lipids, pigments, lignins, tannins, and proteins, whose relative contribution varies in different environments, in relation to its origin. For instance, terrestrially-derived humic acids derived from lignin, which is formed exclusively in vascular plants, contain large amounts of carbon in the form of aromatic carbons and phenols [Lebo et al., 2000]. Microbially-derived amino acids and proteins, on the other

hand, contain a low aromatic and phenolic content in relation to terrestrial sourced DOM [Geider and La Roche, 2002]. Given the huge variety in DOM composition and the wide panel of different approaches employed to analyze it, this article provides a brief review on some of the current methods applied to assess the amount and composition of DOM. Secondly, an overview on the applications of DOM properties as environmental tracers in aquatic systems is presented, with focus on the Arctic marine environment.

2. Quantitative and qualitative methods for DOM assessment

Different methods have been applied for performing chemical analyses of DOM. In general, those methods can be classified into two groups according to the preparation of the sample for analysis: the analyses involving purification and/or pre-concentration and the analyses performed in filtered original water (Figure 1). The purification and pre-concentration are employed to avoid interference of inorganic ions, which can affect highly to sensitive analyses. However, those methods can have analytical errors embedded in their analysis such as oxidation of only a part of DOM and increase in DOM concentration

during drying of samples [Bolan et al., 1996]. A wide range of methods have been developed using such techniques, for instance, solid phase extraction (SPE), ultrafiltration, nanofiltration, reverse osmosis, or electrodialysis. Although those methods have been widely applied in DOM studies, this article focuses on the approaches using filtered original water, which are here further divided into molecular and bulk analyses. The methods for DOM analysis using filtered original water can vary significantly with regards to the analytical procedure, including elemental analysis, isotopic analysis, chromatography, and mass spectrometry.

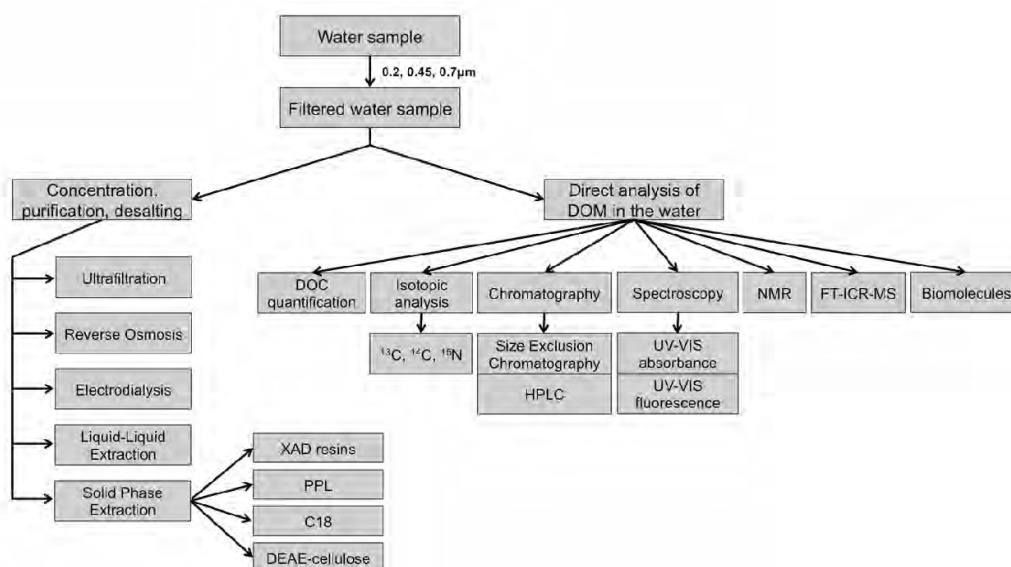


Figure 1. Strategies in the chemical analyses of DOM with respect to the pre-processing of samples [adapted from Dubinenkov, 2015].

2.1. Molecular analysis

By molecular analysis, this article refers to the quantification of an essentially pure type of organic compound or compound class. Two major groups of methods are applied in molecular analysis of DOM, the targeted and the non-targeted (Figure 2). Targeted methods are focused on analyzing specific organic compounds, which structure is well defined in the literature. In

DOM research, such molecules are usually referred to as biomarkers. Non-targeted methods are used to detect the analytical signal (or superposition of signals) from multiple molecular components with the DOM mixture. In addition, non-targeted methods can also be employed for the characterization of bulk DOM, since they can provide information on the carbon content in a water sample.

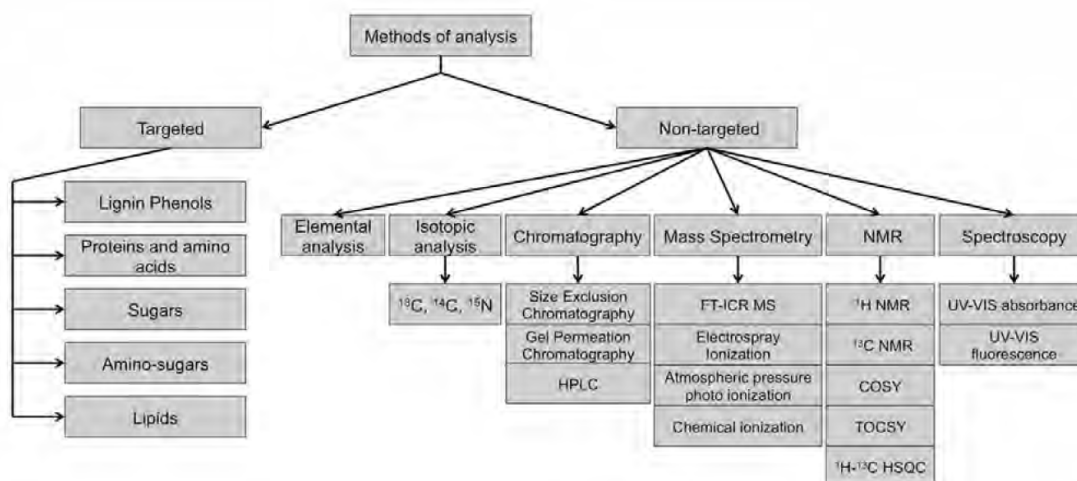


Figure 2. Strategies in the chemical analyses of DOM regarding the methods of analysis [adapted from Dubinenkov, 2015].

2.1.1. Targeted molecules

The analysis of targeted molecules consists of quantifying a specific compound based on its extraction from the water samples. Examples for targeted biomolecules are lignin phenols, proteins and amino acids, sugars, amino-sugars, and lipids. Such molecules can be analyzed by applying different techniques. For example, most proteinogenic

amino acids can be retained and separated by high-performance liquid chromatography (HPLC; Mopper and Lindroth, 1982) whereas some phenols can be separated using both gas chromatography [Benner and Opsahl, 2001] and HPLC.

2.1.2. Non-targeted molecules

Non-targeted approaches focus on the simultaneous detection of multiple molecular components. However, such methods can also provide bulk estimates of DOM. Among the several non-targeted methods for analysis of DOM, the nuclear magnetic resonance (NMR) and the Fourier transform ion cyclotron resonance mass spectrometry (FT-ICR MS) have been applied in many studies focusing on molecular characterization of DOM in the last decades.

Despite of the wide application of both methods, this subsection focuses on the FT-ICR MS method, given the significant increase in the number of studies using that method to chemically characterize DOM.

FT-ICR MS provides a detailed characterization of the diversity of molecular formulas contained in the analyzed DOM samples [Koch and Dittmar, 2006]. Three distinct ways are used to analyze DOM with mass spectrometry,

nevertheless all involving preliminary purification and concentration of samples: hyphenation with HPLC [Dittmar et al., 2007], direct injection of samples extracts [Kim et al., 2003] and chromatographic fractions [Koch et al., 2008]. The FT-ICR MS determines the mass-to-charge ratio (m/z) of ions based on their cyclotron frequency in a fixed magnetic field [Marshall and Hendrickson, 2002]. Given the high accuracy and sensitivity of the method, thousands of different mass peaks of DOM can be resolved

2.2. Bulk analyses

Bulk analyses to quantify and characterize DOM samples can be subdivided into elemental, isotopic, and spectroscopic methods. The most common quantitative representation of DOM in natural waters is dissolved organic carbon (DOC) concentration. It is usually quantified via high temperature catalytic oxidation to CO_2 [Sugimura and Suzuki, 1988]. Carbon isotopic measurements (e.g. ^{13}C and ^{14}C) can also provide information on bulk DOM in aquatic systems. Furthermore, such measurements can provide information on both mass and age of DOM [Williams and Druffel, 1987; Druffel and Bauer, 2000]. Studies have shown that DOC in deep waters presented $\delta^{14}\text{C}$ values

2.2.1. Chromophoric dissolved organic matter

Spectral analyses of DOM have been applied to assess the optically active fraction of DOM, the colored (or chromophoric) and fluorescent DOM (CDOM and FDOM, respectively). CDOM is the DOM fraction that absorbs light in the ultraviolet (UV) and visible wavelength ranges [Siegel et al., 2002], whereas a fraction of CDOM is able to fluoresce, characterizing the FDOM fraction. From the absorbance spectra obtained with spectrophotometers, the Napierian absorption coefficient of CDOM (a) at each wavelength (λ) is obtained from the given equation: $a(\lambda) = (2.303 \times A\lambda) / L$, where $A\lambda$ is the absorbance at specific wavelength and L is the cuvette path length in meters. That coefficient is adopted as an index of CDOM amount and different wavelengths have been chosen to determine a . Studies focusing on ocean color remote sensing previously

2.2.2. Fluorescent dissolved organic matter

FDOM has also been used as an index of DOM amount [Benner et al., 2005; Cooper et al., 2005]. Furthermore, it can provide information on the origin, mixing, and removal of different fractions of DOM [Yamashita and

and their respective molecular formulas can be assigned [Koch et al., 2005]. Several different approaches have been applied for visualizing the molecular information provided by the FT-ICR MS. Among them, the van Krevelen diagram is the most popular method applied [van Krevelen, 1950; Schmidt et al., 2009]. The diagram is constructed based on the atomic ratios of carbon compounds and is obtained from the hydrogen index (hydrogen:carbon) as a function of the oxygen index (oxygen:carbon).

reaching -502‰ (i.e., 5600 years) in the Southern Ocean [Druffel and Bauer, 2000] and -540‰ (i.e., 6240 years) in the central North Pacific Ocean [Williams and Druffel, 1987]. However, this article focuses on the spectroscopic methods, such as absorbance (section 2.2.1) and fluorescence (section 2.2.2) spectra. These parameters can be monitored with in situ autonomous platforms and ocean color remote sensing [Cooper et al., 2005; Siegel et al., 2005; Heim et al., 2014], and the derived optical indices (section 2.2.3) used to characterize and evaluate the transformation and reactivity of DOM.

presented results on absorption in the visible wavelength range, a_{440} or a_{443} [Siegel et al., 2002, 2005; Heim et al., 2014]. Other studies, on the other hand, used the absorption in the UV range (e.g. a_{325} and a_{350}) because of its correlations with DOC and lignin concentration [Spencer et al., 2009; Stedmon et al., 2011], and also because CDOM is the most important optically active constituent of water in the open ocean with regards to absorption in the UV wavelength range [Nelson and Siegel, 2013]. Moreover, DOC has been shown to be strongly correlated with both CDOM and FDOM in the Arctic Ocean [Walker et al., 2013; Gonçalves-Araujo et al., 2015]. Therefore optically active fractions of DOM can be a proxy for the total DOM-pool (based on DOC measurements) in the Arctic environment.

Tanoue, 2003; Chari et al., 2013; Fukuzaki et al., 2014; Gonçalves-Araujo et al., 2015]. By acquiring the excitation-emission-matrices (EEMs), a qualitative evaluation of the different compounds of bulk DOM from spectroscopy

can be performed [Coble, 1996]. With the adaptation of the Parallel Factor Analysis (PARAFAC) for the analysis of DOM, a more holistic differentiation of underlying independent DOM components was possible [Stedmon et al., 2003; Stedmon and Bro, 2008]. The PARAFAC is a multi-way analysis that can be applied to decompose trilinear data arrays such as EEMs. Furthermore, EEMs must be corrected for inner-filter effects and for the Raman and Rayleigh scattering prior to PARAFAC modeling [Murphy et al., 2013]. Recent studies attempted to associate molecular groups and PARAFAC-derived DOM components [Stubbins et al., 2014; Kellerman et al., 2015; Wagner et al., 2015]. They found significant correlations between the humic-like fluorescent peak A [e.g., Coble, 2007] and high molecular weight compounds with little nitrogen, between the protein-like fluorescent peak T and low molecular weight aromatic compounds (such as amino acids) and between the humic-like fluorescent peak C and lignin-derived phenols. Moreover, a recent study pointed

2.2.3. Optical indices for DOM modification

The information contained in the spectral analysis of both CDOM and FDOM cannot only determine the amount and composition of DOM components, but it can also give insights into DOM origin and transformation. For that purpose, several optical indices have been developed. The spectral slope of absorption spectra (S) is obtained by applying an exponential function to the UV-VIS spectral range. It has been shown to be inversely correlated with the molecular weight of DOM and it can also be related to photobleaching [Helms et al., 2008]. The choice of each spectral range for assessment of the spectral slope varies among different studies and sampling regions. For instance, S values acquired in the UV region (e.g., 275–295 nm) can differ from results expressed by means of the VIS region (e.g., 350–400 nm) reflecting differences regarding the origin of DOM, as from terrestrial or marine character [Helms et al., 2008]. Other studies obtained S values considering the full UV-VIS regions, deriving S from the range between 300–650 nm [Stedmon and Markager, 2001]. A recent study showed that nitrate and cytochrome C exert strong influence on CDOM absorption spectra, given their absorbance peaks at 302 and 405 nm, respectively [Catalá et al., 2016]. Furthermore, that same study showed that those two chromophores can lead $S_{275-295}$ and $S_{350-400}$ to an overestimation by $13.3 \pm 6.0\%$ and $14.8 \pm 10.6\%$, respectively. The slope ratio (SR) is

obtained from the ratio between UV and VIS absorption spectral slope (275–295 and 350–400 nm, respectively) and provides strong differentiation between open ocean waters from those of near-shore coastal or estuarine origin [Helms et al., 2008]. The specific UV absorbance (SUVA) index is obtained as a function of the UV absorbance (at 254 nm) and DOC concentration, and it is used to trace the degree of aromaticity in CDOM samples [Weishaar et al., 2003], which is in turn correlated to the molecular weight [Helms et al., 2008].

Fluorescence is widely used to assess the degree of humification of bulk DOM, and thus to provide insights into the origin of DOM. The fluorescence index (FI) can be applied to distinguish sources of isolated aquatic fulvic acids. It is determined based on the ratio of the emission intensity at a wavelength of 450 nm to that at 500 nm, obtained with an excitation of 370 nm [Mcknight et al., 2001]. The humification index (HIX) estimates the degree of maturation of DOM [Zsolnay et al., 1999; Zsolnay, 2003], considering that humification is associated with an increase in the C/H ratio [Stevenson, 1994] and is thus reflected in emissions at longer wavelengths [Senesi et al., 1991]. This index is obtained from the ratio of the areas of two spectral wavelength regions (435–480 nm versus 300–345 nm) in the emission spectra for an excitation at 254 nm [Zsolnay et al., 1999]. An increase in the degree

of aromaticity (humification) leads to a red shift in the emission spectrum, which results in higher HIX values. The biological/autochthonous index (BIX) is used to assess the biological modification of DOM based on UV fluorescence. The BIX index is obtained by calculating the ratio of the emission at 380 and 430 nm, excited at 310 nm [Huguet et al., 2009]. High BIX values correspond to autochthonous origin of DOM, i.e., freshly released DOM, whereas low BIX values indicate allochthonous DOM [Huguet et al., 2009].

3. DOM as an environmental tracer

DOM has been shown to be a useful tool in a wide range of applications, from scientific to management interests. Studies have shown that FDOM measurements provide a fast and sensitive way to monitor the qualitative and quantitative variation of DOM in drinking water, and during the sewage treatment and also recycling water processes [Guo et al., 2010; Hambly et al., 2010; Murphy et al., 2011]. PARAFAC-derived protein-like components (and their relative contribution compared to humic-like components) were suggested to be a reliable tracer to monitor the relative amount of raw or treated sewage in China [Guo et al., 2010]. Another study, conducted with samples from municipal water systems, highlighted the dominance of the terrestrial humic-like PARAFAC-derived component, which has also been identified in other studies performed on engineered, wastewater impact environments [Murphy et al., 2011].

Besides its potential use to monitor water quality and sewage and wastewater treatment, DOM has been shown to be a water mass tracer, especially the fresh water fractions [Stedmon and Markager, 2001; Stedmon et al., 2015]. Strong correlations between CDOM and the fraction of meteoric water, which is a tracer of continental fresh water input [Dodd et al., 2012], can be used as a proxy to monitor the fresh water export from the Arctic to the Atlantic basins, given the high DOM concentrations in those waters. Furthermore, other optical parameters of DOM can be applied to trace the fraction of meteoric water in the Arctic Ocean. Studies have used the correlation between S and a₃₇₅ to detect the fractions of meteoric water [Granskog et al., 2012; Stedmon et al., 2015] by applying the model proposed by Stedmon and Markager [2001]. It has also been demonstrated the potential of the visible wavelength fluorescence of DOM (VIS-FDOM) to trace the fresh

A recent study investigated the correlations between optical indices and molecular families derived from FT-ICR-MS measurements [Wagner et al., 2015]. The authors found that SUVA and HIX are effective in tracking terrestrially-derived groups of highly aromatic compounds with low N, P and S content, which have been previously pointed out by other studies to be photo-labile [Gonsior et al., 2009; Stubbins et al., 2010]. FI and BIX indices have been shown, on the other hand, to be associated to biolabile aliphatic formulae [Wagner et al., 2015].

water content of the Arctic outflow [Gonçalves-Araujo et al., submitted]. Hence, FDOM can be used as a proxy to trace the origin of the waters occupying the Arctic surface layer, based on VIS-FDOM end-members proposed by that study, as being generated either in the Eurasian or Canadian basins, which cannot be detected by traditional analysis of hydrographical data (e.g. T-S diagrams and thermohaline intervals for water masses). Those authors concluded that their results provide an indication of which wavelength regions for DOM fluorescence carry information on DOM source and mixing. Such information has potential for supporting the design of in situ DOM fluorometers as a low-cost mechanism to provide high spatial and temporal resolution data for tracing the freshwater origins and decipher water mass mixing dynamics in the region, given the concern regarding the effects of climate change over the Arctic Ocean.

Given that CDOM absorbs light in both the UV and visible wavelength ranges, it can play an important role in the biogeochemical cycles in coastal and inner-shelf waters, being one of the dominant components interacting with the underwater light field in those environments [Siegel et al., 2002; Nelson and Siegel, 2013]. Furthermore, it can act as a shield for the aquatic biota from harmful UV radiation [Arrigo and Brown, 1996]. As a result of its UV absorbing properties, CDOM is susceptible to photo-degradation, which either induces direct mineralization or produces microbiologically labile low molecular weight compounds, which are subsequently utilized by bacteria [Mopper and Kieber, 2002]. CDOM does not only absorb UV-radiation, it also absorbs heat, thus influencing the light and heat penetration in surface waters [Granskog et al., 2015], especially in coastal and inner-shelf regions.

Finally, given the increased coastal erosion and permafrost thawing rates in the Arctic, with consequent release of ancient organic carbon [Aiken et al., 2014; Dubinenkov et al., 2015], many studies have attempted to trace and elucidate the fate of such compounds in the aquatic environment. A recent study showed that coastal erosion in the Yukon coast releases significant amounts of

DOC to the coastal Beaufort Sea [Tanski et al., 2016]. Based on the results of stable carbon isotope analysis it was also shown that, especially during summer and autumn, ancient DOC is released and will likely contribute to older DOC in the Yukon River and its tributaries in the coming decades [Aiken et al., 2014].

4. Conclusions

DOM has been shown to play an important role on the carbon cycle, acting as a link between terrestrial and aquatic systems. Furthermore, it is an easy-to-measure and affordable tool for monitoring water quality and sewage treatment. DOM is subject to several processes that affect its composition, amount and reactivity. However, the effects of such processes on different compounds, as well as the fate of DOM in aquatic systems are still under debate. With the ongoing climate change over the environment, more effort has been devoted to understand the role and fate of DOM in aquatic systems. A variety of new techniques have emerged in the last decades and better qualitative and quantitative assessment of the DOM is possible. However, there are still unresolved questions and unmet capabilities that need attention in the coming years. For instance, a more comprehensive understanding on the processes governing DOM dynamics, such as photo-oxidation, microbial turnover, adsorption/flocculation, etc. is needed

for a better estimation of DOM production rates as well as the rates of DOM transformation. A recent special issue gathered several papers linking the chemical and optical properties of DOM (“Linking optical and chemical properties of dissolved organic matter in natural waters”, *Frontiers in Journal, Section Marine Biogeochemistry*). Such studies can provide, for instance, a more consistent interpretation of optical indices of DOM modification and PARAFAC-derived fluorescent components. Finally, it is clear that implementation of new observing systems including new ocean color sensors and ocean observing systems, as well as the deployment of autonomous platforms with DOM-fluorometers, will be responsible for much of the future collection of data. Therefore, advances on the analysis and interpretation of the optical properties of DOM are required to improve the sensitivity and specificity of sensors deployable on these platforms.

5. Acknowledgements

The author thanks to Prof. Dr. Astrid Bracher and Lumi Haraguchi for their valuable comments and discussions. Rafael Gonçalves-Araujo is supported by a PhD fellowship from the Coordination for the Improvement of Higher

Level Personnel (CAPES-Brazil, Grant 12362/12-3) in collaboration with the German Academic Exchange Service (DAAD).

6. References

- Aiken, G. R., R. G. M. Spencer, R. G. Striegl, P. F. Schuster, and P. A. Raymond (2014), Influences of glacier melt and permafrost thaw on the age of dissolved organic carbon in the Yukon River basin, *Global Biogeochem. Cycles*, 28(5), 525–537, doi:10.1002/2013GB004764.
- Arrigo, K. R., and C. B. Brown (1996), Impact of chromophoric dissolved organic matter on UV inhibition of primary production in the sea, *Mar. Ecol. Progr. Ser.*, 140, 207–216.
- Benner, R., and S. Opsahl (2001), Molecular indicators of the sources and transformations of dissolved organic matter in the Mississippi river plume, *Org. Geochem.*, 32, 597–611.

- Benner, R., P. Louchouart, and R. M. W. Amon (2005), Terrigenous dissolved organic matter in the Arctic Ocean and its transport to surface and deep waters of the North Atlantic, *Global Biogeochem. Cycles*, 19(2), n/a–n/a, doi:10.1029/2004GB002398.
- Bolan, N. S., S. Baskaran, and S. Thiagarajan (1996), An evaluation of the methods of measurement of dissolved organic carbon in soils, manures, sludges, and stream water, *Commun. Soil Sci. Plant Anal.*, 27(13-14), 2723–2737, doi:10.1080/00103629609369735.
- Catalá, T. S. et al. (2015), Water mass age and aging driving chromophoric dissolved organic matter in the dark global ocean, *Global Biogeochem. Cycles*, 29(7), 917–934, doi:10.1002/2014GB005048.
- Catalá, T. S., I. Reche, C. L. Ramón, À. López-Sanz, M. Álvarez, E. Calvo, and X. A. Álvarez-Salgado (2016), Chromophoric signatures of microbial by-products in the dark ocean, *Geophys. Res. Lett.*, 43(14), 7639–7648, doi:10.1002/2016GL069878.
- Chari, N. V. H. K., S. Keerthi, N. S. Sarma, S. R. Pandi, G. Chiranjeevulu, R. Kiran, and U. Koduru (2013), Fluorescence and absorption characteristics of dissolved organic matter excreted by phytoplankton species of western Bay of Bengal under axenic laboratory condition, *J. Exp. Mar. Bio. Ecol.*, 445, 148–155, doi:10.1016/j.jembe.2013.03.015.
- Coble, P. G. (1996), Characterization of marine and terrestrial DOM in seawater using excitation-emission matrix spectroscopy, *Mar. Chem.*, 51(4), 325–346, doi:10.1016/0304-4203(95)00062-3.
- Coble, P. G. (2007), *Marine Optical Biogeochemistry: The Chemistry of Ocean Color*, *Chem. Rev.*, 107, 402–418.
- Cooper, L. W., R. Benner, J. W. McClelland, B. J. Peterson, R. M. Holmes, P. A. Raymond, D. A. Hansell, J. M. Grebmeier, and L. A. Codispoti (2005), Linkages among runoff, dissolved organic carbon, and the stable oxygen isotope composition of seawater and other water mass indicators in the Arctic Ocean, *J. Geophys. Res.*, 110(G2), G02013, doi:10.1029/2005JG000031.
- Dittmar, T., K. Whitehead, E. C. Minor, and B. P. Koch (2007), Tracing terrigenous dissolved organic matter and its photochemical decay in the ocean by using liquid chromatography/mass spectrometry, *Mar. Chem.*, 107(3), 378–387, doi:10.1016/j.marchem.2007.04.006.
- Dodd, P. A., B. Rabe, E. Hansen, E. Falck, A. Mackensen, E. Rohling, C. Stedmon, and S. Kristiansen (2012), The freshwater composition of the Fram Strait outflow derived from a decade of tracer measurements, *J. Geophys. Res.*, 117(C11005), 1–26, doi:10.1029/2012JC008011.
- Druffel, E. R. M., and J. E. Bauer (2000), Radiocarbon distributions in Southern Ocean dissolved and particulate organic matter, *Geophys. Res. Lett.*, 27(10), 1495–1498, doi:10.1029/1999GL002398.
- Dubinenkov, I., R. Flerus, P. Schmitt-Kopplin, G. Kattner, and B. P. Koch (2015), Origin-specific molecular signatures of dissolved organic matter in the Lena Delta, *Biogeochemistry*, 123(1-2), 1–14, doi:10.1007/s10533-014-0049-0.
- Dubinenkov, I. V (2015), *Molecular biogeochemistry of dissolved organic matter in the permafrost-influenced Lena delta*, University of Bremen.
- Fukuzaki, K., I. Imai, K. Fukushima, K.-I. Ishii, S. Sawayama, and T. Yoshioka (2014), Fluorescent characteristics of dissolved organic matter produced by bloom-forming coastal phytoplankton, *J. Plankton Res.*, 36(3), 685–694, doi:10.1093/plankt/fbu015.
- Geider, R., and J. La Roche (2002), Redfield revisited: variability of C:N:P in marine microalgae and its biochemical basis, *Eur. J. Phycol.*, 37(1), 1–17, doi:10.1017/S0967026201003456.
- Gonçalves-Araujo, R., C. A. Stedmon, B. Heim, I. Dubinenkov, A. Kraberg, D. Moiseev, and A. Bracher (2015), From Fresh to Marine Waters: Characterization and Fate of Dissolved Organic Matter in the Lena River Delta Region, Siberia, *Front. Mar. Sci.*, 2:108, 1–13, doi:10.3389/fmars.2015.00108.
- Gonçalves-Araujo, R., M. A. Granskog, A. Bracher, K. Azetsu-Scott, P. A. Dodd, and C. A. Stedmon (n.d.), Using fluorescent dissolved organic matter to trace and distinguish the origin of Arctic surface waters, *Sci. Rep.*

- Gonsior, M., B. M. Peake, W. T. Cooper, D. Podgorski, J. D'Andrilli, and W. J. Cooper (2009), Photochemically Induced Changes in Dissolved Organic Matter Identified by Ultrahigh Resolution Fourier Transform Ion Cyclotron Resonance Mass Spectrometry, *Environ. Sci. Technol.*, 43(3), 698–703, doi:10.1021/es8022804.
- Granskog, M. A., C. A. Stedmon, P. A. Dodd, R. M. W. Amon, A. K. Pavlov, L. de Steur, and E. Hansen (2012), Characteristics of colored dissolved organic matter (CDOM) in the Arctic outflow in the Fram Strait: Assessing the changes and fate of terrigenous CDOM in the Arctic Ocean, *J. Geophys. Res.*, 117(C12), C12021, doi:10.1029/2012JC008075.
- Granskog, M. A., A. K. Pavlov, S. Sagan, P. Kowalczyk, A. Raczowska, and C. A. Stedmon (2015), Effect of sea-ice melt on inherent optical properties and vertical distribution of solar radiant heating in Arctic surface waters, *J. Geophys. Res. Ocean.*, 120(10), 7028–7039, doi:10.1002/2015JC011087.
- Green, S. A., and N. V. Blough (1994), Optical absorption and fluorescence properties of chromophoric dissolved organic matter in natural waters, *Limnol. Oceanogr.*, 39(8), 1903–1916, doi:10.4319/lo.1994.39.8.1903.
- Guo, W., J. Xu, J. Wang, Y. Wen, J. Zhuo, and Y. Yan (2010), Characterization of dissolved organic matter in urban sewage using excitation emission matrix fluorescence spectroscopy and parallel factor analysis, *J. Environ. Sci.*, 22(11), 1728–1734, doi:10.1016/S1001-0742(09)60312-0.
- Hambly, A. C., R. K. Henderson, M. V. Storey, A. Baker, R. M. Stuetz, and S. J. Khan (2010), Fluorescence monitoring at a recycled water treatment plant and associated dual distribution system – Implications for cross-connection detection, *Water Res.*, 44(18), 5323–5333, doi:10.1016/j.watres.2010.06.003.
- Hedges, J. I. (1992), Global biogeochemical cycles: progress and problems, *Mar. Chem.*, 39(1-3), 67–93, doi:10.1016/0304-4203(92)90096-S.
- Heim, B. et al. (2014), Ocean colour remote sensing in the southern Laptev Sea: evaluation and applications, *Biogeosciences*, 11(15), 4191–4210, doi:10.5194/bg-11-4191-2014.
- Helms, J. R., A. Stubbins, J. D. Ritchie, E. C. Minor, D. J. Kieber, and K. Mopper (2008), Absorption spectral slopes and slope ratios as indicators of molecular weight, source, and photobleaching of chromophoric dissolved organic matter, *Limnol. Oceanogr.*, 53(3), 955–969.
- Huguet, A., L. Vacher, S. Relexans, S. Saubusse, J. M. Froidefond, and E. Parlanti (2009), Properties of fluorescent dissolved organic matter in the Gironde Estuary, *Org. Geochem.*, 40(6), 706–719, doi:10.1016/j.orggeochem.2009.03.002.
- Kellerman, A. M., D. N. Kothawala, T. Dittmar, and L. J. Tranvik (2015), Persistence of dissolved organic matter in lakes related to its molecular characteristics, *Nat. Geosci.*, 8(6), 454–457, doi:10.1038/ngeo2440.
- Kim, S., R. W. Kramer, and P. G. Hatcher (2003), Graphical Method for Analysis of Ultrahigh-Resolution Broadband Mass Spectra of Natural Organic Matter, the Van Krevelen Diagram, *Anal. Chem.*, 75(20), 5336–5344, doi:10.1021/ac034415p.
- Koch, B. P., and T. Dittmar (2006), From mass to structure: an aromaticity index for high-resolution mass data of natural organic matter, *Rapid Commun. Mass Spectrom.*, 20(5), 926–932, doi:10.1002/rcm.2386.
- Koch, B. P., M. Witt, R. Engbrodt, T. Dittmar, and G. Kattner (2005), Molecular formulae of marine and terrigenous dissolved organic matter detected by electrospray ionization Fourier transform ion cyclotron resonance mass spectrometry, *Geochim. Cosmochim. Acta*, 69(13), 3299–3308, doi:10.1016/j.gca.2005.02.027.
- Koch, B. P., K.-U. Ludwigowski, G. Kattner, T. Dittmar, and M. Witt (2008), Advanced characterization of marine dissolved organic matter by combining reversed-phase liquid chromatography and FT-ICR-MS, *Mar. Chem.*, 111(3-4), 233–241, doi:10.1016/j.marchem.2008.05.008.
- van Krevelen, D. V. (1950), Graphical-statistical method for the study of structure and reaction processes of coal, *Fuel*, 29, 269–284.
- Lakowicz, J. R. (2006), *Principles of Fluorescence Spectroscopy*, edited by J. R. Lakowicz, Springer US, Boston, MA.

- Lebo, S. E., J. D. Gargulak, and T. J. McNally (2000), Lignin, Kirk-Othmer Encyclopedia of Chemical Technology, John Wiley & Sons, Inc.
- Marshall, A. G., and C. L. Hendrickson (2002), Fourier transform ion cyclotron resonance detection: principles and experimental configurations, , 215, 59–75.
- Mcknight, D. M., E. W. Boyer, P. K. Westerhoff, P. T. Doran, T. Kulbe, and D. T. Andersen (2001), Spectrofluorometric characterization of dissolved organic matter for indication of precursor organic material and aromaticity, *Limnol. Oceanogr.*, 46(1), 38–48.
- Mopper, K., and D. J. Kieber (2002), Photochemistry and the cycling of carbon, sulfur, nitrogen and phosphorus, in *Biogeochemistry of Marine Dissolved Organic Matter*, edited by C. A. Carlson and D. A. Hansell, pp. 455–508, Academic Press, San Diego, CA.
- Mopper, K., and P. Lindroth (1982), Diel and depth variations in dissolved free amino acids and ammonium in the Baltic Sea determined by shipboard HPLC analysis, *Limnol. Oceanogr.*, 27(2), 336–347, doi:10.4319/lo.1982.27.2.0336.
- Murphy, K. R., A. Hambly, S. Singh, R. K. Henderson, A. Baker, R. Stuetz, and S. J. Khan (2011), Organic Matter Fluorescence in Municipal Water Recycling Schemes: Toward a Unified PARAFAC Model, *Environ. Sci. Technol.*, 45(7), 2909–2916, doi:10.1021/es103015e.
- Murphy, K. R., C. A. Stedmon, D. Graeber, and R. Bro (2013), Fluorescence spectroscopy and multi-way techniques. PARAFAC, *Anal. Methods*, 5(23), 6557, doi:10.1039/c3ay41160e.
- Murphy, K. R., C. A. Stedmon, P. Wenig, and R. Bro (2014), OpenFluor– an online spectral library of auto-fluorescence by organic compounds in the environment, *Anal. Methods*, 6(3), 658–661, doi:10.1039/C3AY41935E.
- Nelson, N. B., and D. A. Siegel (2013), The Global Distribution and Dynamics of Chromophoric Dissolved Organic Matter, *Ann. Rev. Mar. Sci.*, 5(1), 447–476, doi:10.1146/annurev-marine-120710-100751.
- Schmidt, F., M. Elvert, B. P. Koch, M. Witt, and K. U. Hinrichs (2009), Molecular characterization of dissolved organic matter in pore water of continental shelf sediments, *Geochim. Cosmochim. Acta*, 73(11), 3337–3358, doi:10.1016/j.gca.2009.03.008.
- Senesi, N., T. M. Miano, M. R. Provenzano, and G. Brunetti (1991), Characterization, differentiation and classification of humic substances by fluorescence spectroscopy, *Soil Sci.*, 152(4), 259–271, doi:10.1097/00010694-199110000-00004.
- Siegel, D. A., S. Maritorena, N. B. Nelson, D. A. Hansell, and M. Lorenzi-Kayser (2002), Global distribution and dynamics of colored dissolved and detrital organic materials, *J. Geophys. Res.*, 107(C12), 3228, doi:10.1029/2001JC000965.
- Siegel, D. A., S. Maritorena, N. B. Nelson, M. J. Behrenfeld, and C. R. McClain (2005), Colored dissolved organic matter and its influence on the satellite-based characterization of the ocean biosphere, *Geophys. Res. Lett.*, 32(20), L20605, doi:10.1029/2005GL024310.
- Spencer, R. G. M., G. R. Aiken, K. D. Butler, M. M. Dornblaser, R. G. Striegl, and P. J. Hernes (2009), Utilizing chromophoric dissolved organic matter measurements to derive export and reactivity of dissolved organic carbon exported to the Arctic Ocean: A case study of the Yukon River, Alaska, *Geophys. Res. Lett.*, 36(6), L06401, doi:10.1029/2008GL036831.
- Stedmon, C. A., and R. Bro (2008), Characterizing dissolved organic matter fluorescence with parallel factor analysis: a tutorial, *Limnol. Oceanogr. Methods*, 6, 1–6.
- Stedmon, C. A., and S. Markager (2001), The optics of chromophoric dissolved organic matter (CDOM) in the Greenland Sea : An algorithm for differentiation between marine and terrestrially derived organic matter, *Limnol. Oceanogr.*, 46(8), 2087–2093.
- Stedmon, C. A., S. Markager, and R. Bro (2003), Tracing dissolved organic matter in aquatic environments using a new approach to fluorescence spectroscopy, *Mar. Chem.*, 82, 239–254, doi:10.1016/S0304-4203(03)00072-0.

- Stedmon, C. A., R. M. W. Amon, A. J. Rinehart, and S. A. Walker (2011), The supply and characteristics of colored dissolved organic matter (CDOM) in the Arctic Ocean: Pan Arctic trends and differences, *Mar. Chem.*, 124(1-4), 108–118, doi:10.1016/j.marchem.2010.12.007.
- Stedmon, C. A., M. A. Granskog, and P. A. Dodd (2015), An approach to estimate the freshwater contribution from glacial melt and precipitation in East Greenland shelf waters using colored dissolved organic matter (CDOM), *J. Geophys. Res. Ocean.*, 120(2), 1107–1117, doi:10.1002/2014JC010501.
- Steinberg, C. E. W. (2003), *Ecology of Humic Substances in Freshwaters*, Springer Berlin Heidelberg, Berlin, Heidelberg.
- Stevenson, F. J. (1994), *Humus Chemistry: Genesis, Composition and reactions*, 2nd ed., Wiley-Interscience, New York, NY.
- Stubbins, A., R. G. M. Spencer, H. Chen, P. G. Hatcher, K. Mopper, P. J. Hernes, V. L. Mwamba, A. M. Mangangu, J. N. Wabakanghanzi, and J. Six (2010), Illuminated darkness: Molecular signatures of Congo River dissolved organic matter and its photochemical alteration as revealed by ultrahigh precision mass spectrometry, *Limnol. Oceanogr.*, 55(4), 1467–1477, doi:10.4319/lo.2010.55.4.1467.
- Stubbins, A., J.-F. Lapierre, M. Berggren, Y. T. Prairie, T. Dittmar, and P. A. del Giorgio (2014), What's in an EEM? Molecular Signatures Associated with Dissolved Organic Fluorescence in Boreal Canada, *Environ. Sci. Technol.*, 48(18), 10598–10606, doi:10.1021/es502086e.
- Sugimura, Y., and Y. Suzuki (1988), A high-temperature catalytic oxidation method for the determination of non-volatile dissolved organic carbon in seawater by direct injection of a liquid sample, *Mar. Chem.*, 24(2), 105–131, doi:10.1016/0304-4203(88)90043-6.
- Tanski, G., N. Couture, H. Lantuit, A. Eulenburg, and M. Fritz (2016), Eroding permafrost coasts release low amounts of dissolved organic carbon (DOC) from ground ice into the nearshore zone of the Arctic Ocean, *Global Biogeochem. Cycles*, doi:10.1002/2015GB005337.
- Del Vecchio, R., and N. V Blough (2004), On the Origin of the Optical Properties of Humic Substances, *Environ. Sci. Technol.*, 38(14), 3885–3891, doi:10.1021/es049912h.
- Wagner, S., R. Jaffé, K. Cawley, T. Dittmar, and A. Stubbins (2015), Associations Between the Molecular and Optical Properties of Dissolved Organic Matter in the Florida Everglades, a Model Coastal Wetland System, *Front. Chem.*, 3:66, 1–14, doi:10.3389/fchem.2015.00066.
- Walker, S. A., R. M. W. Amon, and C. A. Stedmon (2013), Variations in high-latitude riverine fluorescent dissolved organic matter: A comparison of large Arctic rivers, *J. Geophys. Res. Biogeosciences*, 118(4), 1689–1702, doi:10.1002/2013JG002320.
- Weishaar, J. L., G. R. Aiken, B. A. Bergamaschi, M. S. Fram, R. Fujii, and K. Mopper (2003), Evaluation of Specific Ultraviolet Absorbance as an Indicator of the Chemical Composition and Reactivity of Dissolved Organic Carbon, *Environ. Sci. Technol.*, 37(20), 4702–4708, doi:10.1021/es030360x.
- Williams, P. M., and E. R. M. Druffel (1987), Radiocarbon in dissolved organic matter in the central North Pacific Ocean, *Nature*, 330(6145), 246–248, doi:10.1038/330246a0.
- Wünsch, U. J., K. R. Murphy, and C. A. Stedmon (2015), Fluorescence Quantum Yields of Natural Organic Matter and Organic Compounds: Implications for the Fluorescence-based Interpretation of Organic Matter Composition, *Front. Mar. Sci.*, 2:98, 1–15, doi:10.3389/fmars.2015.00098.
- Yamashita, Y., and E. Tanoue (2003), Distribution and alteration of amino acids in bulk DOM along a transect from bay to oceanic waters, *Mar. Chem.*, 82(3-4), 145–160, doi:10.1016/S0304-4203(03)00049-5.
- Zsolnay, A., E. Baigar, M. Jimenez, B. Steinweg, and F. Saccomandi (1999), Differentiating with fluorescence spectroscopy the sources of dissolved organic matter in soils subjected to drying, *Chemosphere*, 38(1), 45–50, doi:10.1016/S0045-6535(98)00166-0.
- Zsolnay, Á. (2003), Dissolved organic matter: artefacts, definitions, and functions, *Geoderma*, 113, 187–209, doi:10.1016/S0016-7061(02)00361-0.



From Fresh to Marine Waters: Characterization and Fate of Dissolved Organic Matter in the Lena River Delta Region, Siberia

Rafael Gonçalves-Araujo^{1,2*}, Colin A. Stedmon³, Birgit Heim⁴, Ivan Dubinenkov^{2,5}, Alexandra Kraberg⁶, Denis Moiseev⁷ and Astrid Bracher^{1,8}

¹PHYTOOPTICS Group, Physical Oceanography of Polar Seas, Climate Sciences, Alfred Wegener Institute for Polar and Marine Research, Bremerhaven, Germany; ²Faculty of Biology and Chemistry (FB-2), University of Bremen, Bremen, Germany; ³Section for Marine Ecology and Oceanography, National Institute for Aquatic Resources, Technical University of Denmark, Charlottenlund, Denmark; ⁴Periglacial Research, Geosciences, Alfred Wegener Institute for Polar and Marine Research, Potsdam, Germany; ⁵Ecological Chemistry, Biosciences, Alfred Wegener Institute for Polar and Marine Research, Bremerhaven, Germany; ⁶Shelf Sea System Ecology, Biosciences, Biologische Anstalt Helgoland, Alfred Wegener Institute for Polar and Marine Research, Helgoland, Germany; ⁷Murmansk Marine Biological Institute of Kola Science Centre, Russian Academy of Sciences, Murmansk, Russia; ⁸Institute of Environmental Physics, University of Bremen, Bremen, Germany

OPEN ACCESS

Edited by:

Christopher Osburn,
North Carolina State University, USA

Reviewed by:

Karin M. Björkman,
University of Hawaii, USA
John Robert Helms,
Morningside College, USA

*Correspondence:

Rafael Gonçalves-Araujo
rafael.goncalves.araujo@awi.de;
rafaelgoncalvesaraujo@gmail.com

Specialty section:

This article was submitted to
Marine Biogeochemistry,
a section of the journal
Frontiers in Marine Science

Received: 30 September 2015

Accepted: 23 November 2015

Published: 16 December 2015

Citation:

Gonçalves-Araujo R, Stedmon CA, Heim B, Dubinenkov I, Kraberg A, Moiseev D and Bracher A (2015) From Fresh to Marine Waters: Characterization and Fate of Dissolved Organic Matter in the Lena River Delta Region, Siberia. *Front. Mar. Sci.* 2:108. doi: 10.3389/fmars.2015.00108

Connectivity between the terrestrial and marine environment in the Arctic is changing as a result of climate change, influencing both freshwater budgets, and the supply of carbon to the sea. This study characterizes the optical properties of dissolved organic matter (DOM) within the Lena Delta region and evaluates the behavior of DOM across the fresh water-marine gradient. Six fluorescent components (four humic-like; one marine humic-like; one protein-like) were identified by Parallel Factor Analysis (PARAFAC) with a clear dominance of allochthonous humic-like signals. Colored DOM (CDOM) and dissolved organic carbon (DOC) were highly correlated and had their distribution coupled with hydrographical conditions. Higher DOM concentration and degree of humification were associated with the low salinity waters of the Lena River. Values decreased toward the higher salinity Laptev Sea shelf waters. Results demonstrate different responses of DOM mixing in relation to the vertical structure of the water column, as reflecting the hydrographical dynamics in the region. Two mixing curves for DOM were apparent. In surface waters above the pycnocline there was a sharper decrease in DOM concentration in relation to salinity indicating removal. In the bottom water layer the DOM decrease within salinity was less. We propose there is a removal of DOM occurring primarily at the surface layer, which is likely driven by photodegradation and flocculation.

Keywords: DOC, CDOM, FDOM, PARAFAC, optical indices, hydrography, Laptev Sea, Arctic

INTRODUCTION

Colored or chromophoric dissolved organic matter (CDOM) is the fraction of DOM that absorbs light and it is one of the dominant components influencing the underwater light field in coastal and inner-shelf waters (Siegel et al., 2002; Nelson and Siegel, 2013). CDOM absorbs light in the ultraviolet (UV) and visible wavelength ranges and thus it is able to shield aquatic biota from harmful UV radiation (Arrigo and Brown, 1996) and can be detected by ocean color remote sensing

(Siegel et al., 2002, 2005). As a result of its UV absorbing properties, CDOM is susceptible to photodegradation, which either induces direct mineralization or produces microbiologically labile low molecular weight compounds, which are subsequently utilized by bacteria (Mopper and Kieber, 2002). Fluorescent DOM (FDOM), which is the part of CDOM able to fluoresce, can be used to trace the supply, mixing, and removal of different fractions of DOM (Yamashita and Tanoue, 2003, 2004; Coble, 2007; Chari et al., 2013; Fukuzaki et al., 2014). With the recent adaptation of the Parallel Factor Analysis (PARAFAC) for analysis of DOM, a more holistic analysis of excitation-emission matrices (EEMs) allows for the differentiation of wider range of underlying DOM components (Stedmon and Bro, 2008). A recent study showed significant associations between molecular groups and PARAFAC-derived DOM components (Stubbins et al., 2014). For instance, the humic-like fluorescent peak A (e.g., Coble, 2007) is associated with high molecular weight compounds with little nitrogen, whereas the humic-like peak C correlated to lignin-derived phenols and the amino acid-like peak T was associated to low molecular weight and aromatic content compounds, such as hydrolysable amino acids (Stubbins et al., 2014).

By applying the EEMs/PARAFAC technique, the distribution and dynamics of fluorescent DOM have been studied in a wide range of environments varying from lakes (Zhang et al., 2009), estuaries (Stedmon and Markager, 2005; Singh et al., 2010), coastal and shelf (Murphy et al., 2008; Kowalczyk et al., 2010; Para et al., 2010) to pelagic waters (Yamashita et al., 2010; Jørgensen et al., 2011; Kowalczyk et al., 2013). In coastal regions, especially in areas close to river outflows, the riverine input, and its mixing with marine waters are the major factors controlling the distribution and composition of DOM (Stedmon and Markager, 2003; Guo et al., 2007; Alling et al., 2010). In these waters processes such as photobleaching (Opsahl and Benner, 1998; Stubbins et al., 2006; Helms et al., 2008, 2014; Porcal et al., 2013, 2015), sorption to sediments, flocculation (Uher et al., 2001; Shank et al., 2005; Guo et al., 2007; von Wachenfeldt et al., 2008; Asmala et al., 2014), biological uptake (Boyd and Osburn, 2004), biological release (Romera-Castillo et al., 2010), and photo-production of DOM (Helms et al., 2014) can also play a crucial role in controlling the amount, composition, and reactivity of DOM in these environments.

The Arctic Ocean receives considerable input of terrigenous carbon mobilized from high latitude carbon-rich soils and peatlands (Opsahl et al., 1999; Benner et al., 2004). This terrigenous material is supplied by Arctic rivers, which account for more than 10% of the total riverine and terrestrial organic carbon into the global ocean waters (Opsahl et al., 1999; Benner et al., 2004). Among those rivers, the Lena River (eastern Siberia) accounts for the highest annual DOM discharge into the Arctic Ocean (Raymond et al., 2007; Stedmon et al., 2011), with a peak discharge in June (Amon et al., 2012; Fedorova et al., 2015). It contributes approximately 20% to the total fresh water discharge into the Arctic Ocean through its delta into the Laptev Sea (Cauwet and Sidorov, 1996). The Lena Delta and the Laptev Sea inner shelf encompass a large, shallow environment characterized by pronounced physical-chemical gradients (Bauch et al., 2009;

Fofonova et al., 2014) and considerable amounts of sediments, dissolved, and particulate organic matter over the water column (Semiletov et al., 2011; Vonk et al., 2012, 2014; Wegner et al., 2013; Heim et al., 2014; Sánchez-García et al., 2014). Eastern Siberia (including the Lena River and its delta) is known to be affected by global warming with a thawing permafrost (Yang et al., 2002; Schuur et al., 2008), which subsequently affects the fresh water discharge, the production of DOM in river catchments and the riverine transport of organic material input into the shelf seas (Frey and McClelland, 2009; Lyon and Destouni, 2010; Semiletov et al., 2012, 2013; Vonk et al., 2012, 2014; Sánchez-García et al., 2014; Fedorova et al., 2015).

The Lena Delta region and Laptev Sea have high DOC concentrations (>500 μM) and high CDOM associated with low salinity waters (Alling et al., 2010; Stedmon et al., 2011; Semiletov et al., 2013; Walker et al., 2013; Heim et al., 2014; Dubinenkov et al., 2015a), decreasing toward higher salinities through conservative mixing (Cauwet and Sidorov, 1996; Kattner et al., 1999). This is a characteristic also thought to be shared by other Arctic rivers (Dittmar and Kattner, 2003). However, a recent study has indicated non-conservative mixing of DOC within the Lena Delta region, with average losses of 30–50% during mixing along the shelf (Alling et al., 2010). These authors also identified additional sources of DOC in the region (such as primary production and coastal erosion), and pointed out photodegradation, flocculation, sedimentation, and microbial activity as possible processes to be responsible for the removal of DOC and humic substances, although currently poorly resolved. Rectifying this is difficult due to not only the remoteness of the location but also because there is a lack of information on the composition, amount, reactivity, and fate of DOM in these waters. Despite the recent techniques applied for DOM analysis and the advances in the knowledge of the dynamics and composition of DOM in some aquatic environments, there is still a considerable lack of information on this important component of the global carbon pool. This is particularly compounded when accounting for the composition and processes modulating the distribution and reactivity of DOM in the Arctic regions. Hence, further studies addressing these issues are essential for a better understanding of the role of DOM in the carbon cycle within the aquatic environments, especially the Arctic Ocean.

In this study DOM characteristics within the Lena Delta region based on fluorescent properties was investigated. The distribution and transformation of the DOM along the fresh water-marine gradient were investigated, using samples collected in September 2013 at the Lena Delta region in the southern Laptev Sea. The findings provide an insight into the fate of Arctic riverine DOM while it is mixed at the shelf with the waters from the Laptev Sea.

MATERIALS AND METHODS

Sampling

The Lena Expedition was conducted in late summer 2013 (1–7 September) on board the Russian R/V “Dalnie Zelentsy” of the Murmansk Marine Biological Institute, in the surrounding

areas of the Lena River Delta region, Laptev Sea, Siberia. A total of 18 oceanographic stations were occupied and split into four transects (Figure 1A). The hydrographic characteristics of the water column were assessed from vertical profiles acquired with a CTD-profiler SEACAT SBE 19+. Prior to the cruise, temperature, conductivity, and pressure sensors were calibrated at laboratories of the All-Russia D. I. Mendeleyev Scientific and Research Institute for Metrology. Water samples were taken using Niskin bottles at surface and discrete depths chosen based on CTD profiles. The amount of samples per profile and station varied according to the local depth, ranging from two samples at shallow water (<5 m) and six samples at deeper water stations (e.g., 20–35 m). The full data set used to compose this work is available online in two published datasets (Dubinenkov et al., 2015b; Gonçalves-Araujo et al., 2015a).

Water Column Structure Assessment

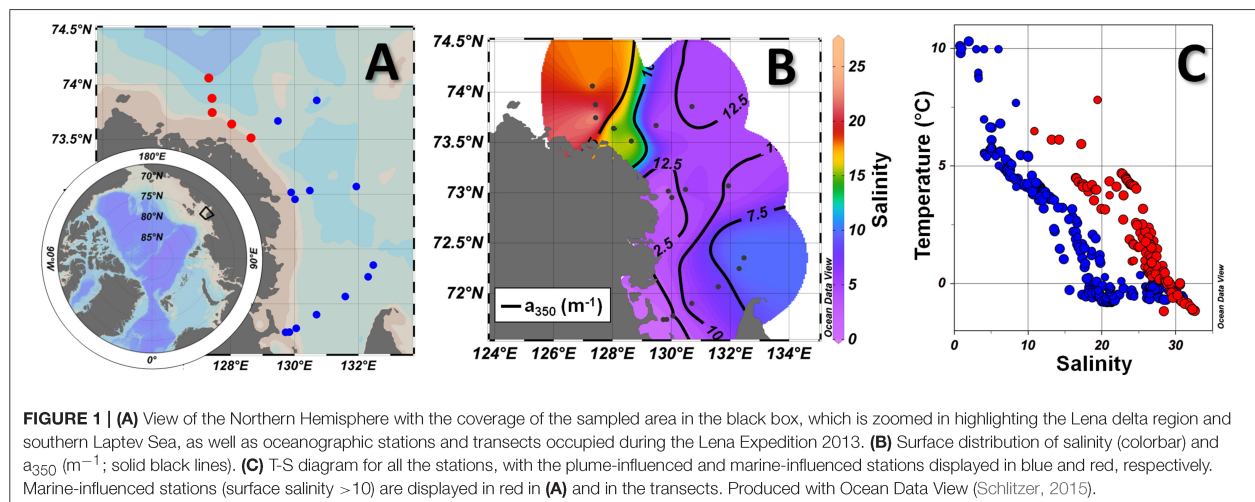
To assess the structure of the water column, vertical profiles of temperature and salinity from the CTD casts were used to obtain potential water density (ρ) profiles. The depth where variations in density were equal or greater than 0.125 kg m^{-3} over a 5-m depth interval was considered the upper mixed layer depth (UMLD), as adapted from Levitus (1982) and Kara et al. (2000a). The bottom depth was adopted as UMLD for inner shelf stations with vertically mixed profiles. The water column stability parameter (E) was obtained from vertical density variations assessed by the buoyancy or Brunt-Väisälä frequency (N^2), which is defined by $N^2 = \frac{g}{\rho} \frac{\partial \rho}{\partial z}$ ($\text{rad}^2 \text{ s}^{-2}$) leading to $E = \frac{N^2}{g}$ ($10^{-8} \text{ rad}^2 \text{ m}^{-1}$), where g is gravity. The maximum stability immediately below the UMLD was considered to represent the strength of the pycnocline/stratification (Gonçalves-Araujo et al., 2015b; and references therein).

DOC and DOM Sample Processing and Data Analysis

Water samples for DOC analysis were filtered through $0.7 \mu\text{m}$ GF/F filters (Whatman, pre-combusted, 4 h, 450°C) and dark

stored in a freezer until further analysis in the laboratory. DOC concentrations were measured using high temperature catalytic oxidation (TOC-VCPN, Shimadzu). For external calibration of the instrument potassium hydrogen phthalate (KHP, Merck) was used. All samples were acidified (0.1 M HCl suprapur, Merck) and purged with O_2 for >5 min. Performance of the instrument was recorded by daily analysis of in-lab KHP standard solutions and reference samples (deep sea reference, DSR, Hansell research lab). The instrument blank was $\sim 2 \mu\text{M C}$ and quality of analysis was monitored continuously based on results of DSR reference samples.

The samples for CDOM analysis were immediately syringe-filtered after sampling with Whatman Spartan 13 filters ($0.2 \mu\text{m}$) and then stored in amber glass bottles (100 mL) and kept cooled in the fridge (4°C) until further analysis. Before analysis, the samples were mixed and filtered once more through Whatman Spartan 13 syringe filters ($0.2 \mu\text{m}$). Fluorescence EEMs were collected using an Aqualog[®] fluorescence spectrometer (HORIBA Jobin Yvon, Germany). Freshly produced Milli-Q water was used as reference. Fluorescence intensity was measured across emission wavelengths 220–620 nm (resolution 1.77 nm, 4 pixel) at excitation wavelengths from 240 to 600 nm with 3 nm increments, and an integration time of 2 s. The blank-corrected absorbance spectra was converted into Napierian absorption coefficient (a) at each wavelength (λ), using the given equation: $a_\lambda (\text{m}^{-1}) = (2.303 \times A_\lambda)/L$, where A_λ is the absorbance at specific wavelength and L is the cuvette path length in meters. The absorption coefficients in the visible (440 nm— a_{440}) and UV (350 nm— a_{350}) bands are generally adopted as indicators of CDOM magnitude. Although many studies have presented their results using the absorption coefficient at 440 nm (a_{440}) due to its application to ocean color remote sensing (e.g., Siegel et al., 2005; Heim et al., 2014), in this study we determined the absorption coefficients in both visible (a_{440}) and UV (a_{350}) ranges. Nevertheless, we focus our results and discussions on the a_{350} coefficient because of its correlations to DOC and lignin concentrations and to permit comparison



with earlier results (Spencer et al., 2009; Stedmon et al., 2011; Walker et al., 2013). The raw EEMs acquired with Aqualog[®] were corrected for inner-filter effects and for the Raman and Rayleigh scattering (Murphy et al., 2013). The different fluorescent components of DOM were isolated from combined signal by PARAFAC modeling using the “drEEM Toolbox” and following the recommendation of Murphy et al. (2013). The DOM components derived from PARAFAC modeling were compared with PARAFAC components from other studies through the OpenFluor database (Murphy et al., 2014). The complete absorption and emission spectra of the fluorescent components derived from PARAFAC are available on the OpenFluor database after publication (<http://www.openfluor.org>). We have estimated the hypothetical conservative mixing of DOM (i.e., a_{350} , DOC, and fluorescence intensity of each of the PARAFAC components) by considering the average of two values of the respective parameter at the highest and at the lowest salinity extremities, respectively, as the end points of the conservative line.

DOM Modification Indices, Statistical Analyses, and Graphical Tools

Besides the determination of the magnitude and characterization of DOM components, the optical characteristics of CDOM and FDOM can also be used to assess the origin and degree of transformation of DOM through the calculation of optical indices. By applying an exponential function to the 275–295 nm spectral range it is possible to derive the spectral slope of absorption spectra (S_{CDOM} , in μm^{-1}) that varies in relation to the source of CDOM. It has also been shown to be inversely correlated with the molecular weight of DOM and can be related to photobleaching (Helms et al., 2008; Fichot and Benner, 2012; Fichot et al., 2013). The specific UV absorbance (SUVA) is used as a proxy for the degree of aromaticity in CDOM samples (Weishaar et al., 2003) and it is defined by $SUVA = A_{254}/[DOC]$, where A_{254} is the absorbance at 254 nm and the concentration of DOC, [DOC], is measured in mg CL^{-1} . Due to the high absorption of aromatic compounds in the UV-visible, higher SUVA values indicate higher aromaticity from allochthonous input (e.g., humic compounds), while lower SUVA values are associated to more autochthonous or modified terrestrial CDOM with lower aromaticity (Weishaar et al., 2003).

Two optical indices, that take FDOM into account, were also used to investigate both the degree of humification and biological degradation of the DOM. The humification index (HIX) estimates the degree of maturation of DOM (Zsolnay et al., 1999; Zsolnay, 2003), considering that humification is associated with an increase in the C/H ratio (Stevenson, 1982) and is thus reflected in emissions at longer wavelengths (Senesi et al., 1991). The HIX index is the ratio of the areas of two spectral wavelength regions in the emission spectra for an excitation at 254 nm and it is obtained as: $HIX = H/L$, where H is the area between 435 and 480 nm in the emission spectra and L is the area in the emission spectra between 300 and 345 nm (Zsolnay et al., 1999). An increase in the degree of aromaticity (humification) leads to a red shift in the emission spectrum, which will be associated with higher HIX values. The biological/autochthonous index (BIX) is

used to assess the biological modification of DOM based on UV fluorescence. The BIX index is obtained by calculating the ratio of the emission at 380 and 430 nm, excited at 310 nm: $BIX = I_{Em380}/I_{Em430}$ (Huguet et al., 2009). High BIX values correspond to autochthonous origin of DOM, i.e., freshly released DOM, whereas low BIX values indicate allochthonous DOM (Huguet et al., 2009).

The relationships between all pairs of variables were investigated using Spearman correlation coefficients. To compare the variables among themselves or among different groups of samples, Kruskal–Wallis H tests were applied, after performing normality tests. Furthermore, the relationship between each pair of variables was determined based on linear regressions.

RESULTS

Hydrography and Water Column Structure

Pronounced environmental variability was observed within the studied region, with sampling varying from fresh to marine waters, as demonstrated by the noticeable hydrographical gradients in the T-S diagram (Figure 1C). Salinity varied between 0.90 and 32.63, with the lowest values associated with fresh water input from the Lena River and plume (Figures 1B,C). Temperature ranged from -1.2 to 10.3°C , with higher values related to the warmer and fresher Lena river plume and the lowest values attributed to the presence of the colder and saltier Laptev Sea shelf waters. In addition, a strong horizontal frontal zone was found within the NW portion of the study area, with the isohaline of 10 depicting the surface limit between two hydrographic provinces observed: the sites under direct influence of fresher Lena River plume and the sites under influence of the saltier waters from the Laptev Sea shelf (Figures 1A,B), hereafter named as plume- and marine-influenced stations. Note that, although named marine-influenced stations, those sites were still under influence of the continental fresh water input, however less than the plume-influenced ones, given the still low salinity observed at surface (varying from 13.21 to 25.60; Figure 1B).

A low salinity surface layer generated by the influence of the fresh waters from the Lena River was observed along the entire sampled area (Figure 1). The occupation of the surface layer by the river plume leads to the establishment of an upper mixed layer of ~ 10 m and a pronounced vertical gradient of density. Nevertheless, a few shallower stations (< 5 m deep) close to the main outflows of the Lena River (Bykovskaya and Trofimovskaya) were characterized by vertically mixed profiles with very low salinity (< 3) waters from the Lena plume. The stability parameter (E) was obtained for all the stations where a vertical stratification was observed. The strength of the pycnocline was inversely related to the surface salinity ($r^2 = 0.82$; $p < 0.01$). Thus, the plume-influenced stations exhibited a greater stratification in comparison to the marine-influenced ones, with averaged E -values of about $7.01 \pm 2.84 \times 10^{-8}$, $4.32 \pm 1.79 \times 10^{-8}$, and $3.98 \pm 1.80 \times 10^{-8} \text{ rad}^2 \text{ m}^{-1}$ for stations located at the inner-plume (surface salinity < 5), outer-plume ($5 < \text{surface salinity} < 10$) and marine-influenced stations (surface salinity > 10), respectively).

CDOM and DOC Spatial Variability

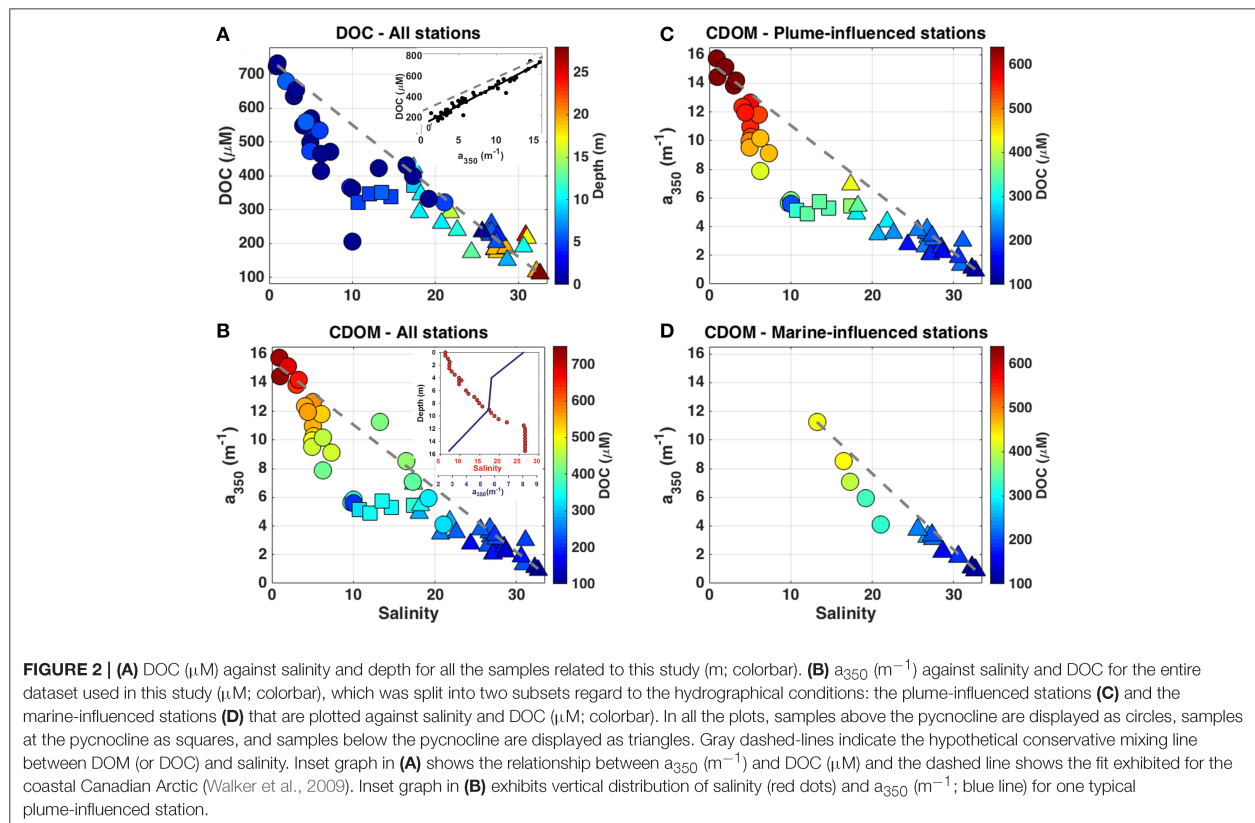
CDOM displayed a distribution tightly coupled with salinity (see **Figures 1B, 2**). a_{350} ranged from 0.9 to 15.7 m^{-1} (**Figure 2**) and showed a significant negative correlation with salinity [$a_{350} = -0.377(\text{salinity}) + 12.774$; $r^2 = 0.96$; $p < 0.0001$]. The highest a_{350} values were observed within the fresher waters under the influence of the Lena plume with a decrease in a_{350} toward the saltier waters from the Laptev Sea. DOC ranged from 110 to 732 μM and was highly correlated to a_{350} [DOC = $38.529(a_{350}) + 106.889$; $r^2 = 0.99$; $p < 0.0001$], exhibiting a very similar behavior as CDOM across the salinity gradient [DOC = $-14.878(\text{salinity}) + 605.236$; $r^2 = 0.96$; $p < 0.0001$] (**Figure 2**). Additionally, a_{440} varied between 0.12 and 2.97 m^{-1} and it was significantly highly correlated to a_{350} [$a_{440} = 5.188(a_{350}) + 0.361$; $r^2 = 0.99$; $p < 0.0001$] and DOC [DOC = $199.057(a_{440}) + 121.760$; $r^2 = 0.98$; $p < 0.0001$].

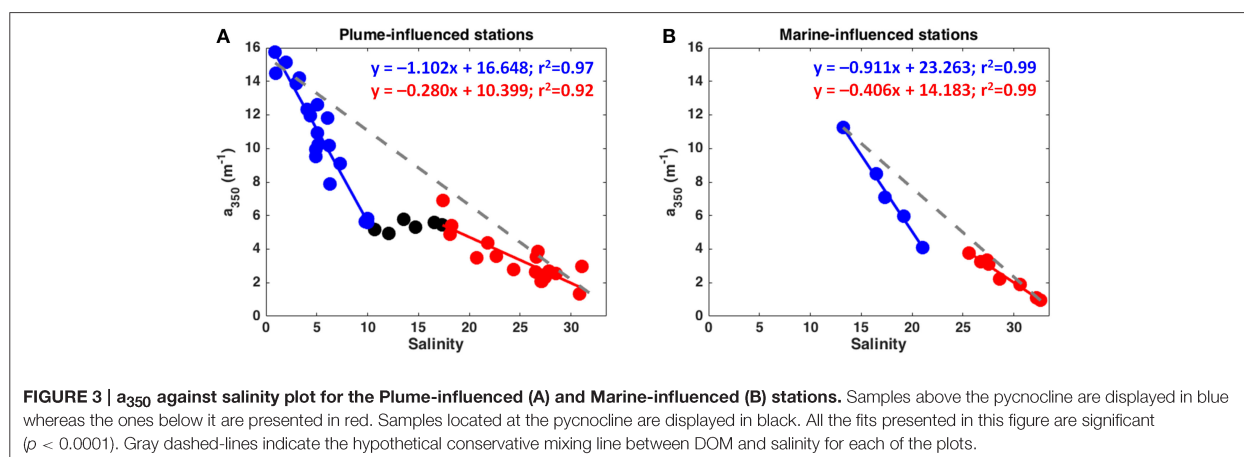
When taking into account the relationship between DOM and salinity for each of the hydrographic provinces separately, some features/patterns become clear (**Figures 2, 3**): a higher DOM amount is associated to the plume-influenced sites; a steeper curve is exhibited by samples above the pycnocline in relation to the samples below it; and there is low variability in DOM along the pycnocline itself. In addition, the a_{350} vs. salinity curve above the pycnocline displayed by the plume-influenced sites was even steeper than the same curve for the marine-influenced sites (**Figure 3**). Overall, a non-conservative behavior

is observed in the low salinity, surface layer (given the deviation in relation to the hypothetical conservative mixing line) with an indication of removal of DOM (deviating up to 56% from the hypothetical conservative mixing line). That deviation decreases at the underlying layer, suggesting a conservative mixing of DOM in those waters (see **Figures 2, 3**).

FDOM Components by PARAFAC

Six fluorescent components (C1-C6) were identified by the PARAFAC model (**Figure 4**). Four components had broad emission and excitation spectra, with emission maxima at visible wavelengths typical of humic-like material (C1, C2, C4, and C5). C3 and C6 had comparably narrow UVA emission maxima. The fluorescence intensity of the components differed greatly, with C1 having the greatest values (reaching up to 2.08 nm^{-1}) and C6 the lowest (up to 0.18 nm^{-1} ; **Figure 4**). The humic-like components C1 and C2 were the dominant fluorescent signals, accounting for more than 50% of total FDOM in all the samples. The humic-like contribution to total FDOM reached up to 86% at low salinity (see colorbar in **Figure 5**), and was inversely related to salinity ($p < 0.0001$). C1, C2, C3, and C4 presented a similar scattered pattern in relation to salinity. A steeper curve at low salinity (< 10) suggests removal in that layer, whereas a less steep curve fit at high salinity (> 10) indicates the presence of a conservative mixing (**Figure 4**, right panel). Although being likewise inversely correlated with salinity, C5 and C6 presented distinct patterns





when compared to the other components (Figure 4). Both components exhibited a non-conservative mixing, however with indication of release/production during the transit from the river to the outer shelf (Figure 4, right panel).

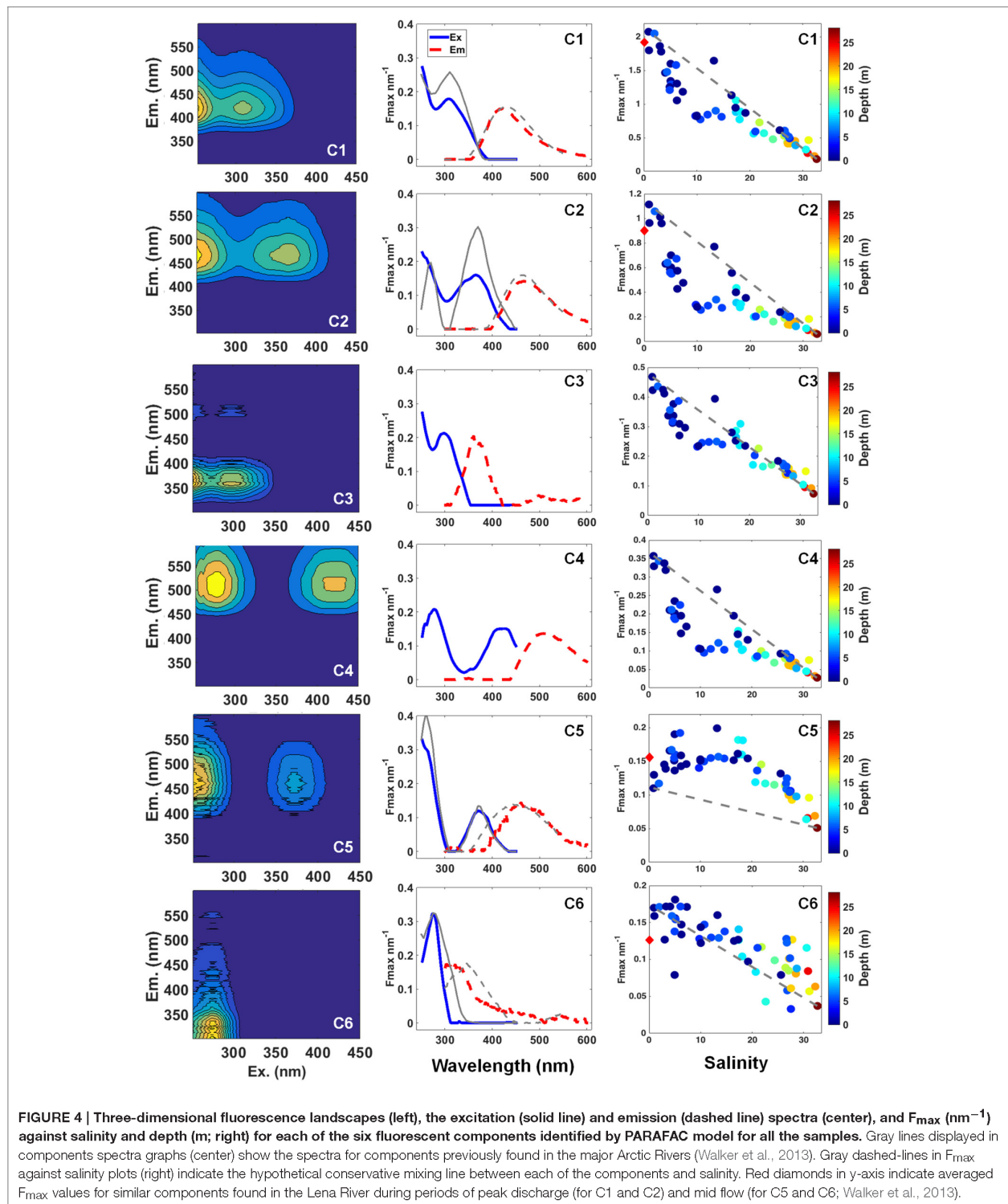
Optical Indices of DOM Modification

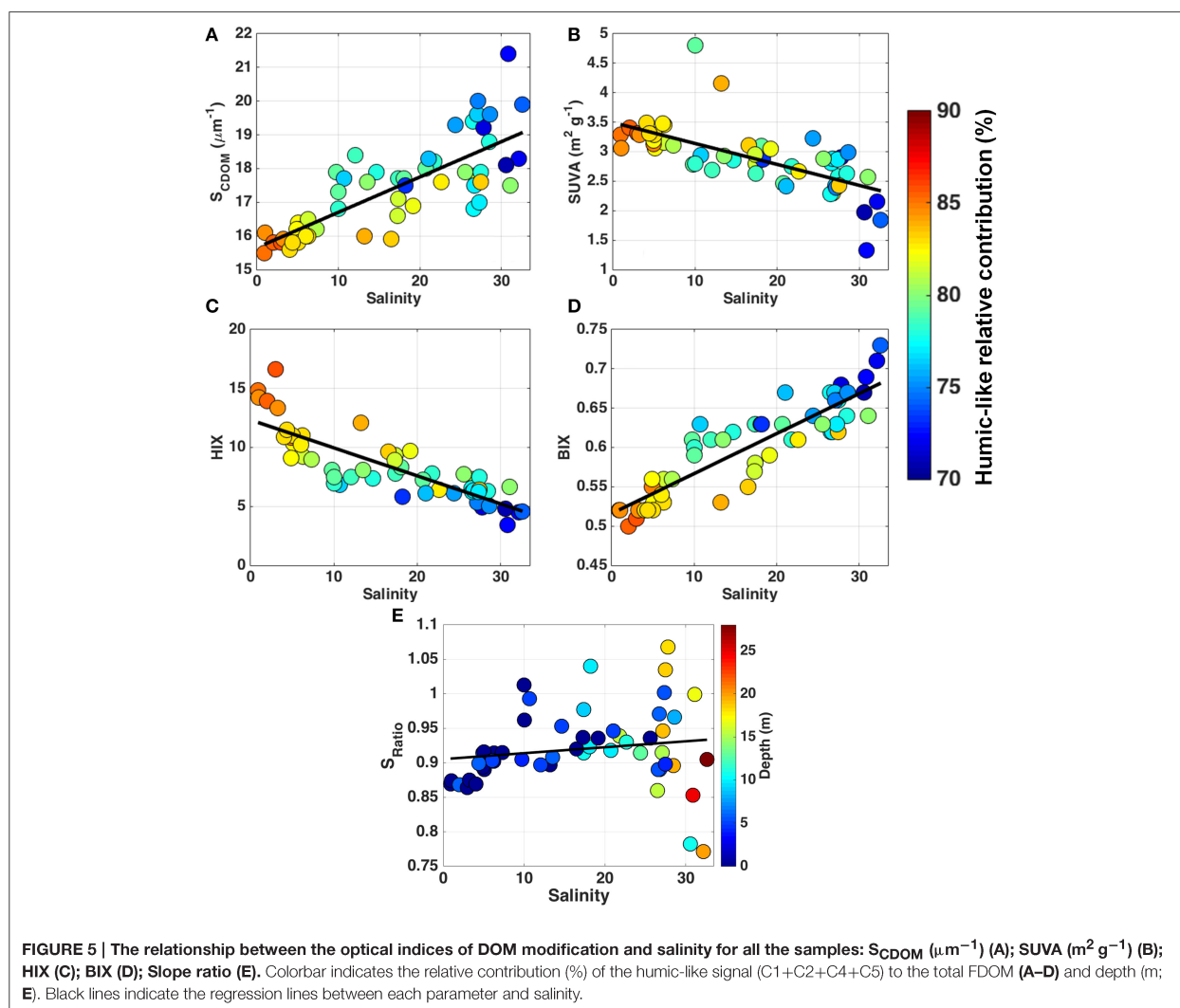
Different optical indices including S_{CDOM} , SUVA, HIX, and BIX indices (in Figure 5 shown in relation to salinity), as well as the slope ratio (S_{Ratio} ; Helms et al., 2008) and the fluorescence index (FI; McKnight et al., 2001; not shown) were evaluated within all samples. All indices, except S_{Ratio} ($p > 0.05$), were significantly correlated with salinity, a_{350} , DOC and FDOM, and by that also to each other ($p < 0.0001$). Although it was not significantly correlated to salinity ($p > 0.05$), the S_{Ratio} indicated a dominance of terrigenous signal over the entire sample area, given that most of the samples (~93%) presented S_{Ratio} values below 1 (Figure 5E). In addition, the lack of significance between S_{Ratio} and salinity might be due to an increase in the signal-to-noise ratio for the absorbance spectra at wavelengths longer than 350 nm observed in samples at higher salinity that, in turn, presented the greatest variability in S_{Ratio} values. S_{CDOM} ranged from 15.5 to 21.4 μm^{-1} and was directly related to salinity (Figure 5A), suggesting a decrease in the molecular weight with increased salinity (Helms et al., 2008). The values observed for the SUVA index were high, ranging from 1.33 to 4.80 $\text{m}^2 \text{g}^{-1}$, and was inversely related to salinity ($p < 0.0001$), evidencing a decrease in the aromaticity of the molecules toward high salinity (Figure 5B). The HIX index values ranged from 3.4 to 16.6, and the BIX index values were lower than 0.73 (Figures 5C,D, respectively), indicating a high degree of humification and low autochthonous contribution within our sample set, respectively. Moreover, HIX and BIX showed a decrease (increase) in the degree of humification (DOM from biological activity) with increase in salinity, given the significant relationship ($p < 0.0001$) displayed by those indices and salinity (Figures 5C,D). FI presented values below 1.3 and was inversely related ($p < 0.0001$) to salinity (not shown), indicating a consistent predominance of terrestrial sources of DOM to the region.

DISCUSSION

Characterization and Transformation of DOM

The results characterize the DOM composition (here using the EEM/PAFARAC approach and optical indices of DOM modification) along the fresh water-marine gradient within the Lena delta region and Laptev Sea. Four of the six fluorescent components identified by PARAFAC analysis, three humic-like (C1, C2, and C5) and one protein-like (C6; see Figure 4-center), were already reported in the Lena River and in other large Arctic rivers (Walker et al., 2013). In addition, a recent study reported the presence of three of those components (C1, C2, and C6) in the Amerasian basin (Guéguen et al., 2015), which seem to be common components of the Arctic DOM pool. Although, our sampling was carried out during a period of mid discharge flow (Stedmon et al., 2011), C1 and C2 presented similar fluorescence intensities to the average observed for the Lena River during the discharge peak (~1.6 and 0.9 nm^{-1} , respectively; Walker et al., 2013). C5 and C6, on the other hand, presented intensities close to the average observed in the Lena during the mid discharge flow (see Figure 4-right column; Walker et al., 2013). Our results demonstrate that the FDOM composition in the Lena Delta region was mainly characterized by the dominance of riverine humic-like compounds. This is evidenced by the high contribution of the allochthonous humic-like components with fluorescence in the visible range (C1, C2, C4, and C5) observed in relation to the total FDOM (Figure 4), as well as by the optical indices of DOM modification (Figure 5). A recent study has identified PARAFAC components similar to our humic-like C1 (also referred in the literature as the classical peak C) and C4, which presented strong correlation to lignin phenol concentrations (Yamashita et al., 2015). Dominance of humic-like compounds has been already reported in the Lena Delta in late summer 1995, when high concentrations of lignin, and high contribution of terrigenous DOC (about 60% of total DOC) were observed (Kattner et al., 1999). The humic-like component 1 is a dominant component of the FDOM signal not only in the Lena River and Delta, but it has also been found to be





dominant in other Arctic rivers such as Mackenzie, Kolyma, Ob, and Yenisei (Walker et al., 2009, 2013), in the Amerasian basin (Guéguen et al., 2015) and in shelf waters in the North Atlantic (Kowalczyk et al., 2009; Yamashita et al., 2013). In accordance to the results obtained with the EEM/PARAFAC approach, the optical indices of DOM modification have also pointed to a dominance of humic-like compounds within the samples (see Figure 5).

Despite the dominance of allochthonous humic-like components over the entire sampled area, autochthonous components (such as the marine-humic like C3 and the protein-like C6) have their relative contribution (to total FDOM signal) enhanced toward high salinity (see colorbar in Figure 5). Increased relative contribution of C6 was also observed during the base flow of the Lena River, when the terrestrial input is reduced (Walker et al., 2013). In addition, the component C6, also referred in other studies as tryptophan-like, seems

to be a useful indicator of bioavailability of DOM, given the strong correlation showed by it and total dissolved amino acids concentrations (Yamashita et al., 2015). The increase observed in the relative contribution of autochthonous compounds toward the high salinity waters of the Laptev Sea shelf region was also evident when observing the ranges presented by the optical indices of DOM modification (see Figure 5). Furthermore, those indices can provide more information on the transformation of the DOM during the transit from the river to the outer shelf. The use of optical indices has been successfully applied to assess the transformation of DOM along wide salinity ranges in some estuary regions worldwide (Benner and Opsahl, 2001; Helms et al., 2008, 2014; Huguet et al., 2009; Asmala et al., 2014). The values obtained for the optical indices at low salinity in our study are in agreement with previous studies conducted in the Lena River. For instance, those studies have reported S_{CDOM} , $SUVA$, and BIX values around $16 \mu\text{m}^{-1}$, $2.8 \text{m}^2 \text{g}^{-1}$ and 0.52,

respectively (Stedmon et al., 2011; Walker et al., 2013). All the optical indices taken into account in this study demonstrated that the DOM in the Lena delta region experiences an evident transformation along the riverine-marine transition. This is supported by the reduction on the molecular weight, aromaticity and humification degree of DOM observed toward high salinity, with the more photochemically reactive compounds associated to the surface (with lower salinity) layer and components with more refractory character being associated to the high salinity-Laptev Sea shelf waters (Figure 5). The possible mechanisms driving the observed transformation in DOM are discussed in the following section.

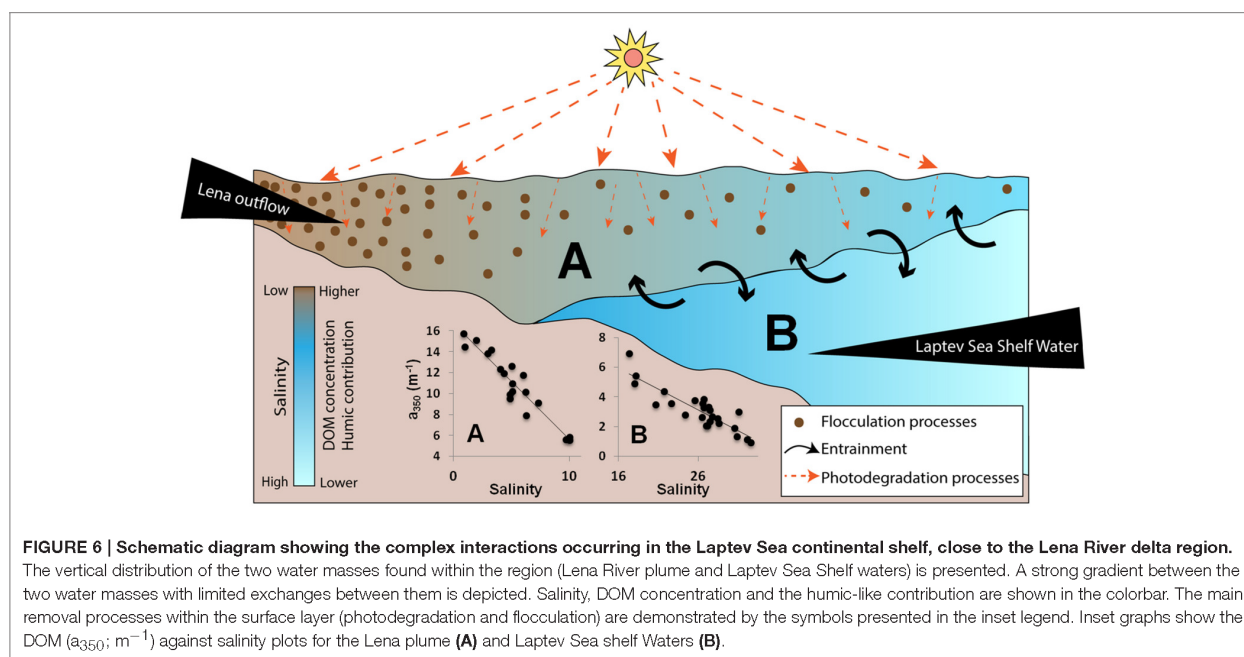
Dynamics and Fate of DOM in the Lena Delta Region

The hydrographic observations during our campaign revealed strong gradients, with noticeable northward propagation of the Lena River plume along the study region. This generated a shallow, low salinity surface mixed layer with strong stratification, which separates the surface layer from the underlying high salinity layer with Laptev Sea shelf water (see Figure 1). The propagation of the plume along the Laptev Sea shelf has also induced the establishment of a strong frontal system in the NW part of our study area (see Figure 1). Such hydrographic characteristics were previously described as offshore wind conditions, when the predominant winds from the continent drive the offshore propagation of the Lena waters generating a strong stratification and a frontal system NW of the Lena Delta region (Bauch et al., 2009; Wegner et al., 2013). Thus, we have identified the presence of two hydrographic provinces within the sampled area: the plume- and marine-influenced sites (see Figure 1).

The noticeable variability in hydrographic conditions due to the dynamics between fresh water input from the Lena River and the Laptev Sea shelf waters were also reflected in the striking differences of the amount and composition of DOM (Figures 2, 3). The association of the highest DOM concentrations with the low salinity waters of the Lena outflow decreasing toward the high salinity Laptev Sea shelf waters (see Figure 2) re-emphasizes the importance of the Lena River as a major source of DOM to the Laptev Sea. Such inverse relationship has previously been indicated for this region (Cauwet and Sidorov, 1996; Kattner et al., 1999; Alling et al., 2010; Semiletov et al., 2013; Heim et al., 2014) and it is the case for many other estuary regions (Benner and Opsahl, 2001; Guo et al., 2007; Huguet et al., 2009). Both CDOM and DOC were highly correlated, displaying a similar relationship as found for the coastal Canadian Arctic (Walker et al., 2009; see Figure 2), although with a higher a_{350} relative to DOC in the Lena delta waters. The presented values are comparable to other studies previously conducted in this region, with a_{350} (a_{440}) values of about 15 m^{-1} (2.9 m^{-1}) at low salinity and DOC concentrations ranging from 500–700 to $100 \mu\text{M}$ at low and high salinity, respectively (Alling et al., 2010; Stedmon et al., 2011; Semiletov et al., 2013; Walker et al., 2013; Heim et al., 2014; Dubinenkov et al., 2015a).

Our results show a coupled relationship between DOM and the two hydrographic provinces identified in this work. Plume-influenced stations presented higher DOM concentrations at surface as compared to marine-influenced stations ($p < 0.001$; see Figure 1). Despite these differences within the surface layers, both hydrographic provinces exhibited similar patterns regarding the relationship between DOM and salinity. Distinct DOM mixing patterns (in relation to salinity) were observed for samples above and below the pycnocline, i.e., the low and high salinity layers, respectively (Figure 6). The mixing curves derived from samples above the pycnocline exhibited higher slope than the ones below it (see Figures 2, 3, 6). The same pattern is observed when looking at the results from an expedition conducted at the Lena Delta region in September 2005 (see Figure 9 in Semiletov et al., 2013); however, the possible causes of this pattern were not addressed in that study. We suggest that such an increase in the slope of the relationship can be interpreted as a non-conservative decrease in DOM concentration along with the surface layer. This DOM removal in the surface (lower salinity) layer occurred despite the short residence time (of about 2 months) the Lena River plume waters in the Laptev Sea (Alling et al., 2010). Release/production of the components C5 and C6 was observed along the entire riverine-marine transition (see Figure 4, right panel). The autochthonous protein-like C6 is known to be released by microbial metabolism (Romera-Castillo et al., 2010; Fukuzaki et al., 2014) and its release in our sampling area can be related to the microbial community presented within the region. On the other hand, the humic-like C5 could have had its release associated with photoproduction, given that some humic-like components, such as alkyl, have been shown to be produced via that process (Helms et al., 2014). Although the components C5 and C6 presented indication of release/production along the riverine-marine transition, the contribution of those components to the total fluorescence signal was small (less than 20%). Thus, the overall DOM mixing curve mirrored the curves displayed by C1–C4 (accounting for more than 80% of the total FDOM signal), with a removal of DOM at low salinities and a conservative mixing behavior related to the saltier Laptev Sea shelf waters. Non-conservative mixing characterized by removal at low salinities seems to be a characteristic shared by other estuarine regions in the Baltic Sea (Kowalczyk et al., 2010; Asmala et al., 2014).

Given the strong stratification observed within the sampled area, we assume that exchanges between surface and underneath layer are limited (Kara et al., 2000b) compared to well-mixed conditions. As a result, the humic-like-dominated, highly photo-reactive DOM (Helms et al., 2014; Timko et al., 2015) is exposed longer to photochemical degradation (Fichot and Miller, 2010). This process is evidenced by the relationship between S_{Ratio} and salinity (Figure 5E), with high S_{Ratio} values (>0.95) observed in intermediate salinity (10–20). Furthermore, the influence of particulate matter and sediments in coastal and shelf environments has to be taken into account given their influence on DOM removal through the process of sorption and flocculation (Uher et al., 2001; Shank et al., 2005; Guo et al., 2007; Asmala et al., 2014). The flocculation process, in turn, can be increased either due to the presence of the salt in the



marine water (Asmala et al., 2014, and references therein) and to the exposition to high light intensities that, together with photochemical processes, can synergistically enhance the DOM removal from the dissolved phase (von Wachenfeldt et al., 2008; Porcal et al., 2013, 2015). A sharp decrease in POC concentrations at low salinity has been reported in the Lena delta region and was attributed to sinking of particles (Cauwet and Sidorov, 1996). We speculate that the main drivers on the apparent removal of highly humic content DOM observed within the surface layer are the photodegradation and flocculation, given the high susceptibility of those aromatic carbons to those processes (von Wachenfeldt et al., 2008; Porcal et al., 2013, 2015; Asmala et al., 2014; Helms et al., 2014). Those processes have also been indicated to modulate the non-conservative mixing behavior in other estuaries such as the Mississippi delta (Benner and Opsahl, 2001). Our findings from late summer 2013 corroborate the indication of DOM removal within the region as observed in late summer 2008 (Alling et al., 2010); however, with a more refined spatial coverage, we have demonstrated that the removal of DOM occurs mostly in the low salinity surface layer (Figure 6).

Considering that the impact of temperature increases to the Arctic and Siberian environments, an increase in permafrost thawing rates, changes in the freshwater budget, catchment vegetation and hydrology, and subsequent DOM discharge into the Arctic Ocean are expected (Peterson et al., 2002; McClelland et al., 2004; Frey and McClelland, 2009). As a consequence, changes in concentration and composition of DOM are expected, given the release of ancient DOM trapped in the permafrost layer due to its thaw (Aiken et al., 2014; O'Donnell et al., 2014), and given the variability of DOM composition in response to variations in river discharge (Walker

et al., 2013). Subsequently, with an enhanced input of DOM (especially CDOM) into the Arctic Ocean, changes in the radiant heating in the upper meters of the ocean as well as a possible increase in the sea-ice melt rates might be foreseen (Granskog et al., 2015). Furthermore, the characteristics of DOM have been shown to be a powerful proxy for tracing organic substances with permafrost origin (Aiken et al., 2014; O'Donnell et al., 2014; Dubinenkov et al., 2015a). Moreover, long-term studies concerning the quantification, composition and dynamics of DOM, from fresh to marine waters in the main rivers flowing into the Arctic Ocean, are needed to improve the understanding of DOM dynamics, its role in the carbon cycle pathways. Thus, a better comprehension of DOM composition and its fate, as presented in this study, can be used as baseline for further monitoring of the sources, biogeochemical implications and export of riverine DOM with regard to climate change effects in northern Siberian environments and Arctic Ocean.

SUMMARY

This study brings new insights on the composition, transformation and fate of DOM in the Lena Delta region. DOM composition evaluated through PARAFAC modeling showed dominance of strong humic-like signal over the entire sampled area. We have demonstrated that the dynamics between the Lena River outflow and Laptev Sea shelf waters is the main driver controlling the hydrographical conditions and, consequently, the DOM behavior within the region. Higher DOM concentrations (also with higher humic-like content) were associated to the low salinity waters of the Lena River that showed to be the main DOM source for the region. The concentration of

DOM, as well as its humic-like content and reactivity, decreased along the fresh water-marine gradient toward high salinity. Although being limited by sampling within a synoptic scale, we have identified different mixing behaviors of DOM coupled with the dynamics between the Lena River plume and the Laptev Sea shelf waters, which were expressed through the vertical structure of the water column: a sharper decrease in DOM concentration in relation to salinity is observed in waters above the pycnocline, under influence of the low salinity waters from the continental runoff. This indicates that different processes modulating the distribution, composition, and reactivity of DOM occur within the two layers and that there is evidence of removal of DOM in the surface mixed layer. Thus, we suggest photodegradation and flocculation as the main drivers on modulating the removal of highly humified DOM within the surface layer of the Lena Delta region.

ACKNOWLEDGMENTS

The authors acknowledge the Captain and the crew of the R/V “Dalnie Zelentsy” and the researchers E. Druzhkova and

K. Bobrov for their assistance during the field sampling. We are thankful to the logistics department of the Alfred Wegener Institute (AWI) particularly Waldemar Schneider for the support, and to Sonja Wiegmann for the work in the laboratory. This work was funded by the Helmholtz Impulse Fond (HGF Young Investigators Group Phytooptics), and by the Presidium of Russian Academy of Sciences program “Prospecting fundamental research in the interest of the Russian Arctic Zone development in 2014–2015” through the project “Biological resources of the Russian Arctic Seas: current state, influence of natural changes and anthropogenic impacts, scientific principles, and perspectives of use.” RG is funded by a Ph.D. fellowship from the Coordination for the Improvement of Higher Level Personnel (CAPES–Brazil) in collaboration with the German Academic Exchange Service (DAAD), and a visiting fellowship from the Helmholtz Graduate School for Polar and Marine Research (POLMAR–AWI). CS acknowledges funding from Danish Research Council for Independent Research (DFR 1323-00336). BH acknowledges grants from the German Science Foundation (DFG 4575) and the Helmholtz Climate Initiative REKLIM.

REFERENCES

- Aiken, G. R., Sepner, R. G. M., Striegl, R. G., Schuster, P. F., and Raymond, P. A. (2014). Influences of glacier melt and permafrost thaw on the age of dissolved organic carbon in the Yukon River basin. *Global Biogeochem. Cycles* 28, 525–537. doi: 10.1002/2013GB004764
- Alling, V., Sanchez-Garcia, L., Porcelli, D., Pugach, S., Vonk, J. E., van Dongen, B., et al. (2010). Nonconservative behavior of dissolved organic carbon across the Laptev and East Siberian seas. *Global Biogeochem. Cycles* 24, GB4033. doi: 10.1029/2010GB003834
- Amon, R. M. V., Rinehart, A. J., Duan, S., Louchouart, P., Prokushkin, A., Guggenberger, G., et al. (2012). Dissolved organic matter sources in large Arctic rivers. *Geochim. Cosmochim. Acta* 94, 217–237. doi: 10.1016/j.gca.2012.07.015
- Arrigo, K. R., and Brown, C. W. (1996). Impact of chromophoric dissolved organic matter on UV inhibition of primary productivity in the Sea. *Mar. Ecol. Prog. Ser.* 140, 207–216. doi: 10.3354/meps140207
- Asmala, E., Bowers, D. G., Autio, R., Kaartokallio, H., and Thomas, D. N. (2014). Qualitative changes of riverine dissolved organic matter at low salinities due to flocculation. *J. Geophys. Res. Biogeosci.* 119, 1919–1933. doi: 10.1002/2014JG002722
- Bauch, D., Dmitrenko, I. A., Wegner, C., Hölemann, J., Kirilov, S. A., Timokhov, L. A., et al. (2009). Exchange of Laptev Sea and Arctic Ocean halocline waters in response to atmospheric forcing. *J. Geophys. Res.* 114, C05008. doi: 10.1029/2008JC005062
- Benner, R., Benitez-Nelson, B., Kaiser, K., and Amon, R. M. W. (2004). Export of young terrigenous dissolved organic carbon from rivers to the Arctic Ocean. *Geophys. Res. Lett.* 31, L05305. doi: 10.1029/2003gl019251
- Benner, R., and Opsahl, S. (2001). Molecular indicators of the sources and transformations of dissolved organic matter in the Mississippi river plume. *Org. Geochem.* 32, 597–611. doi: 10.1016/S0146-6380(00)00197-2
- Boyd, T. J., and Osburn, C. L. (2004). Changes in CDOM fluorescence from allochthonous and autochthonous sources during tidal mixing and bacterial degradation in two coastal estuaries. *Mar. Chem.* 89, 189–210. doi: 10.1016/j.marchem.2004.02.012
- Cauwet, G., and Sidorov, I. S. (1996). The biogeochemistry of Lena river: organic carbon and nutrient distribution. *Mar. Chem.* 53, 211–227. doi: 10.1016/0304-4203(95)00090-9
- Chari, N. V. H. K., Keerthi, S., Sarma, N. S., Rao Pandi, S., Chiranjeevulu, G., Kiran, R., et al. (2013). Fluorescence and absorption characteristics of dissolved organic matter excreted by phytoplankton species of western Bay of Bengal under axenic laboratory condition. *J. Exp. Mar. Biol. Ecol.* 445, 148–155. doi: 10.1016/j.jembe.2013.03.015
- Coble, P. G. (2007). Marine optical biogeochemistry: the chemistry of ocean color. *Chem. Rev.* 107, 402–418. doi: 10.1021/cr050350+
- Dittmar, T., and Kattner, G. (2003). The biogeochemistry of the river and shelf ecosystem of the Arctic Ocean: a review. *Mar. Chem.* 83, 103–120. doi: 10.1016/S0304-4203(03)00105-1
- Dubinenkov, I., Flerus, R., Schmitt-Kopplin, P., Kattner, G., and Koch, B. P. (2015a). Origin-specific molecular signatures of dissolved organic matter in the Lena Delta. *Biogeochemistry* 123, 1–14. doi: 10.1007/s10533-014-0049-0
- Dubinenkov, I., Kraberg, A., Bussmann, I., Kattner, G., and Koch, B. P. (2015b). *Data from: Physical Oceanography and Dissolved Organic Matter in the Coastal Laptev SEA in 2013*. PANGAEA. Available online at <http://doi.pangaea.de/10.1594/PANGAEA.842221>
- Fedorova, I., Chetverova, A., Bolshiyarov, D., Makarov, A., Boike, J., Heim, B., et al. (2015). Lena Delta hydrology and geochemistry: long-term hydrological data and recent field observations. *Biogeosciences* 12, 345–363. doi: 10.5194/bg-12-345-2015
- Fichot, C. G., and Benner, R. (2012). The spectral slope coefficient of chromophoric dissolved organic matter ($S_{275-295}$) as a tracer of terrigenous dissolved organic carbon in river-influenced ocean margins. *Limnol. Oceanogr.* 57, 1453–1466. doi: 10.4319/lo.2012.57.5.1453
- Fichot, C. G., Kaiser, K., Hooker, S. B., Amon, R. M. W., Babin, M., Bélanger, S., et al. (2013). Pan-Arctic distributions of continental runoff in the Arctic Ocean. *Sci. Rep.* 3:1053. doi: 10.1038/srep01053
- Fichot, C. G., and Miller, W. L. (2010). An approach to quantify depth-resolved marine photochemical fluxes using remote sensing: application to carbon monoxide (CO) photoproduction. *Remote Sens. Environ.* 114, 1363–1377. doi: 10.1016/j.rse.2010.01.019
- Fofonova, V., Androsov, A., Danilov, S., Janout, M., Sofina, E., and Wiltshire, K. (2014). Semidiurnal tides in the Laptev Sea Shelf zone in the summer season. *Cont. Shelf Res.* 73, 119–132. doi: 10.1016/j.csr.2013.11.010
- Frey, K. E., and McClelland, J. W. (2009). Impacts of permafrost degradation on arctic river biogeochemistry. *Hydro. Process.* 23, 169–182. doi: 10.1002/hyp.7196
- Fukuzaki, K., Imai, I., Fukushima, K., Ishii, K.-I., Sawayama, S., and Yoshioka, T. (2014). Fluorescent characteristics of dissolved organic matter produced by bloom-forming coastal phytoplankton. *J. Plankton Res.* 36, 685–694. doi: 10.1093/plankt/fbu015
- Gonçalves-Araujo, R., de Souza, M. S., Tavano, V. M., and Garcia, C. A. E. (2015b). Influence of oceanographic features on spatial and interannual variability of

- phytoplankton in the Bransfield Strait, Antarctica. *J. Mar. Syst.* 142, 1–15. doi: 10.1016/j.jmarsys.2014.09.007
- Gonçalves-Araujo, R., Stedmon, C. A., Heim, B., Dubinenkov, I., Kraberg, A., Moiseev, D., et al. (2015a). *Data from: Dissolved Organic Matter in the Lena River Delta Region, Siberia, Russia*. PANGAEA. Available online at: <http://doi.pangaea.de/10.1594/PANGAEA.844928>
- Granskog, M., Pavlov, A. K., Sagan, S., Kowalczyk, P., Raczkowska, A., and Stedmon, C. A. (2015). Effect of sea-ice melt on inherent optical properties and vertical distribution of solar radiant heating in Arctic surface waters. *J. Geophys. Res. Oceans* 120, 7028–7039. doi: 10.1002/2015jc011087
- Guéguen, C., Itoh, M., Kikuchi, T., Eert, J., and Williams, W. J. (2015). Variability in dissolved organic matter optical properties in surface waters in the Amerasian Basin. *Front. Mar. Sci.* 2:78. doi: 10.3389/fmars.2015.00078
- Guo, W., Stedmon, C. A., Han, Y., Wu, F., Yu, X., and Hu, M. (2007). The conservative and non-conservative behavior of chromophoric dissolved organic matter in Chinese estuarine waters. *Mar. Chem.* 107, 357–366. doi: 10.1016/j.marchem.2007.03.006
- Heim, B., Abramova, E., Doerffer, R., Günther, F., Hölemann, J., Kraberg, A., et al. (2014). Ocean colour remote sensing in the southern Laptev Sea: evaluation and applications. *Biogeosciences* 11, 4191–4210. doi: 10.5194/bg-11-4191-2014
- Helms, J. R., Mao, J., Stubbins, A., Schmidt-Rohr, K., Spencer, R. G. M., Hernes, P. J., et al. (2014). Loss of optical and molecular indicators of terrigenous dissolved organic matter during long-term photobleaching. *Aquat. Sci.* 76, 353–373. doi: 10.1007/s00027-014-0340-0
- Helms, J. R., Stubbins, A., Ritchie, J. D., Minor, E. C., Kieber, D. J., and Mopper, K. (2008). Absorption spectral slopes and slope ratios as indicators of molecular weight, source, and photobleaching of chromophoric dissolved organic matter. *Limnol. Oceanogr.* 53, 955–969. doi: 10.4319/lo.2008.53.3.0955
- Huguet, A., Vacher, L., Relexans, S., Saubusse, S., Froidefond, J. M., and Parlanti, E. (2009). Properties of fluorescent dissolved organic matter in the Gironde Estuary. *Org. Geochem.* 40, 706–719. doi: 10.1016/j.orggeochem.2009.03.002
- Jørgensen, L., Stedmon, C. A., Kragh, T., Markager, S., Middelboe, M., and Søndergaard, M. (2011). Global trends in the fluorescence characteristics and distribution of marine dissolved organic matter. *Mar. Chem.* 126, 139–148. doi: 10.1016/j.marchem.2011.05.002
- Kara, A. B., Rochford, P. A., and Hurlburt, H. E. (2000a). An optimal definition for ocean mixed layer depth. *J. Geophys. Res.* 105, 16803–16821. doi: 10.1029/2000JC900072
- Kara, A. B., Rochford, P. A., and Hurlburt, H. E. (2000b). Mixed layer depth variability and barrier layer formation over the North Pacific Ocean. *J. Geophys. Res.* 105, 16783–16801. doi: 10.1029/2000JC900071
- Kattner, G., Lobbes, J. M., Fitznar, H. P., Engbrodt, R., Nöthig, E.-M., and Lara, R. J. (1999). Tracing dissolved organic substances and nutrients from the Lena River through Laptev Sea (Arctic). *Mar. Chem.* 65, 25–39. doi: 10.1016/S0304-4203(99)00008-0
- Kowalczyk, P. M., Durako, J., Young, H., Kahn, A. E., Cooper, W. J., Gonsior, M., et al. (2009). Characterization of dissolved organic matter fluorescence in the South Atlantic Bight with use of PARAFAC model: interannual variability. *Mar. Chem.* 113, 182–196. doi: 10.1016/j.marchem.2009.01.015
- Kowalczyk, P. M., Zablocka, S., Sagan, and Kuliński, K. (2010). Fluorescence measured *in situ* as a proxy of CDOM absorption and DOC concentration in the Baltic Sea. *Oceanologia* 52, 431–471. doi: 10.5697/oc.52-3.431
- Kowalczyk, P., Tilstone, G. H., Zablocka, M., Röttgers, R., and Thomas, R. (2013). Composition of dissolved organic matter along an Atlantic Meridional transect from fluorescence spectroscopy and parallel factor analysis. *Mar. Chem.* 157, 170–184. doi: 10.1016/j.marchem.2013.10.004
- Levitus, S. (1982). *Climatological Atlas of the World Ocean*. NOAA Professional Paper 13. Washington, DC: U.S. Govt. Print. Off.
- Lyon, S. W., and Destouni, G. (2010). Changes in catchment-scale recession flow properties in response to permafrost thawing in the Yukon River basin. *Int. J. Climatol.* 30, 2138–2145. doi: 10.1002/joc.1993
- McClelland, J. W., Holmes, R. M., Peterson, B. J., and Stieglitz, M. (2004). Increasing river discharge in the Eurasian Arctic: consideration of dams, permafrost thaw, and fires as potential agents of change. *J. Geophys. Res.* 109, D18102. doi: 10.1029/2004JD004583
- McKnight, D. M., Boyer, E. W., Westerhoff, P. K., Doran, P. T., Kulbe, T., and Andersen, D. T. (2001). Spectrofluorometric characterization of dissolved organic matter for indication of precursor organic material and aromaticity. *Limnol. Oceanogr.* 46, 38–48. doi: 10.4319/lo.2001.46.1.0038
- Mopper, K., and Kieber, D. J. (2002). “Photochemistry and the cycling of carbon, sulfur, nitrogen and phosphorus” in *Biogeochemistry of Marine Dissolved Organic Matter*, eds C. Carlson and D. Hansell (San Diego, CA: Academic Press), 455–508.
- Murphy, K. R., Stedmon, C. A., Graeber, D., and Bro, R. (2013). Fluorescence spectroscopy and multi-way techniques. *PARAFAC. Anal. Methods* 5, 6557–6566. doi: 10.1039/c3ay41160e
- Murphy, K. R., Stedmon, C. A., Waite, T. D., and Ruiz, G. M. (2008). Distinguishing between terrestrial and autochthonous organic matter sources in marine environments using fluorescence spectroscopy. *Mar. Chem.* 108, 40–58. doi: 10.1016/j.marchem.2007.10.003
- Murphy, K. R., Stedmon, C. A., Wenig, P., and Bro, R. (2014). OpenFluor – an online spectral library for auto-fluorescence by organic compounds in the environment. *Anal. Methods* 6, 658–661. doi: 10.1039/C3AY41935E
- Nelson, N. B., and Siegel, D. A. (2013). The global distribution and dynamics of chromophoric dissolved organic matter. *Annu. Rev. Mar. Sci.* 5, 447–476. doi: 10.1146/annurev-marine-120710-100751
- O'Donnell, J. O., Aiken, G. R., Walvoord, M. A., Raymond, P. A., Butler, K. D., Dornblaser, M. M., et al. (2014). Using dissolved organic matter age and composition to detect permafrost thaw in boreal watersheds of interior Alaska. *J. Geophys. Res. Biogeosci.* 119, 2155–2170. doi: 10.1002/2014JG002695
- Opsahl, S., and Benner, R. (1998). Photochemical reactivity of dissolved lignin in river and ocean waters. *Limnol. Oceanogr.* 43, 1297–1304. doi: 10.4319/lo.1998.43.6.1297
- Opsahl, S., Benner, R., and Amon, R. M. W. (1999). Major flux of terrigenous organic matter through the Arctic Ocean. *Limnol. Oceanogr.* 44, 2017–2023. doi: 10.4319/lo.1999.44.8.2017
- Para, J., Coble, P. G., Charrière, B., Tedetti, M., Fontana, C., and Sempéré, R. (2010). Fluorescence and absorption properties of chromophoric dissolved organic matter (CDOM) in coastal surface waters of the northwestern Mediterranean Sea, influence of the Rhône River. *Biogeosciences* 7, 4083–4103. doi: 10.5194/bg-7-4083-2010
- Peterson, B. J., Holmes, R. M., McClelland, J. W., Vörösmarty, C. J., Lammers, R. B., Shiklomanov, I. A., et al. (2002). Increasing river discharge to the Arctic Ocean. *Science* 298, 2171–2173. doi: 10.1126/science.1077445
- Porcal, P., Dillon, P. J., and Molot, L. A. (2013). Photochemical production and decomposition of particulate organic carbon in a freshwater stream. *Aquat. Sci.* 73, 469–482. doi: 10.1007/s00027-013-0293-8
- Porcal, P., Dillon, P. J., and Molot, L. A. (2015). Temperature dependence of photodegradation of dissolved organic matter to dissolved inorganic carbon and particulate organic carbon. *PLoS ONE* 10:e0128884. doi: 10.1371/journal.pone.0128884
- Raymond, P. A., McClelland, J. W., Holmes, R. M., Zhulidov, A. V., Mull, K., Peterson, B. J., et al. (2007). Flux and age of dissolved organic carbon exported to the Arctic Ocean: a carbon isotopic study of the five largest arctic rivers. *Global Biogeochem. Cycles* 21, GB4011. doi: 10.1029/2007GB002934
- Romera-Castillo, C., Sarmiento, H., Álvarez-Salgado, X. A., Gasol, J. M., and Marrasé, C. (2010). Production of chromophoric dissolved organic matter by marine phytoplankton. *Limnol. Oceanogr.* 55, 446–454. doi: 10.4319/lo.2010.55.1.0446
- Sánchez-García, L., Vonk, J. E., Charkin, A., Kosmach, D., Dudarev, O., Semiletov, I., et al. (2014). Characterisation of three regimes of collapsing Arctic ice complex deposits on the SE Laptev Sea coast using biomarkers and dual carbon isotopes. *Permafrost Periglacial Process.* 25, 172–183. doi: 10.1002/ppp.1815
- Schlitzer, R. (2015). *Ocean Data View*. Available online at: <http://odv.awi.de>
- Schuur, E. A. G., Bockheim, J., Canadell, J. G., Euskirchen, E., Field, C. B., Goryachkin, S. V., et al. (2008). Vulnerability of permafrost carbon to climate change: implications for the global carbon cycle. *Bioscience* 58, 701–714. doi: 10.1641/B580807
- Semiletov, I. P., Pipko, I. I., Shakhova, N. E., Dudarev, O. V., Pugach, S. P., Charkin, A. N., et al. (2011). Carbon transport by the Lena River from its headwaters to the Arctic Ocean, with emphasis on fluvial input of terrestrial particulate organic carbon vs. carbon transport by coastal erosion. *Biogeosciences* 8, 2407–2426. doi: 10.5194/bg-8-2407-2011

- Semiletov, I. P., Shakhova, N. E., Pugach, S. P., Charkin, A. N., Dudarev, O. V., Kosmach, D. A., et al. (2013). Space-time dynamics of carbon and environmental parameters related to carbon dioxide emissions in the Buor-Khaya Bay and adjacent part of the Laptev Sea. *Biogeosciences* 10, 5977–5996. doi: 10.5194/bg-10-5977-2013
- Semiletov, I. P., Shakhova, N. E., Sergienko, V. I., Pipko, I. I., and Dudarev, O. V. (2012). On carbon transport and fate in the East Siberian Arctic land-shelf-atmosphere system. *Environ. Res. Lett.* 7, 015201. doi: 10.1088/1748-9326/7/1/015201
- Senesi, N., Miano, N. T., Provenzano, M. R., and Brunetti, G. (1991). Characterization, differentiation and classification of humic substances by fluorescence spectroscopy. *Soil Sci.* 152, 259–271. doi: 10.1097/00010694-199110000-00004
- Shank, G. C., Zepp, R. G., Whitehead, R. F., and Moran, M. A. (2005). Variations in the spectral properties of freshwater and estuarine CDOM caused by partitioning onto river and estuarine sediments. *Estuar. Coast. Shelf Sci.* 65, 289–301. doi: 10.1016/j.ecss.2005.06.009
- Siegel, D. A., Maritorena, S., Nelson, N. B., Behrenfeld, M. J., and McClain, R. (2005). Colored dissolved organic matter and its influence on the satellite-based characterization of the ocean biosphere. *Geophys. Res. Lett.* 32, L20605. doi: 10.1029/2005gl024310
- Siegel, D. A., Maritorena, S., Nelson, N. B., Hansell, D. A., and Lorenzi-Kayser, M. (2002). Global distribution and dynamics of colored dissolved and detrital organic materials. *J. Geophys. Res.* 107, 3228. doi: 10.1029/2001jc000965
- Singh, S., D'Sa, E. J., and Sweson, E. M. (2010). Chromophoric dissolved organic matter (CDOM) variability in Barataria Basin using excitation-emission matrix (EEM) fluorescence and parallel factor analysis (PARAFAC). *Sci. Total Environ.* 408, 3211–3222. doi: 10.1016/j.scitotenv.2010.03.044
- Spencer, R. G. M., Aiken, G. R., Butler, K. D., Dornblaser, M. M., Striegl, R. G., and Hernes, P. J. (2009). Utilizing chromophoric dissolved organic matter measurements to derive export and reactivity of dissolved organic carbon exported to the Arctic Ocean: a case study of the Yukon River, Alaska. *Geophys. Res. Lett.* 36, L06401. doi: 10.1029/2008gl036831
- Stedmon, C. A., Amon, R. M. W., Rinehart, A. J., and Walker, S. A. (2011). The supply and characteristics of colored dissolved organic matter (CDOM) in the Arctic Ocean: par Arctic trends and differences. *Mar. Chem.* 124, 108–118. doi: 10.1016/j.marchem.2010.12.007
- Stedmon, C. A., and Bro, R. (2008). Characterizing dissolved organic matter fluorescence with parallel factor analysis: a tutorial. *Limnol. Oceanogr.* 6, 572–579. doi: 10.4319/lom.2008.6.572
- Stedmon, C. A., and Markager, S. (2003). Behaviour of the optical properties of coloured dissolved organic matter under conservative mixing. *Est. Cost. Shelf Sci.* 57, 1–7. doi: 10.1016/s0272-7714(03)00003-9
- Stedmon, C. A., and Markager, S. (2005). Resolving the variability in dissolved organic matter fluorescence in a temperate estuary and its catchment using PARAFAC analysis. *Limnol. Oceanogr.* 50, 686–697. doi: 10.4319/lo.2005.50.2.0686
- Stevenson, F. J. (1982). *Humus Chemistry*. New York, NY: Genesis, Composition, Reactions, Wiley-Interscience.
- Stubbins, A., Lapiere, J.-F., Berggren, M., Prairie, Y. T., Dittmar, T., and del Giorgio, P. A. (2014). What's in an EEM? Molecular signatures associated with dissolved organic fluorescence in boreal Canada. *Environ. Sci. Technol.* 48, 10598–10606. doi: 10.1021/es502086e
- Stubbins, A., Uher, G., Law, C. S., Mopper, K., Robinson, C., and Upstill-Goddard, R. C. (2006). Open-ocean carbon monoxide photoproduction. *Deep Sea Res. II* 53, 1695–1705. doi: 10.1016/j.dsr2.2006.05.011
- Timko, S. A., Maydanov, A., Pittelli, S. L., Conte, M. H., Cooper, W. J., Koch, B. P., et al. (2015). Depth-dependent photodegradation of marine dissolved organic matter. *Front. Mar. Sci.* 2:66. doi: 10.3389/fmars.2015.00066
- Uher, G., Hughes, C., Henry, G., and Upstill-Goddard, R. C. (2001). Non-conservative mixing behavior of colored dissolved organic matter in a humic-rich, turbid estuary. *Geophys. Res. Lett.* 28, 3309–3312. doi: 10.1029/2000GL012509
- von Wachenfeldt, E., Sobek, S., Batsviken, D., and Tranvik, L. J. (2008). Linking allochthonous dissolved organic matter and boreal lake sediment carbon sequestration: the role of light-mediated flocculation. *Limnol. Oceanogr.* 53, 2416–2426. doi: 10.4319/lo.2008.53.6.2416
- Vonk, J. E., Sánchez-García, L., van Dongen, B. E., Alling, V., Kosmach, D., Charkin, A., et al. (2012). Activation of old carbon by erosion of coastal and subsea permafrost in Arctic Siberia. *Nature* 489, 137–140. doi: 10.1038/nature11392
- Vonk, J. E., Semiletov, I., Dudarev, O., Eglinton, T., Andersson, A., Shakhova, N., et al. (2014). Preferential burial of permafrost-derived organic carbon in Siberian-Arctic shelf waters. *J. Geophys. Res.* 119, 8410–8421. doi: 10.1002/2014JC010261
- Walker, S. A., Amon, R. M. W., and Stedmon, C. A. (2013). Variations in high-latitude riverine fluorescent dissolved organic matter: a comparison of large Arctic rivers. *J. Geophys. Res. Biogeosci.* 118, 1689–1702. doi: 10.1002/2013jg002320
- Walker, S. A., Amon, R. M. W., Stedmon, C., Duan, S., and Louchouart, P. (2009). The use of PARAFAC modeling to trace terrestrial dissolved organic matter and fingerprint water masses in coastal Canadian Arctic surface waters. *J. Geophys. Res.* 114, G00F06. doi: 10.1029/2009jg000990
- Wegner, C., Bauch, D., Hölemann, J. A., Janout, M. A., Heim, B., Novikhin, A., et al. (2013). Interannual variability of surface and bottom sediment transport on Laptev Sea shelf during summer. *Biogeosciences* 10, 1117–1129. doi: 10.5194/bg-10-1117-2013
- Weishaar, J. L., Aiken, G. R., Bergamaschi, B. A., Fram, M. S., Fujii, R., and Mopper, K. (2003). Evaluation of specific ultraviolet absorbance as an indicator of the chemical composition and reactivity of dissolved organic carbon. *Environ. Sci. Technol.* 37, 4702–4708. doi: 10.1021/es030360x
- Yamashita, Y., Boyer, J. N., and Jaffé, R. (2013). Evaluating the distribution of terrestrial dissolved organic matter in a complex coastal ecosystem using fluorescence spectroscopy. *Cont. Shelf Res.* 66, 136–144. doi: 10.1016/j.csr.2013.06.010
- Yamashita, Y., Cory, R. M., Nishioka, J., Kuma, K., Tanoue, E., and Jaffé, R. (2010). Fluorescence characteristics of dissolved organic matter in the deep waters of the Okhotsk Sea and the northwestern North Pacific Ocean. *Deep Sea Res. II* 57, 1478–1485. doi: 10.1016/j.dsr2.2010.02.016
- Yamashita, Y., Fichot, C. G., Shen, Y., Jaffé, R., and Benner, R. (2015). Linkages among fluorescent dissolved organic matter, dissolved amino acids and lignin-derived phenols in a river-influenced ocean margin. *Front. Mar. Sci.* 2:92. doi: 10.3389/fmars.2015.00092
- Yamashita, Y., and Tanoue, E. (2003). Chemical characterization of protein-like fluorophores in DOM in relation to aromatic amino acids. *Mar. Chem.* 82, 255–271. doi: 10.1016/S0304-4203(03)00073-2
- Yamashita, Y., and Tanoue, E. (2004). Chemical characteristics of amino acid-containing dissolved organic matter in seawater. *Org. Chem.* 35, 679–692. doi: 10.1016/j.orgchem.2004.02.007
- Yang, D., Kane, D. L., Hinzman, L. D., Zhang, X., Zhang, T., and Ye, H. (2002). Siberia Lena River hydrologic regime and recent change. *J. Geophys. Res.* 107, 4694. doi: 10.1029/2002JD002542
- Zhang, Y., van Dijk, M. A., Liu, M., Zhu, G., and Qin, B. (2009). The contribution of phytoplankton degradation to chromophoric dissolved organic matter (CDOM) in eutrophic shallow lakes: field and experimental evidence. *Water Res.* 43, 4685–4697. doi: 10.1016/j.watres.2009.07.024
- Zsolnay, Á., Baigar, E., Jimenez, E., Steinweg, B., and Saccomandi, F. (1999). Differentiating with fluorescence spectroscopy the source of dissolved organic matter in soils subjected to drying. *Chemosphere* 38, 45–50. doi: 10.1016/S0045-6535(98)00166-0
- Zsolnay, Á. (2003). Dissolved organic matter: artefacts, definitions and functions. *Geoderma* 113, 187–209. doi: 10.1016/S0016-7061(02)00361-0

Conflict of Interest Statement: The authors declare that the research was conducted in the absence of any commercial or financial relationships that could be construed as a potential conflict of interest.

Copyright © 2015 Gonçalves-Araujo, Stedmon, Heim, Dubinenkov, Kraberg, Moiseev and Bracher. This is an open-access article distributed under the terms of the Creative Commons Attribution License (CC BY). The use, distribution or reproduction in other forums is permitted, provided the original author(s) or licensor are credited and that the original publication in this journal is cited, in accordance with accepted academic practice. No use, distribution or reproduction is permitted which does not comply with these terms.

SCIENTIFIC REPORTS

OPEN

Using fluorescent dissolved organic matter to trace and distinguish the origin of Arctic surface waters

Rafael Gonçalves-Araujo^{1,2,3}, Mats A. Granskog⁴, Astrid Bracher^{1,5}, Kumiko Azetsu-Scott⁶, Paul A. Dodd⁴ & Colin A. Stedmon³

Received: 14 June 2016
Accepted: 06 September 2016
Published: 26 September 2016

Climate change affects the Arctic with regards to permafrost thaw, sea-ice melt, alterations to the freshwater budget and increased export of terrestrial material to the Arctic Ocean. The Fram and Davis Straits represent the major gateways connecting the Arctic and Atlantic. Oceanographic surveys were performed in the Fram and Davis Straits, and on the east Greenland Shelf (EGS), in late summer 2012/2013. Meteoric (f_{mw}), sea-ice melt, Atlantic and Pacific water fractions were determined and the fluorescence properties of dissolved organic matter (FDOM) were characterized. In Fram Strait and EGS, a robust correlation between visible wavelength fluorescence and f_{mw} was apparent, suggesting it as a reliable tracer of polar waters. However, a pattern was observed which linked the organic matter characteristics to the origin of polar waters. At depth in Davis Strait, visible wavelength FDOM was correlated to apparent oxygen utilization (AOU) and traced deep-water DOM turnover. In surface waters FDOM characteristics could distinguish between surface waters from eastern (Atlantic + modified polar waters) and western (Canada-basin polar waters) Arctic sectors. The findings highlight the potential of designing *in situ* multi-channel DOM fluorometers to trace the freshwater origins and decipher water mass mixing dynamics in the region without laborious samples analyses.

Arctic rivers supply high loads of freshwater and dissolved organic matter (DOM) to the Arctic Ocean^{1–3}. A major fraction of this DOM, which is mobilized from high latitude carbon-rich soils and peatlands^{4,5}, is transported across shelf seas⁶ and is widely distributed across the surface waters of the Arctic Ocean. This makes the Arctic Ocean globally unique being highly impacted by both freshwater and terrestrial organic carbon compared to other ocean basins⁵. With the expected permafrost thaw due to the effects of global warming over the Arctic⁷, changes in freshwater export, production of DOM in river catchments and riverine transport of organic material into the shelf seas are foreseen^{8,9}.

The strong relationship between riverine DOM and freshwater in the Arctic Ocean presents the opportunity of using DOM measurements to isolate and trace the contribution of Arctic riverine freshwater to the Arctic surface waters¹⁰. Inflow from the Pacific Ocean through the Bering Strait is also an important component of the Arctic Ocean freshwater budget due to its lower salinity^{11,12}. In addition to regional input from North American and East Siberian rivers the high productivity of the Chukchi shelf results in these waters also having a high DOM signal although less terrestrial in nature¹. Initial studies have indicated that the optical properties of DOM in surface and halocline (polar) waters of the Eurasian and Canada basin differ¹ and suggest that there may be potential to utilize this to trace the contribution of these two freshwater sources to water exiting the Arctic Ocean into the North Atlantic through the two major gateways; Fram Strait and the Canadian Arctic Archipelago (CAA)/Davis Strait. It is important to understand the fate and any changes in the export of Arctic freshwater as two major sites of meridional overturning circulation bottom water formation lie directly in recipient waters; the Nordic Seas and the Labrador Sea¹³.

¹Alfred Wegener Institute Helmholtz Centre for Polar and Marine Research (AWI), Climate Sciences Division, Physical Oceanography of Polar Seas, Bussestraße 24, 27570 Bremerhaven, Germany. ²University of Bremen, Faculty of Biology and Chemistry (FB2) - PO Box 330440, 28334 Bremen, Germany. ³Technical University of Denmark, National Institute for Aquatic Resources, Section for Marine Ecology and Oceanography, Kavalergården 6, 2920 Charlottenlund, Denmark. ⁴Norwegian Polar Institute, Fram Centre, Postbox 6606 Langnes, 9296 Tromsø, Norway. ⁵University of Bremen, Institute of Environmental Physics, PO Box 330440, 28334 Bremen, Germany. ⁶Fisheries and Ocean, Canada, Bedford Institute of Oceanography, PO Box 1006, Dartmouth, Nova Scotia, BY2 4A2 Canada. Correspondence and requests for materials should be addressed to R.G.-A. (email: rafael.goncalves.araujo@awi.de) or C.A.S. (email: cost@aqu.dtu.dk)

The Fram Strait is characterized by two main currents: to the west, the Arctic outflow carrying the cold polar waters, and to the east the Atlantic inflow^{12,14}. Additionally, it has been demonstrated that there is recirculation of Atlantic water within the region¹⁵. During summer, the polar waters are characterized by a shallow surface layer influenced by high fractions of seasonal sea-ice melt forming a low salinity surface layer over the underlying polar waters with brine excess and high fractions of meteoric water (a combination of river water, precipitation and glacial melt)^{16,17}. After passing through the Fram Strait, the polar waters are transported along the east Greenland shelf by the East Greenland Current (EGC). On the eastern side of Fram Strait, the Atlantic inflow is primarily characterized by warm and saline Atlantic water with little or no influence from meteoric waters^{12,14,17}.

The Davis Strait, at approximately 67°N between Canada and Greenland, represents a transition from Arctic to North Atlantic environments. In the western Davis Strait, the Baffin Island Current (BIC) transports polar waters southwards, towards the Labrador Sea^{8,19}. These waters have similar characteristics to their equivalent in Fram Strait: relatively low salinity, near freezing temperatures, high meteoric water fractions and brine excess^{20,21}. The surface waters of eastern Davis Strait are mainly characterized by the presence of the West Greenland Shelf Water (WGSW) and the West Greenland Irminger Water (WGIW). The WGSW originates from the EGC after it turns northward at the southern tip of Greenland, and continues as the West Greenland Current (WGC)^{18,19}. The WGIW is of Atlantic origin (high temperature and salinity) and is transported northward along the western Greenland slope by the West Greenland Slope Current (WGSC), parallel to WGC^{18,19}.

A fraction of DOM is colored (CDOM) absorbing light (especially in the ultraviolet – UV – range), and in the Arctic this influences light and heat penetration in surface waters^{22,23}. When present in high concentrations CDOM imparts a brown color to water easily visible by eye or in satellite ocean color measurements near the mouths of Arctic rivers⁶. Despite considerable dilution the color signal from Arctic riverine CDOM can be easily traced across the Arctic. In addition the spectral properties of the absorption spectrum can be used to differentiate between contrasting CDOM sources such as marine productivity and rivers¹. A fraction of CDOM also emits a fluorescence signal (hereafter FDOM) which provides not only quantitative information on DOM, but also qualitative information regarding the composition and origin²⁴. Fluorescence measurements are well suited for *in situ* sensors and studies have shown that visible wavelength DOM fluorescence (VIS-FDOM) can be linked to Arctic upper halocline waters^{3,25} and used to map DOM distribution at higher resolution. Detailed measurement and characterization of DOM fluorescence properties offers the potential to optimize the design and use of these *in situ* fluorometers, which typically measure at single excitation and emission wavelength pairs. Laboratory-based spectroscopic analysis of DOM results in an excitation-emission-matrix (EEM), which maps the UV-visible fluorescence properties. These EEMs represent a combined quantitative and qualitative measure of different signals present in FDOM, which can subsequently be separated into independent underlying DOM components using Parallel Factor Analysis (PARAFAC). Some of those components have been shown to match with fluorescence of specific organic compounds²⁶ and are related to some DOM molecular species^{27,28}. PARAFAC characterization of FDOM has been recently used to assess DOM variability in the Arctic Ocean^{29–31}, and here we seek to build on this and link the distribution of different FDOM components to bulk water fractions and mixing. Although having a less sensitive signal in comparison to FDOM^{24,32}, CDOM has shown to be a robust proxy for halocline (polar) waters^{10,33}. Based on that this study aims primarily to assess the potential of FDOM, especially VIS-FDOM, as a tracer of polar waters along two important export pathways of Arctic waters: Fram Strait (as well as the eastern Greenland shelf) and Davis Strait. Secondly the biogeochemical dynamics of FDOM was evaluated in Davis Strait. The results here can be further applied on the development of *in situ* profilers, as well as autonomous platforms (such as ROVs and AUVs), focusing on monitoring the freshwater fluxes exiting the Arctic Ocean. Moreover, it would increase the sampling resolution and accelerate the data processing, given that waters samples (especially $\delta^{18}\text{O}$, alkalinity and nutrient analysis) would be taken only for calibration purposes and lab work time would be reduced.

Results

Water mass distribution. Six water masses were identified in Fram Strait, on east Greenland shelf and Iceland Sea, based on published thermohaline characteristics^{22,34} (Table S1), as shown on the T-S diagram (Fig. 1b): Atlantic Water, Polar Water and Arctic Surface Water (ASW) in the surface layer (<~200 m); and upper and lower Arctic Intermediate Water (uAIW and lAIW, respectively) and Norwegian Sea Deep Water (NSDW) in the deep layers. In Davis Strait a similar pattern for the temperature versus salinity relation was observed, however with lower salinity values (Fig. 1c). For Davis Strait the following waters masses were observed: West Greenland Shelf Water (WGSW), West Greenland Irminger Water (WGIW), Polar Water, Arctic Surface Water (ASW), Transitional Water (TrW) at depth >300 m and Baffin Bay Deep Water (BBDW) at depth >900 m (adapted from Tang *et al.*¹⁸, Azetsu-Scott *et al.*²¹, Curry *et al.*¹⁹). In cruises east of Greenland temperature ranged from –1.77 °C to 7.92 °C with the highest values associated with Atlantic Water in eastern Fram Strait (Figs 1b, 2a and 3a). In Davis Strait the highest temperatures (>3 °C) were associated with WGSW and WGIW (in eastern Davis Strait) whereas the lowest values (down to –1.63 °C) were found within the Polar Water in the western Davis Strait (Figs 1c and 4a). Salinity in Fram Strait and east Greenland shelf varied typically between 28 and 35 with highest salinity associated with Atlantic Water and the deeper waters (>~500 m; lAIW and NSDW), while the lowest values were observed in surface waters in central Fram Strait and inner Greenland shelf (Figs 1b, 2b and 3b). In Davis Strait, salinity ranged from 31.40 to 34.87, with highest salinity in warm subsurface waters of WGIW and TrW (Figs 1c and 4b). BBDW occupied the deepest parts of the Davis Strait section (>750 m) and had lower temperatures than the layer above it, characterized by TrW. The distribution of apparent oxygen utilization (AOU) in Davis Strait showed a clear pattern with lowest values (<60 $\mu\text{mol kg}^{-1}$) in western Greenland and surface waters, whereas these values increase toward the bottom layer reaching up to 216 $\mu\text{mol kg}^{-1}$ within BBDW (Fig. 4i). Although we have sampled for temperature and salinity over the entire water column, in Fram Strait we hereafter focus our results on the surface layer (300 m).

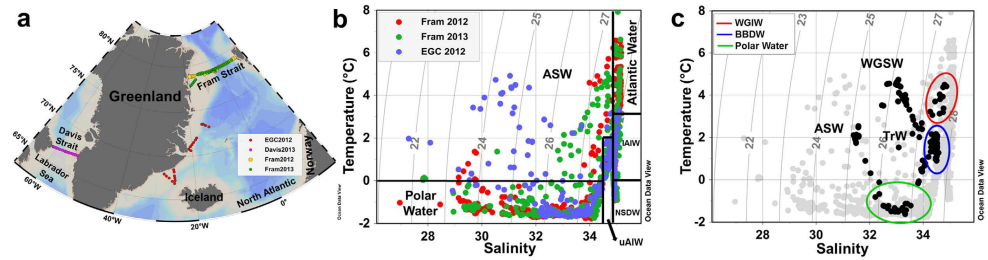


Figure 1. Study area and water masses. (a) Map of the study area and sampling stations in 2012 and 2013. (b) T-S diagram for all the oceanographic stations (except Davis 2013) considered for this study with the identified water masses^{22,34} (Table S1): Atlantic Water, Polar Water, Arctic Surface Water (ASW), upper Arctic Intermediate Water (uAIW), lower Arctic Intermediate Water (lAIW) and Norwegian Sea Deep Water (NSDW). (c) T-S diagram showing the eastern Greenland cruises (gray) and Davis 2013 (black) with the identified water masses for the latter region (adapted from *Tang et al.*¹⁸, *Azetsu-Scott et al.*²¹, *Curry et al.*¹⁹): West Greenland Shelf Water (WGSW), West Greenland Irminger Water (WGIW), Polar Water, Arctic Surface Water (ASW), Baffin Bay Deep Water (BBDW) and Transitional Water (TrW). Isopycnals [potential density (σ , kg m^{-3})] are indicated as gray lines in (b) and (c). Produced with Ocean Data View⁶⁰.

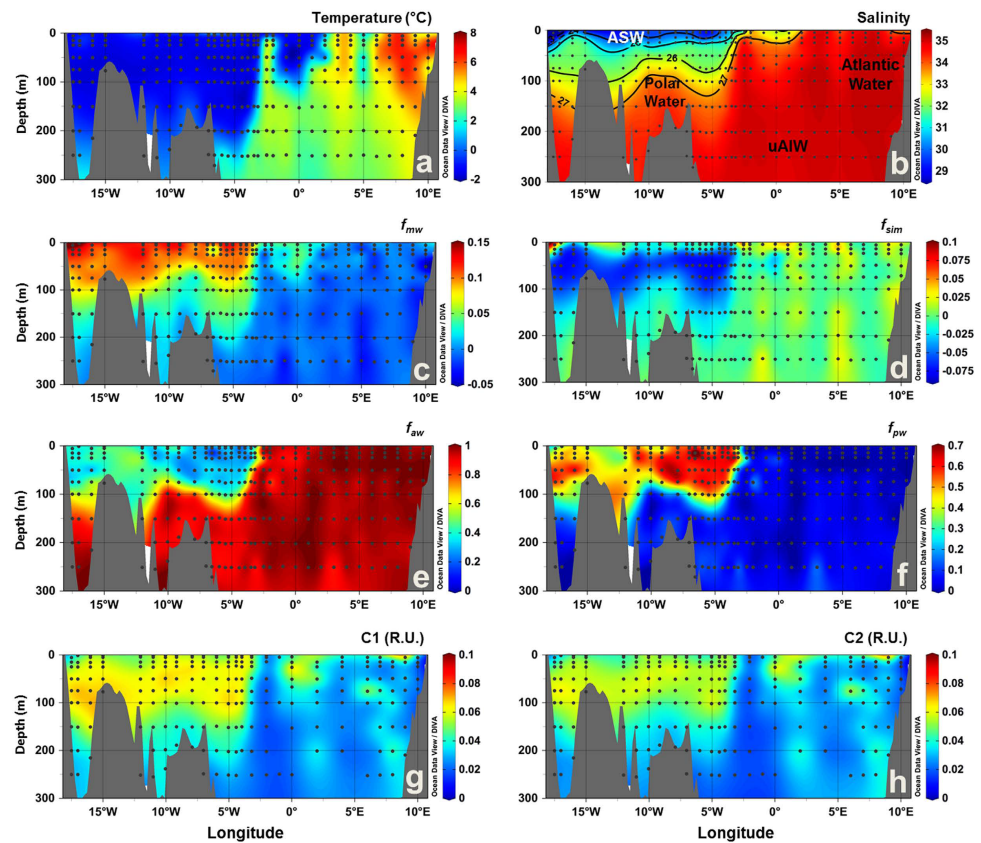


Figure 2. Vertical sections across the surface layer of Fram Strait in September 2012. (a) temperature ($^{\circ}\text{C}$), (b) salinity, fractions of (c) meteoric water (f_{mw}), (d) sea-ice melt (f_{sim}), (e) Atlantic water (f_{aw}), and (f) Pacific water (f_{pw}), (g) C1 (R.U.) and (h) C2 (R.U.). In (b) black lines indicate the potential density (σ , kg m^{-3}) and the abbreviations indicate the position of the water masses defined based on T-S diagrams (Fig. 1). Produced with Ocean Data View⁶⁰.

Dissolved organic matter fluorescence characterization. Three fluorescent components (C1–C3) were identified during the different PARAFAC runs. C1 and C2 had broad emission and excitation spectra, with emission maxima at visible wavelengths, whereas C3 had an emission maximum at ultraviolet-A wavelengths

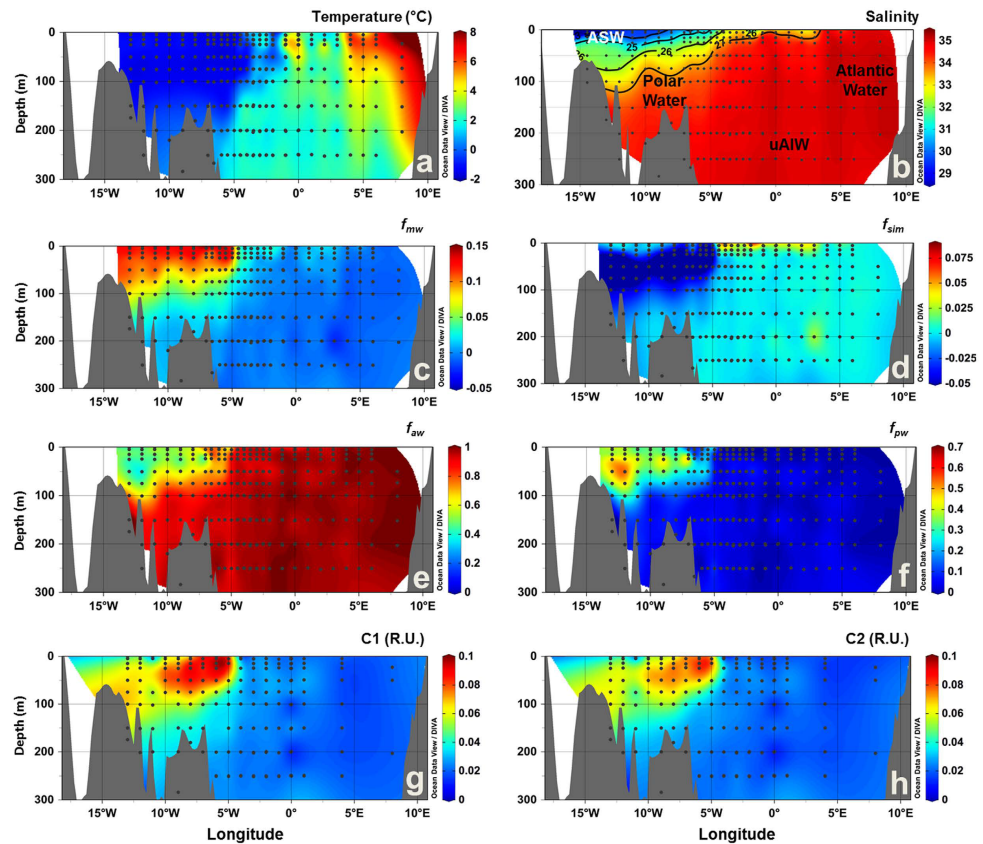


Figure 3. Vertical sections across the surface layer of Fram Strait in September 2013. (a) temperature ($^{\circ}\text{C}$), (b) salinity, fractions of (c) meteoric water (f_{mw}), (d) sea-ice melt (f_{sim}), (e) Atlantic water (f_{aw}) and (f) Pacific water (f_{pw}), (g) C1 (R.U.) and (h) C2 (R.U.). In (b) black lines indicate the potential density (σ , kg m^{-3}) and the abbreviations indicate the position of the water masses defined based on T-S diagrams (Fig. 1). Produced with Ocean Data View⁶⁰.

(UV-A) (Fig. 5, bottom panel). The fluorescence intensities of C1 and C2 ranged from 0 to 0.1 and to 0.09 R.U., respectively, with highest values observed in the polar waters in Fram Strait (Figs 2g,h and 3g,h). In Davis Strait, C1 and C2 fluorescence values were notably lower, only reaching 0.05 and 0.04 R.U., respectively (Fig. 4g,h). In surface waters (depth <300 m) C1 and C2 were significantly correlated ($C1 = 1.109 * C2 + 0.001$; $r^2 = 0.99$; $p < 0.0001$), however, this correlation was not apparent in Davis Strait deep waters (Fig. 4k). There was a clear addition of C1 in TrW and BBDW, without a proportional increase in C2.

The UV-A fluorescence signal of C3 ranged typically from 0 to 0.04 R.U. and was independent of C1 or C2. Its fluorescence was linked to productivity in surface waters, rather than water mass distribution, as evident from the significant correlation between C3 and chlorophyll-a fluorescence ($r^2 = 0.65$, $p < 0.0001$; Figure S2c). Across the region fluorescence intensities of C3 were generally higher in surface waters (Figure S2b) and profiles often exhibited maxima at or just below phytoplankton chlorophyll fluorescence maxima (Figure S2a).

Distribution of water fractions. In Fram Strait and on east Greenland shelf f_{mw} and f_{pw} followed the distribution patterns of C1. The highest values for f_{mw} and f_{pw} were observed on the Greenland shelf, associated with the cold, high DOM, polar waters exiting the Arctic (Figs 2c,f and 3c, 3f). These waters also had negative f_{sim} values indicating the fact that freshwater has been lost to sea-ice formation and they have experienced brine accumulation in the Arctic Basin (Figs 2d and 3d). In surface waters f_{sim} was generally less negative or even positive representing the contribution of freshwater from seasonal sea-ice melt. Warmer waters off the Greenland shelf and further east were largely of Atlantic origin with high f_{aw} (Figs 2e and 3e). Pacific water contribution (f_{pw}) to the polar waters on the Greenland Shelf in Fram Strait was significantly higher in 2012 than in 2013 ($p < 0.001$) (Figs 2f and 3f).

Some similarities in the distribution of the water masses in Fram Strait could be observed in Davis Strait (Fig. 4c–f). In western Davis Strait, cold polar waters occupied the sub-surface layer, characterized by sub-zero temperatures and high contribution of f_{mw} (Fig. 4c). Similarly the highest f_{sim} values were at the very surface (0–30 m), indicating sea-ice melt, and the lowest (negative values) were associated with the polar waters in western Davis Strait (Fig. 4d). The f_{aw} was the most dominant fraction on the west Greenland shelf and in deeper

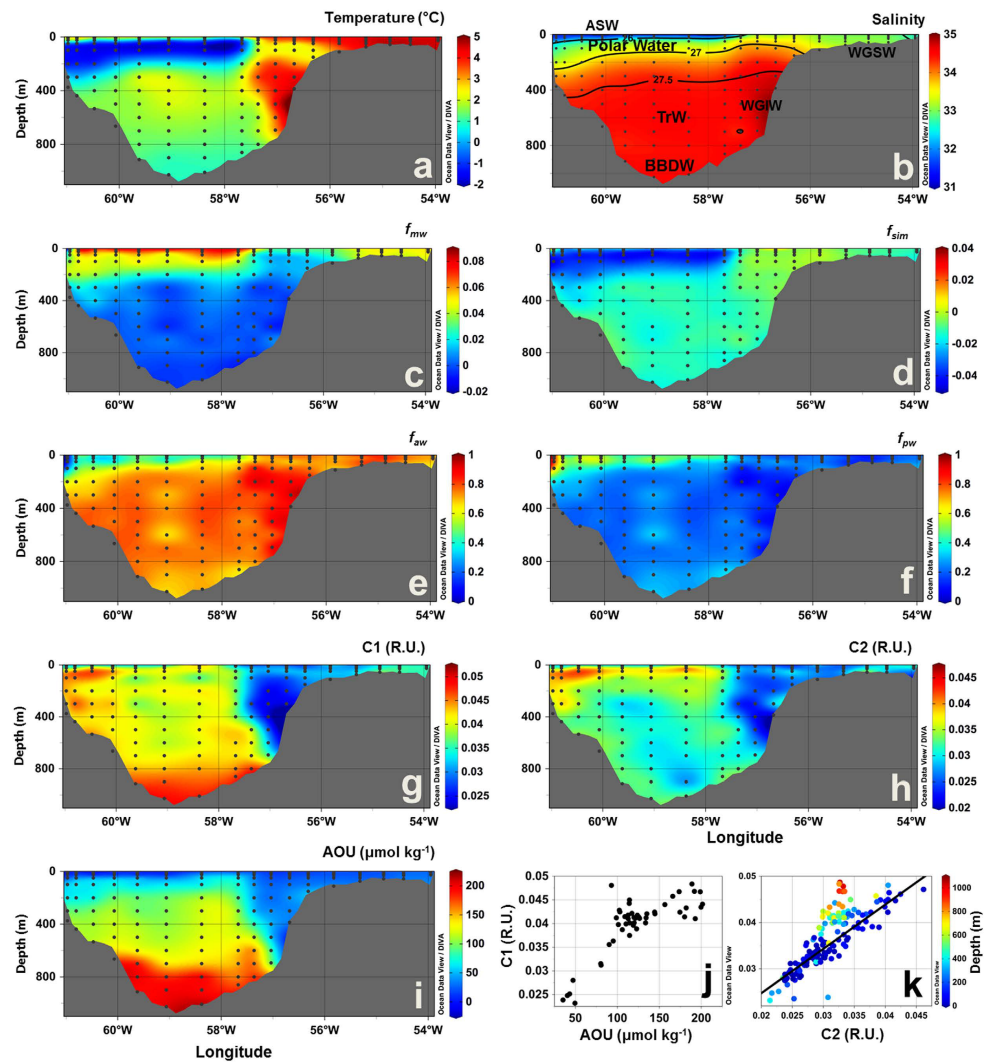


Figure 4. Vertical sections across Davis Strait in September 2013. (a) temperature ($^{\circ}\text{C}$), (b) salinity, fractions of (c) meteoric water (f_{mw}), (d) sea-ice melt (f_{sim}), (e) Atlantic water (f_{aw}) and (f) Pacific water (f_{pw}), (g) C1 (R.U.), (h) C2 (R.U.) and (i) apparent oxygen utilization (AOU, $\mu\text{mol kg}^{-1}$). (j) AOU ($\mu\text{mol kg}^{-1}$) vs. C1 (R.U.) for samples under influence of TrW and BBDW (below 300 m). (k) C2 vs. C1 plots for all the samples collected in the Davis Strait 2013, with colorbar indicating depth (m). In (b) black lines indicate the potential density (σ , kg m^{-3}) and the abbreviations indicate the position of the water masses defined based on T-S diagrams (Fig. 1). Produced with Ocean Data View⁶⁰.

waters (Fig. 4e). The contribution of Pacific water (f_{pw}) was associated with the cold polar waters exported from the Arctic (Fig. 4f).

Linking visible organic matter fluorescence to water fractions. The T-S diagram (Fig. 6a) shows a clear distinction of polar waters exiting the Arctic, with respect to C1. Highest C1 fluorescence was associated with polar waters and ASW. The latter had comparatively lower values, indicating the dilution of surface waters by sea-ice melt and precipitation (glacial input and snow). The correlation of C1 with both temperature (not shown) and salinity (Fig. 6b–d) presented a very similar, however tighter, pattern than portrayed by absorption alone^{10,33}. When considering the salinity versus C1 relation for each cruise individually (except for Davis Strait), two distinct mixing curves for the dilution of polar waters are apparent (Fig. 6). C1 was also strongly inversely correlated to f_{sim} (Figure S3) linking the high DOM signal to brine. In Davis Strait, different patterns were observed. The relationships C1 and C2 vs. salinity indicate two mixing curves (Fig. 7) in agreement with the mixing curves visible on the T-S diagram (Fig. 7a,b), where a clear separation of stations from eastern and western Davis Strait is apparent. The correlation between C1 and C2 in the East Greenland data could be harnessed tested if the FDOM in the Davis Strait had the same characteristics (relative proportions of C1 and C2) and hence similar origins. A

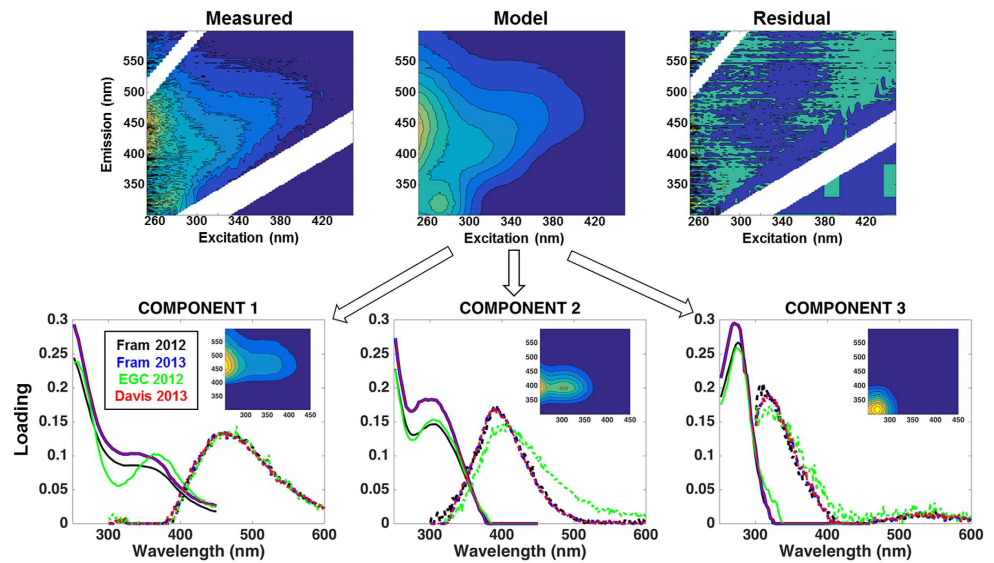


Figure 5. PARAFAC model and isolated components. (top) Three-dimensional fluorescence landscapes example of the measured, modeled and residual EEMs of the PARAFAC analysis. (bottom) The excitation (solid line) and emission (dashed line) spectra for the three fluorescent components identified by PARAFAC model for each of the cruises. Inset plots show the three-dimensional fluorescence landscapes for each of the final PARAFAC-derived component used in this work (with all cruises merged into one dataset).

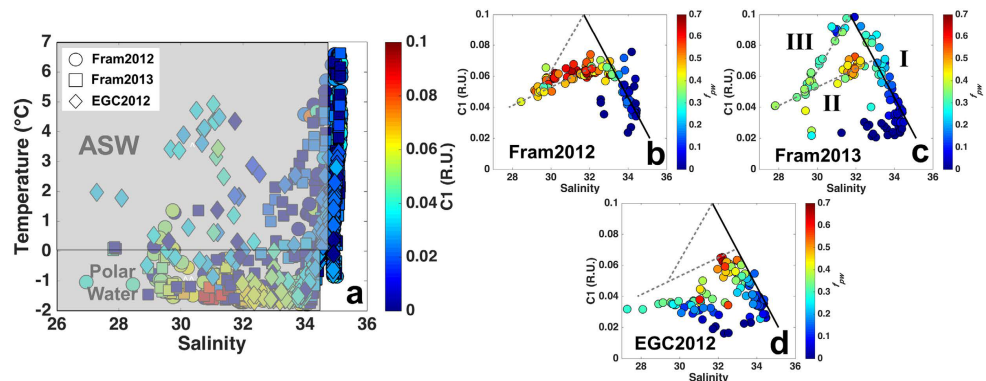


Figure 6. T-S diagram and correlations between salinity and C1 in the east of Greenland. (a) Temperature (°C) vs. salinity with colorbar indicating C1 (R.U.) for all the samples collected in the eastern Greenland cruises. (b–d) Salinity vs. C1 (R.U.) and f_{pw} , as colorbar for polar waters and ASW for each of the eastern Greenland cruises. Black solid line (I) indicates the mixing curve for the polar waters (based on Fram 2012 and 2013 datasets). Gray dashed lines (II and III) indicate the two distinct mixing curves of polar waters over the Greenland shelf. The regressions were obtained by combining the three datasets. (I) $y = -0.02 * (\text{Sal}) + 0.723$, $r^2 = 0.90$, $p < 0.0001$, $n = 240$. (II) $y = 0.0042 * (\text{Sal}) - 0.0698$, $r^2 = 0.90$, $p < 0.0001$, $n = 126$. (III) $y = 0.0183 * (\text{Sal}) - 0.4816$, $r^2 = 0.98$, $p < 0.0001$, $n = 18$.

regression was derived for C1 fluorescence based on C2 considering all the surface data (<200 m). This was then applied to the Davis Strait data to predict expected C1 fluorescence, C1*, for the surface layer in Davis Strait. The difference between measured and predicted C1 fluorescence, C1–C1*, is plotted against C2 (Fig. 7d) and indicates significant differences ($p < 0.05$) between eastern and western Davis Strait DOM. Samples in eastern Davis Strait have similar properties to those from the Fram Strait, whereas on the Canadian side of the strait the DOM has comparatively less C1. Finally for Davis Strait deep waters (>300 m), C1 was highly correlated with AOU, with the highest values of both parameters in BBDW (Fig. 4g,i). C2 showed no indication of elevated values at depth (Fig. 4h).

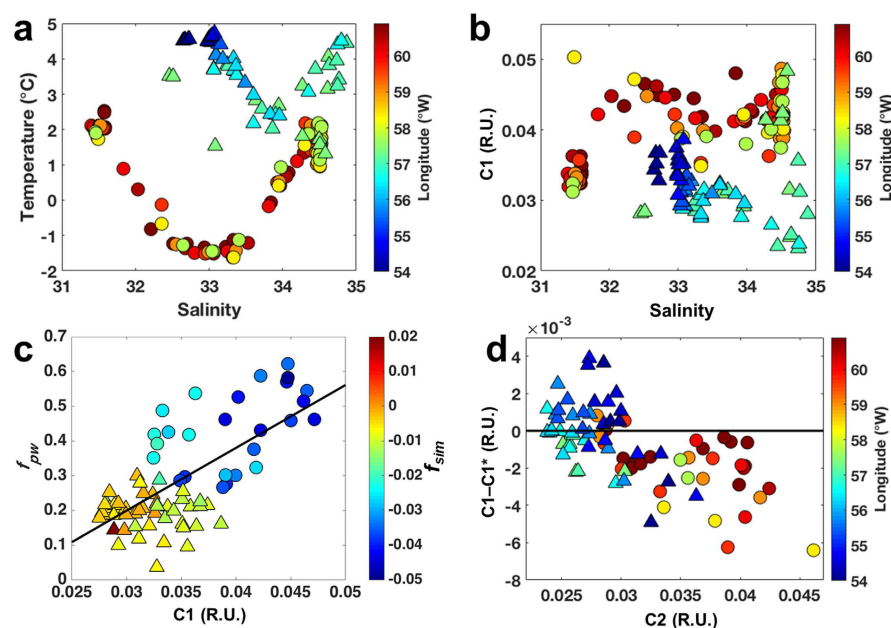


Figure 7. VIS-FDOM as a water mass tracer in the Davis Strait. Plots for the Davis2013 cruise. **(a)** T-S diagram with longitude ($^{\circ}$ W) as colorbar. **(b)** Salinity vs. C1 (R.U.), with colorbar indicating longitude ($^{\circ}$ W). **(c)** C1 (R.U.) vs. f_{pw} for the surface layer (<300 m) and f_{sim} as colorbar. **(d)** C2 (R.U.) vs. $C1-C1^*$ (R.U.) for the surface layer (<300 m), with longitude ($^{\circ}$ W) as colorbar. Triangles indicate the samples within the eastern part of Davis Strait, whereas circles refer to samples located in the western sector (separated by the 57.5° W longitude). Black line in (c) indicate the best fit.

Discussion

The distribution of the water fractions in the surface layer (0–300 m) of the Fram Strait followed the overall patterns and values reported for the region^{17,33,35} (Figs 2c–f and 3c–f). Similar hydrographic features were also observed in the distributions of temperature and salinity (Figs 2ab and 3ab), agreeing with previous reports^{12,14,22}. f_{mw} was related to the Arctic outflow through the EGC and the highest values (up to 0.15) were observed in the western section and aligned with earlier reports^{10,14,17,33}. Evidence for sea-ice melt was apparent in the surface layer with generally more positive f_{sim} values than immediately below. f_{sim} and f_{mw} were inversely correlated in polar waters indicating the origins from brine rejection during sea ice formation on coastal waters influenced by riverine inputs^{10,17,36}. The f_{pw} was associated with polar waters with values up to 0.7, and within the range reported in previous multi-year analysis conducted in the region¹⁷. Interannual variability in the contributions of f_{pw} to polar waters exiting the Arctic Ocean in the Fram Strait is related to variability in atmospheric forcing, and consequently ocean surface circulation, over the Arctic^{35,37}.

The three fluorescent components identified by PARAFAC modeling (Fig. 5) are similar to fluorescent components identified in previous studies conducted in Fram and Davis Straits^{38–40}, but also in other regions of the Arctic Ocean^{29,41}. The visible wavelength fluorescence character of C1 and C2 has been linked to aromatic, high molecular weight organic matter (humic-like) with terrestrial character^{27,28} and correlated to lignin phenol concentrations²⁵. However, the precise chemical origin of those signals is currently unknown and the subject of much research. In Fram Strait, these components (C1 and C2; Figs 2g,h and 3g,h) presented similar distribution as CDOM (a_{350})^{10,22,33}. Their fluorescence intensities were highly correlated and both had their maximum associated with the relatively low salinity polar waters and ASW (Fig. 6a) in agreement with previous *in situ* VIS-FDOM measurements (Ex: 350–460 nm; Em: 550 nm) in the region²⁵.

The UV-A FDOM signal (C3) is associated with compounds with lower aromaticity, such as dissolved and combined amino acids⁴² and is often linked to aquatic productivity^{39,40,43–45}. As can therefore be expected C3 fluorescence in this study was not correlated to polar waters; but rather linked to phytoplankton productivity in surface waters (Figure S2). In support of this C3 fluorescence in Greenland shelf waters are correlated to amino acid concentrations [Jørgensen & Stedmon, *unpublished data*].

In Davis Strait the distributions of temperature and salinity followed previous reports^{18,19,21,46} (Fig. 4a,b). The surface layer in western Davis Strait was occupied by sub-zero temperature polar waters, characterizing the Arctic outflow with the BIC. Similarly to the Fram Strait, the impact of freshening by seasonal sea-ice melt was observed in a shallow surface layer (~ 40 m)^{19,21}. The bottom layer was characterized by the presence of BBDW²¹. While the origin of this water mass is still under debate¹⁸ the high AOU values (over $220 \mu\text{mol kg}^{-1}$) associated with it (Fig. 4i,j) are comparable to AOU values observed for very old deep ocean waters and waters beneath productive upwelling regions¹³.

The distribution and contribution of water fractions in Davis Strait were in agreement with previous studies applying different approaches^{20,21,46} (Fig. 4c–f). As in Fram Strait, polar waters were found in the western sector, with the highest values of f_{mw} and f_{pw} ^{20,21,46}. However, f_{pw} contributions were greater than the ones found in Fram Strait, with values for polar waters varying between 0.5 and 1, indicating a great contribution of polar waters originating from the Canada basin. The lowest values of f_{sm} were associated with the polar waters, reflecting the fact that they have been modified by sea-ice formation. This layer was underneath a thin surface layer highly influenced by sea-ice melt^{20,21,46}. The contribution of f_{ow} was highest in the eastern Davis Strait, associated with the WGC²¹.

The distribution of the components C1 and C2 in Davis Strait surface waters resembled the general hydrographic conditions in the region^{19,21,46} with the highest fluorescence intensities associated with polar outflow to the west, as portrayed in the Fram Strait. Those components were, however, found in lower concentrations than in Fram Strait polar waters. This can be due to either a greater dilution of polar waters from Canada basin passing through the CAA and Baffin Bay³⁸ or an indication of lower FDOM levels in the source Canada basin polar waters relative to Eurasian Basin polar waters. The elevated levels of C1 and C2 observed on the west Greenland shelf likely originates from the diluted, reminiscent FDOM signal from polar waters transported through Fram Strait, with the EGC and subsequently the WGC (see discussion later). Although there is a detectable input of meteoric water from eastern Greenland to the EGC, there is little terrestrial DOM contribution from Greenland to shelf waters¹⁰.

The fluorescence intensities of C1 and C2 were highly correlated in the whole dataset; however, there were two clear exceptions. In Davis Strait deep waters there had an excess C1 relative to C2. Organic matter with these spectral characteristics has previously been linked to bacterial biomass^{47,48}, microbial respiration and degradation of organic material^{45,49}. Earlier studies have linked the generation of visible wavelength FDOM to AOU in ocean bottom waters^{43,49}, which was also proven by incubation experiments³⁹. A similar correlation is apparent in the deep layer of the Baffin Bay for C1 vs. AOU (Fig. 4j). Since ~90% of the oxygen consumption in the deep ocean is due to particle remineralization⁵⁰, our results thus suggest that the observed increase in C1 at the bottom layer is likely derived from the turnover of sinking particulate organic matter. This is supported by the fact that waters from the deeper layers of Davis Strait have a relatively long residence time⁵¹ where such a signature from the microbial production of bio-refractory material would persist and be easily detectable.

The second exception to the correlation between C1 and C2 was in the surface waters of the western Davis Strait (Fig. 4k). If the DOM fluorescence signal in polar waters present in Davis Strait and Fram Strait would have common origins one would expect all data to lie on one relationship as dilution would influence both C1 and C2 in the same fashion. The fact that the DOM in the WGC has the same proportions of C1 and C2 as that found in polar waters of the EGC (Fig. 7d) strongly suggests that it represents here the same material transported along the Greenland shelf and gradually diluted. In contrast, the lower levels of C1 relative to C2 in polar waters in the western Davis Strait suggest a different DOM source (Fig. 7d). This could be reflecting the documented differences in DOM in polar waters originating from the Canada and Eurasian Basins, marine production and terrestrial material, respectively¹. This is supported by the correlation of C1 fluorescence to f_{pw} in Davis Strait (Fig. 7c) and to f_{mw} in Fram Strait (Fig. 8b).

In Fram Strait Pacific water contribution varied between 2012 and 2013. Although the Davis Strait results discussed above suggest that visible wavelength DOM fluorescence might distinguish between polar waters from Eurasian and Canada basins, there were no such systematic deviations in Fram Strait C1 vs. C2 relationship, which could be linked to Pacific water contribution. However, plots of C1 fluorescence against salinity and f_{mw} clearly reveal a segregation into three groups where polar waters highly influenced by f_{pw} (waters from Canada basin) have lower C1 fluorescence than those of Eurasian origin which have a C1 fluorescence greater than 0.08 R.U. (Figs 6 and 8). Such clear distinction between the origins of polar waters is not apparent for CDOM (a_{350})^{10,33}, most likely due to the lesser sensitivity of this bulk measurement.

Freshening of polar waters at the very surface layer (<40 m) was clearly detected in the relationship between f_{mw} and f_{sm} (Fig. 8d), where dilution of both Atlantic and polar waters by sea-ice melt at the surface layer is apparent^{10,33,52}. Dilution of CDOM absorption (a_{350}) was observed in previous studies where samples deviating from the correlation line (to f_{mw}) indicated the dilution by sea-ice melt and/or precipitation (at the very surface layer)^{10,33}. However, the correlations observed for fluorescence in this study had a better fit than the ones for a_{350} . This can again be expected due to the general higher sensitivity of fluorescence measurements in comparison to absorbance spectroscopy³². Thus, we surmise VIS-FDOM is a more reliable tracer of polar waters and the mixing processes associated to those waters (sea-ice melt and sea-ice formation). This result holds great promise for further developments in the use of DOM visible wavelength fluorescence in tracer studies in the Arctic and warrants further investigation.

Summary

The visible wavelength DOM fluorescence components identified by PARAFAC modeling were correlated to the fraction of meteoric and Pacific water determined using established techniques^{17,53}. The ratio of the two fluorescence signals was linked to the dominant organic matter sources in polar waters exiting the Arctic from the Canada and Eurasian basins. In 2012 a greater fraction of Pacific waters in the Fram Strait suggests greater contribution of waters from the Canada basin which is reflected in organic matter fluorescence intensities. Such changes were not detectable from CDOM absorption measurements^{10,33}. Our results demonstrate that Eurasian polar waters have higher visible wavelength DOM fluorescence signal than waters from the Canada basin. The result also show that the organic matter exported through the Davis and Fram straits differ in quality reflecting the contrasting dominant sources of DOM in polar waters from the two basins. In addition, in deep waters of the Davis Strait there was a production of bio-refractory organic matter fluorescence signal linked to microbial respiration driven by degradation of sinking particulate matter.

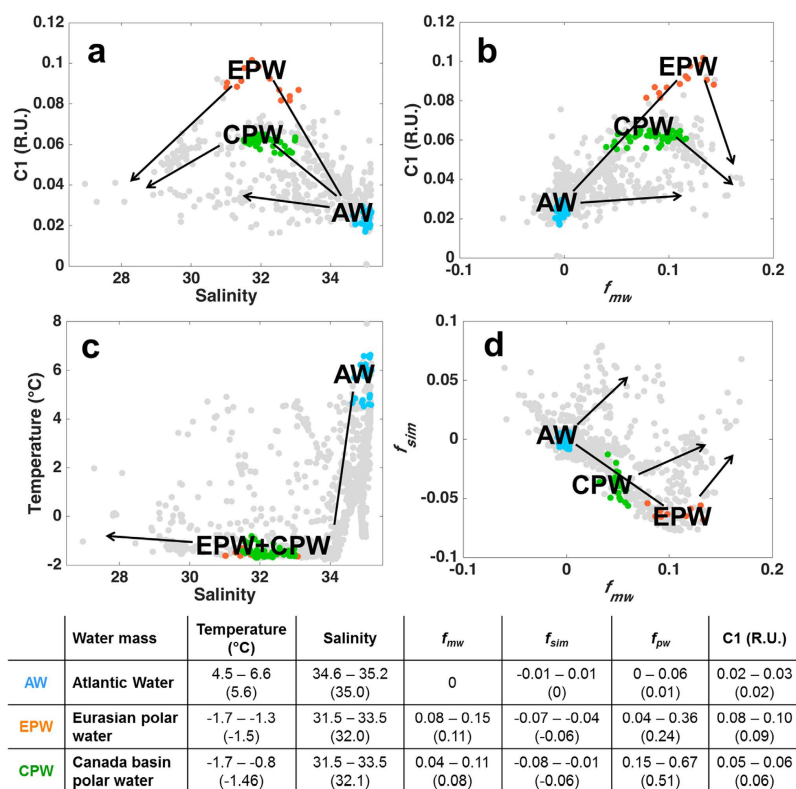


Figure 8. Schematic graphs for eastern Greenland. Schematic graphs showing the behavior during mixing of distinct waters defined in the text (Atlantic water, Eurasian and Canada basin polar waters, whose end members in this study are colored accordingly): for (a) C1 and salinity, (b) C1 and f_{mw} , (c) temperature and salinity, (d) f_{sim} and f_{mw} . All data used in this study is shown with gray dots. Lines indicate the mixing between different waters, whose end-members for this study are tabulated below. Arrows represent the approximate direction of the deviation expected by dilution with sea-ice melt and precipitation (including glacial melt). The table shows information (range and average) on some parameters for the end members of each water type identified in this study.

The results presented here provide an indication of which wavelength regions of DOM fluorescence carry information on DOM source and mixing. As fluorescence is well suited for use *in situ* instrumentation, these measurements can aid the design of new multi-channel fluorometers for different platforms. These can provide additional insight into the physical oceanography of the region and complement current hydrographic measurements focused on monitoring freshwater fluxes and circulation.

Methods

Sampling strategy. Samples for salinity, dissolved organic matter fluorescence (FDOM), dissolved inorganic nutrients (nitrate and phosphate) and $\delta^{18}\text{O}$ were collected during several cruises around Greenland (Fig. 1a). Two cruises were along a section in the Fram Strait at 78°55'N in Aug/Sep of 2012 and 2013 onboard *R/V Lance*, hereafter referred to as Fram2012 and Fram2013, respectively. A cruise onboard *R/V Dana* (September 2012, hereafter EGC2012) collected samples in the Denmark Strait region, Iceland Sea and along a number of sections across the EGC. Data from Fram2012 and EGC2012 cruises (including hydrography, water fractions and CDOM absorption) are also presented in other study¹⁰. In addition, samples were collected across the Davis Strait onboard *R/V Knorr* (September 2013, hereafter Davis2013). During all cruises temperature and salinity profiles were acquired with a CTD attached to a rosette system at all the stations, which was calibrated with salinity from water samples.

Analyses of salinity, dissolved inorganic nutrients, dissolved oxygen and $\delta^{18}\text{O}$. For calibration of the CTD, salinity samples were collected in glass bottles and analyzed using a Guildline 8410A Portasal salinometer (Fram and EGC). For the Fram2012, Fram2013 and EGC2012 cruises, nutrient samples were collected directly into acid-washed polyethylene bottles and frozen immediately after collection, and were kept at -20°C until analysis. Nutrient analyses were conducted at Aarhus University (Roskilde, Denmark) using an autoanalyzer (Skalar)⁵⁴. For those cruises, $\delta^{18}\text{O}$ samples were collected in 40 mL glass vials that were filled completely, closed tightly and sealed with Parafilm, and were analyzed by equilibration with carbon dioxide. Measurements were carried out with isotope ratio mass spectrometers at the G.G. Hatch Stable Isotope Laboratory, University of Ottawa, Canada (Thermo Delta Plus XP).

For the Davis 2013 cruise nutrient samples were frozen and later analyzed at Bedford Institute of Oceanography, Canada, following the World Ocean Circulation Experiment (WOCE) protocols using a Technicon Autoanalyzer with the precision of $0.19 \text{ mmol kg}^{-1}$ for nitrate and nitrite ($\text{NO}_3 + \text{NO}_2$), and $0.04 \text{ mmol kg}^{-1}$ for phosphate (PO_4). Oxygen isotope samples were collected in 60 mL Amber Boston Rounds with Poly-Seal-Lined caps secured with electrical tape, stored at room temperature. They were analyzed with a FISIONS PRISM III with a Micromass multiprep automatic equilibration system at Lamont-Doherty Earth Observatory, USA. Two-milliliter subsamples were equilibrated with CO_2 gas (8 h at 35°C). Data are reported with respect to standard mean ocean water (SMOW) with the $\delta^{18}\text{O}$ notation. The external precision based on replicates and standards is $\pm 0.033\%$. Additionally, 293 samples for dissolved oxygen were collected only in the Davis 2013 cruise and analyzed using Winkler titration (with precision of 0.5%), to calibrate oxygen sensors on CTD.

DOM samples processing. Water samples for DOM analysis (CDOM and FDOM) were collected through prerinsed $0.2 \mu\text{m}$ Millipore Opticap XL filter capsules, except on the EGC2012 cruise precombusted GF/F filters (nominal pore size $0.7 \mu\text{m}$) were used. The samples were stored in pre-combusted amber glass vials in dark at 4°C until analysis at the Technical University of Denmark, within two months of collection (Fram and Davis Straits) or analyzed immediately onboard (EGC2012). It should be noted that the optimal situation would be to have all samples $0.2 \mu\text{m}$ filtered (removing bacteria and colloids) and analyzed immediately onboard however, logistical constraints and practicalities of collaborative sampling hindered this. An analysis of histograms of the fluorescence properties of DOM from the Fram Strait (sterile filtered and stored) and the EGC (GFF and analyses immediately) indicated no clear systematic bias resulting from the two approaches.

Spectroscopic measurements and PARAFAC modeling. CDOM absorbance was measured across the spectral range from 250 to 700 nm using a Shimadzu UV-2401PC spectrophotometer and 100 mm quartz cells with ultrapure water as reference⁵⁵. Absorbance was used to correct fluorescence EEMs.

Fluorescence EEMs were collected using an Aqualog fluorescence spectrometer (HORIBA Jobin Yvon, Germany). Fluorescence intensity was measured across emission wavelengths 300–600 nm (resolution 1.64 nm) at excitation wavelengths from 250 to 450 nm, with 3 nm increments, and an integration time of 8 s. EEMs were corrected for inner-filter effects and for Raman and Rayleigh scattering⁵⁶ (Fig. 5, top panel). The underlying fluorescent components of DOM in the EEMs were isolated by applying PARAFAC modeling using the “drEEM Toolbox”⁵⁶. In this study different PARAFAC model fits were explored. At first, individual PARAFAC models were derived and split-half validated for each cruise individually. The split-half analysis consists in producing identical models from independent subsamples (halves) of the dataset, generally randomly generated. Similar PARAFAC components were identified (Fig. 5, bottom panel) and these results were then compared to a model derived on the combined dataset (1022 samples). The fluorescent components derived from PARAFAC modeling were compared with PARAFAC components from other studies using the OpenFluor database⁵⁷.

Water masses fractionation. The fractions of meteoric water (f_{mw}), sea-ice melt water (f_{sim}), Pacific seawater (f_{pw}) and Atlantic seawater (f_{aw}) in discrete water samples were derived using a combination of procedures established by Östlund and Hut⁵⁸ and Jones *et al.*¹¹ as described in Dodd *et al.*¹⁷. The details behind the choice of end-member values and for the sensitivity of the estimates of freshwater fractions to variations in the end-member composition can be found in Jones *et al.*¹⁶, Dodd *et al.*¹⁷ and Hansen *et al.*⁵⁹. In brief, the contribution from Atlantic water, Pacific water, meteoric water, and sea-ice melt was carried out with the following equations:

$$P_{pw} = 0.065N + 0.94, \quad (1)$$

$$P_{aw} = 0.060N + 0.120, \quad (2)$$

$$f_{mw} + f_{sim} + f_{pw} + f_{aw} = 1 \quad (3)$$

$$f_{mw}S_{mw} + f_{sim}S_{sim} + f_{pw}S_{pw} + f_{aw}S_{aw} = S, \quad (4)$$

$$f_{mw}\delta^{18}O_{mw} + f_{sim}\delta^{18}O_{sim} + f_{pw}\delta^{18}O_{pw} + f_{aw}\delta^{18}O_{aw} = \delta^{18}O, \quad (5)$$

$$f_{mw}P_{mw} + f_{sim}P_{sim} + f_{pw}P_{pw} + f_{aw}P_{aw} = P, \quad (6)$$

N and P in the equations above correspond to the nitrate and phosphate concentrations, respectively (Figure S1a). The salinity (S) of meteoric water, sea-ice melt, Pacific water, and Atlantic water were 0, 4, 32.0, and 34.9, respectively, and the $\delta^{18}\text{O}$ end-members -18.4 , 0.5 , -1.3 , and 0.3 , respectively¹⁷.

References

1. Stedmon, C. A., Amon, R. M. W., Rinehart, A. J. & Walker, S. A. The supply and characteristics of colored dissolved organic matter (CDOM) in the Arctic Ocean: Pan Arctic trends and differences. *Mar. Chem.* **124**, 108–118 (2011).
2. Dittmar, T. & Kattner, G. The biogeochemistry of the river and shelf ecosystem of the Arctic Ocean: a review. *Mar. Chem.* **83**, 103–120 (2003).
3. Cooper, L. W. *et al.* Linkages among runoff, dissolved organic carbon, and the stable oxygen isotope composition of seawater and other water mass indicators in the Arctic Ocean. *J. Geophys. Res.* **110**, G02013 (2005).

4. Benner, R., Benitez-Nelson, B., Kaiser, K. & Amon, R. M. W. Export of young terrigenous dissolved organic carbon from rivers to the Arctic Ocean. *Geophys. Res. Lett.* **31**, (2004).
5. Opsahl, S., Benner, R. & Amon, R. M. W. Major flux of terrigenous dissolved organic matter through the Arctic Ocean. *Limnol. Oceanogr.* **44**, 2017–2023 (1999).
6. Fichot, C. G. *et al.* Pan-Arctic distributions of continental runoff in the Arctic Ocean. *Sci. Rep.* **3**, 1053 (2013).
7. Schuur, E. A. G. *et al.* Expert assessment of vulnerability of permafrost carbon to climate change. *Clim. Change* **119**, 359–374 (2013).
8. Frey, K. E. & McClelland, J. W. Impacts of permafrost degradation on arctic river biogeochemistry. *Hydrol. Process* **23**, 169–182 (2009).
9. Vonk, J. E. *et al.* Activation of old carbon by erosion of coastal and subsea permafrost in Arctic Siberia. *Nature* **489**, 137–140 (2012).
10. Stedmon, C. A., Granskog, M. A. & Dodd, P. A. An approach to estimate the freshwater contribution from glacial melt and precipitation in East Greenland shelf waters using colored dissolved organic matter (CDOM). *J. Geophys. Res. Ocean.* **120**, 1107–1117 (2015).
11. Jones, P. E., Anderson, L. G. & Swift, J. H. Distribution of Atlantic and Pacific water in the upper Arctic Ocean: Implications for circulation. *Geophys. Res. Lett.* **25**, 765–768 (1998).
12. Beszczynska-Möller, A., Fahrback, E., Schauer, U. & Hansen, E. Variability in Atlantic water temperature and transport at the entrance to the Arctic Ocean, 1997–2010. *ICES J. Mar. Sci.* **69**, 852–863 (2012).
13. Aagaard, K. & Carmack, E. C. The role of sea ice and other fresh water in the Arctic circulation. *J. Geophys. Res.* **94**, 14485 (1989).
14. Rabe, B. *et al.* Freshwater components and transports in the Fram Strait – recent observations and changes since the late 1990s. *Ocean Sci.* **5**, 219–233 (2009).
15. Hattermann, T., Isachsen, P. E., von Appen, W.-J., Albretsen, J. & Sundfjord, A. Eddy-driven recirculation of Atlantic Water in Fram Strait. *Geophys. Res. Lett.* **43**, 3406–3414 (2016).
16. Jones, E. P., Anderson, L. G., Jutterstro, S., Mintrop, L. & Swift, J. H. Pacific freshwater, river water and sea ice meltwater across Arctic Ocean basins: Results from the 2005 Beringia Expedition. *J. Geophys. Res.* **113**, 1–10 (2008).
17. Dodd, P. A. *et al.* The freshwater composition of the Fram Strait outflow derived from a decade of tracer measurements. *J. Geophys. Res.* **117**, 1–26 (2012).
18. Tang, C. C. *et al.* The circulation, water masses and sea-ice of Baffin Bay. *Prog. Oceanogr.* **63**, 183–228 (2004).
19. Curry, B., Lee, C. M., Petrie, B., Moritz, R. E. & Kwok, R. Multiyear Volume, Liquid Freshwater, and Sea Ice Transports through Davis Strait, 2004–10*. *J. Phys. Oceanogr.* **44**, 1244–1266 (2014).
20. Alkire, M. B., Falkner, K. K. & Boyd, T. Sea ice melt and meteoric water distribution in Nares Strait, Baffin Bay, and the Canadian Arctic Archipelago. *J. Mar. Res.* **68**, 767–798 (2010).
21. Azetsu-Scott, K., Petrie, B., Yeats, P. & Lee, C. Composition and fluxes of freshwater through Davis Strait using multiple chemical tracers. *J. Geophys. Res. Ocean.* **117**, n/a–n/a (2012).
22. Pavlov, A. K. *et al.* Contrasting optical properties of surface waters across the Fram Strait and its potential biological implications. *J. Mar. Syst.* **143**, 62–72 (2015).
23. Granskog, M. A. *et al.* Effect of sea-ice melt on inherent optical properties and vertical distribution of solar radiant heating in Arctic surface waters. *J. Geophys. Res. Ocean.* **120**, 7028–7039 (2015).
24. Coble, P. G. Marine Optical Biogeochemistry: The Chemistry of Ocean Color. *Chem. Rev.* **107**, 402–418 (2007).
25. Amon, R. M. W., Budéus, G. & Meon, B. Dissolved organic carbon distribution and origin in the Nordic Seas: Exchanges with the Arctic Ocean and the North Atlantic. *J. Geophys. Res.* **108**, 3221 (2003).
26. Wünsch, U. J., Murphy, K. R. & Stedmon, C. A. Fluorescence Quantum Yields of Natural Organic Matter and Organic Compounds: Implications for the Fluorescence-based Interpretation of Organic Matter Composition. *Front. Mar. Sci.* **2**, 98, 1–15 (2015).
27. Wagner, S., Jaffé, R., Cawley, K., Dittmar, T. & Stubbins, A. Associations Between the Molecular and Optical Properties of Dissolved Organic Matter in the Florida Everglades, a Model Coastal Wetland System. *Front. Chem.* **3**, 66, 1–14 (2015).
28. Stubbins, A. *et al.* What's in an EEM? Molecular Signatures Associated with Dissolved Organic Fluorescence in Boreal Canada. *Environ. Sci. Technol.* **48**, 10598–10606 (2014).
29. Dainard, P. G., Guéguen, C., McDonald, N. & Williams, W. J. Photobleaching of fluorescent dissolved organic matter in Beaufort Sea and North Atlantic Subtropical Gyre. *Mar. Chem.* **177**, 630–637 (2015).
30. Gonçalves-Araujo, R. *et al.* From Fresh to Marine Waters: Characterization and Fate of Dissolved Organic Matter in the Lena River Delta Region, Siberia. *Front. Mar. Sci.* **2**, 108, 1–13 (2015).
31. Guéguen, C., Itoh, M., Kikuchi, T., Eert, J. & Williams, W. J. Variability in dissolved organic matter optical properties in surface waters in the Amerasian Basin. *Front. Mar. Sci.* **2**, 78, 1–9 (2015).
32. Blough, N. V. & Del Vecchio, R. In *Biogeochemistry of marine dissolved organic matter* (eds Hansell, D. A. & Carlson, C. A.) 509–546 (Academic Press, 2002).
33. Granskog, M. A. *et al.* Characteristics of colored dissolved organic matter (CDOM) in the Arctic outflow in the Fram Strait: Assessing the changes and fate of terrigenous CDOM in the Arctic Ocean. *J. Geophys. Res.* **117**, C12021 (2012).
34. Swift, J. H. & Aagaard, K. Seasonal transitions and water mass formation in the Iceland and Greenland seas. *Deep Sea Res. Part A. Oceanogr. Res. Pap.* **28**, 1107–1129 (1981).
35. Rabe, B. *et al.* Liquid export of Arctic freshwater components through the Fram Strait 1998–2011. *Ocean Sci.* **9**, 91–109 (2013).
36. Bauch, D. *et al.* Origin of freshwater and polynya water in the Arctic Ocean halocline in summer 2007. *Prog. Oceanogr.* **91**, 482–495 (2011).
37. Falck, E., Kattner, G. & Budéus, G. Disappearance of Pacific Water in the northwestern Fram Strait. *Geophys. Res. Lett.* **32**, n/a–n/a (2005).
38. Guéguen, C., Cuss, C. W., Cassels, C. J. & Carmack, E. C. Absorption and fluorescence of dissolved organic matter in the waters of the Canadian Arctic Archipelago, Baffin Bay, and the Labrador Sea. *J. Geophys. Res. Ocean.* **119**, 2034–2047 (2014).
39. Jørgensen, L., Stedmon, C. A., Granskog, M. A. & Middelboe, M. Tracing the long-term microbial production of recalcitrant fluorescent dissolved organic matter in seawater. *Geophys. Res. Lett.* **41**, 2481–2488 (2014).
40. Jørgensen, L., Stedmon, C. A., Kaartokallio, H., Middelboe, M. & Thomas, D. N. Changes in the composition and bioavailability of dissolved organic matter during sea ice formation. *Limnol. Oceanogr.* **60**, 817–830 (2015).
41. Guéguen, C., Granskog, M. A., McCullough, G. & Barber, D. G. Characterisation of colored dissolved organic matter in Hudson Bay and Hudson Strait using parallel factor analysis. *J. Mar. Syst.* **88**, 423–433 (2011).
42. Yamashita, Y. & Tanoue, E. Chemical characterization of protein-like fluorophores in DOM in relation to aromatic amino acids. *Mar. Chem.* **82**, 255–271 (2003).
43. Jørgensen, L. *et al.* Global trends in the fluorescence characteristics and distribution of marine dissolved organic matter. *Mar. Chem.* **126**, 139–148 (2011).
44. Romera-Castillo, C., Sarmiento, H., Álvarez-Salgado, X. A., Gasol, J. M. & Marrase, C. Production of chromophoric dissolved organic matter by marine phytoplankton. *Limnol. Oceanogr.* **55**, 446–454 (2010).
45. Catalá, T. S. *et al.* Turnover time of fluorescent dissolved organic matter in the dark global ocean. *Nat. Commun.* **6**, 5986 (2015).
46. Azetsu-Scott, K. *et al.* Calcium carbonate saturation states in the waters of the Canadian Arctic Archipelago and the Labrador Sea. *J. Geophys. Res.* **115**, C11021 (2010).
47. Rochelle-Newall, E. J. & Fisher, T. R. Production of chromophoric dissolved organic matter fluorescence in marine and estuarine environments: an investigation into the role of phytoplankton. *Mar. Chem.* **77**, 7–21 (2002).

48. Shimotori, K., Omori, Y. & Hama, T. Bacterial production of marine humic-like fluorescent dissolved organic matter and its biogeochemical importance. *Aquat. Microb. Ecol.* **58**, 55–66 (2009).
49. Yamashita, Y. & Tanoue, E. Production of bio-refractory fluorescent dissolved organic matter in the ocean interior. *Nat. Geosci.* **1**, 579–582 (2008).
50. Aristegui, J. *et al.* Dissolved Organic Carbon Support of Respiration in the Dark Ocean. *Science* (80-) **298**, 1967–1967 (2002).
51. Punshon, S., Azetsu-Scott, K. & Lee, C. M. On the distribution of dissolved methane in Davis Strait, North Atlantic Ocean. *Mar. Chem.* **161**, 20–25 (2014).
52. Bauch, D. *et al.* Correlation of river water and local sea-ice melting on the Laptev Sea shelf (Siberian Arctic). *J. Geophys. Res. Ocean.* **118**, 550–561 (2013).
53. Bauch, D. *et al.* Atmospheric controlled freshwater release at the Laptev Sea continental margin. *Polar Res.* **30**, 1–14 (2011).
54. Hansen, H. P. & Koroleff, F. In *Methods of Seawater Analysis* (eds Grasshoff, K., Kremling, K. & Ehrhardt, M.) 159–228 (Wiley-VCH Verlag GmbH, 1999), doi: 10.1002/9783527613984.ch10.
55. Stedmon, C. A. & Markager, S. The optics of chromophoric dissolved organic matter (CDOM) in the Greenland Sea: An algorithm for differentiation between marine and terrestrially derived organic matter. *Limnol. Oceanogr.* **46**, 2087–2093 (2001).
56. Murphy, K. R., Stedmon, C. A., Graeber, D. & Bro, R. Fluorescence spectroscopy and multi-way techniques. *PARAEAC. Anal. Methods* **5**, 6557 (2013).
57. Murphy, K. R., Stedmon, C. A., Wenig, P. & Bro, R. OpenFluor— an online spectral library of auto-fluorescence by organic compounds in the environment. *Anal. Methods* **6**, 658–661 (2014).
58. Østlund, H. G. & Hut, G. Arctic Ocean water mass balance from isotope data. *J. Geophys. Res.* **89**, 6373–6381 (1984).
59. Hansen, M. O., Nielsen, T. G., Stedmon, C. A. & Munk, P. Oceanographic regime shift during 1997 in Disko Bay, Western Greenland. *Limnol. Oceanogr.* **57**, 634–644 (2012).
60. Schlitzer, R. Ocean Data View. at <http://odv.awi.de> (2015).

Acknowledgements

The authors thank the captain, crew and scientists onboard *R/V Lance*, *R/V Dana* and *R/V Knorr* for their assistance during the campaigns. Study was supported by the Danish Strategic Research Council for the NAACOS project (grant 10–093903), the Danish Center for Marine Research (grant 2012–01), the Danish Research Council for Independent Research (DFF 1323–00336). The funding for Davis Strait program comes from the U.S. National Science Foundation (ARC1022472) and the International Governance Strategy (IGS) fund for the Fisheries and Oceans, Canada. The authors acknowledge the “Fram Strait Arctic Outflow Observatory” for providing data from the Fram Strait. Authors also acknowledge the chief scientist and lead of the Davis Strait program, Dr. Craig Lee of University of Washington. R.G.-A. was supported by a PhD fellowship from the Coordination for the Improvement of Higher Level Personnel (CAPES-Brazil, Grant 12362/12-3) in collaboration with the German Academic Exchange Service (DAAD), and by an impulsive grant from the University of Bremen. M.A.G. was supported by the Polish–Norwegian Research Program operated by the National Centre for Research and Development under the Norwegian Financial Mechanism 2009–2014 in the frame of Project Contract Pol-Nor/197511/40/2013, CDOM-HEAT and the Fram Centre Ocean Acidification Flagship programme. M.A.G. and P.A.D. were supported by the Centre for Ice, Climate and Ecosystems (ICE) at the Norwegian Polar Institute.

Author Contributions

Designed the sampling strategy and acquired and analyzed the samples: M.A.G., P.A.D., K.A.-S. and C.A.S. Analyzed the data: R.G.-A., M.A.G., A.B., P.A.D. and C.A.S. Prepared the figures: R.G.-A., M.A.G. and C.A.S. Wrote the manuscript: R.G.-A. All authors reviewed the manuscript.

Additional Information

Supplementary information accompanies this paper at <http://www.nature.com/srep>

Competing financial interests: The authors declare no competing financial interests.

How to cite this article: Gonçalves-Araujo, R. *et al.* Using fluorescent dissolved organic matter to trace and distinguish the origin of Arctic surface waters. *Sci. Rep.* **6**, 33978; doi: 10.1038/srep33978 (2016).



This work is licensed under a Creative Commons Attribution 4.0 International License. The images or other third party material in this article are included in the article's Creative Commons license, unless indicated otherwise in the credit line; if the material is not included under the Creative Commons license, users will need to obtain permission from the license holder to reproduce the material. To view a copy of this license, visit <http://creativecommons.org/licenses/by/4.0/>

© The Author(s) 2016